EUV, X-ray and Optical Studies of White Dwarf Binary Systems

CHRISTIAN MARC JOMARON

Mullard Space Science Laboratory
Department of Space and Climate Physics
University College London

A thesis submitted to the University of London
for the Degree of Doctor of Philosophy

January 1994

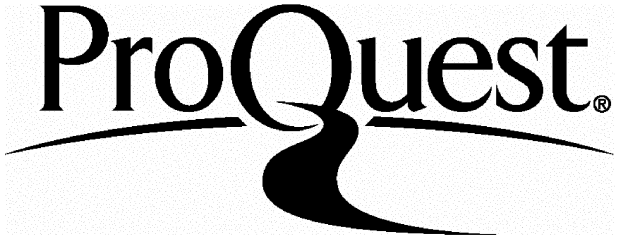

Abstract

This thesis describes an EUV, X-ray and optical study of white dwarfs, concentrating on those in binary systems with a late-type companion star.

In the introductory chapter I outline the types of binary systems known to include white dwarf components and the observed characteristics of binary and single white dwarfs. Chapter 2 discusses *WFC*-discovered white dwarfs which appear isolated. I derive magnitudes and temperatures both from optical spectra and EUV data, and compare this population to that of known field white dwarfs. I also report on a search for any further 'hidden' white-dwarf/red-dwarf systems. Chapter 3 presents extensive work on RE1016−05, a white-dwarf/red-dwarf candidate pre-cataclysmic binary, discovered in the *ROSAT* all-sky-survey. EUV, X-ray and optical data are analysed to determine the parameters and nature of the system. In chapters 4 and 5 I describe work undertaken on other white-dwarf/red dwarf systems: several discovered with the *ROSAT WFC* ; and several pre-cataclysmic systems known before the all-sky-survey. EUV and X-ray observations (obtained during the *ROSAT* survey and pointed phases) and optical follow-up spectra are analysed to determine parameters of both components in the systems and extract information about their evolutionary state and the structure and composition of the white dwarf atmospheres. The main results and conclusions to be drawn from this thesis are summarised in chapter 6. Appendix A describes software I wrote to aid in the reduction of the large volumes of spectral data accumulated by the *ROSAT* Optical Identification Programme. Appendix B contains a brief description of the *ROSAT* spacecraft and our (MSSL) participation in the *WFC* survey data reduction.

Contents

List of Figures

List of Tables

Chapter 1

Introduction

Of all the communities available to us, there is not one I would want to devote myself to except for the society of the true searchers, which has very few living members at any one time.

Albert Einstein, quoted by Max Born

This chapter provides a historical introduction to the current state of understanding of white dwarfs (WD), both in isolated and binary systems, gained from data obtained in the optical, EUV and X-ray bands. I shall summarise the relevant knowledge about these stars' structure, their formation, and their evolution. This knowledge has recently been modified due to the availability of *ROSAT* data, and new conclusions will be summarised at the end of this thesis.

1.1 *ROSAT* : an introduction

ROSAT (an abbreviation of Röntgensatellit) is a multinational space-borne observatory designed to carry out the first ever simultaneous all-sky extreme-ultraviolet (EUV) and X-ray survey. This is now being followed up by an extensive 'pointed' phase during which many individual targets are observed for extended periods.

The X-ray and EUV energy bands are two regions of the electromagnetic spectrum which, until fairly recently ($\sim$ 1970), received little attention compared to that given the optical. In particular, the EUV and X-ray emission from astronomical sources has been poorly studied due to the problems of transmission through the Earth's atmosphere. Absorption of the EUV (and to a lesser extent X-rays) by Galactic neutral hydrogen has also proved a problem, requiring the development of extremely sensitive detectors.

The *ROSAT Wide Field Camera* (*WFC*) conducted a six month all-sky survey in two EUV bandpasses: one defined by the S1a filter (90–190 eV or 65–135 Å) and one by the S2a filter (60–110 eV or 110–200 Å). The *WFC*, which has a 5° diameter field-of-view, is co-aligned with the German imaging X-ray Telescope (XRT; spectral range 0.05–2.5 keV). During the survey, both of these instruments scanned a swath normal to the ecliptic plane, and this scan plane rotated (because of the Earth's orbital motion) by 1° per day in ecliptic longitude. The data collected were stored and transmitted back to Earth each day. For a more detailed description of the *ROSAT* mission, see appendix B.

The wealth of data returned by the various instruments aboard *ROSAT* has provided a fertile ground for astrophysical research in many areas where current knowledge is limited. Much still needs to be done in order to gain an understanding of many of the fundamental properties of stellar structure and evolution, the interstellar medium and extragalactic astronomy.

One of the areas to benefit most from *ROSAT* EUV data is that of degenerate-star research. The study of some of these objects—white dwarfs—forms the basis of this thesis.

1.2 EUV and X-ray astronomy

The first EUV observations were performed by sounding rocket experiments carried out in the 1970s. Data from these experiments produced constraints on the

luminosity of sources in certain areas of sky (10^{-7} erg s^{-1} cm^{-2}; Riegler & Garmire 1974; Henry *et al.* 1975, 1976), but otherwise failed to produce direct observational evidence for any extra-Solar EUV sources. One of the first successful EUV instruments was the *Apollo-Soyuz* EUV telescope (Margon & Bowyer 1975) which returned about 20 hours of observations and led to the discovery of the first non-Solar EUV source—the hot white dwarf HZ43 (Lampton *et al.* 1976).

HZ43 was also observed in X-rays as early as in 1972 (Hayakawa *et al.* 1975a, 1975b); X-ray astronomy also began via sounding rockets, but by this time was more advanced than EUV astronomy, having progressed to the use of satellites such as UHURU.

The first UV and EUV satellite observations of hot white dwarf stars were made using the *Astronomical Netherlands Satellite* (Wesselius & Koester 1978) and the *International Ultraviolet Explorer* (Greenstein & Oke 1979; Böhm-Vitense, Dettman & Kapranidis 1979).

Since these early observations, the study of white dwarfs (and many other objects) with EUV and X-ray instruments has become an invaluable tool in understanding their structure. This is especially so because the bulk of the luminosity of a white dwarf is emitted in the UV/EUV region, and it is here that many of the important spectral features form, as we shall see later in this chapter.

1.3 White dwarfs

In general a star can be classified as a white dwarf if it lies five or more magnitudes below the Main Sequence (MS). The name 'white dwarf' was attributed to this class of objects because the first such star to be studied, 40 Eri B (Adams 1914), was classified as spectral type A, yet appeared very sub-luminous. Until this time, all dwarf stars had been found to be red. Thus the term was coined to point out the apparent discrepancy between the luminosity and the colour of the star. Another term used to describe these stars is degenerates, since they are composed of

degenerate matter [1]. Thus it was seen to be an important task for the completeness of stellar evolution theory to determine if any more of these stars existed.

1.4 White dwarf surveys

1.4.1 Isolated stars

The first real white dwarf survey was carried out by Luyten from 1931 onwards. He isolated a set of nearby stars, based on their proper motions, then extracted the subset of stars with unusually blue colours. This eventually led to the production of a catalogue of some 3000 degenerate stars. Humason & Zwicky (1947) employed a different technique: a spectroscopic search for blue objects, in an area of the Hertzsprung-Russell diagram where no intrinsically luminous stars are expected to lie. An example of a more recent, and one of the more important surveys for degenerate stars, is the Palomar-Green survey (Fleming, Liebert & Green 1986). Covering a 10 000 square degree region of sky and extending down to $B = 16.2$, 3000 stars with blue colours were selected and observed. From these, 700 degenerates were selected.

1.4.2 Binary systems

Luyten (1969, 1979) searched for wide binary systems containing white dwarf components by looking for nearby stars exhibiting similar proper motions. He found that degenerate stars are present in a remarkably high number of nearby systems containing MS stars. In most cases, the degenerate was the fainter of the two components (explaining their non-detection until this survey technique was utilised).

[1] In degenerate matter the electrons and/or nucleons are forced so close together that they occupy every available energy state. There are essentially no free energy levels to allow movement of a particle from one energy state to another. Since the same state cannot be occupied by more than one fermion (electron or nucleon), expressed as the Pauli exclusion principle, further inward contraction is resisted, and this resistance is termed the degeneracy pressure of the matter.

These degenerates included α CMa B, α CMi B, 40 Eri B, L145-141. Very few binary systems were observed to contain two degenerate stars.

Searching for close binary systems is much harder, since it must be done purely on the basis of the colours or spectra of the systems. Thus it is easiest to detect binaries combining a degenerate with a late (K–M) star than an early (O–G) star since the stars' flux output will occupy largely exclusive spectral regions.

Such searches were performed by Greenstein & Sargent (1974), Lanning (1982), Probst (1983) and, prior to *ROSAT* , $\sim$ 10 spectroscopic binaries of this type (WD + dK–M, with P $<$ 1.5 d) were known.

More recent surveys (Berg *et al.* 1992; Zuckerman & Becklin 1992) have shown that many faint white dwarfs (up to 27%) have low mass MS companions. Most of these systems do not appear to interact, in the sense that the two stars are structurally unaffected by the presence of their companion. Apart from their orbital motions the stars behave as if they were isolated. However, white dwarfs are also present in the type of close, interacting binary systems which have provoked much study in modern astronomy: the cataclysmic binary system.

1.5 Classification of white dwarfs

As white dwarfs were discovered after non-degenerate stars, their classification has tended to follow the stellar classification system. Thus, they have been classified on the basis of the elements visible in their optical spectra.

The classification of degenerate stars as a separate class was begun by Kuiper in 1940. Until recently, the classification used was based on that proposed by Luyten (1952) and Greenstein (1958). Nearly all white dwarf stars appeared upon discovery to have either mono-elemental hydrogen or helium atmospheres (i.e. H and He are the only elements whose absorption lines were visible in the optical spectra). These were termed DA (H lines only), DB (He I lines only) and DO (He II lines, but He I and H allowed). DA stars were found to represent two-thirds of

all degenerate stars. A few stars were found with other elements present, and with elements co-existing (DF, DG, C_2), but degenerates could be broadly divided into two categories; DA and non-DA stars, since very few showed hydrogen co-existing with other elements (only 3 out of 600 stars exhibited both H I and He lines, and a handful showed both H I and Ca II [Greenstein 1979]). Some stars appeared to have no lines in the optical region, these being termed DC (for 'continuous' spectra stars). However, upon examination with superior resolution and/or signal-to-noise, many of these have been reclassified.

Today, the classification is based on the scheme proposed by Sion *et al.* (1983). This is a more satisfactory scheme in that it not only classifies the stars based on spectra, but also takes into account other parameters important in degenerate star structure. The refinement of spectroscopic equipment and observing techniques, plus the opening up of other major portions of the electromagnetic spectrum such as UV and EUV, has revealed more anomalous stars showing trace elements and co-existent elements than known before.

The scheme is as follows (see table 1.1). An uppercase D denotes that the star is degenerate. A second uppercase letter denotes the predominant atmospheric species, and an optional third uppercase letter for a secondary atmospheric species if necessary. Appended to this is a temperature index ranging from 0–9, given by $50\,400/T_{eff}$ where T_{eff} is the effective temperature measured for the star. Further symbols may be assigned for other peculiarities, such as magnetic stars (H), polarised magnetic stars (P), or variable stars (V).

In this scheme, DA stars account for 75% of all known white dwarfs. The helium stars (DO and DB) account for another 10%, as do the DC stars. The remainder are metal-lined, carbon or peculiar type stars.

The visual classifier of spectra may also use other suffixes, such as wk (weak lines), e (emission features), s (sharp lines), or n (wide lines).

White dwarfs, as any other type of star, can be divided into two further categories: those found as isolated objects, and those occurring in binary or multiple

Designation	Old class	Features visible in spectra	Examples
DC	DC	No lines deeper than 5% of continuum	EG 1 (DC6)
DA	DA	HI lines only	EG 157 (DA1)
DB	DB	He I lines only	L 1573-31 (DB3)
DO	DO	He II lines. May have H or He I	HZ21 (DO2?)
DZ	DF/DG	Metal lines only	Ross 640 (DZA7)
DQ	C_2	Atomic or molecular Carbon	L 879-14 (DQ6)
DX		Unclassifiable spectra	GD 229 (DXH3)

Table 1.1: *White dwarf classification scheme, based on Sion et al. (1983).*

star systems. This division is useful, since there is a vast difference in the evolutionary path of a star not only once it becomes a white dwarf but also on its way to becoming a white dwarf, depending on whether it is isolated or part of a multiple system.

This thesis discusses *ROSAT* EUV and X-ray data and optical follow-up data, obtained on white dwarf stars both as isolated objects (chapter 2) and as part of binary systems (chapters 3–5). It contains work covering two types of systems: the normal WD + red-dwarf binaries, and interacting WD + red-dwarf binaries. That is, binary systems where the gravitation and/or radiative energy from one star (usually the white dwarf) can be seen to have an effect on the other star. There is apparently no large scale mass transfer taking place in these binary systems, which is a characteristic of the class of interacting binaries called cataclysmic binaries (CB, also called cataclysmic variables). These CB exhibit many effects due to the mass transfer from a normal star onto the degenerate companion and the possible presence of an accretion disc around the white dwarf. However, that is not to say that the systems discussed in this thesis have never undergone mass-transfer

phases. Indeed, these phases may be quite common in the evolutionary history of many of the WD + MS binary systems currently known.

1.6 Formation of a white dwarf: in theory

There are many sources which give detailed accounts of the theoretical and observational evidence for the formation mechansims of white dwarf stars. I present here a condensed overview of the currently accepted formation routes. For more thorough treatments (and the source of much of the information in the following overview) see Iben 1991, 1985; Bowers & Deeming 1984; Weidemann 1990; Sion 1986; de Kool & Ritter 1993; Smith & Jacobs 1973; Vassiliadis & Wood 1993; Jaschek & Jaschek 1987.

1.6.1 An isolated star

A white dwarf is one possible endpoint of stellar evolution. However, there is more than one way to form a white dwarf assuming a MS star as the progenitor. For an isolated MS (hydrogen-burning) star, the situation is straightforward. When its central fuel source is diminished to a low level, the core (and initially also the envelope) will slowly begin to contract due to the loss of the (fusion-generated) radiation pressure which normally counterbalances the gravitational attraction. Eventually, all the hydrogen in the core is exhausted. Owing to gravitational attraction, material just around the core is pulled inwards and a hydrogen-burning shell forms around the now helium-rich core, gradually increasing its mass. The core initially has a steep enough pressure gradient to support most of the weight above it, so contraction is slow until the mass of the core exceeds the Schönberg-Chandrasekhar limit ($0.12\,M_{\odot}$; Bowers & Deeming 1984). As more mass is added the core becomes denser and gravitational pressure further exceeds the gas pressure. Now the core contracts more rapidly. Energy production in the shell is accelerated by the increase of material falling into the fusion zone, and the envelope is thus

forced to expand outwards, cooling as it does so. This expansion causes a deep convective layer to develop in the stellar envelope, increasing the effectivity of the energy transport, thus halting the cooling. This is the red-giant phase. The core will continue to heat up as it becomes denser. A brief ignition of core helium-burning (via the triple-α process) occurs, but soon extinguishes and the star cools once more (Iben 1991). The next stages depend critically on the mass of the progenitor star.

Eventually, the core temperature will be forced high enough to re-ignite helium fusion. If the star is of low mass ($<2.3\,M_{\odot}$), the core will become electron-degenerate before this ignition. The efficient electron superconduction in the degenerate core effectively holds the core at a much lower temperature than that of a high-mass star whose core is not degenerate. At the point of helium ignition, the core of a star above $2.3\,M_{\odot}$ will comprise approximately one-tenth the total stellar mass, whereas the core of a low mass stars must grow to 0.4–$0.5\,M_{\odot}$ before ignition. Helium burning in a degenerate core is violent and initially generates energy faster than it can be conducted outwards. This is termed the 'helium core flash'. Degeneracy is lifted and the helium burning continues quiescently, as is the case for helium burning in a higher mass star from the point of ignition. The envelope once again heats up significantly as the core helium burning dominates over the shell hydrogen burning. The outer atmosphere of the star may become unstable with the introduction of two energy generation processes, leading to the formation of variable ionisation zones of hydrogen and helium. The star may appear as one of the variable class of stars such as a Cepheid if it is a higher mass star ($>2.3\,M_{\odot}$) or RR Lyrae if it is a lower mass star ($\sim 1\,M_{\odot}$).

When the helium in the core is exhausted, the now carbon-oxygen rich core contracts, becoming highly degenerate. This time a helium burning shell is formed around the core. The star's envelope may again expand, placing the star on the asymptotic giant branch (AGB) of the Hertzsprung-Russell diagram, as a super-giant star. For a star of mass $<8\,M_{\odot}$, the core will not heat up enough to ignite

carbon fusion; the electron conductivity and neutrino losses efficiently diffuse all the energy (released by gravitational collapse and the influx of material from the shell-burning). As before, the contraction of the core accelerates the shell burning and the extra energy generation causes the outer envelope to expand and cool extremely rapidly. Mass is often lost due to a 'wind' emanating from the stellar surface, approximately quantified by the Reimers equation: $M_{\odot}\ \mathrm{yr}^{-1} = 10^{-13} L_{\star} R_{\star} M_{\star}^{-1}$ (with $L_{\star}$, $R_{\star}$ and $M_{\star}$ in Solar units). The dominant fusion process alternates between the hydrogen-burning and helium-burning shells, leading to eventual thermonuclear runaway in the helium shell. This thermal pulse process (Weigert 1966) occurs up to ten times during this evolutionary phase (the star may become a Long Period Variable—LPV). The envelope expansion becomes so violent that the entire outer atmosphere separates from the core in a radiatively-driven 'superwind' (Vassiliadis & Wood 1993). The initial stages of this heavy mass loss may be the cause of the IRAS (OH/IR) sources (Weidemann 1990) and later on some Wolf-Rayet stars (Sion 1993). This superwind terminates the AGB evolution of the central star (now essentially the giant core surrounded by a thin hydrogen shell) which continues to contract. The material thrown off becomes a planetary nebula (PN) when it is photoionised by radiation from the heating pre-white dwarf star (>30 000 K), now called the planetary nebula nucleus (PNN). The PNN continues to contract until the pressure becomes so great that the matter is forced into a degenerate state. The resultant star is a conventional white dwarf, with no significant core fusion processes remaining. However, the white dwarf does not necessarily only radiate away the thermal energy from the non-degenerate ions as is usually assumed. There may still be significant shell hydrogen-fusion (Iben 1985) contributing up to 50% of the total luminosity.

There is one final possible variation. Depending on the mass of the helium-rich zone (below the hydrogen-burning shell) when the star leaves the AGB, it may undergo one final helium shell flash either during or after the phase of significant hydrogen shell-burning (e.g., V605 Aql = Abell 58; Bond 1993) becoming a tem-

porarily 'born-again' red giant. This may occur in up to 25% of all PNN. The important result is that the remaining vestiges of the hydrogen envelope may be almost completely stripped away. In fact, whether this envelope is ejected or not may lead to the formation of some of the different classes of white dwarf star: 'thick' or 'thin' hydrogen envelopes retained on the core may alter the stellar appearance between DA and non-DA (by affecting whether He and metals are visible at the surface). The masses of the various types of white dwarf star are very similar since there is little mass contained even in the 'thick' envelope. However, it would be over-simplistic to suggest this is the only reason for the divergence into different types of white dwarf star. At most it is only a part of the story, since several ensuing processes are efficient at altering the visible stellar surface composition and structure.

Examples of degenerate stars which may have evolved via these two different routes include PG 0108+101, a hot DO (Reynolds 1987), and PG 0950+139, a hot DA still losing mass (Liebert *et al.* 1989). Both stars are still embedded in faint PN.

For a somewhat less massive isolated star ($\sim 0.45\,M_{\odot}$), the core helium-burning may never become dominant due to insufficient central temperatures. In this case, the star may contract to become a white dwarf without ejecting significant portions of its outer envelope. However, stars below $1\,M_{\odot}$ will not yet have evolved off the MS, and thus cannot constitute any of the degenerate stars we see today. In the distant future, these stars may evolve into a significantly different class of degenerate star than those we see today (if mass is not lost in the form of a wind after the white dwarf stage is reached [Liebert *et al.* 1989]).

1.6.2 A binary star

More massive stars (up to $\sim 10\,M_{\odot}$) may also become white dwarfs, but only if they are part of a binary system. Isolated massive stars will ignite carbon fusion in a non-degenerate C–O core, with the higher temperatures produced under contrac-

tion. Many heavy elements will be produced in these nuclear reactions, forming a central portion of the core rich in heavy nuclei, such as ^{56}Fe. When the carbon is in turn exhausted, this central core contraction is extremely violent. The imploding core emanates a shock wave strong enough to blow away the entire mantle, driven by neutrino energy deposition (Wilson 1980, 1983) and the outer core 'bouncing' when nucleon pressure becomes important (Bowers & Deeming 1984). This energy deposition simultaneously causes the photo-disintegration of the mantle and heats up the envelope sufficiently to synthesize post-iron peak elements. These phenomena are what we observe as a type II supernova explosion. The inner core continues collapsing, yet the available degeneracy pressure is only a finite quantity: if the mass of the core is greater than the Chandrasekhar limit ($1.4\,M_{\odot}$), the gravitational attraction will overcome the degeneracy pressure and the star will collapse further. The core will become a neutron star, in which most of the protons and electrons are forced to combine into neutron rich matter. The core contraction may halt here, supported by the nucleonic degeneracy. Cores which are more massive than the Tolman-Oppenheimer-Volkoff limit ($\sim 2\,M_{\odot}$; Bowers & Deeming 1984) may undergo further gravitational collapse and form a black hole (Woosley & Weaver 1986).

Thus only stars whose core mass remains below this $1.4\,M_{\odot}$ threshold can end up as white dwarfs (not proceed to form neutron stars or black holes). A star does not have to be below this mass threshold as a hydrogen-burning MS star, as long as there is a mass-loss mechanism which can drop it below this threshold. This is where the binarity of a star comes in: there is a mass-loss mechanism that may allow initially massive stars to become white dwarfs.

The more massive star in a binary system will evolve off the MS before its companion. It will essentially follow the path described in § 1.6.1, as its core contracts and its envelope expands outwards. It may fill its Roche lobe[2] while

[2] The Roche lobe of a star is its equipotential zero-gravitational surface (Roche 1849a, 1849b, 1851, 1873; Kopal 1978).

the envelope has a deep convective layer. After this point, events depart from those followed by an isolated star. The matter overflowing the Roche lobe will create dynamically unstable mass transfer between the primary and its companion (Paczyński 1976; Webbink 1979; Law & Ritter 1983) creating a common-envelope (CE) around the two stars. This is termed a 'mode III' mass-transfer event in the notation of de Kool & Ritter (1993). The stars will lose angular momentum inside the CE due to friction, magnetic braking (Eggleton 1976; Spruit & Ritter 1983) and gravitational radiation (Rappaport, Joss & Webbink 1982). The stars thus spiral in towards each other. Eventually, so much angular momentum is transferred into the envelope that it breaks up. The whole envelope is ejected. This rapid mass-loss from the primary terminates its evolution early, preventing a climb up the AGB as for isolated stars; rather, these objects evolve directly from the Horizontal Branch (HB) and Extended Horizontal Branch (E-HB), and hydrogen shell-fusion is extinguished early (Wood, Zhang & Robinson 1993).

If the mass transfer occurs before the donor star has ignited helium in its core, it may uncover layers previously within a large convective core during the MS phase. This material has experienced significant hydrogen burning, and its exposure truncates the mass-loss before all of the envelope is lost. The star continues to contract, however, and subsequently burns helium in the core, then later in a shell, after a second brief phase of Roche-lobe overflow driven mass-loss.

In either case, the material thrown off from the primary becomes a PN, and the system is observed as a double-cored planetary nebula (DCPN).

The pre-white dwarf primary appears as a subdwarf (sd) star on the H-R diagram (midway between the MS and the white dwarf cooling track). These subdwarf stars exhibit lines of He II and ionised metals, which are the visible effects of the exposure of the processed material. As before, the larger the mass of the primary, the smaller is the ratio of hydrogen to helium at the surface after mass-loss terminates. Thus a massive core He-burning remnant may appear as a sdO star (or possibly PG 1159 or WC/O Wolf-Rayet star depending upon the time-scale and

surface hydrogen content), whereas a less massive example ($<0.50\,M_{\odot}$; Caloi 1989) appears as an sdOB star, or sdB star. This hydrogen layer gradually diminishes in mass due to either nuclear burning at its base or a wind loss mechanism. High-mass systems will thus become WD + MS binaries before the dispersal of the PN. Lower mass subdwarf stars will take longer to reach the stage of white dwarf, and thus appear as sd + MS stars devoid of a planetary nebula shell for some time before evolving into a WD + MS binary. Some very low mass progenitors may not even become classifiable as subdwarf stars until after the PN has dispersed (Iben & Tutukov 1986a), and if the contracting star has not become hot enough to photoionise the PN by this time, the PN may never be observed.

It may be that, due to the increased mass loss possible in binary systems, all high surface-density planetary nebulae are formed in binaries. Isolated stars produce much fainter nebulae due to the reduced mass of the ejecta shell.

It is possible for the massive star in a binary system to evolve into a white dwarf without a CE stage if the primary has a radiative envelope when it initiated mass transfer. The mass-transfer will then be conservative rather than unstable (a 'mode II' mass-transfer event). The evolution of this star will be similar to an isolated star with an added mass-loss mechanism. It should lead to a binary of larger separation/period than the CE type, since there will be less orbital angular momentum loss. Such a system is thus a good candidate for the formation of a double degenerate system, since the two stars may be prevented from merging at this stage. There will be a CE stage when the secondary evolves off the MS, and if the two again avoid coalescence will emerge as a binary degenerate system. If the two stars do merge, they may form a subdwarf or R CrB star. That white dwarf and PN birth rates agree (Weidemann 1977) would suggest that nearly all stars do pass through a PN stage in forming a white dwarf. However, there is some evidence that PN can be formed via other mechanisms and that not all white dwarf pre-cursors produce appreciable PN (see Iben 1991).

Figure 1.1 illustrates the various routes to a white dwarf for stars in binary

systems. In the notation of de Kool & Ritter (1993), a 'mode III' mass-transfer event is one in which the primary has a convective envelope when it fills its Roche lobe. This leads to dynamically unstable mass-transfer and a CE phase. A 'mode II' mass-transfer event occurs if the primary fills its Roche lobe when it has a radiative envelope. In this case, mass-transfer is considered to be conservative and no CE phase follows.

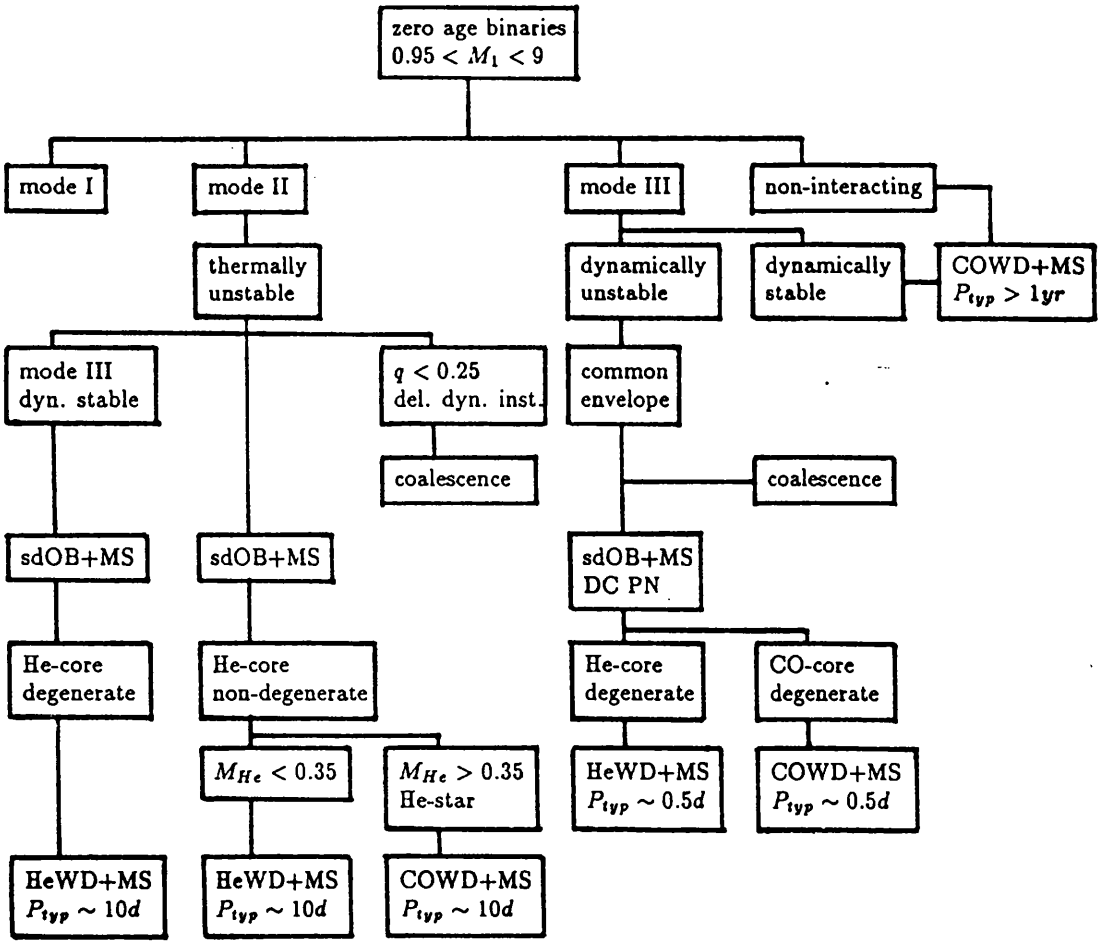

Figure 1.1: *Schematic illustration of various evolutionary routes to and during the white dwarf stage. Taken from de Kool & Ritter (1993).*

1.7 Evolutionary considerations

We can ascribe an upper mass-limit of $\sim 10\,M_{\odot}$ to the stars in binary systems able to evolve into white dwarfs. Above this mass they will almost certainly form neutron stars (or black holes) irrespective of which mass loss mechanism is in operation. Isolated stars cannot lose as much mass as those in a binary system, thus the progenitor must be initially somewhat less massive ($<7\,M_{\odot}$).

There is also in practice a lower mass-limit, since stars below a certain mass will not have had enough time in which to evolve off the MS since the Galaxy was formed. In theory, any star which contains enough matter ($\sim 0.05\,M_{\odot}$) in order for the core to heat to fusion temperatures will eventually provide enough pressure to force the matter into degeneracy, when the star does evolve. The practical lower limit for stars to have formed into white dwarfs within the lifetime of the Galaxy is $\sim 1\,M_{\odot}$ (de Kool & Ritter 1992). The formation method of the white dwarf may also be constrained by observations, since isolated evolution within the lifetime of the Galaxy could not account for enough mass loss to produce degenerates with final mass below $0.5\,M_{\odot}$ (the He core limit). In a study performed by de Kool & Ritter (1992) the number of binary systems formed which contain white dwarfs and subdwarf stars are calculated. They estimate that 10% of all zero-age binaries will undergo and survive a CE phase, whereas about 50% are too wide to interact at all. This agrees with observational studies, such as that of Bergeron, Saffer & Liebert (1992), who deduce that 10% of DA stars are the product of close binary evolution, from a low-mass tail to the observed mass distribution of DA degenerates. Bergeron, Saffer & Liebert also conclude that the appearance of some high-mass degenerates is due to the coalescence of double degenerate systems.

Figures 1.2 and 1.3 illustrate the mass and interior composition of a white dwarf as a function of the progenitor mass and mass-loss mechanisms operating. In the notation of Kippenhahn & Weigert (1967), a 'case B' mass-transfer event is one where the primary fills its Roche lobe after the exhaustion of core hydrogen but before the ignition of helium. A 'case C' mass-transfer event occurs after a

degenerate core has developed.

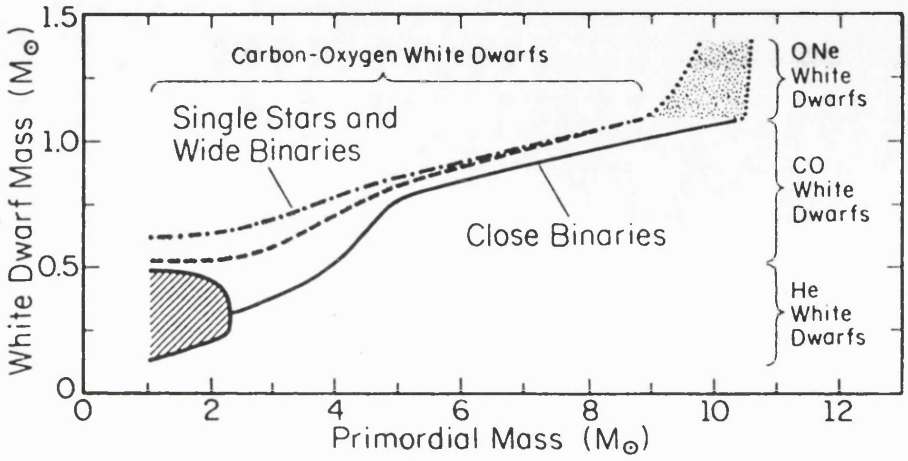

Figure 1.2: *Mass and interior composition of a white dwarf as a function of the progenitor mass, for single stars and binary components after a case B mass-transfer event. A case C event (in an initially wide binary) will result in a remnant of similar mass to that produced by an isolated progenitor. Taken from Iben (1991)*

Accurate assessments of the fractions of white dwarfs evolving through each of the above channels is not yet possible. It is estimated that roughly one third form via each of the the post-AGB, binary, and non-PN channels, with little contribution via direct evolution from the HB or E-HB (Weidemann 1990). The channel followed by an individual star depends both on its initial mass and binarity, but also on many, as yet poorly understood, factors. Which type of white dwarf is formed by each mechanism is also a matter of controversy; many people believe all white dwarfs are initially DO, and later evolve into DA, given the absence of very hot DA stars in the PN stage. However Napiwotzki & Schönberner (1993) report the recent discovery of many very hot DAO stars embedded in PN, and argue that there is thus a distinct feeder channel rather than a temperature evolutionary sequence.

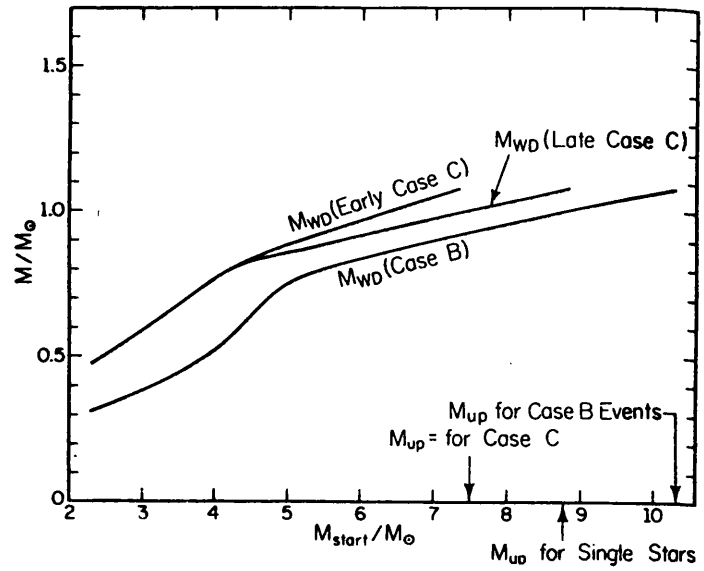

Figure 1.3: *Mass of a white dwarf as a function of the progenitor mass and mass-loss scenario. M_{up} is the progenitor mass upper limit. This assumes a Population I progenitor. Taken from Iben (1991)*

1.8 Why study white dwarfs?

The study of degenerate stars is important because it can in principle be used to reconstruct the entire history of star formation in the Galactic disc. To do this both the luminosity function and the mass distribution of degenerate stars need to be determined precisely, and we need to understand the relationship between the initial mass and final mass of a star. In fact, theoretical relationships between progenitor mass and white dwarf mass have been calculated, which are in agreement with the observed mass distribution functions (e.g., Mazzitelli 1989).

Accurate measurement of the effective temperatures for DA stars is a crucial factor for many areas of investigation. Temperatures are used to derive the luminosity function of the DA stars. This will in turn provide information on their cooling rate. It is important to determine the upper temperature limit for DA stars (assumed to lie at $\sim 65\,000$ K) since this constrains the post MS evolution mod-

els. The mass distribution is also an important physical parameter. The width of this distribution puts constraints on the theories of stellar formation in the Solar neighbourhood (Fusi-Pecci & Renzini 1976), so accurate determinations are vital.

1.9 Physical parameters

1.9.1 Effective temperatures, radii and masses

Fleming, Liebert & Green (1986) find that DA degenerates account for 21% of faint blue stars (identified from the Palomar-Green survey) to a limiting magnitude of $B = 16.1$. Field white dwarfs have temperatures ranging up to 150 000 K (the hotter of which are non-DA). White dwarf radii are clustered narrowly around a mean of $0.0127\,R_{\odot}$ (Shipman 1979). With a Hamada-Salpeter mass-radius relation (Hamada & Salpeter 1961) this implies a mean mass of $0.55\,M_{\odot}$, and a mean surface gravity of $\log(g) = 8.0$. The typical mass of white dwarfs in CB was long thought to be somewhat larger, $\sim 1\,M_{\odot}$ (Robinson 1976). This has now been shown to be almost entirely a selection effect (Ritter & Burkert 1986); the true average mass of the degenerates in CB is $0.62\,M_{\odot}$.

In calculating the luminosity function of their sample, Fleming, Liebert & Green note a problem with the hottest stars (>70 000 K) which are very young and still contracting to their final radii (Koester & Schönberner 1986). They arrive at a figure of ~ 0.5 white dwarfs per $1000\,\mathrm{pc}^3$, for $M_V < 12.75$. These authors find no evidence for any DA stars with T_{eff} >100 000 K or $\log(g) < 7.0$.

Bergeron, Saffer & Liebert (1992) derive a mean DA mass of $0.56\,M_{\odot}$ ($\log(g) = 7.9$). They find that 75% of DA stars lie within only $\pm 0.1\,M_{\odot}$ of the mode of the sample, which lies at 0.50–0.55 $M_{\odot}$. The mass distribution appears remarkably symmetric, unlike that suggested by earlier determinations (e.g. McMahan 1989). There is a sloping tail-off from the low-mass end (0.4–0.45 $M_{\odot}$) due to binary star evolution, and a sloping tail-off towards high masses (1 $M_{\odot}$), which results by convolving the white dwarf production mechanism with the initial galactic mass func-

tion (Weidemann & Koester 1983, 1984), plus the merger products of binary star evolution. These data support a single cooling evolutionary sequence for DA stars rather than a two-sequence model. The extremely narrow mass-distribution supports the galactic evolution and mass-loss theories of Fusi-Pecci & Renzini (1976) and Weidemann & Koester (1983). The data also requires a narrow mass distribution in the extragalactic PNN formation; PNN do appear to have such a narrow mass-distribution, centred about $0.58\,M_{\odot}$ (Schönberner 1983) and mostly contained within $\pm 0.03\,M_{\odot}$. This may mean that over half of white dwarfs develop with insignificant (low surface brightness) nebulae.

1.9.2 Magnetic fields

The highest stellar magnetic fields measured are found to occur in degenerate stars, as evidenced by the Zeeman splitting of absorption lines. Neutron stars may exhibit field strengths of up to 10^{12} G, wheares white dwarfs have field strengths roughly a million times less intense. For example, the Hβ line in the spectrum of GD90 implies a field strength of 5×10^6 G (Angel *et al.* 1974) and fields of up to 50×10^6 G have been found in some polars (a class of highly magnetised, accreting white dwarfs, which emit polarised radiation; see Cropper 1990). However, it appears that large magnetic fields are not particularly common among white dwarf stars, since most spectra show no Zeeman splitting of line components.

1.9.3 Rotational velocities

White dwarfs stars show a remarkably low average rotational velocity of $\sim 27\,\mathrm{km\,s^{-1}}$ (Trimble & Greenstein 1972; Pilachowski & Milkey 1984), implying that they have lost most of their angular momentum during earlier evolutionary stages. This fits in with the expulsion of the atmosphere explained in § 1.6.2, as there is postulated to be an exchange of momentum between the core and envelope (Greenstein *et al.* 1977). It would also appear that magnetic degenerates are in general slower rotators than non-magnetic degenerates, which is presumably evidence for a magnetic

braking mechanism.

It should be noted that there is not enough matter contained in the cooled-down degenerate component of the stellar population to affect the Oort limit deficit (dark matter/missing mass), unless the formation rate was much higher in the past or most degenerates cannot be observed (Fleming, Liebert & Green 1986).

Iben (1984) postulated that the difference between DA and non-DA stars is of primordial origin (i.e. before the object becomes degenerate) and depends only upon the thickness of the H-layer left over when the star undergoes its final thermal pulse. This scenario predicts little difference in the masses and kinematics of the two types of stars, which is indeed what is observed. Furthermore, it may also account for the fraction (25%) of non-DA stars. However, it cannot be the full solution: at the hottest temperature ranges ($> 80\,000$ K), DO stars outnumber the DA stars (Wesemael, Green & Liebert 1985). Between 45 000–30 000 K this situation is reversed, with many more DA stars, but no DB star is known (Sion 1984). Below this temperature He stars reappear, and by very cool temperatures (< 6000 K) they dominate over the H-rich DA stars once more (Sion 1984). These data indicate that there is at least some evolutionary change in the structure of degenerate stars.

1.10 Cataclysmic and pre-cataclysmic binaries

Cataclysmic binaries (CB) are historically those binary systems which were found to exhibit sudden brightening events. In general, they comprise a late-type star near the MS (usually the less massive of the two) which fills its Roche lobe and which is transferring matter via the inner Lagrangian point onto a more massive white dwarf. In many systems the transferred material accretes onto the white dwarf via a disc, a bright spot forming where the stream of matter impacts the disc. The secondary star is tidally distorted by the white dwarf's gravitational field. CB emit copious amounts of X-rays, EUV, UV and optical radiation, most of

which arises from the disc and bright spot. In a few cases, the secondaries may not be a near-MS star; they may be a giant star (e.g. T CrB), a subgiant (e.g. V1341 Cyg), an H degenerate (possibly WZ Sge?) or an He degenerate (possibly AM CVn?). If the degenerate star is highly magnetised (polars) then accretion may be via a magnetically channelled flow rather than an accretion disc. Low mass X-ray binaries (LMXB) are similar to CB in many respects, but have a neutron star primary instead of a white dwarf.

While it is not the intent of this introduction to provide a complete insight into the various classes of CB, I will briefly outline the types and their makeup, as they are closely related to the white dwarf systems studied in this thesis: they are the evolutionary descendants of PCB and the type of CB formed depends upon the parameters of the ancestor PCB.

Cataclysmic binaries are classified into four categories based on their optical light variations: novae, recurrent novae, dwarf novae (subclasses U Gem, Z Cam and SU UMa) and nova-like variables (subclasses UX UMa, VY Scu, DQ Her or 'intermediate polars', AM Her or 'polars' and AM CVn). The cause of outbursts in novae may be a thermonuclear runaway in a degenerate, accreted, hydrogen shell around the white dwarf. Dwarf novae suffer outbursts caused by a brightening of the accretion disc, which is due to a disc instability or temporary increase in the accretion rate onto the white dwarf. Comprehensive reviews of the subject may be found in Córdova & Mason (1981), Patterson (1979), Robinson (1976), Webbink *et al.* (1987).

Pre-cataclysmic binaries (PCB) are those systems which are thought to be the progenitors of fully fledged cataclysmic systems (Bond 1985). They do not exhibit the eruptive behaviour of the CB, but are comprised of similar stellar types, and it is thought that they eventually evolve into CB. The systems discussed in chapters 3, 4 and 5 of this thesis include some pre-cataclysmic binary systems. There are three classes of PCB, and they have been described in §1.6: DCPN, close sd + MS, and close WD + MS. These are the only systems considered capable of evolving

into CB, and in a sense they belong to the same category, being related by an evolutionary sequence: DCPN → sd + MS → WD + MS (§1.6).

The early assertion that CB are evolved from contact binaries of the W UMa type (Kraft 1967) was disproven by Webbink (1976) showing that these systems would coalesce before the primary has left the MS. The current view is as follows:

A CB is formed when the late-type star in a PCB overflows its Roche lobe and initiates mass transfer onto the degenerate companion. As mentioned above, there are two ways in which a late-type star might fill its Roche lobe. In the case of the earlier type secondary stars (G–K) the star might evolve off the MS, (i.e. it physically expands to overflow its Roche lobe). However, a later (M-type) star cannot have evolved off the MS within the current age of the Galactic disc. The only other possibility is that some mechanism must have drained angular momentum from the system causing the two companions to spiral in until they are close enough for the secondary star to fill its Roche lobe under the influencing gravitational field of the degenerate star (i.e. the Roche lobe contracts to meet the stellar surface).

It is thought that the binary systems which evolve into the PCB must have an initial period ranging from months to years. The secondaries should all be lower MS stars. In the evolutionary sequence (described in § 1.6.2) for the formation of a white dwarf in a binary system, if the stars are too close together (P < months), they may merge to form a single star. If they are very far apart (P > years), they may emerge from the CE phase still too wide to form a CB. With initial periods in the range months to years they should emerge as close binaries (Eggleton 1976; Paczyński 1976; Ritter 1976; Livio 1982). Their orbital periods should be < 2 days in order for the CB to form via orbital decay rather than secondary evolution. As for the masses of the resultant stars, if the primary is above $\sim 10\,M_{\odot}$, the system may become a neutron star binary. These may progress to form LMXB as a consequence of angular momentum loss.

1.10.1 Close binary remnants of CE evolution

The parameters of several short-period remnants of binary evolution (thought to have formed via orbital decay) are summarised in table 1.10.1.

There are two principle mechanisms thought to be responsible for the angular momentum loss: gravitational radiation and magnetic braking (during the CE phase or in a stellar wind from the secondary). CB should thus be the short period tail of a whole distribution of WD + MS binaries, many of which are left too far apart for significant angular momentum loss (and whose companions are not massive enough to evolve off the MS) within the current lifetime of the Galactic disc. Bond (1985) calculated the likely rate of loss of angular momentum/period change of two typical PCB due solely to gravitational radiation, based upon the equations of Kraft, Mathews & Greenstein (1962). He concludes that systems with periods over 10 h cannot evolve to CB in less than the age of the Galactic disc if gravitational radiation is the only momentum sink. There is, however, evidence for another angular momentum sink: both UU Sge and V471 Tau were detected as soft X-ray sources by van Buren, Charles & Mason (1980) who attribute the activity to coronal emission from a late type star forced into rapid rotation by tidal synchronism. There is also evidence for chromospheric activity and stellar winds in some PCB e.g., V471 Tau and Feige 24. These winds should lead to magnetic braking, and when this is included into the momentum-loss equations (Verbunt & Zwaan 1981; Patterson 1983) it is estimated that PCB with periods of up to 1.5 d may have evolved into CB via angular-momemtum loss.

1.10.2 Long period remnants of CE evolution

Many systems with periods longer than 1.5 d are also known. They will not become CB via orbital decay, but may do so via evolution of the secondary (if it is massive enough). In fact several systems already show evidence for evolution of the secondary (FF Aqr, 39 Cet, HD 128220). A long-period nova similar to GK Per (Crampton, Cowley & Fisher 1986) may well form from a system such as HD 49798.

Name	Components	M_s/M_p $M_\odot$	T_p 10^3 K	P_{orb} d^{-1}	Ref.
(i) *DCPN*					
MT Ser	sdO + MS	0.6?	?	0.11	17, 18
KV Vel	sdO + MS	0.55/0.25	?	0.36	17, 18
UU Sge = Abell 63	sdO + dK	0.7/0.5	?	0.46	1
V477 Lyr = Abell 46	sd + dK-M	?	?	0.47	2
V664 Cas	?	?	?	0.58	17, 18
VW Pyx	neu? + MS	?	?	0.67	3
Abell 65	?	?	?	1.00	17, 18
(ii) *sd + MS*					
Abell 41	sdO + dM	?	?	0.11	4
HW Vir	sdB + MS	0.25/0.12	33	0.12	12
Feige 36	sdB + sd/MS	0.5?	30	0.21	15
AA Dor = LB 3459	sdO + MS	0.25/0.04	?	0.26	5
HZ 22 = UX CVn	sdB + MS/D?	0.39/0.42	28	0.57	6
(iii) *WD + MS*					
NN Ser	DA + dM5	0.54/0.12	60	0.13	16
RE2013+400	DAO + dMe	?	50	0.15?	11
PG0308+096	DA4 + dM2	?		0.29	17, 18
RR Cae	DAwk + dMe	?	?	0.30	17, 18
GK Vir	DAO + dM3	0.7/0.4	50	0.34	7
V471 Tau	DA2 + dK2e	0.71/0.73	33	0.52	8
HZ 9	DA2 + dM4.5e	0.51/0.28	22	0.56	9
PG1026+002	DA + dM2	?	?	0.60	17, 18
Case 1 = EG UMa	DA + dM4.5e	0.38/0.26	13	0.67	10
RE1016−053	DAO + dM2e	0.57	56	<	13
PG 0824+289	DA + dC	?	40	<	14

Table 1.2: *Detached binaries with $P < 1.5\,d$ (PCB). M_p and T_p are the mass and surface temperature of the primary. P_{orb} is the systemic orbital period.*
References: 1, Bond 1976; 2, Grauer & Bond 1981; 3, Kohoutek 1964; 4, Grauer & Bond 1983; 5, Kilkenny, Hilditch & Penfold 1978; 6, Young, Nelson & Mielbrecht 1972; 7, Green, Richstone & Schmidt 1978; Fulbright et al. 1993; 8, Nelson & Young 1970; 9, Lanning & Pesch 1981; Stauffer 1987; 10, Stephenson 1971; Stauffer 1987; 11, Barstow et al. 1993a; 12, Wood, Zhang & Robinson; 13, Jomaron et al. 1993; Tweedy et al. 1993; 14, Jordan & Heber 1993; 15, Reid, Saffer & Liebert; 16, Wood & Marsh 1991; 17, de Kool & Ritter 1992; 18, Ritter 1990;

A recurrent nova may eventually form from a system such as HD 128220 (Bond 1985).

System	Components	P_{orb} d	Reference
HD 49798	sdO + dF-K	1.55	Kudritzki & Simon 1978
BE UMa	DO1 + dM2e	2.29	Ferguson *et al.* 1981, 1987
Feige 24	DA1wk + dM1e	4.23	Vennes *et al.* 1991
NGC 1360	DCPN sdO + ?	8.2	Mendez & Niemela 1977
FF Aqr	sdO + G8 III	9.2	Dorren 1982
NGC 4326	DCPN ? + dA3	16	Mendez & Niemela 1981
39 Ceti	DA + G5 III	77	Simon *et al.* 1983
HD 128220	sdO + G0 III	870	Wallerstein & Wolff 1966

Table 1.3: *Example detached binaries with $P > 1.5\,d$*

It is clear that many systems can emerge from a PN with periods much longer than those of the typical CB. Thus not all will end up as CB (for instance none of those with M star secondaries).

Still more WD/sd + MS systems are known of the type where the stars must have evolved essentially independently due to a very large separation, for example HR 3080, Zeta Cap, 56 Peg. There are also many other systems where no period information is available. These stars may or may not be close binary remnants of CE evolution (see Bond 1985).

Essentially, from the observations we can conclude that most CE evolution will result in wide binaries destined not to become CB (e.g., Bond 1985), a conclusion confirmed in theoretical studies such as that of de Kool & Ritter 1992.

It is possible that CB may also be formed by stellar capture, say in dense stellar regions like globular clusters (Lightman & Grindlay 1982). It is unlikely

that this method is important in the Galactic disc. LMXB may be formed if the degenerate star in a CB is driven over the Chandrasekhar limit by continuous accretion (Labay *et al.* 1983).

1.11 Evolution from a PCB to a CB

If a close WD + MS binary does have the right parameters to be considered a PCB, and then undergoes mass transfer, what type of CB will it form? If the mass transfer rate is low, the accretion disc outer edges will be cool and the disc accretion will be unstable. This may lead to dwarf novae or X-ray transients (Smak 1971; Hoshi 1979, 1981, 1982; Cannizzo, Wheeler & Ghosh 1982). High mass transfer rates lead to stable accretion and the nova-like CB systems. Intermediate rates may lead to a stable or unstable disc, and the CB may look like Z Camelopardalis.

High accretion rates onto the degenerate star may lead to build up of an envelope if the nuclear processing is not fast enough. Thus the system may become a contact or CE system. Lower accretion rates mean the burning is unstable, giving rise to nova explosions (Fujimoto 1982).

Eventually, the accretion may cease if the secondary is depleted sufficiently to fall within its Roche lobe, or the two stars coalesce due to excessive angular momentum loss. Another possible end-state is that the degenerate star is pushed over the Chandrasekhar limit, inducing degenerate helium or carbon ignition; the most likely situation to give rise to a type I supernova explosion (Mazurek 1973; Greggio & Renzini 1983).

Figure 1.4 illustrates the positions of interacting binary systems in the H-R diagram.

There are several problems with this evolutionary scenario. One of the most important is the missing 'evolved' binaries with mass ratio close to unity. Most of the systems which formed the known CB must have had an initial mass ratio very different from unity, as the degenerate star is usually observed to be the

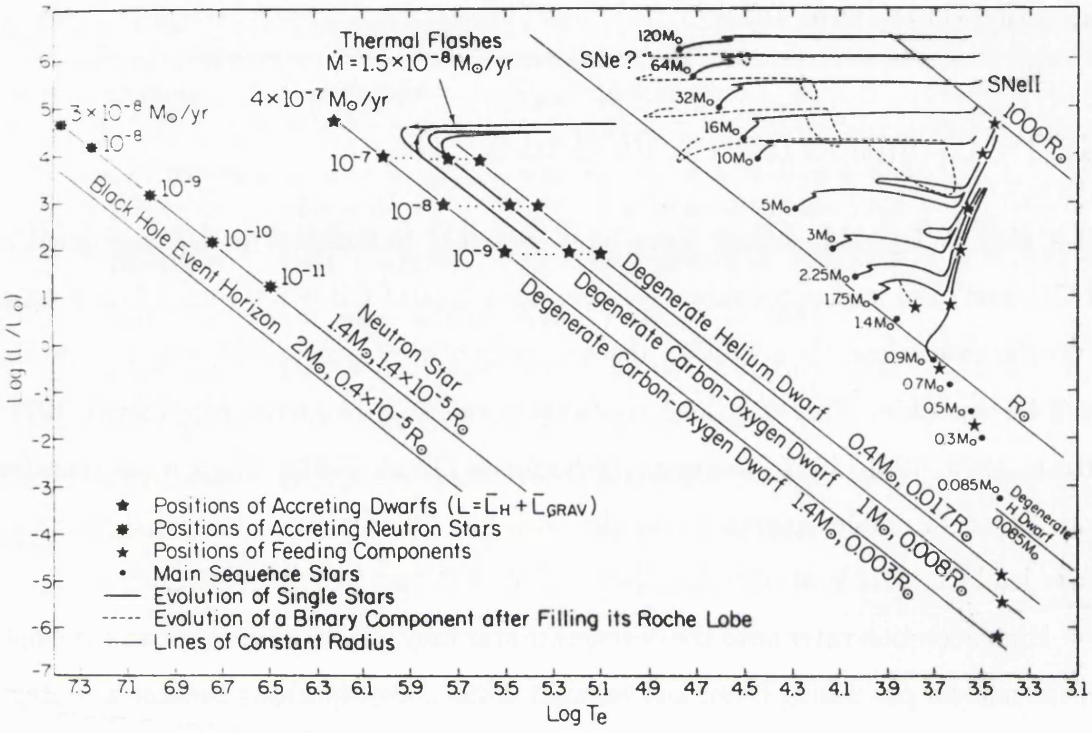

Figure 1.4: *Positions of interacting binary systems in the H-R diagram. From Iben & Tutakov (1984).*

more massive and must have been even more so before the CE phase. However, Lucy & Ricco (1979) show that MS binaries with mass ratio of unity are common. As these systems evolve, the first mass-transfer stage may not be violent as both stars are of equivalent mass. Thus a CE phase is unlikely. The star to evolve first will become a degenerate and the secondary will shortly also evolve to red giant. This system may be observed as a symbiotic star (Paczyński & Rudak 1980). Further evolution leads to violent mass transfer and a CE phase, then later the emergence of a double degenerate system (if the stars do not coalesce

during the CE phase). However, there are extremely few of these systems observed, when in fact they should be more common than CB, if the initial ratio of the two types of system is a guide (e.g., the Algol systems should form this type of binary if the two components avoid coalescence). There should be many double degenerate star, neutron star and possibly black hole systems (Nather, Robinson & Stover 1981), unless some mechanism prevents their formation or a selection effect prevents their discovery. The only system known until recently was the binary radio pulsar PS1913+16 (Taylor & Weisberg 1982). The stars L870−2 (Saffer, Liebert & Olszewski 1988), WD0957−666 (Braggaglia *et al.* 1990), L151−8A/B (Oswalt *et al.* 1988) and HS2240+1234 (Jordan & Heber 1993) seem to be further systems of this type. However, these objects are still not numerous enough. Since the end product of the evolution should be two very low mass degenerate stars in a close orbit, they may show up as a single low mass degenerate in any searches (due to the large apparent surface area of the 'combined' stellar appearance). Thus any degenerate stars with mass $<0.45\,M_{\odot}$ (which is believed to be the limit for formation from an isolated star; Weidemann & Koester 1983) must be candidates for a close double degenerate system formed via binary evolution. The most efficient survey method of finding these systems is to look for high radial velocity variations in the spectra of apparently isolated white dwarfs. These double degenerate systems may eventually form a DB degenerate star (Nather, Robinson & Stover 1981), a He-rich mass-transferring CB (AM CVn), an R CrB star (Paczyński & Trimble 1973) or give rise to a type I supernova (SN). It is postulated that these double degenerate systems may be more efficient at creating type I SN than the regular types of CB (Paczyński 1985). This would alleviate the current problem of necessitating all normal CB having to become type I SN, since the birth rate of normal CB has been found to equal the rate of type I SN (Trimble 1982).

In fact, Bergeron, Saffer & Liebert (1992) do find a low-mass tail to the distribution of white dwarfs, which they attribute to a class of low-mass degenerate stars resulting from close binary evolution. They put the number of dwarfs formed

this way at 10%, in agreement with the theoretical calculations of de Kool (1992).

1.12 White dwarf atmospheres

Böhm & Kapranidis (1980) state that the basic (qualitative) difference between DA and non-DA atmospheric structures can be attributed to (a) the importance of electron scattering in DA stars only (a consequence of the very low absorption coefficient in the EUV), (b) the different surface cooling and backwarming effects in the two types of star (due to the difference in absorption edge frequencies), (c) differences in atmospheric densities due to the different transparence of both types of atmosphere.

The composition and thickness of a degenerate star's surface can have much influence on their evolutionary sequence. The average white dwarf consists of a C–O core overlaid by a thick He-layer of $10^{-2}\,M_{\odot}$, overlaid by a thinner H-layer of mass 10^{-14}–$10^{-4}\,M_{\odot}$ (Winget & Fontaine 1982) depending upon the exact route taken to become a white dwarf.

Initially it was thought that the spectral flux output of a degenerate star would be easier to model than that of a normal non-degenerate star, since its atmosphere was thought to be highly mono-elemental, and the underlying flux emission extremely blackbody-like in nature. In practice, while it is indeed somewhat easier than for non-degenerate stars, and some very good models have been developed (e.g., Wesemael *et al.* 1980; Jordan & Koester 1986), it has recently emerged that there are significant discrepancies at short-wavelengths between observations and the current model predictions.

1.12.1 Physics of white dwarf atmospheres

It has been known for a long time that the time-scale for downwards gravitational diffusion of heavy elements in the high-gravity photosphere of a degenerate star is much shorter than the cooling time for such a star (e.g., Muchmore 1984). In

the absence of any competing mechanisms, the photosphere of a degenerate star should appear mono-elemental; however, recent observations show that many DA stars which exhibit pure H spectra in the optical band have significant opacity in the EUV (Auer & Shipman 1977; Heise & Huizenga 1980; Maline *et al.* 1982; Kahn *et al.* 1984; Paerels & Heise 1989; Barstow *et al.* 1993c). Uniformly mixed helium (in a predominantly hydrogen atmosphere) has been shown to be theoretically implausible at any significant quantities (Vennes *et al.* 1988), thus we can rule this out as the cause of absorption. There are currently two competing theories as to what causes the opacity: the first theory is of a stratified atmosphere. This consists of a layer of essentially pure hydrogen on top of a layer of essentially pure helium (Jordan & Koester 1986; Heise 1986), where the H/He diffusion is in equilibrium, but the H-layer is so thin ($10^{-15}\,M_{\odot}$) that the H/He transition zone will extend into the photosphere, where the stellar continuum is formed. Thus the EUV continuum will be partly formed in the underlying helium-layer, allowing some He features to be visible in the EUV. Since the H opacity is much higher in the optical than in the EUV, however, the optical continuum is effectively formed higher up in the photosphere than the EUV continuum—above the H/He transition region—and will appear as a pure H atmosphere in optical spectra. The alternative theory is that of trace heavy elements in a homogenous atmosphere (such as C, N, O, Si, Na, Fe) radiatively levitated by intercepting the EUV flux. Which of these scenarios (or a combination) is applicable and the mechanism by which it is maintained is the subject of much discussion. This problem is only now beginning to be resolved, with data from *ROSAT* and *EUVE*.

There are several effects which must be considered as competitors with gravitational diffusion in the determination of the atmospheric structure of any white dwarf star. These are convection (Fontaine & van Horne 1976), radiative levitation (Fontaine & Michaud 1979), magnetism, accretion (Alcock & Illarionov 1980), wind-loss (Bruhweiler & Kondo 1983) and meridonial/poloidal currents. All these processes, apart from diffusion, are very sensitive to temperature, thus it is clear

that temperature will be a key factor in determining the chemical abundances in degenerate stars.

Below 15 000 K, DA stars have convective atmospheres. In cooler examples (< 12 000 K), significant helium may be dredged up to the surface via convection, yet remain spectroscopically invisible (in the optical region) due to the low temperature. Moreover, Bergeron *et al.* (1991) show that optical spectroscopy cannot resolve the difference between pressure effects caused by increased helium abundance in the atmosphere and those from an increased surface gravity. Above 15 000 K the DA atmosphere is radiative, which means that gravitational settling dominates the chemical composition, and atmospheres are hydrogen-rich. Radiative levitation is one proposed mechanism for supporting heavy elements in the atmosphere (Chayer *et al.* 1987). In this process, radiative collisions with ions which have EUV resonance transitions near the star's Planck radiation peak provide enough pressure to buoy these elements. However, levitation is not a significant contributor of helium in DA atmospheres (Vennes *et al.* 1988) due to its small cross-section for radiation capture, and convection is not effective for metals when levitation is absent, since the metals sink below the convective layer into the core. Vauclair (1989) and others have shown that significant quantities of C, N and Si can be levitated in DA atmospheres with temperatures >40 000 K. No truly self-consistent models of levitated trace metals in a DA atmosphere have yet been developed (but see Finley *et al.* 1993). If the EUV deficits are caused by flux-blocking, there should be a backwarming effect resulting in FUV flux excesses, which may be searched for in future studies.

In a star with a surface convection zone, it is the diffusion at the base of the zone which affects the surface composition, since the convection is turbulent (Böhm 1979). The diffusion will only separate material in the deeper layers. Furthermore, the relation between the surface temperature and central temperature and the structure of the convection zone are sensitive to the opacity of the material at the stellar surface. Any material which sinks downwards out from the convection zone

will progress downwards more and more slowly (Muchmore 1984). It should be noted that the convection zone can never overtake and dredge up original metals which had fallen out of the convection zone (as proposed by Strittmatter & Wickramasinghe 1971), since the timescale for diffusion at the bottom of the convection zone is always shorter than the cooling age of the star (Muchmore 1984).

The number of degenerate stars that exhibit H lines varies significantly as a function of effective temperature (Fontaine & Wesemael 1987), indicating that the processes competing with diffusion in the atmospheric composition change with the evolutionary cooling of a degenerate star.

Helium in a newly formed degenerate star, composed of both hydrogen and helium, should be depleted from the surface (by diffusion) within mere decades. In hotter stars with no convection, these elements are expected to form stratified atmospheres, with possibly thin H-layers depending on the original H mass. For cooler (<20 000 K) stars with thin H-layers, it is calculated that convective mixing (Koester 1976) will mix the H back into the He until it becomes invisible. Thus layered atmospheres are not possible for these stars, and the atmospheres are essentially homogenous unless acted upon by one of the other selective enhancement mechanisms described above (§ 1.12).

The continuum from a degenerate star is, however, formed deep enough within the atmosphere to give rise to significant differences between the homogenous and layered models. In homogenous models, He features such as the 228 Å He I and He II edges may still be visible when the continuum flux is high shortward of 200 Å. For layered atmospheres, this is not the case. If He features can be seen, then the flux must be low since the continuum is also formed in He-rich layers and suffers from the high He opacity. Thus the EUV emission from degenerate stars provides a crucial test of these atmospheric models.

DA stars may have sharp cores to the Hα and possibly Hβ lines due to a departure from local thermodynamic equilibrium (L.T.E.) in the population of the atomic levels of hydrogen in the upper layers of the atmosphere (i.e. a strong

overpopulation of the $n = 2$ level; Wesemael *et al.* 1980). Other Balmer lines are formed deeper in the atmosphere and thus are unaffected by this anomaly. In fact, Kuzma (1979) calculated that it was possible for Hα to appear in emission in stars cooler than $\sim 10\,000$ K.

1.12.2 Current problems

There are several outstanding problems with the evolutionary model of degenerate stars. There is deficiency of He-rich stars (the hot DO and cooler DB stars) between 30 000 K and 45 000 K (the so-called 'DO–DB gap'; Liebert, Fontaine & Wesemael 1987). Also, as stated previously, the DA stars outnumber the DO stars by a large factor, yet the progenitor PNN have roughly equivalent numbers of H- and He-rich stars. Thus there must be some mechanism to effectively rid many degenerates of helium. This is believed to be gravitational diffusion.

1.12.3 The evolutionary scenario

For a very hot star, with an atmosphere consisting predominantly of helium with trace hydrogen, the diffusion time-scale may be short enough to initially hide the hydrogen so the star appears as a DO (Nather, Robinson & Stover 1981; hereafter NRS). As the star cools, hydrogen floats to the surface, giving the star the characteristics of a DAO (Vennes *et al.* 1988). Over time a thin surface H-layer builds up, eventually reaching $10^{-11}\,M_{\odot}$ by the time the star has cooled to 45 000 K, and the star is classified as a DA. As the star cools further, the onset of convection may mix in some He from the transition zone, making the star a DAB/DBA (Shipman *et al.* 1986). Enough may have been mixed in by the time T_{eff} is down to 30 000 K to convert the temporary DA star into a DB. Finally, when the star cools to a level such that no H or He line transitions are apparent, it appears as a DZ, DQ or DC. A possible example of this sequence is GD323 (Liebert, Fontaine & Wesemael 1987). The DO–DB gap may then be understood and it sets a lower limit to the H abundance. However, the implied H-layer must be much less massive ($10^{-11}\,M_{\odot}$)

than that derived by evolutionary calculations ($10^{-4}\,M_{\odot}$; Koester & Schönberner 1986). NRS find no mechanism to allow such a small H-layer to remain on the star after the PN stage. Wind loss or diffusion-induced nuclear burning are two possibilities (Michaud, Fontaine & Charland 1984); however, NRS conclude that either all of the hydrogen or only a very small amount of the hydrogen should be dispersed.

1.12.4 Thick or thin H layers

Evidence has been accumulating that the evolutionary model may be incorrect, and H-layers may, in fact, be much thinner ($\sim 10^{-12}\,M_{\odot}$). Several lines of evidence argue for this. Modelling shows that ZZ Ceti stars[3] require H-layers of mass $<10^{-8}\,M_{\odot}$ in order for their atmospheres to become unstable. In addition, if He-rich stars are predominant at low temperatures, due to convective mixing, then the H-layers in most DA stars must be thin in order for the H to be invisible in a re-mixed atmosphere.

Fleming, Liebert & Green (1986) argue that DA stars must have thick H layers since no very hot DA stars (>70 000 K) are observed. The evolutionary calculations of Iben & Tutakov (1984) show that stars with thin H-layers evolve essentially identically to He stars, while those with thick H-layers evolve differently from He/thin H-layer stars. Since there is a class of very hot, high-gravity He stars (PG1159 stars) Wesemael, Green & Liebert (1985; hereafter WGL) argue that an analagous class of very hot DA stars should be observed if DA stars have thin H-layers. These, however, are not seen in the number expected. WGL note that this contradicts the thin H layers required by the ZZ Ceti stars. They also find that the birthrate for degenerate stars is consistent with the birthrate of PN to within the error limits (although speculating that some degenerate stars are formed without recourse to

[3] A class of pulsating white dwarf star (Nather 1978). These DA stars pulsate for similar reasons to non-degenerate stars—the varying ionisation zones of hydrogen and helium—and are to be found inside the same instability strip in the H-R diagram. See 1.12.7

a PN stage, by direct evolution from subdwarf O stars [AGB] and B stars [HB]).

NRS find that diffusion-induced nuclear burning will decrease the H content of an envelope to reduce the H/He ratio as a star cools. This agrees with the data: most hot DA stars have high H/He ($\sim 10^5$–10^6) while the 30 000 K 'DA' stars have low H/He ($\sim$100).

Bergeron *et al.* (1990, 1991) find subtle distortions of the high-order Balmer line profiles of most cool (<11 500 K) DA stars, which they attribute to the presence of He (Liebert & Wehrse 1983). These data imply that nearly all DA stars below 11 500 K have atmospheres contaminated by significant amounts of He, some stars even acquiring He as the dominant component. This is probably due to the onset of convective remixing at this temperature threshold. This He content had not been noticed previously since He at these low temperatures cannot be detected spectroscopically. These data strongly support the thin H-layer scenario, implying a mass of 10^{-14}–$10^{-11}\,M_\odot$ in order to produce the He/H ratios observed for most DA stars. ZZ Ceti stars may have pure H upper atmospheres and represent the evolutionary phase just prior to the onset of convection. Furthermore, this convective remixing should produce DA type stars with significant 'hidden' He content, but will not visibly turn DA into non-DA stars. Thus most cool non-DA stars must originate from the cooling of DB stars. The less He-rich stars must have an extra source of H in order to to dilute the He. The proposed mechanism is accretion (Wesemael 1979). However, if accretion is common an explanation must be found as to why some cool degenerates show no H at all (Greenstein 1986). Moreover, Vennes *et al.* (1988) provide evidence that accretion is not, in fact, a significant contributor for DA stars.

As will be seen later in this thesis, data from *ROSAT* provides new insight into the atmospheric thickness debate.

1.12.5 Rotation, magnetism, accretion

NRS also investigate rotation-induced mixing (which mixes white dwarf envelopes) and magnetism (which stabilises them). Using Tassoul & Tassoul (1983) data they conclude that radial and poloidal components of circulation currents lead to a mixing timescale of 10^{11} yr, which is far too slow to affect the composition significantly. This could only be significant if the stars' rotational speed was $> 500\,\mathrm{km\,s^{-1}}$, which, given the data, seems implausible. Magnetism has also been investigated by Michaud & Fontaine (1982) who conclude that for a field of 1 MG the surface H would be concentrated in a very thin layer at optical depths $< 10^{-4}$. However, observations have not supported these field strengths. Overall, NRS and Michaud & Fontaine conclude that it seems unlikely that either rotation or magnetic fields play a significant rôle in the DBA stars. In investigating accretion to explain the H in DBA stars NRS note several points. If H were accreted, why are no DBA stars seen with H $\gg 10^{-4}$? There would seem to be no mechanism to prevent continued H accretion, to much higer abundances. NRS also question why there are no accreted metals seen in most DBA stars, and postulate that the metals might sink rapidly into the core. However, the only stars in this temperature range to show accreted metals (i.e. the DBZ stars GD40 and CBS78) have no H accretion. It has been proposed that this is due to the propeller mechanism (Illarionov & Sunyaev 1975; Wesemael & Truran 1982)[4]. However, it seems unlikely that there should be two opposing processes for these two classes of stars; one to accrete hydrogen but not metals, one to accrete metals but not hydrogen!

If metals are accreted when the degenerate star passes through a dense interstellar cloud, then the mean time between accretion events should be roughly 10^8 yr, and the duration of each event $\sim 10^6$ yr. Most metals are found in He-rich cool stars, for which the diffusion timescales for the separation of these metals is

[4] Metals (evaporated from grains) with large mass-to-charge ratios can accrete onto a rotating, weakly magnetised white dwarf. Ionised hydrogen couples to the rotating magnetosphere and is pushed away.

10^6–10^8 yr (e.g., Koester 1987). Thus these metals will never reach an equilibrium state. For a H degenerate star, diffusion is much quicker, say 10^4 yr. Equilibrium (as stated by Vauclair, Vauclair & Greenstein 1979) will always occur. If material with cosmic abundances is accreted, then the abundance of metals to hydrogen should always be less than cosmic. However, it is observed to be more than cosmic for the helium stars for which it can be measured, thus accretion may well be fractionated (different elements accreted at different rates). Abundances in H dominated stars are not generally known, but in most cases would seem to be less than solar (Fontaine & Michaud 1979a), except for the case of LP701-29 (Cottrell, Bessel & Wickramasinghe 1977). If metals do accrete with cosmic abundances, we should be able to predict the changes that will happen by diffusion from the relative elemental diffusion rates (e.g., Mg and Ca diffuse at the same rate in hot He degenerates, but for cooler stars Ca sinks at twice the rate). Interestingly, Mg is enhanced to Ca in most stars in which they have both been detected (Liebert 1980), except in the case of GD40 (Shipman & Greenstein 1983).

A second DB star with accreted calcium was discovered in 1986 (CBS 78; Sion *et al.*). Comparing this to GD40 and other metal line degenerates supports the relation between T_{eff} and [H/Ca] as proposed by Liebert, Wehrse & Green (1987). They conclude that there is a critical temperature above which an accretion screening mechanism operates, suggesting the propeller mechanism of Wesemael & Truran (1982). This implies that the DBA stars (Shipman, Liebert & Green 1986) are due to some mechanism other than accretion. In contrast, Sion *et al.* (1990) and Dupuis, Fontaine & Wesemael (1993) both reject the threshold temperature (after analysis of CBS 127 and other DZ stars), conjecturing that the screening mechanism operates at variable (and low) efficiency over most temperatures. Sion *et al.* speculate that bimodal accretion (from normal clouds or volatile-depleted material) could account for the two opposing atmospheric contents. Dupuis, Fontaine & Wesemael propose a similar two-phase accretion model, and argue that it can theoretically explain metal levels in all DZ stars, in combination with other selec-

tion mechanisms.

1.12.6 Atmospheric content of DB stars

Shipman, Liebert & Green (1987) analyse the DB stars in the PG survey and find that at least 20% are actually DBA stars, containing significant trace H in their atmospheres. They speculate that at least as many again may have trace H present, albeit below their detection limit, and that in reality all DB stars may be DBA at some level of sensitivity. They speculate further that the H may be either primordial (convectively mixed with the helium) or accreted, but neither hypothesis is entirely consistent with their data. They find that DB stars have a much higher Balmer decrement, as Greenstein (1986) proposed earlier would be the case in He-rich atmospheres. However, one problem Shipman, Liebert & Green quote is the apparent absence of many cooler non-DA stars with trace H, which they state should be quite abundant (if the 20% figure for a significant H/He ratio is carried on throughout the degenerate class). Another problem they state is that they find it hard to account for why there are no stars with greater H abundances, if the H is gained by accretion, or much smaller abundances if it is convectively mixed with the He. This result is interesting in the light of the discovery that cool DA stars have He in their atmospheres (Bergeron *et al.* 1990, 1991) which had previously remained undetected. These stars could be the missing cool He-rich stars with trace H: they could have been mis-identified as DA stars. Also a number of DZA stars too cool to show He lines are now found to have significant amounts of He present (Zeidler, Weidemann & Koester 1986). The survey of DQ stars by Wegner & Yackovich (1984) is also consistent with 20% having H/He = 10^{-4}. The small amount may be due to the propeller mechanism and thus depend on the temperature and magnetic field of the DB stars.

A search for carbon in the atmospheres of DB stars by Wegner & Nelan (1987) revealed none to within limits consistent with the convective dredge-up process (Koester, Weidemann & Zeidler 1982), which is thought to account for carbon

presence in the cooler DQ stars of the He-rich degenerate sequence (Pelletier *et al.* 1986). However they did find additional DBA stars.

Fundamental questions about the origin and evolution of DB stars and their atmospheres still exist. Some authors have suggested that DB stars can evolve from DA stars as they cool, and can evolve into DA stars again by accretion of H by passing through interstellar clouds. However the diffusive H-burning can complicate the picture. Accretion could be an important source of metals in the DZ stars, but could be modified by magnetism (via the propeller mechanism), suggesting that DB stars are more magnetic since they usually show no metals or H by accretion. However some magnetic stars do have H spectra (Grw +70 8247; Greenstein, Henry & O'Connell 1985), and some DBA stars do exist. A small minority of DB stars (GD40, CBS 78) do show metals. Other investigators have proposed that the differences are in the progenitor stars. DB stars might evolve from hot subdwarfs, or via a binary mechanism (Nathan, Robinson & Stover 1981).

More information on envelope structure can be obtained from the DQ stars (they lie just below DB in effective temperature). It appears accretion is important for these and that C can diffuse out from the core due to an abundance gradient and is then brought to the surface by convection. The surface C abundance depends on the He layer mass and convection theory. This can explain the carbon found in a particular T_{eff} range of DQ and DC stars (Wegner & Yackovich 1983), and why it is not found in the DB stars, since the convection zone reached maximum depth at the T_{eff} found in the former stars.

Zeidler, Weidemann & Koester (1986) conclude that for He-rich degenerates (types DZ and DQ) the dredge-up hypothesis may account satisfactorily for the observed carbon abundances (as well as its non-appearance in DB stars). However the metals cannot be explained satisfactorily since they will have sunk into the core, and they propose cloud accretion followed by diffusion (Wesemael & Truran 1982), since the stars are too cool for levitation to have much effect as they would in the hot DA stars. This is supported by the fact that the stars are observed to

have a range of abundances, reflecting the time since the last cloud encounter.

1.12.7 ZZ Ceti stars

Pulsating DA degenerates, ZZ Ceti stars, are one of the most homogenous classes of stars (McGraw 1979). Studies prove they are restricted to a very narrow strip of instability. Evidence is accumulating that these stars represent an evolutionary phase though which nearly all DA degenerates must cool (Fontaine *et al.* 1982). Measurement of the blue edge of the instability strip has become important since it could be sensitive to both the efficiency of convective mixing in the H envelope, and the mass of the envelope. Thus it could provide information on the whole evolution of all DA degenerates and the hydrodynamic structure of their atmospheres. Variability in DB stars (Winget *et al.* 1982) provides information on their ionisation zones and indicates outer He-rich envelope masses similar to the range of H-layer masses found in the ZZ Ceti stars.

1.13 Ionisation effect of white dwarf population

Dupree & Raymond (1983) argue that degenerate stars are a significant contributor to the total ionisation of the interstellar medium, which has hitherto been mostly ignored. The degenerate stellar population has a much harder[5] flux distribution than the population of non-degenerate stars, and this should allow the production of highly ionised species. Also, degenerate stars are now calculated to have a higher local space density than non-degenerate stars (Koester 1978) and this seems to agree with observations (Green 1980; Liebert 1980). Furthermore, degenerate stars have a larger scale height than non-degenerates (Hills 1972) so their radiation can escape the Galactic plane. They argue that degenerates should leave a fossil Strömgren trail due to their relatively high space velocity and the long recombination timescale for many of the ionised species in the interstellar medium. Thus

[5] the spectral flux distribution has relatively more energy at shorter wavelengths.

there should be a network of these patchily ionised trails pervading the Galactic disc (even extending out of the Galactic plane), and the ionisation balance of the interstellar medium should be significantly altered by the degenerate star contribution. HD149499B, a He rich degenerate, was discovered by Sion & Guinan (1983) to show sharp absorption lines, which they concluded were of photospheric origin. Dupree & Raymond argue that this is an example of a photoionised region around a white dwarf. They conclude that the local interstellar medium density can be measured by the detection or non-detection of highly ionised species around degenerate stars. This effect could also account for the detection of HII (Reynolds 1977, 1980) and CIV pervading the Galaxy (Jenkins 1978; Cowie, Taylor & York 1981).

1.14 Summary

Close, detached WD + MS binary systems are well suited for studying orbital angular momentum loss mechanisms such as magnetic braking, without having to cope with the effects of mass-transfer seen in CB. If we can deduce the formation rate of these WD + MS binaries with respect to orbital period, and can map the current period distribution, then we can infer the orbital angular momentum loss rate. It is also valuable to study these systems to determine the formation rate of binaries containing two degenerate stars (which may lead to type I supernovae). These systems provide an excellent laboratory for investigation of the binary star 'reflection effect': the study of the effect of the irradiation of one, or both components, by the other (see Wilson 1990; Vaz 1985). In many of the other systems in which a reflection effect is seen or postulated, there are complicating factors, such as mass transfer or a CE.

The entire area of white dwarf envelope research is currently very active. EUV observations of white dwarfs, such as those reported in this thesis, are crucial in determining their atmospheric structure and composition, and the mechansims by which these atmospheres are formed and evolve; are their atmospheres 'thick'

or 'thin', do they change with time, what are the roles of accretion, magnetism, convection and cooling? Several key areas in the production of the various types of white dwarf are still poorly understood; their relation to the MS progenitor stars and the myriad intermediate stages of stellar evolution via the giant branches to final white dwarf are also unclear. How the white dwarf visual classification types may change as the stars cool is yet another subject of much controversy; do the various classes evolve from separate feeder channels and remain distinct, or can one star change its type?

As mentioned, thin H-layer masses are at odds with the evolutionary calculations of Iben & Tutakov (1984) and Koester & Schönberner (1986) which require much thicker atmospheres. They also predict radii of hot degenerates must lie above the Hamada-Salpeter zero-temperature relation, which is again not addressed by the results of Finley, Basri & Bowyer (1990). There is obvious conflict between theory and observation, and it is important to determine the causes of these discrepancies.

Determination of white dwarf luminosity functions and mass distributions will eventually allow us to constrain the history of star formation at our galactocentric radius, and the evolutionary paths of stars from the MS.

Chapter 2

White dwarfs detected with the WFC

Imagination is more important than knowledge.

Albert Einstein.

2.1 Introduction

In this chapter I study the observational characteristics of the white dwarf population sample selected in the *WFC* All-Sky-Survey. I compare the EUV-selected population of 'new' white dwarfs with the optically-selected population of previously-known white dwarfs. I perform a search for faint, late-type companion stars to all the apparently isolated white dwarfs found within the *WFC* optical ID database.

2.2 Optical ID programme

The mandate of the *WFC* optical ID programme (Mason *et al.* 1991) was to determine the optical counterparts to the *WFC* EUV survey detections. For my part in this project, aside from being an observing team member, I developed an automated data-reduction system (FARCE), which was run on each observing night's data, at the end of the observing session, producing a set of fully-calibrated (debiased,

flat-fielded, wavelength calibrated, extinction corrected, flux level calibrated, atmospheric absorption lines removed, both spectral orders merged) optimally extracted spectra for examination before the next night's observing session. For a detailed description of the software and data-reduction techniques, and a performance summary of the data-reduction pipeline in operation, please refer to appendix A. In brief, the software will run essentially intervention-free to completion under almost all circumstances, producing results comparable to, and in some respects, superior to, those achieved via a manual reduction by the observer on each individual object. The data reduced by this system is online to the astronomical community in the ROSCO database.

2.3 Optical data

Table 2.2 lists all the white dwarfs detected with the *ROSAT WFC*, for which optical spectra were obtained during the optical ID programme and are thus not listed as being correlated with known sources in the Bright Source Catalogue (Pounds *et al.* 1992). This does not mean that *all* of them were previously unknown—further research reveals that 2 of them do have catalogued identifications in the Edinburgh-Cape survey. Those stars with entries in other catalogues have their alternative names listed in the table.

The corresponding optical spectra of the white dwarfs listed in table 2.2 were reduced using my data-reduction system (FARCE) and are shown in figure 2.3.

Table 2.2 also gives the V magnitude, colour indices and two independent determinations of the effective temperature of each star. The magnitudes and colours were obtained via a convolution of the flux-calibrated optical spectra with the Johnson filter functions. Since various instruments were used to obtain these spectra (FOS on the INT at La Palma; RCPS on the 1.9 m at SAAO) the wavelength ranges vary and thus not all the spectra cover the same filter bands (see table 2.1). However, all of them at least fully cover the B and V filter bands and 50–100% of

the U filter band. A portion also have R band filter information.

The effective temperature information is derived via two different methods. Firstly, the *WFC* EUV count rates have been modelled with the PHOTAN code, developed by Martin Barstow at Leicester (see § A.4.2.1 and § 3.3.2 for a description of the procedure). Secondly, I have performed individual fits to each of the the Balmer absorption lines in the optical spectra of the white dwarfs (c.f. Bergeron *et al.* 1992). I have obtained a grid of model atmospheres from D. Koester (Koester 1991), which are based opon calculations of a pure hydrogen (DA) atmosphere spanning the temperature range 20 000–60 000 K and a surface gravity range of log (g) = 7.5–8.5 (see § A.3.1). The models cover the wavelength range 10–10000 Å. To this end, I have written a program, DWARF, which allows the comparison of the models with the optical data. Each of the models within the grid is read in turn, and the particular wavelength region to be compared with the data is flagged and nomalised to the same flux level as the optical data. On the first pass, the optical data is cross-correlated with a coarse subset of the available models and the correlation statistic used to narrow down the range of models to inspect more closely. Then, each individual model within the narrowed range is compared in turn to the optical data, and the χ^2 between the two spectra is calculated. The model with the lowest χ^2 is determined to be the best fit to the data. The confidence interval can then be calculated by rechecking the χ^2 minimisation as the models either side of the best fit are compared against the optical data.

An example of the output from my DWARF software fit of the DA model atmospheres to the optical spectrum of the EUV source RE0648−25 is shown in figure 2.1 and an example of a PHOTAN fit to the EUV count rates of a typical white dwarf can be seen in figure 2.2.

For the EUV-derived effective temperatures in table 2.2, I give the 1σ error ranges. The models used were for DA atmospheres, (pure H, no trace He). For the optically-dervied effective temperatures, I give the temperature of the best fit model atmosphere and the 1 σ error limits, after combining the individual line

fits for each star. It was found that the fits were insensitive to the gravity of the models, and thus this parameter was kept fixed at the canonical log $(g) = 8$.

Spectrograph	Telescope	λ range	observing dates
FOS-1	INT/La Palma	3600–11000	Jan, Feb, May, Aug, Dec 91
			Feb 92
RPCS	1.9 m/SAAO	3300–8000	Nov, Dec 90
			Feb, Jul, Aug, Oct, Nov, Dec 91
			Jan 92

Table 2.1: *Parameters of observing instruments.*

One point to note is that although the spectral observations may not all be 'wide slit', they can still be used to obtain magnitude information. Generally, if the photometric flux calibration standard star is observed through the *same* instrumental setup and atmospheric conditions as the target stars, the flux calibration should be accurate. In the vast majority of our target stars, the instrumental setup did remain the same. The second condition, for atmospheric stability, is harder to meet, and in some cases the conditions are known to have changed. The effect of varying atmospheric conditions between observations of standard star and target star will be to introduce a random element into the calculation of the flux levels for these targets, resulting in an increased scatter of the data points about the true value.

In order to validate this hypothesis of accurate flux calibration, I have compared the spectroscopically and photometrically derived magnitudes and colours of the two white dwarf stars which have both optical identification spectra and previous observations in the literature. It should become clear if there is any significant systematic error in the spectroscopic magnitudes. However, since there are only two such stars, I augment this by looking at the difference in the spectroscopic

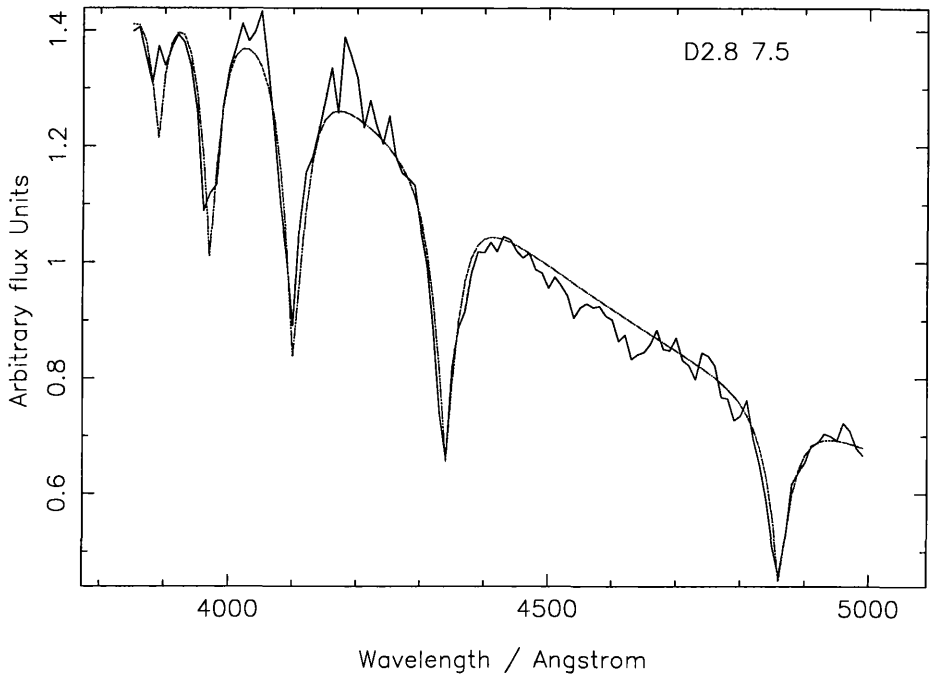

Figure 2.1: *Example of a DWARF model fit to the Balmer profiles in RE0648−25*

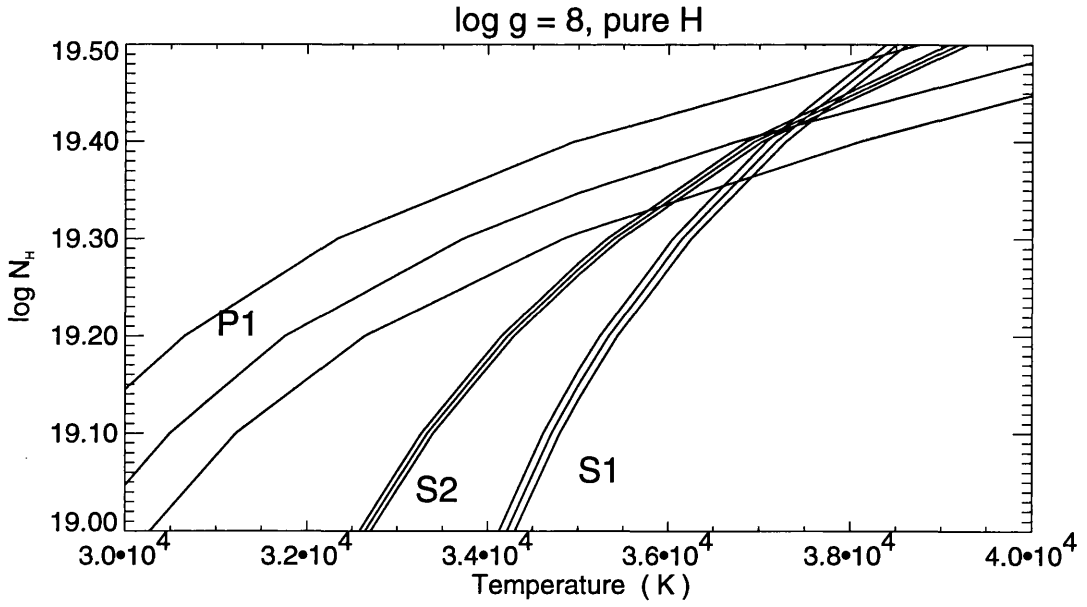

Figure 2.2: *Example of a PHOTAN fit to* WFC *EUV counts rates. In this case there are S1, S2 and P1 count rates.*

magnitudes determined from several optical spectra of the same object taken at different times. This cannot give information on any systematic errors, but should reveal the scatter of the spectroscopic magnitudes. The available data show that the spectroscopically determined magnitudes and colour indices are consistent with the photometric values to within ± 0.2 and ± 0.07 magnitudes respectively.

Source	V	Colour Indices			T_{eff} / 10^3 K		Comment
Designation	magnitude	$U-B$	$B-V$	$V-R$	EUV	Balmer	
RE0003+43	16.8	-1.62	-0.41	0.36	< 47	50 ± 5	
RE0029−63	15.7	-0.44	-0.09	-0.34	40–43	42 ± 3	n, e
RE0053+36	14.1	-0.95	-0.07	0.31	< 32	26 ± 3	
RE0239+50	16.1	-1.34	-0.24	0.29	30-38	38 ± 1	?
RE0427+74	15.7	-1.15	-0.17	0.30	44-48	48 ± 2	
RE0443−03	16.5	-0.84	-0.15	0.62	< 53	45 ± 8	
RE0457−28	14.0	-1.37	-0.29	1.14	no fit	no fit	
RE0512−00	13.8	-1.20	-0.26	0.54	30–31	33 ± 2	
RE0512−41	16.4	-1.29	-0.34	-0.17	40–45	50 ± 3	
RE0521−10	15.7	-1.06	-0.15	-0.18	no fit	32 ± 1	
RE0534−02	17.0	-0.89	-0.15	-	29–31	23 ± 2	n
RE0550−24	17.3	-0.79	-0.02	-0.06	< 41	no fit	n
RE0558−37	14.9	-1.36	-0.26	0.32	no fit	61 ± 1	
RE0605−48	16.2	-1.33	-0.28	-0.31	no fit	33 ± 2	
RE0616−64	17.0	-	-	-	< 29	no fit	
RE0620+13	15.3	-1.26	-0.25	0.30	26–28	47 ± 1	n
RE0623−37	12.9	-1.44	-0.18	0.23	> 24	58 ± 2	c
RE0632−05	15.8	-1.29	-0.19	0.30	69–77	43 ± 1	
RE0633+20	17.5	-1.21	-0.28	0.22	< 47	60 ± 1	
RE0648−25	14.0	-1.09	-0.13	0.32	30–31	27 ± 1	
RE0715−70	?	-	-	-	37–39	38 ± 2	e

Table 2.2: *Effective temperature, V magnitude and colours for the White Dwarfs in the* WFC *EUV survey.*

Source	V	Colour Indices			T_{eff} / 10^3K		Comment
Designation	magnitude	$U-B$	$B-V$	$V-R$	EUV	Balmer	
RE0720−31	15.0	-1.12	-0.07	0.38	no fit	55 ± 6	e, c
RE0831−53	14.5	-0.89	-0.09	-0.01	27–28	29 ± 2	c
RE0841+03	14.8	-1.21	-0.16	0.28	34–38	42 ± 3	
RE0902−04	13.4	-1.04	0.03	0.43	25–29	23 ± 2	
RE0916−19	17.5	-1.29	-0.24	0.26	43–54	60 ± 5	n
RE0957+85	16.4	-1.15	-0.08	0.33	41–48	38 ± 2	
RE1019−14	15.5	-1.07	-0.07	0.34	28–30	30 ± 1	
RE1032+53	14.5	-0.97	0.07	0.38	39–40	45 ± 4	
RE1043+49	16.2	-1.24	-0.16	0.33	38–41	45 ± 4	
RE1440+75	15.6	-1.08	-0.12	0.32	34–41	47 ± 4	
RE1446+63	16.0	-1.18	0.04	0.54	31–38	49 ± 3	n
RE1529+48	14.5	-1.27	-0.30	0.21	26–29	46 ± 2	
RE1650+40	15.9	-1.17	-0.15	0.32	> 26	40 ± 4	
RE1738+66	14.3	-0.95	0.13	0.57	31–35	>60	n
RE1746−70	16.7	-0.77	-0.20	-	35–40	43 ± 3	n, e
RE1820+58	14.1	-1.26	-0.19	0.34	31–33	42 ± 1	
RE1847−22	14.2	-1.40	-0.25	0.28	26–33	33 ± 1	
RE1943+50	14.6	-1.05	-0.21	0.24	27–33	36 ± 1	
RE2009−60	13.2	-1.30	-0.31	-0.06	35–38	46 ± 2	1
RE2127−22	14.6	-1.34	-0.38	0.07	28–33	58 ± 3	e
RE2154−30	14.2	-1.27	-0.29	-0.07	27–29	28 ± 1	
RE2156−41	15.5	-1.36	-0.40	-1.37	38–44	43 ± 2	e
RE2156−54	14.3	-1.49	-0.51	0.17	38–39	50 ± 5	
RE2207+25	14.4	-1.10	-0.11	0.29	no fit	28 ± 1	
RE2210−30	14.0	-1.14	-0.25	-0.07	26–30	28 ± 1	
RE2214−49	11.8	-1.26	-0.36	0.47	no fit	57 ± 2	e, c
RE2324−54	15.0	-1.41	-0.49	-0.19	34–36	43 ± 2	
RE2334−47	13.6	-1.33	-0.29	-0.05	no fit	55 ± 5	c
RE2353−24	15.8	-1.11	-0.26	-	28–36	28 ± 1	e, 2

Table 2.2: *1 = EC20048−6034; 2 = GD1706, EC23504−2448. In the comment column 'n' indicates a noisy spectrum, 'e' indicates emission features, 'c' indicates a possible companion. A 'no fit' in the effective temperature column indicates that there was no acceptable fit to the data.*

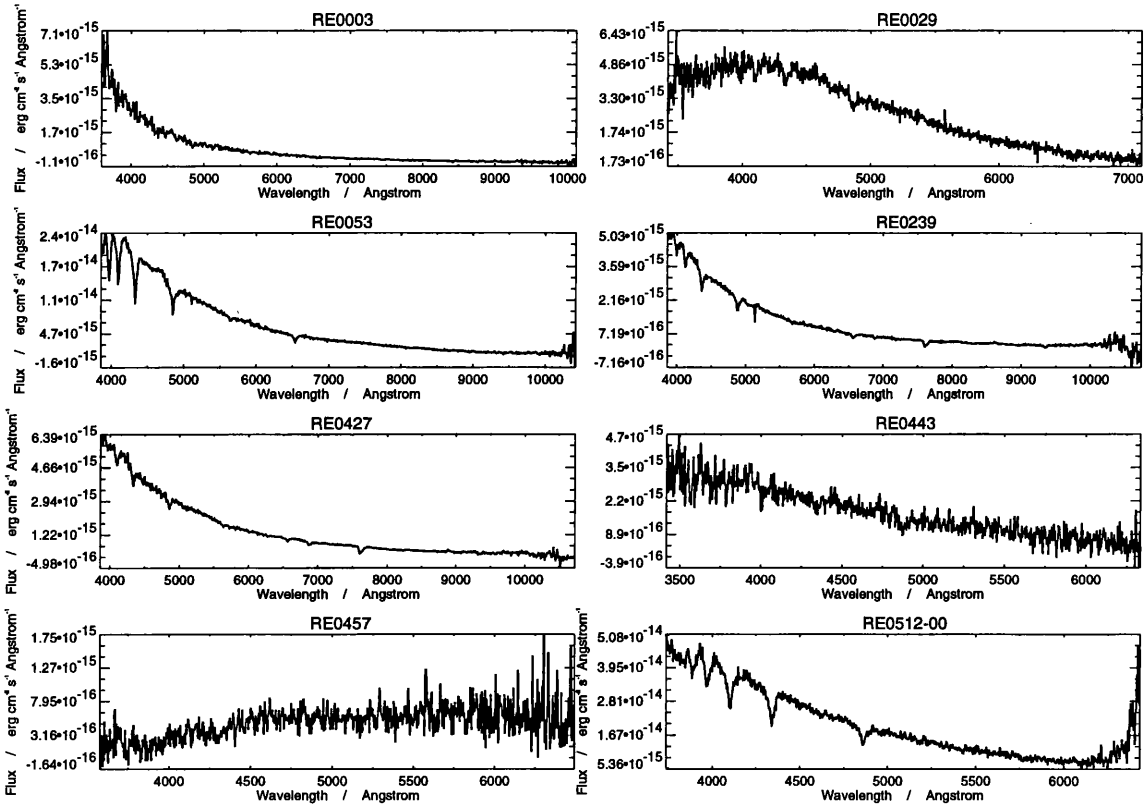

Figure 2.3: *Optical spectra of my sample of white dwarfs.*

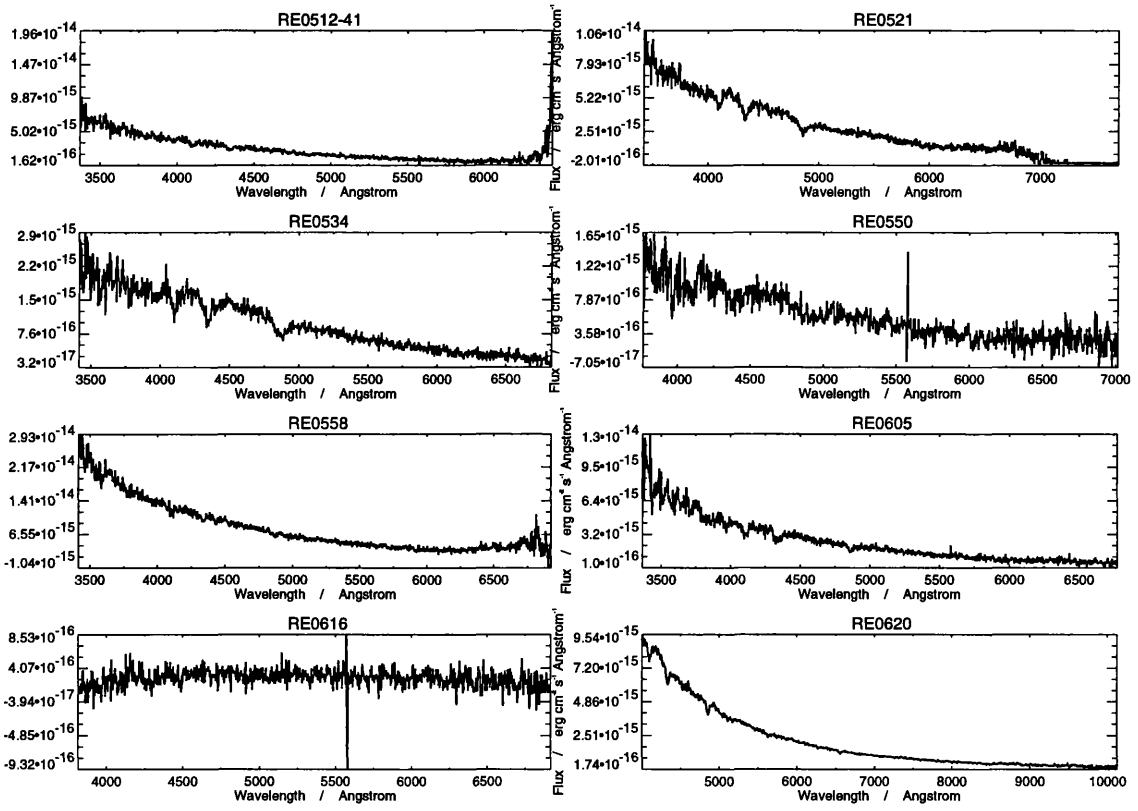

Figure 2.3: *Optical spectra of my sample of white dwarfs.*

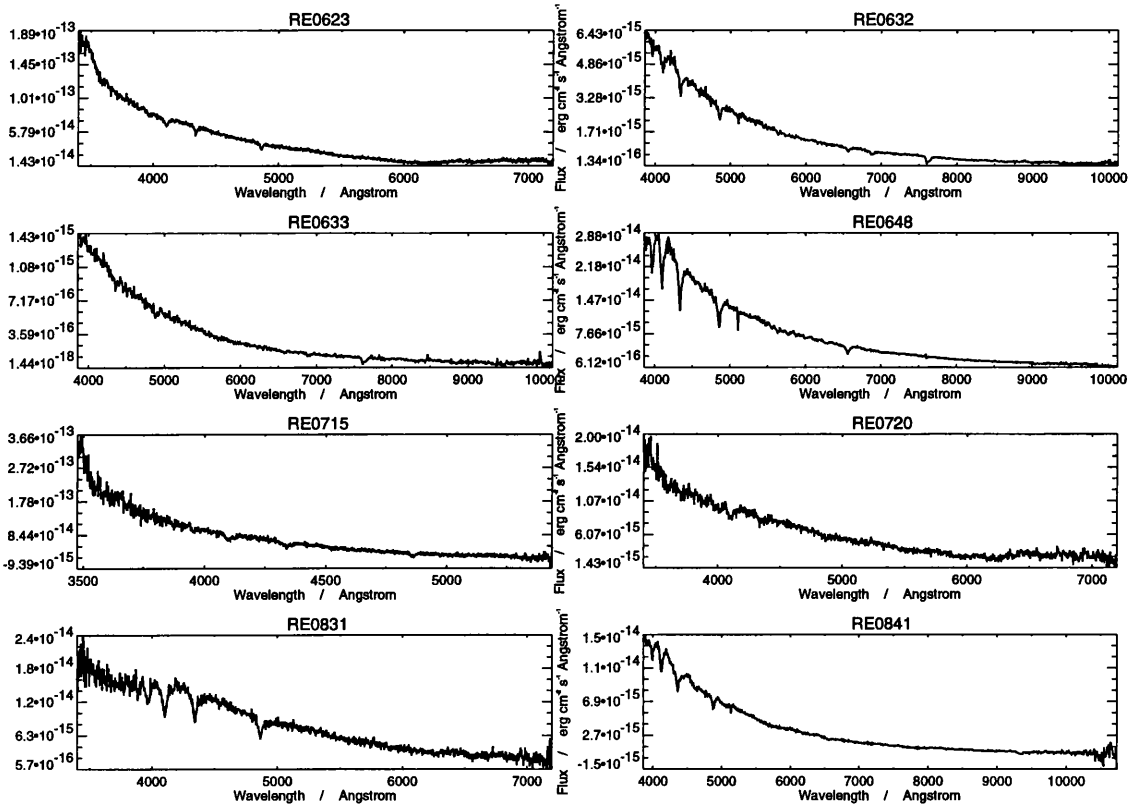

Figure 2.3: *Optical spectra of my sample of white dwarfs.*

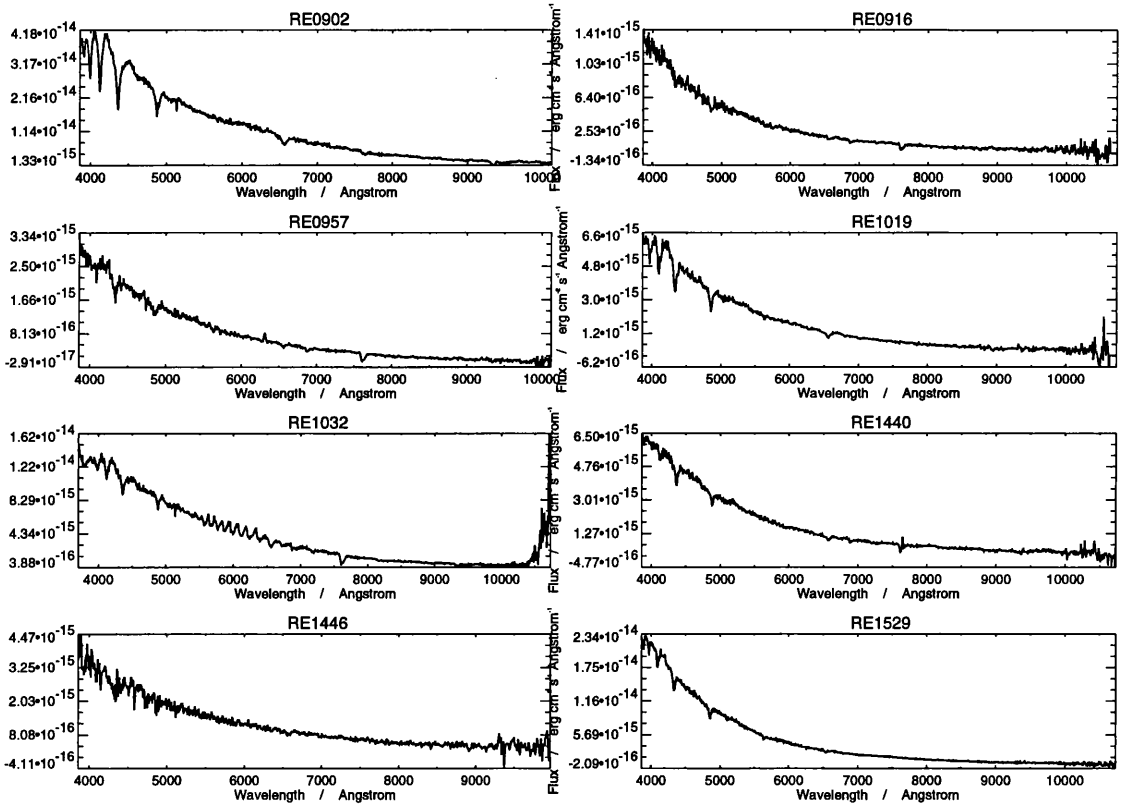

Figure 2.3: *Optical spectra of my sample of white dwarfs.*

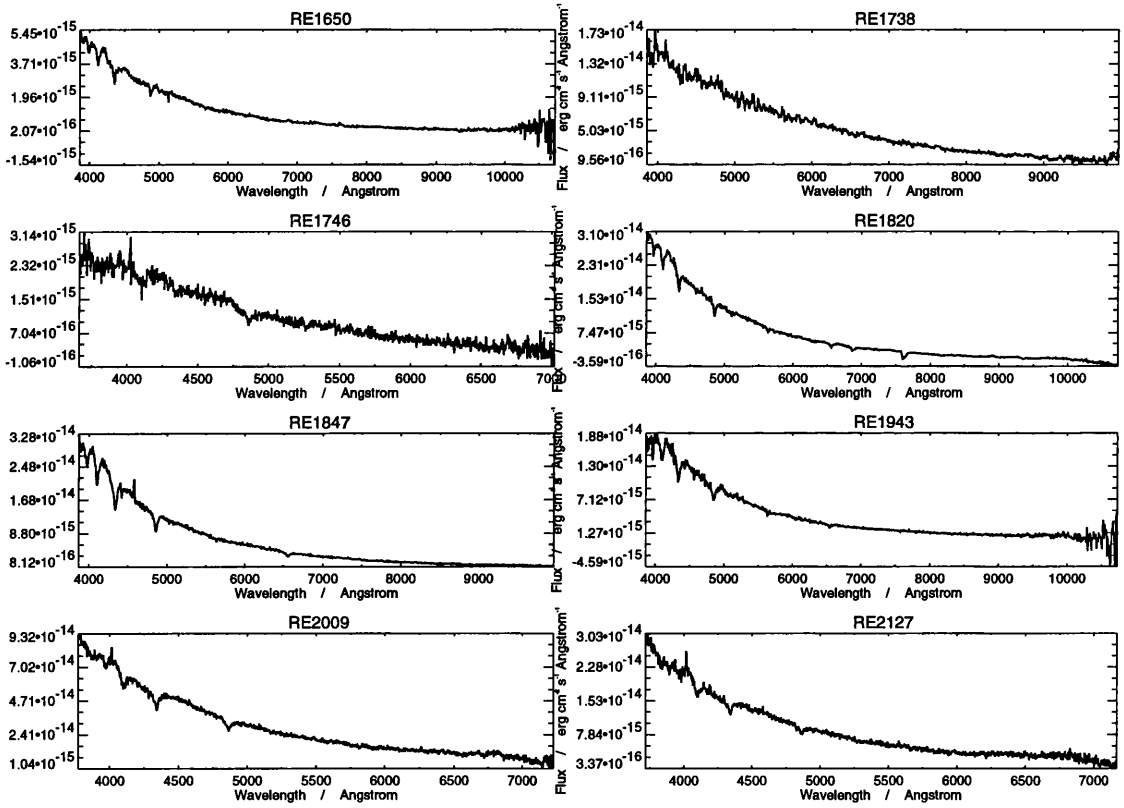

Figure 2.3: *Optical spectra of my sample of white dwarfs.*

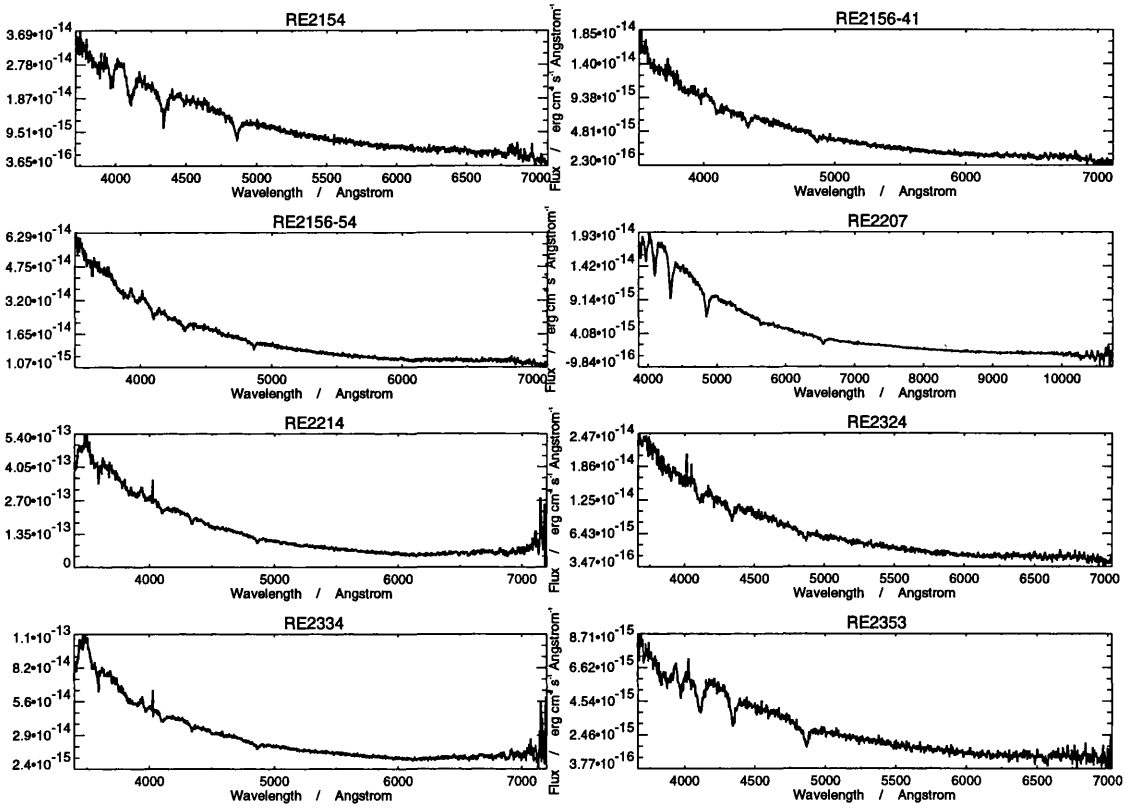

Figure 2.3: *Optical spectra of my sample of white dwarfs.*

2.4 Sample parameters

The observed number distribution with V magnitude (in 1 magnitude bins centred on the half magnitude) of white dwarfs from the *WFC* survey is shown in figure 2.4. The top, centre and bottom panels show respectively the distributions for the 'new' (EUV-selected) stars, the known (optically-selected) stars, and the complete sample of white dwarfs detected with the *WFC* .

The 'new' IDs do not contain any stars brighter than $V = 11.8$, and in fact, only two stars brighter than $V = 13.0$. This is expected since all the optically-bright stars should have been catalogued from previous surveys in the optical and UV, such as the Palomar-Green (PG) survey (Fleming, Liebert & Green 1986) and the UVX survey (Green, Schmidt & Liebert 1986).

The EUV-selected white dwarfs are perhaps fainter in V magnitude than those with previous optically-catalogued identifications, although given the precision of the current measurements this is not categorical. If it is true, it may be expected, since the majority of the catalogued stars have been optically selected in various spectroscopic or photometric surveys for unusually blue objects (thus are EUV- *and* optically-selected in this sample, whereas the 'new' IDs are EUV-selected only). Typically, most spectroscopic surveys have been limited to $V < 16$. This means that most surveys have been restricted to within $\sim 100\,\mathrm{pc}$ of the Sun, providing limited information on the galactic scaleheight of the degenerate population. Certain surveys (e.g. Boyle 1989) have attempted to redress this matter.

The bolometric magnitudes of this sample of DA stars may be calculated, in order to transform figure 2.4 into more meaningful information.

We may relate the surface temperature and radius of a degenerate star to its luminosity by a simple application of the blackbody law

$$F = \sigma T^4 \, erg\, s^{-1}\, cm^{-2} \tag{2.1}$$

where $\sigma = 5.669 \times 10^{-5}\, erg\, s^{-1}\, cm^{-2}\, K^{-4}$. Thus over the whole star,

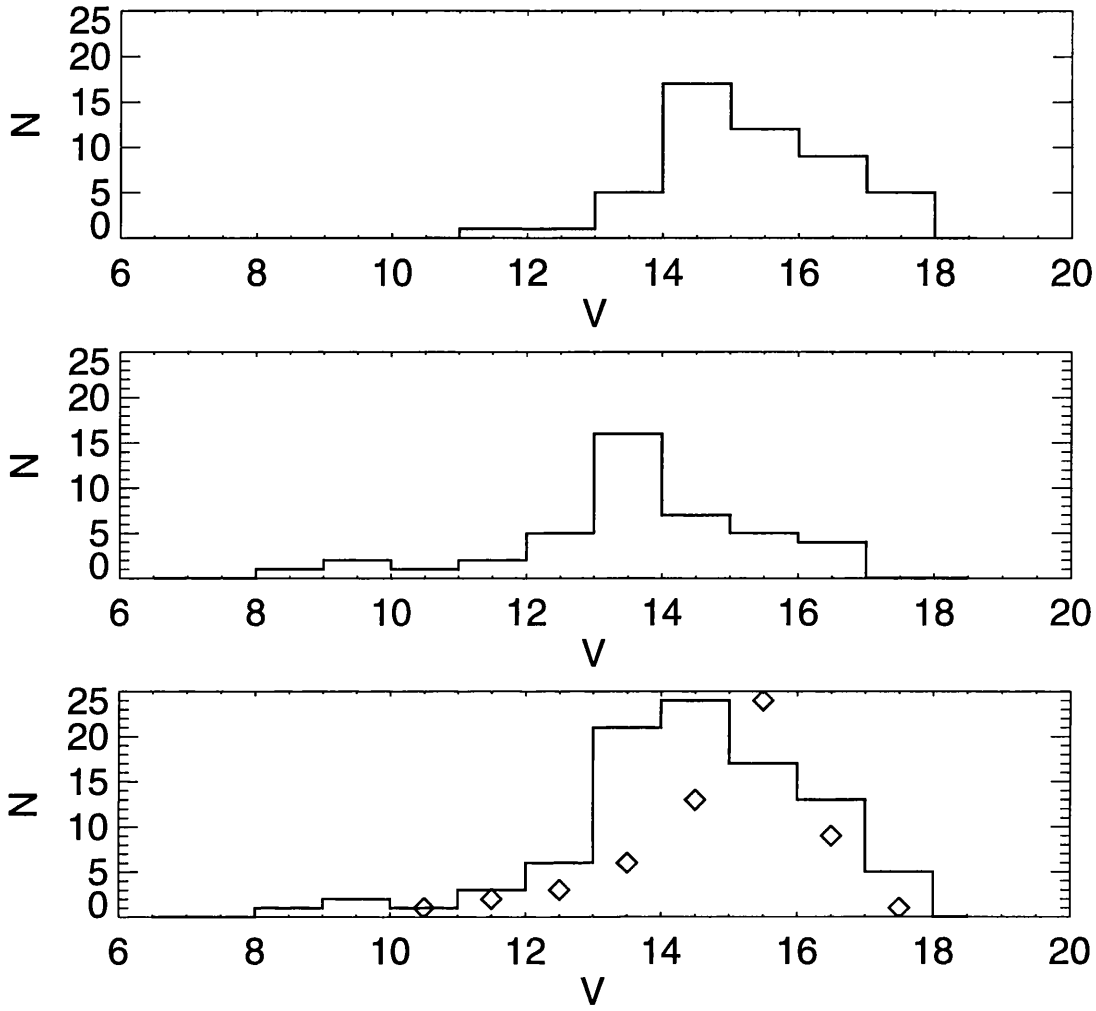

Figure 2.4: *Magnitude versus number for WFC-selected white dwarfs. The top, centre and bottom panels show the EUV-selected stars, optically-selected stars, and the combined sample, respectively. Diamonds indicate a scaled PG survey distribution.*

$$L_\star = 4\pi R_\star^2 \sigma T^4 \, erg\, s^{-1} \tag{2.2}$$

with R in cm and T in K. If we rewrite this in terms of solar units, where $R_\star = X.R_\odot$

$$\frac{L_\star}{L_\odot} = \frac{4\Pi\sigma R_\odot^2}{L_\odot} T^4 X^2 \tag{2.3}$$

which, given $R_\odot = 6.96 \times 10^{10}\, cm$ and $L_\odot = 3.83 \times 10^{33}\, erg\, s^{-1}$ (Zombeck 1982; Smith & Jacobs 1977) reduces to

$$\frac{L_\star}{L_\odot} = T^4 X^2 \left[9.01 \times 10^{-16}\right] \tag{2.4}$$

We also have the standard magnitude-luminosity relation, which we can express as

$$M_{bol\star} - M_{bol\odot} = -2.5 \log \left(\frac{L_\star}{L_\odot}\right) \tag{2.5}$$

Combining 2.4 and 2.5 leaves

$$M_{bol\star} = M_{bol\odot} - 2.5 \log \left[T^4 X^2 \left(9.01 \times 10^{-16}\right)\right] \tag{2.6}$$

Simplifying and using $M_{bol\odot} = 4.75$ (Zombeck 1982; Smith & Jacobs 1977) we arrive at

$$M_{bol\star} = 42.36 - 2.5 \log \left[T^4 X^2\right] \tag{2.7}$$

For the stellar radii I use the tabulations of Koester & Schönberner (1986), for a $0.55 M_\odot$ model, $M_H = 10^{-6}$. The values of T_{eff} I use are those derived from the Balmer line fitting. The results are tabulated in table 2.3. This is rather a crude technique when compared to those of e.g., Liebert, Dahn & Monet (1988). However, the paucity of data constrain the methods available for calculating these parameters. Furthermore, for such a hot sample of stars as this, it may well be a sufficient technique, given that the greatest errors should occur in the coolest ($<$ 5000 K) degenerates, which are expected to depart from the radius relation used in the above technique.

An alternative method for calculating the absolute magnitudes, and hence the bolometric magnitudes of these stars is available: Boyle (1989) describes how the

broadband $U-B$ colours can be transformed into $B-V$ colours via a set of relations he derives from the broadband colours listed in the McCook & Sion (1987) catalogue for DA stars.

$$(B-V) = 0.63(U-B) + 0.50 \qquad (U-B < -0.6) \tag{2.8}$$

$$(B-V) = 2.05(U-B) + 1.35 \qquad (-0.6 < U-B < -0.5) \tag{2.9}$$

$$(B-V) = 0.75(U-B) + 0.70 \qquad (U-B > -0.5) \tag{2.10}$$

This allows the application of the empirical relations of Sion & Liebert (1977)

$$M_v = 11.246(B-V+1)^{0.60} - 0.045 \tag{2.11}$$

or Greenstein (1988)

$$M_v = 11.61 + 5.11(B-V) - 1.11(B-V)^2 \tag{2.12}$$

to derive the absolute magnitudes. Since I have both $B-V$ and $U-B$ colours I can not only calculate the absolute magnitudes, but perform a consistency check between the colour indices. To transform these absolute magnitudes into bolometric magnitudes, I take the bolometric corrections from Wesemael *et al.* (1980). Note that Boyle (1989) estimates that an error of ± 0.2 in $U-B$ will results in an error of ± 0.75 in M_v.

I find that in all cases, the values I derive for the bolometric magnitudes from the $B-V$ and $U-B$ colours are within ± 0.5 and ± 0.7 magnitudes respectively of those derived from the T_{eff} relation. The internal consistency between the colour indices is ± 0.3 magnitudes. The $B-V$ relation to magnitude is expected to be more accurate than the $U-B$ relation since it requires less transformations. However, the errors I propagate through the T_{eff} relation for bolometric magnitude are comparible or smaller to those predicted by Boyle (1989) for the colour relations. Thus, I have also calculated the absolute magnitudes from the T_{eff} relation by subtracting the bolometric corrections from the bolometric magnitudes, and in the table I give the mean of the three determination methods for the absolute magnitude.

Using equation 2.5, I derive the luminosities of the stars, which are also listed in table 2.3.

Having derived the absolute magnitude (from the colours and effective temperatures) of the stars, and having the apparent magnitudes from the spectra, it is trivial to calculate their distances. The distance moduli are also given in the table. The distances can be calculated assuming no intervening optical absorption, since the stars are all close-by in order to be detected by the *WFC* . This is supported by Boyle's (1989) estimate that even for his AAT sample of stars, which is on average further away, the extinction, A, < 0.05 magnitudes (Sandage 1973) for the most distant stars in the sample. When combined with the reddenning, this means at most a 0.1 magnitude error in the absolute magnitude estimate. From the table it may be seen that my sample of stars spans a distance range of 40–570 pc, with a mean at 130 pc. The extreme of 570 pc may seem rather large. However when examining the star responsible, RE0003+43, we see it is one of the hottest and bluest stars (60 000 K, $B - V$ = -0.41), yet at $V = 16.8$, one of the faintest. The other star at the extreme upper limit ($m - M = 8.5$), RE0633+20, is fitted at the hottest model (60 000 K) and faintest magnitude seen in my sample, $V = 17.5$. We may expect a noisy spectrum to produce higher temperature estimates than the true value, since the shallow Balmer absorption lines will be lost in the low S/N of the spectrum. Looking at the relevant FOS spectra reveals that all three are indeed noisy, and virtually no Balmer absorption can be seen in the spectra, if at all. Thus this sample of stars may well be offset to a slightly overestimated mean distance, due to the low S/N of many of the spectra, and resultant uncertainty/overestimation of the temperatures. A higher S/N spectral survey of the stars should alleviate this problem.

From the radii I have derived in table 2.3 it is theoretically possible to derive the stellar masses, assuming a model for the mass-radius relation, such as the zero-temperature models of Hamada & Salpeter (1961). However, Bergeron, Saffer & Liebert (1992b) show that, especially in the case of hot stars, it is necessary to

Source	$log(R/R_\odot)$	M_{bol}	$log(L/L_\odot)$	M_v	m - M
RE0003+43	-1.808	4.41	0.13	8.00	8.8
RE0029−63	-1.828	5.27	-0.20	10.74	4.9
RE0053+36	-1.859	7.51	-1.10	10.38	3.7
RE0239+50	-1.838	5.75	-0.40	9.12	6.9
RE0427+74	-1.815	4.62	0.05	9.44	6.2
RE0443−03	-1.821	4.93	-0.07	9.98	6.5
RE0512−00	-1.847	6.40	-0.66	9.37	4.4
RE0512−41	-1.808	4.41	0.13	8.75	7.6
RE0521−10	-1.849	6.55	-0.72	9.89	5.8
RE0534−02	-1.863	8.05	-1.32	10.34	6.6
RE0558−37	-1.775	3.38	0.54	8.70	6.1
RE0605−48	-1.847	6.40	-0.66	9.10	7.0
RE0620+13	-1.816	4.71	0.01	9.06	6.2
RE0623−37	-1.784	3.64	0.44	8.80	4.0
RE0632−05	-1.826	5.15	-0.16	9.23	6.5
RE0633+20	-1.778	3.46	0.51	8.90	8.5
RE0648−25	-1.857	7.33	-1.03	9.96	4.0
RE0715−70	-1.838	5.75	-0.40	9.89	5.1
RE0720−31	-1.794	3.92	0.32	9.88	4.6
RE0831−53	-1.854	7.00	-0.90	9.66	5.1
RE0841+03	-1.828	5.26	-0.20	10.17	3.2
RE0902−04	-1.863	8.05	-1.32	9.50	7.9

Table 2.3: *Radius, bolometric magnitude, absolute magnitude, luminosity and distance modulus for the EUV-selected sample of white dwarfs.*

Source	$log(R/R_\odot)$	M_{bol}	$log(L/L_\odot)$	M_v	m - M
RE0916−19	-1.778	3.46	0.51	9.48	6.9
RE0957+85	-1.838	5.75	-0.40	9.96	5.5
RE1019−14	-1.852	6.84	-0.83	10.53	3.9
RE1032+53	-1.821	4.93	-0.07	9.35	6.8
RE1043+49	-1.821	4.93	-0.07	9.70	5.9
RE1440+75	-1.816	4.71	0.01	9.87	6.1
RE1446+63	-1.811	4.51	0.09	8.88	5.6
RE1529+48	-1.818	4.82	-0.02	9.45	6.4
RE1650+40	-1.833	5.50	-0.30	10.52	3.7
RE1746−70	-1.826	5.15	-0.16	9.99	6.7
RE1820+58	-1.828	5.26	-0.20	9.31	4.7
RE1847−22	-1.847	6.40	-0.66	9.06	5.1
RE1943+50	-1.842	6.00	-0.50	9.66	4.9
RE2009−60	-1.818	4.82	-0.02	8.84	4.3
RE2127−22	-1.784	3.64	0.44	8.46	6.1
RE2154−30	-1.856	7.16	-0.96	9.28	4.9
RE2156−41	-1.826	5.15	-0.16	8.57	6.9
RE2156−54	-1.808	4.41	0.13	7.93	6.3
RE2207+25	-1.856	7.16	-0.96	9.99	4.4
RE2210−30	-1.856	7.16	-0.96	9.59	4.4
RE2214−49	-1.788	3.74	0.40	8.64	3.1
RE2324−54	-1.826	5.15	-0.16	8.23	6.7
RE2334−47	-1.794	3.92	0.32	8.71	4.8
RE2353−24	-1.856	7.16	-0.96	9.61	6.1

Table 2.3: *Radius, bolometric magnitude, absolute magnitude, luminosity and distance modulus for the EUV-selected sample of white dwarfs.*

use models including finite-temperature effects, such as the carbon-core models of Wood (1990). These require accurate determinations of the effective temperature and surface gravity of the degenerate stars. With the poor precision of the current data on surface temperature and especially surface gravity (where my fits are insensitive due to the low S/N) it is not possible to construct a meaningful mass-distribution of this sample.

2.5 Comparison to optically-selected sample

Recently, a study of an optically-selected subset of the known degenerate stars detected by the *WFC* has been performed by Barstow *et al.* (1993c, hereafter B93). I have compared this with my sample of *WFC*-selected white dwarfs. B93 have included additional data in their modelling, in the form of the PSPC survey count rates on the stars. Their models are also slightly more advanced than the models I have used in this chapter, having improved flux calculations and the ability to fit stratified atmosphere models. In addition, it is possible to calculate varying hydrogen layer masses in the case of the stratified atmosphere models. Despite the differences, I find that my results are consistent with the B93 results, wherever the analyses have overlapped. i.e. my results fall within the same parameter space. I shall henceforth use their parameters when quoting results on the catalogued white dwarfs detected with the *WFC*. Where I plot both sets of data (EUV-selected and optically-selected), the B93 results are indicated by squares, while those results from the uncatalogued sample I have reduced are denoted by diamonds.

Firstly, for my sample of stars, I have plotted the results from both methods of temperature determination (EUV and Balmer line modelling) against each other. Figure 2.5 overlays the white dwarf data points (shown as diamonds) with the 1:1 correlation line. I have determined rough error limits to the correlation line by the following formalism: I divided the maximum and minimum allowable values of the individual temperature determinations (eg. if $T_{e1} = 30\,000 \pm 5000$ K and $T_{e2} =$

25 000 ± 5000 K, then the upper limit is 35 000 divided by 20 000 and the lower limit is 25 000 divided by 30 000. The final error limits on the graph are calculated from the total set of error values thus derived from the total set of effective temperature determinations).

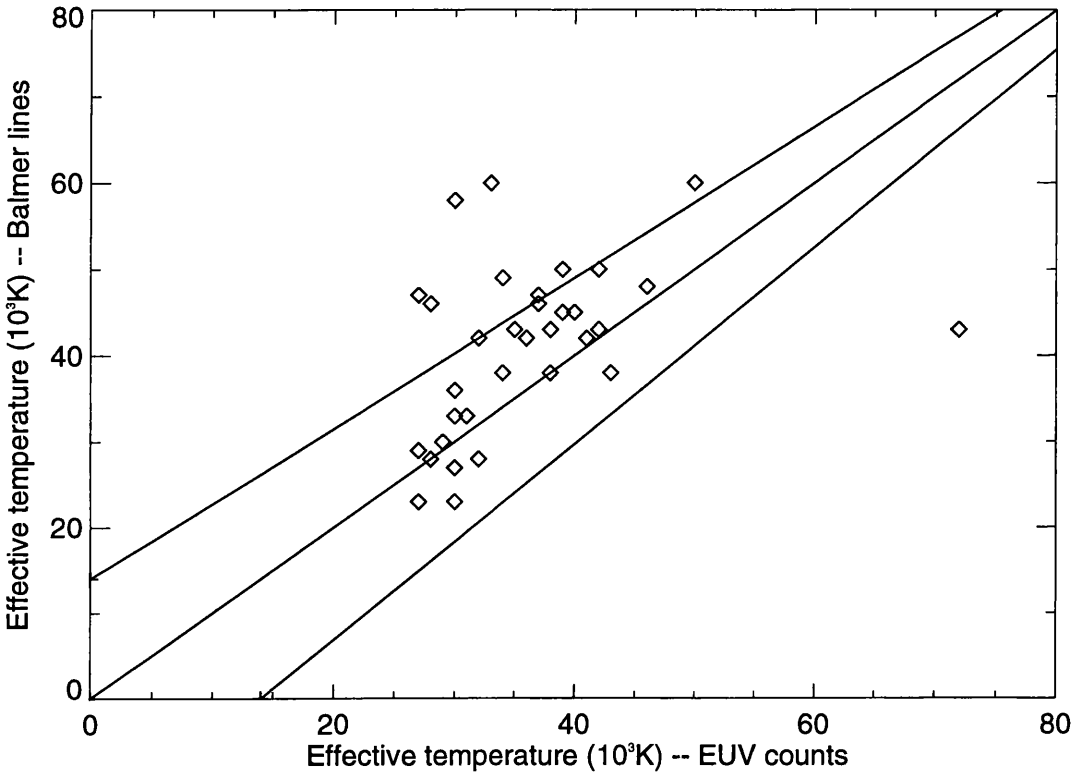

Figure 2.5: *Temperature–Temperature diagram for the white dwarf sample: the Balmer line derived temperatures are plotted against those derived from the EUV count rates. The solid lines indicate the 1:1 correlation and the associated error limits.*

It is interesting to note that while the majority of the degenerates lie inside the error limits and a sizeable proportion lie notably above the agreement limits (RE2156−54, RE2127−22, RE1738+66, RE1529+48, RE0720−31, RE0239+50), only one lies below it (RE0632−05). This means that in all cases but one, the Balmer line derived temperature either agrees with, or is higher than, the EUV derived temperature. This, however, is not wholly unexpected. The atmospheric

models I have used to model the EUV count rates are essentially DA model atmospheres with trace Helium abundances, essentially homogenous and with no significant metal content. The atmospheres I have used for the Balmer line modelling are all homogenous pure hydrogen DA atmospheres. In the case of a degenerate star with a stratified atmosphere having a relatively thin topmost hydrogen layer, or an atmosphere with a non-negligible metal content, the EUV flux is expected to be extinguished preferentially as compared to the optical flux, with little or no visible effect on the optical line regions (Jordan & Koester 1986). Thus for such a star the EUV models will not be able to successfully fit the short wavelength flux unless assuming the star is at a lower temperature than in reality. The Balmer line profile fitting should be relatively unaffected and thus give a truer indication of the actual effective temperature in these cases (until improved atmospheric models become available). This under-estimation of the EUV-derived temperature leads to the systematic shift of these stars upwards in the plot. However, this situation can be turned to our advantage. We can deduce that any star above this correlation line must have either a high metal content or a stratified atmosphere with relatively thin layer of hydrogen, and thus is automatically worthy of further investigation, since these two characteristics are amongst the features that are currently under close scrutiny in degenerate atmosphere research. The modelling used in this chapter does not allow a meaningful distinction between the two causes (levitated metals or stratified atmospheres) of flux blanketing. Also note that (if one assumes the Balmer line profile determined temperatures are more accurate) it is only those stars which lie at the hotter end of the temperature scale ($T_{eff} >$ 45 000 K in a sample which spans 20 000 K $< T_{eff} <$60 000 K) that actually deviate from a 1:1 correlation between the two derived temperatures. Also, the hotter the star, the greater the deviation possible. This indicates that not only is it the hotter of the DAs which exhibit the flux extinguishing agent (either metals or an underlying He layer) but that the hotter the star, the greater the flux blocking. This is what one would expect if, for example, metals are one of the causes of

this effect, since radiative acceleration will levitate more metal species at higher atmospheric temperatures. The magnitude of the discrepancy between the two methods indicates the amount of EUV flux-blanketing taking place in the stellar atmosphere, although it must be remembered that this is not the sole cause of any deviations between the two methods. Independently, B93 find a similar trend in their data, (whilst having in general superior optically-determined temperatures [Finley *et al.* 1993; Kidder 1991] due to the more extensive optical work on these known stars), and thus confirm this interpretation. This could explain why very few extremely hot ($> 55\,000$ K) DA stars were detected in the *WFC* survey, since at that temperature, enough metals may be levitated to almost totally block the EUV flux. This unforseen opacity may also explain the discrepancy between the Barstow (1989) estimation of the number of DA stars which were expected to be discovered during the *WFC* survey, and the actual number discovered.

To quantify the flux extinction, I have used the formula of B93 to calculate a first order estimate of the each star's absolute flux in the *WFC* S1 and S2 bandpasses. The fluxes are derived by folding the observed *WFC* count rates through an estimated effective area and mean bandpass energy, given the V magnitude of the star as the normalisation. For comparison with the B93 results, I adopt the same normalisation, effective area and mean energy values.

$$C_E = 4 \times 10^{-5}.C_{obs}/(E.A_{eff}.10^{-0.4V}) \tag{2.13}$$

where $A_{eff} = 7,8\,\mathrm{cm}^2$ (S1 and S2), and $E = 0.085, 0.14\,\mathrm{keV}$ (S1 and S2).

Figure 2.6 displays the absolute fluxes versus temperatures for my sample of stars, along with the predicted curves for a pure hydrogen DA white dwarf. Pluses and diamonds indicate the S1 and S2 points respectively. As can be seen, the cooler stars ($< 40\,000$ K) tend to lie very close to the predicted values for low column density, pure hydrogen stars. However, the large discrepancies exhibited by some of the hotter stars cannot be explained by, say, enhanced interstellar opacity, because absorption would be greater at the longer wavelength, which is

clearly not the case for all the stars in this sample; some exhibit more extinction in the S1 band, some exhibit more extinction in the S2 band. Thus I conclude that in some cases the opacity is intrinsic to the star (it would also seem that the nature of the opacity varies, given the variation in extinction from star to star). Again, this confirms the trend found in the optically-selected white dwarf sample analysed by B93.

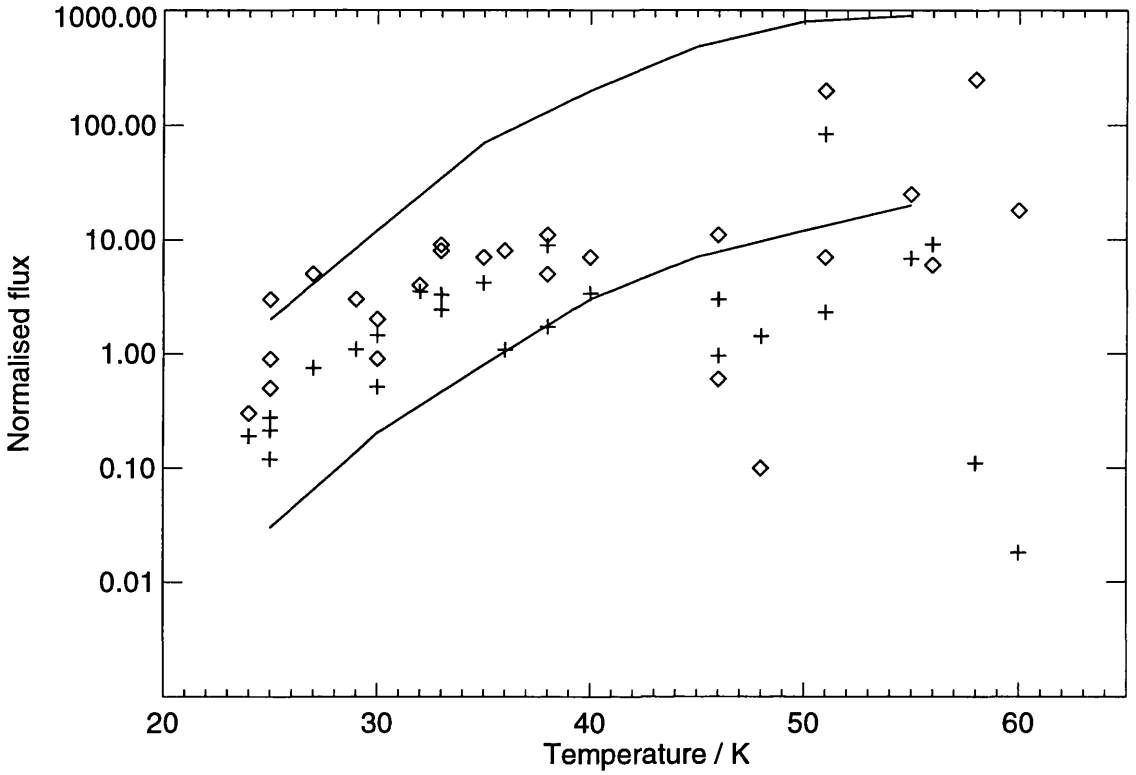

Figure 2.6: *Normalised fluxes versus effective temperature for EUV-selected sample of white dwarf stars. Pluses and diamonds indicate the S1 and S2 fluxes respectively. The top and bottom curves represent the S2 and S1 fluxes for a pure H atmosphere, with* $N_H = 10^{18}\, atm\, cm^{-2}$.

It should be noted that if one can fit a star with a particular H/He abundance homogenous model, then usually *any* other H/He abundance homogenous model within limits (given that the star must remain optically a DA, i.e. no helium absorption visible) including pure hydrogen atmospheres, gives an acceptable fit.

There are no cases where a pure hydrogen atmosphere will not fit, but adding trace helium achieves a good fit. Thus I can place these stars into two rough groups: those fitted with homogenous atmospheres, for which I cannot usefully constrain the helium abundances within the known DA boundaries; and those that are not fitted by *any* homogenous H+He model. This again reinforces the view that the discrepancies arise because of stratification and/or levitated metals, rather than helium abundances in a homogenous atmosphere. Amongst the stars I can fit successfully, there are also two distinct groups: those which show agreement between optical and EUV temperatures, and which are well fitted by the homogenous H+He models; and those whose optical temperatures are higher than their EUV temperatures.

It is tempting to speculate if the causes of the two groups of stars I find difficulty in fitting are mutually exclusive: one caused by, say, levitated metals in an otherwise homogenous atmosphere, the other caused by having stratified atmospheres with thin topmost hydrogen layers. However, it is not possible to say that all of the stars which I can fit well must have homogenous atmospheres, since, with the available data, it is not possible to distinguish between a homogenous atmosphere with relatively very little trace helium, and a stratified atmosphere with a larger hydrogen layer.

Consider a stratified atmosphere with a moderately thick H-layer: If we now assume the layer becomes gradually thinner until the H/He transition zone is within the continuum-forming photosphere, it will at some point ($\sim 10^{-13}\,M_{\odot}$) become more and more transparent to the EUV photons ($\sim 100\,\mathrm{eV}$) leaving the underlying He-layer, allowing us to see He line features in the EUV, while maintaining enough optical depth to the less energetic optical photons ($\sim 1\,\mathrm{eV}$) to prevent any contamination of the spectrum with optical He line features from the underlying He-layer. As the H-layer becomes thinner still, it will eventually become transparent to optical photons ($\sim 10^{-15}\,M_{\odot}$) and, assuming the effective temperature is high enough to cause He line transitions, the star will exhibit He absorption lines in the optical

spectra.

Now consider a homogenous atmosphere with trace contamination of heavy metals, such as C, N, O, Ca, Na, Si, Fe: these have strong transitions near the EUV peak of the flux-distribution (indeed, must, if they are to be levitated into the photosphere). These elements have fewer transitions in the optical, and those that exist are generally weaker then the EUV transitions, so overall are much less evident. Thus it is feasible that significant enough quanties of metals may be present to cause noticeable EUV blanketing, yet remain invisible optically, especially with my low-resolution, low S/N FOS spectra.

It should be noted that the UV is a fruitful area for study of these phenomena. There are many heavy-element line-transitions evident in this spectral region and, for example, IUE spectra can (and have been) be used to identify whether there are significant metal abundances in the atmospheres of white dwarf stars.

In order to separate the two above cases, it would be desireable to study these stars more closely in the EUV and UV, where most of the important transitions are located. With the launch of *EUVE*, it now becomes possible to resolve some of the EUV lines (in brighter stars) which may be caused as a result of metal or He abundances. This is a potent technique which may soon aid the resolution of this long standing debate about the source of the opacities in white dwarf atmospheres.

In the case of the stars with an assumed extra photospheric opacity, we may at first think it is hard to justify a stratified atmosphere with levitation of metals, since by definition that should levitate more helium giving an effectively homogenous atmosphere anyway. However the radiative cross-section for helium is only a fraction of that for metals, since helium has many fewer transitions, and is it likely that a stratified atmosphere can exist with significant metal levitation (Chayer *et al.* 1987; Vennes *et al.* 1988; Vauclair 1988) for stars with T_{eff} >40 000 K.

However, it is not a necessity to be able to spectrally resolve EUV lines in order to rule out a particular model, if enough *ROSAT* data-points are available. A subset of the B93 sample stars cannot be fitted satisfactorily by either homogenous

or stratified H+He atmospheres. This suggests that atmospheric stratification can not be regarded as the only cause of the poor fitting in my sample either, but that, in at least some cases, there must be extra opacity in the photosphere due to levitation of metals. This is important as a proof of the radiative acceleration theory as a true competitor in the debate on atmospheric evolution in degenerate stars, since until recently it has been a theoretical argument which has had little evidence to argue either for or against.

I have investigated whether there is any correlation between the extra opacity detected in some of the stars and their surface gravity. If metal abundances are a cause of the opacities, one would expect the stars with the lowest gravities to depart most from an agreement between the two temperature measuring techniques, since it is the balance between gravitation and radiative acceleration which determines the metal abundance in the photosphere (indeed this is precisely what is found by B93).

However, the model fitting of the Balmer line profiles to the FOS spectra turns out to be largely insensitive to the surface gravity determination, due to the low S/N and resolution of the spectra. The error limits span the range of gravities allowed in my models. Thus no meaningful gravity estimates can be assigned to these stars, and no correlation with the opacity may be inferred.

2.6 Colour diagrams

In figures 2.7a & 2.7b I plot the sample of degenerate stars in magnitude–colour (Hertzsprung–Russell) diagrams. Figure 2.7a shows the newly-identified (EUV-selected) white dwarfs as diamonds and those previously known (optically-selected) as squares, on the same plot. Figure 2.7b shows the EUV-selected sample transformed into an absolute magnitude versus colour plot. On each plot I have also indicated the positions of the stellar luminosity classes I, III, V and VII, i.e. supergiant, giant, main-sequence and degenerate (the cooling curve for an average mass

degenerate star). For figure 2.7a these luminosity class curves have been shifted to represent a population of stars at a nominal distance of 115 pc, which I use as a first order estimate of the mean distance of the white dwarf population detected with the *WFC* (see § 2.4). I assume the optically-selected stars are at the same mean distance as my EUV-selected sample.

The large scatter in V magnitude of the data points about the standard luminosity class VII cooling curve in figure 2.7a is mostly due to this 115 pc distance assumption, as evidenced by the almost total absence of scatter in the absolute magnitude plot, where the distance to each star is effectively corrected for. This validitates the accuracy of the colour-magnitude and temperature-luminosity relations used to calculate the absolute magnitudes.

There will be, of course, a natural scatter even in an absolute magnitude plot due to the varying masses of the individual white dwarfs. However, the white dwarf mass function is tightly bunched about the mean ($0.6\,M_{\odot}$; see § 1.9) and the important parameter in determining the flux output, the radius, is even more constrained about its mean value ($0.0127\,R_{\odot}$). I expect the residual scatter visible in the absolute magnitude plot is due to the intrinsic population distribution combined with other sources: firstly, the data-points used to derive the absolute magnitudes—the fitted T_{eff} and colour indices—were subject to significant errors of their own. When propagated through the relations I use to derive the magnitudes, I find that these errors are less than the scatter due to intrinsic radius variations; secondly, the error, or approximations, in the relationships used to derive the magnitudes from the colour indices. The effect of these approximations is uncertain, but I expect it to produce a systematic rather than random effect on the data. The data-points in figure 2.7b may be fitted with a straight line, of slope 7.3 ± 1.3 (3σ).

The mean position of the sample coincides with the positions of the standard degenerate star cooling curves. Moreover, all the points are sufficiently far away from the luminosity class VI (subdwarf) region to conclude that it is highly unlikely

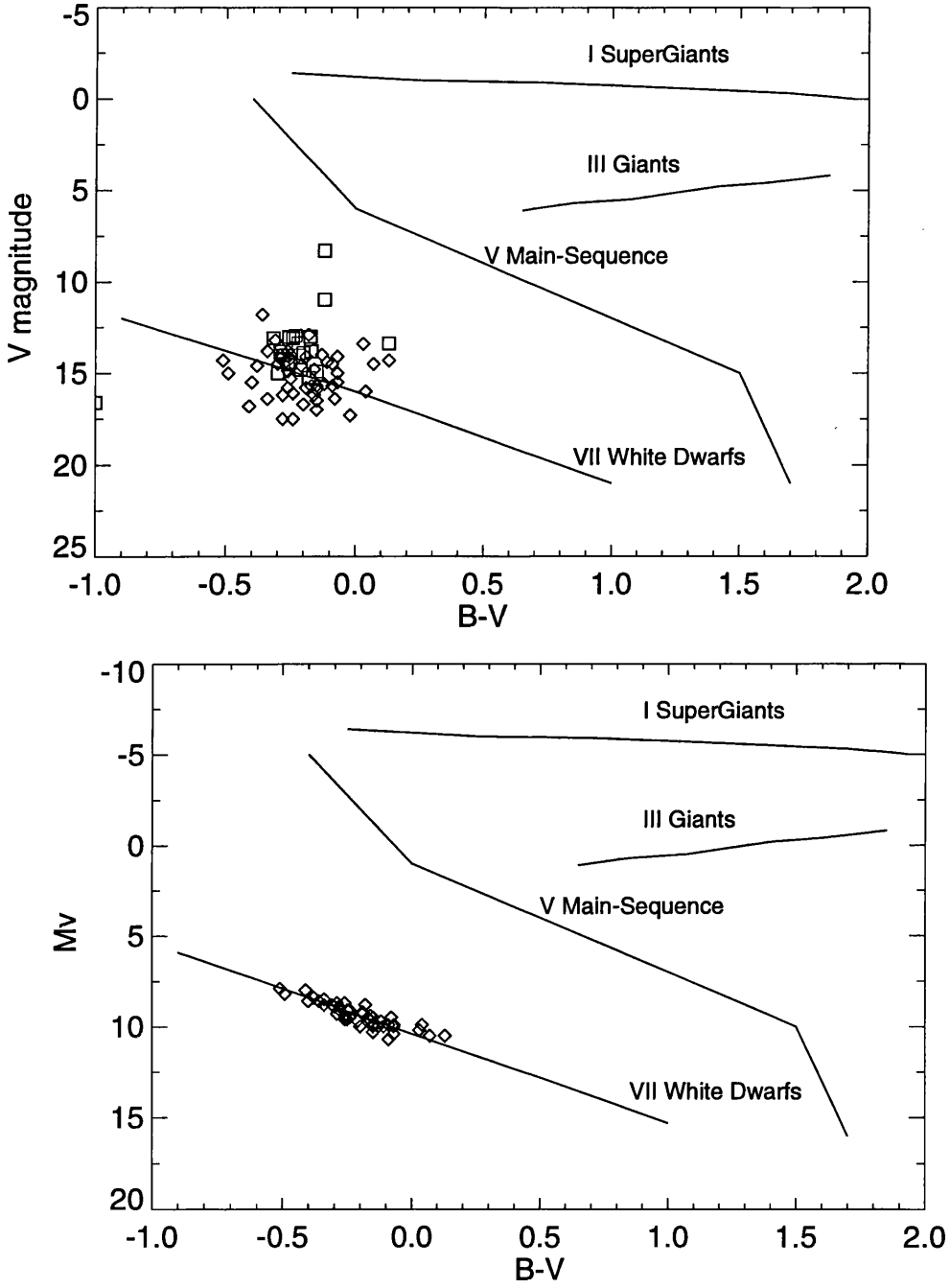

Figure 2.7: *Magnitude–Colour diagrams for (a) the uncatalogued white dwarf sample (shown as diamonds) and catalogued white dwarf sample (shown as squares) (b) transformed into an absolute magnitude plot. The solid lines indicate the Hertzsprung–Russell curves for luminosity classes I (supergiant), III (giant), V (main–sequence) and VII (white dwarf).*

any of the sample are mis-identified subdwarfs.

The EUV selected sample of degenerates appears distinctly bluer than the general population of degenerate stars (e.g., Astrophysics I: stars 1984; Introductory Astronomy and Astrophysics 1977; Zombeck 1982). This can be interpreted as due to a combination of several factors. The optical 'blueness' of a degenerate star is, of course, a measure mainly of its effective temperature and partly of its composition (since wide absorption lines can affect the colour indices). Thus we have in reality a sample of hotter than average degenerate stars, slightly skewed to those with less line blanketing in the B band than the V band. Since the *WFC* is selecting EUV bright objects, these type of stars are exactly what we expect—a cross-section of hot, mainly DA stars.

Plotting a colour–colour diagram for the white dwarf sample can also reveal useful information. Figures 2.8a & 2.8b show the sample of degenerate stars overlaid with the lines for the Main-Sequence, a blackbody radiator, and the typical reddening for an O star.

Most of the sample stars lie above the blackbody curve. However, several are prominently below the line, two of which are especially close to the main-sequence curve. Examination of the spectra of these 'low lying' stars reveals that nearly all appear to be anomalous. The two stars closest to the main sequence line are RE0029−63 and RE1746−70. The RE0029−63 spectrum is noisy, appears to show no prominent Hα absorption, and possible emission cores to the remaining observable Balmer lines (β, γ, δ). The 5577 Å night sky line is improperly subtracted from the spectrum. RE1746−70 also has a noisy spectrum, with no visible Hα absorption and the rest of the Balmer lines very weak, with possible emission core components, and emission at He II 4026 Å. Of the other stars deviating from the norm RE0443−03, RE0534−02 and RE0550−24 are all very noisy spectra with flux levels amongst the lowest of the sample. I conclude that all of these stars deviate from the norm by virtue of having either companion stars, emission features, badly fluxed spectra or absence of Balmer absorption lines.Thus, this colour technique

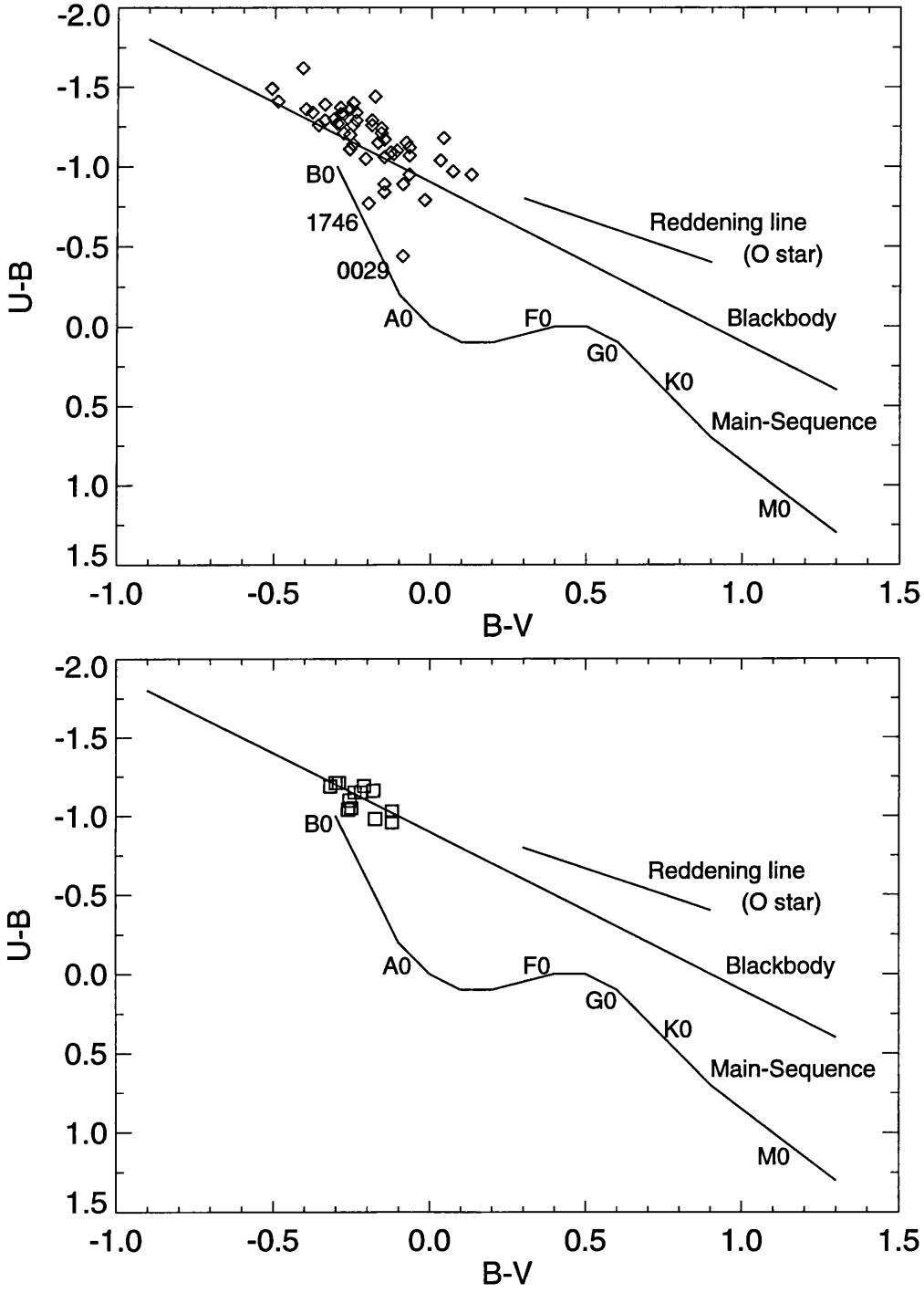

Figure 2.8: *Two-colour diagrams for (a) EUV selected and (b) EUV/optically selected white dwarf samples, shown as diamonds and squares respectively. Also shown are the blackbody radiation line, the Main-Sequence curve and a typical reddening line for an O star.*

seems to be a versatile method of separating out the anomalous stars for further investigation.

Plots of the effective temperature versus the spectrally determined colour indices, shown in figure 2.9, do show a trend of increasing temperature with increasingly negative colour index (i.e. bluer) as expected. However the scatter is very large, reflecting many causes, both intrinsic (such as composition differences) and extrinsic (error in spectrally determined colours and temperatures). The relationship is seen much more clearly in the plot of the optically-selected white dwarfs, for which much better temperature and colour determinations exist, effectively removing the scatter along these axes in the plot. There is thus little chance at present of these colour-temperature relationships constraining the parameters of the newly identified (EUV-selected) degenerate stars in any way.

2.7 Late-type binary systems

During the optical ID programme there were several white dwarf binary systems discovered, mostly by virtue of having recognizable components of two different stars in their composite spectra, or else line emission or other anomalous features which caused further investigation into those systems. Other systems had more detailed investigation because of the pecularities of their *WFC* count rates. These systems include RE1629+78 (Cooke *et al.* 1992), RE1016−05 (Tweedy *et al.* 1993a; Jomaron *et al.* 1993), RE2013+40 (Barstow *et al.* 1993a). However, up to this point, I am not aware of any *systematic* search for binary systems amongst the spectra taken for the optical ID programme. Thus, I decided to perform such a search. I am mainly interested in binary systems where the white-dwarf has a late-type companion star (dK–dM). These type of systems lend themselves to discovery more easily than, say a white dwarf and A star binary system, since the flux output of the two stars is in different wavelength regions. This means that most of these systems detected in the *WFC* survey (which have thus been looked at

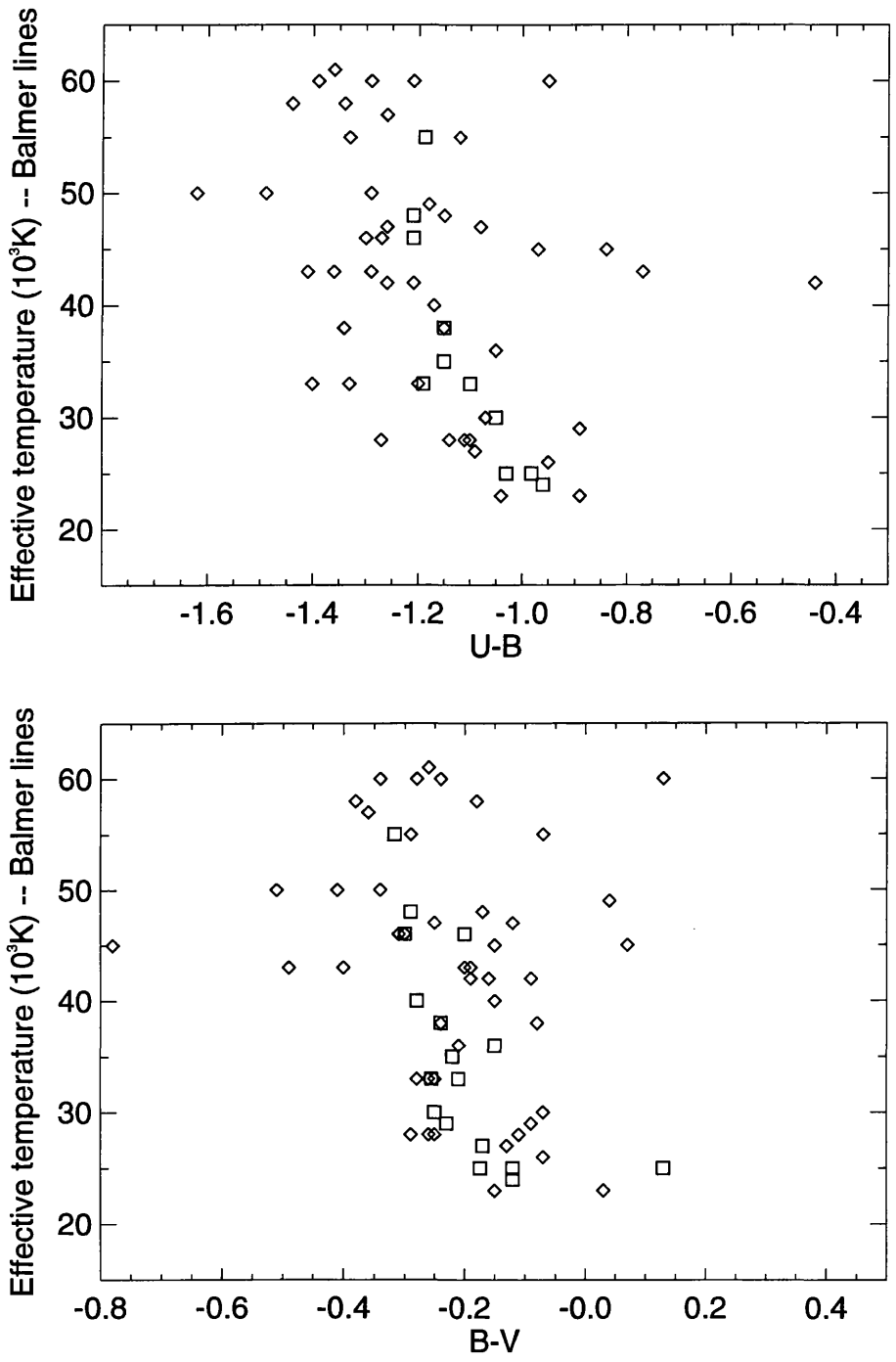

Figure 2.9: *Temperature–Colour diagrams for EUV-selected white dwarf sample. A plot of the Balmer profile derived temperatures versus the spectrally derived $U-B$ (top panel) and $B-V$ (bottom panel) colours. Diamonds indicate uncatalogued (EUV-selected) stars, squares indicate catalogued (optically-selected) stars.*

optically during the follow-up programme) have probably already been discovered (because they do exhibit an obvious spectral pecularity) except for a few systems where one component is much fainter than the other.

2.8 Search for further binary systems

To determine if any further late-type binary systems are 'hidden' in the survey data I have performed a systematic search amongst the optical spectra of all the newly identified white dwarf stars observed during the Optical ID programme. The first technique I use is as follows: I derive the $U-B$ and $B-V$ colour for each white dwarf spectrum and compare this against the usually very blue colours typical of a white dwarf. Any reddening of these colours may indicate a late-type companion star. In order to then gain information about any companion the contribution of the white dwarf must be compensated for.

I fit the EUV data from the *WFC* survey (as explained above) to determine an effective temperature for each white dwarf with unusual colours. This was augmented by Balmer line fitting to the optical spectra, where possible. Then I scaled the best fitting white dwarf model to the optical spectrum at a point where there should be negligible contribution from any late companion (i.e. $< 5000\,\text{Å}$) and subtracted the scaled model from the target spectrum. If visible late-type features were present in the residual I have concluded the system is a binary.

If the companion is very faint, however, the colours may only be slightly changed and the companion remain unnoticed. Thus I have actually checked *every* white dwarf with an optical spectrum from the *WFC* optical ID programme, by subtraction of the best fit white dwarf model (determined from the EUV and Balmer line fits) and examining the residual spectrum. Even if the companion is very faint, it may still be possible to detect one or two of the absorption and/or emission features which will have little effect on the broadband colours since they are narrow compared to the Johnson filter bands.

The sample in table 2.2 consists of 52 previously unknown white dwarfs discovered in the *WFC* survey. I passed all of these stars' spectra through my software, and after checking through the results I conclude that there are a further five candidates for binary systems with late-type companions (in addition to those mentioned earlier). These are: RE0623-37; RE0720-31; RE0831-53; RE2214-49; RE2334-47.

However, one problem arose with the flux-calibration of the RPCS; the long-wavelength end of the spectrum often shows an excess, which can to a certain extent mimic the excess seen when a faint late-type companion star is present. In order to confirm the authenticity of these systems as binaries, I have correlated the residual spectra against a set of standard star templates. I have also studied the form of the red-excess exhibited by the RPCS, in all the available spectra taken with that device, and looked for similarities in the long wavelength spectra of the candidate binaries.

After this analysis, it it seen that there is good evidence for 4 of the initial 5 systems showing real late-type dwarf star features in the red end of their spectra; that is, bands of TiO and CaOH. RE0831-53 shows no conclusive evidence of molecular bands and I thus discount it as a binary system. The surviving binaries are detailed in table 2.4.

Source	V	$U-B$	$B-V$	$V-R$	$T_{Eff-EUV}$ (K)	$T_{Eff-Balmer}$ (K)
RE0623-37	12.9	-1.44	-0.18	0.23	> 24	55
RE0720-31	15.0	-1.12	-0.07	0.38	no fit	45e
RE2214-49	11.8	-1.26	-0.36	0.47	no fit	60e
RE2334-47	13.6	-1.33	-0.29	-0.05	no fit	60

Table 2.4: *Systems postulated to have late-type companions. An 'e' indicates possible emission features in the optical spectra.*

It is notable that two of these stars (RE0623−37 and RE2214−49) are amongst those with the steepest EUV cutoffs (Tweedy 1993b) of any seen in the *WFC* survey. RE2214−49 is found to exhibit strong heavy-element lines in its IUE spectra, yet no detectable He. The divergence between the optical and EUV derived effective temperatures of this set of stars is very large. Note also that the other stars listed have no acceptable fit to the EUV data (except RE0831−53, which was the one to be discounted after the correlation stage...!). This may imply a relationship between the binarity of a system and atmospheric EUV opacities.

It should also be noted that all of these systems are in the south. However, this is not surprising: most of the similar systems (non-CV WD + dK-M) from the WFC EUV survey discovered up until now have been discovered in the north, from La Palma, and even some of those discovered in the south were identified at La Palma. One reason for this might be the much longer wavelength coverage afforded by the FOS. Reaching up to 10 000 Å, it would allow any late-type companion to be much more visible than the RPCS, which was only covering up to 7000 Å. Plus, the red excess in the RPCS tends to mask any real stellar features. Thus most of the systems visible from La Palma (i.e in the north or low south) I expect to have been discovered visually at the telescope, during the optical ID programme. This seems to be borne out by the fact my search finds no new systems in the north. However, because of the aforementioned problems, the southern systems may well remain hidden unless exhibiting line emission, and thus not be found until a systematic survey such as this.

2.9 Summary

The main points to be gleaned from these data are as follows. For most of the stars with effective temperatures below 45 000 K the EUV data can be fit with homogenous H+He models. The EUV-derived effective temperatures agree with the optically-derived effective temperatures for these stars. A portion of those

above that temperature (45 000 K) seem to have an extra source of opacity, which cannot always be attributed to interstellar column, and must therefore be in the stellar photosphere, probably in the form of levitated metals (such as Si, C, Fe, N, O) or an underlying helium layer in a stratified atmosphere. It is not possible to discriminate between the two causes with these data. Chapters 4 and 5 attempt to resolve this problem with the aid of further observations of white dwarf systems.

The profile of the population distribution of the total sample of degenerates detected with the *WFC* is in agreement with that of known white dwarfs (e.g., Bergeron, Saffer & Liebert 1992b; McCook & Sion 1987) to within my error limits. Both profiles exhibit a steady rise in number fraction from $V \sim 8$–9 to a peak at $V \sim 15$, then a sharp drop-off in number fraction to $V \sim 17$–18. We might have expected the distributions to be different, since the *WFC* detected only a subset of the degenerates (due to their EUV opacities) whereas optical studies should pick up all these stars (given that optical regions are not flux-blanketed by the opacity sources). The fact that the profiles are similar implies that, within the limits of the errors on my magnitude determinations, the EUV opacity in these stars has roughly the same correlation to the V magnitude as the optical opacity. Since the V magnitude is essentially a function of the distance to the star, this tells us that there is no stronger correlation of opacity to distance in the EUV than in the optical i.e. that the EUV opacity source preferentially obscuring many optically-detected degenerates is *not* interstellar column, and thus must be intrinsic to the star. In actual fact, the profile of the EUV-selected stars does exhibit a slightly less steep drop-off than the profile of the optically-selected stars, implying that the EUV is less attenuated by increasing interstellar column than the optical, as we expect, since hydrogen has a larger opacity to optical than EUV wavelengths. The conclusion that the selective obscuration is intrinsic to the star and not interstellar column is an important conclusion, in agreement with that reached by other authors, but via different techniques. Of course, the V magnitude is also a function of the effective temperature (absolute magnitude) of

the star. However, since there is no correlation between the absolute magnitude of the star and its distance from us i.e. it is essentially a random distribution, this dependence will not affect our results. Or, to turn the argument around, this profile also tells us that there is no correlation between the distance to the star and its temperature.

The mean distance of the sample is 115 pc, spanning a range of 25-550 pc (although the upper limit may be an overestimation). The stars all lie on the standard cooling curves and none of the sample appear to be mis-identified subdwarf stars.

After an in depth examination of the set of optical spectra taken of the white dwarfs detected with the *WFC*, a number of systems are flagged for further attention, being possible late-type companion binary systems.

An important task to perform (with the acquisition of more data on these sources, such as accurate surface gravity determinations) would be the calculation of a formal luminosity function and mass distribution for the white dwarf sample detected with the *WFC* (including the catalogued white dwarfs). Luminosity functions, such as those derived with the $1/V_{max}$ technique, as in Boyle (1989) and Liebert, Dahn & Monet (1988), and mass distributions such as those in Bergeron, Saffer & Liebert (1992b) will constrain the parameters of white dwarf formation and evolution and in turn those of non-degenerate stellar formation and evolution at our galactic radius.

A further discussion of the implications of these data will be made in later chapters.

Addendum

Since the writing of this thesis, it has been confirmed that RE0720−31 is a binary system (Vennes & Thorstensen; 1994).

Chapter 3

RE1016−05: Discovery and follow-up

If the facts don't fit the theory, change the facts

Albert Einstein.

3.1 Abstract

This chapter is concerned with the extreme-ultraviolet source RE1016−05, discovered in the *ROSAT Wide Field Camera* All-Sky Survey.

The *ROSAT WFC* scanned the region containing RE1016−05 during November 1990. Routine analysis of the EUV data (see appendix B) detected a source with a combined filter significance of 80σ (68σ in the S1a filter, 52σ in the S2a filter) positioned at $\alpha_{2000} = 10^h\ 16^m\ 27\overset{s}{.}7$, $\delta_{2000} = -05°\ 20'\ 47''$, with a 90% confidence error radius of $41''$.

The measured PSS count rates were $0.52 \pm 0.02\,\mathrm{ct\,s^{-1}}$ in the *WFC* S1a filter, and $0.62 \pm 0.03\,\mathrm{ct\,s^{-1}}$ in the *WFC* S2a filter, the exposure times being 1966 s and 1512 s respectively.

The S1/S2 ratio (~ 0.84) is similar to that of many other DA white dwarfs detected with the *WFC* . The actual value of S1/S2 varies according to the spectral distribution of the star (thus the abundance of helium or trace metals levitated in

the atmosphere, or the mass of a top-most hydrogen layer) and the intervening column.

Spectroscopy of possible optical counterparts reveals an object with a composite DA white dwarf and M dwarf spectrum, offset only 19″ from the *WFC* source coordinates. The spectra exhibit hydrogen Balmer line emission in the cores of wide Balmer absorption lines (the latter arising from the white dwarf) together with weaker He I line emission. There is evidence for variability in the optical emission line flux on time scales of hours, but no variation in EUV output is detected. I classify the cool companion in the range dM1–dM3, and determine the white dwarf temperature to be in the range 37 000–47 000 K. The distance modulus derived from the red dwarf data is 5.3 ± 0.8. In this chapter, after presenting the observational work and data analysis, I discuss possible production mechanisms for the emission line spectrum and the nature of the system. I also note the presence of a dM0 star only 3″ away from RE1016−05, and conclude that it may be a distant third member of the system.

3.2 Optical observations and identification

A finding chart of the sky region containing RE1016−05 was produced from the COSMOS scans of the SERC UK Schmidt Plates (see Appendix B) and is displayed in Figure 3.1.

The associated astrometric position-magnitude listing is presented in Table 3.1.

These show that object A is the most likely candidate for the optical counterpart, being the closest to the position of the *WFC* source and brighter ($V = 13.2$) by seven magnitudes than any other object within the error circle. The coordinates of star A are $\alpha_{2000} = 10^h\,16^m\,28\overset{s}{.}6$, $\delta_{2000} = -05°\,20'\,33''$, only 19″ distant from the *WFC* position.

Object A was observed in February 1991 as part of a programme to identify *WFC* survey sources using the Isaac Newton Telescope (INT) on La Palma. I was

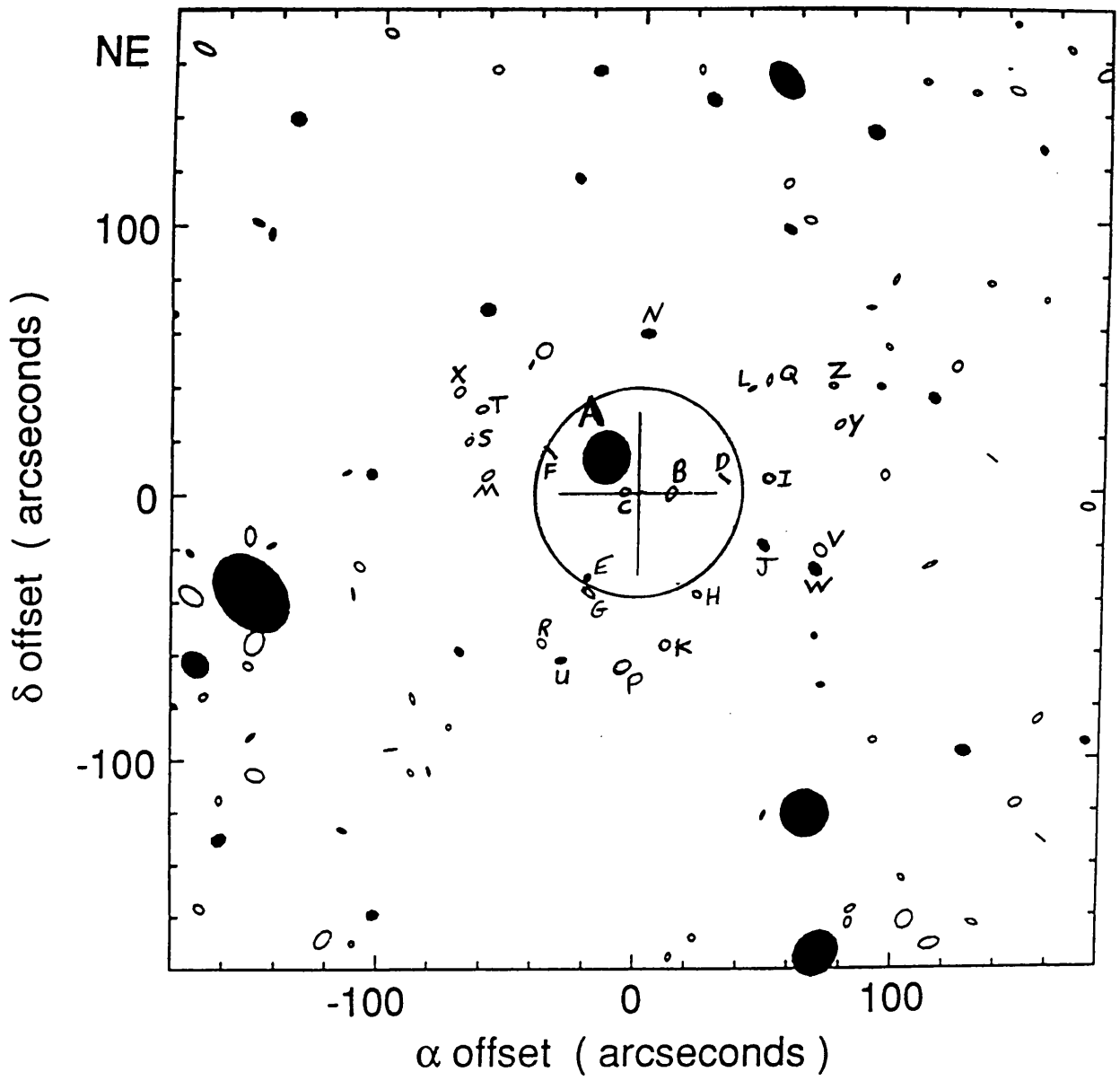

Figure 3.1: *Optical finding chart centred on the* WFC *position of RE1016−05* ($\alpha_{2000} = 10^h\,16^m\,27\overset{s}{.}7$, $\delta_{2000} = -05°\,20'\,47''$) *which is indicated by the cross. The error circle has a 90% confidence radius of 41″. The optical counterpart of the EUV source is marked as star 'A'. Note that the solid circles indicate stellar objects, open circles indicate non-stellar objects.*

Star	α_{2000} h m s	δ_{2000} ° ′ ″	J mag.	Separation ′
A	10 16 28.55	-5 20 33.7	13.27	0.31
B	10 16 26.89	-5 20 47.3	22.08	0.20
C	10 16 28.07	-5 20 46.6	23.45	0.09
D	10 16 25.50	-5 20 42.2	23.68	0.56
E	10 16 29.01	-5 21 18.3	20.04	0.61
F	10 16 30.00	-5 20 31.7	23.30	0.63
G	10 16 28.06	-5 21 23.9	22.52	0.69
H	10 16 26.17	-5 21 24.7	23.16	0.73
I	10 16 24.36	-5 20 41.8	21.99	0.84
J	10 16 24.46	-5 21 06.6	18.55	0.87
K	10 16 26.99	-5 21 44.0	22.09	0.96
L	10 16 24.82	-5 20 08.3	23.56	0.97
M	10 16 31.60	-5 20 40.0	22.64	0.98
N	10 16 27.51	-5 19 47.8	18.24	0.99
O	10 16 30.51	-5 19 59.0	23.67	1.06
P	10 16 28.08	-5 21 52.1	21.27	1.09
Q	10 16 24.36	-5 20 05.0	23.25	1.09

Table 3.1: *Astrometric position-magnitude listing for COSMOS finding chart of sky region containing RE1016−05. 'Separation' indicates the offset from the* WFC *position. Coordinates are J2000*

in attendance at two runs as an observing team member and to set up and modify the data processing software. Inspection of the field in the telescope acquisition camera showed object A to be double, with the two components aligned approximately North-South (referred to as A(N) and A(S) from here on), separated by 3″.2. Spectra of each star were obtained individually (with the companion object rotated out of the slit plane and a narrow slit to exclude its light) at both low and high resolution. In addition, spectra were taken of several calibration sources: flux standard stars HZ44 and EG247 (observed with the same slit width to calibrate for slit losses), F8 stars close to the target object on the sky (to calibrate for atmospheric absorption features), and spectral arc lamps (Cu-Ar and Cu-Ne). Low resolution work was carried out with the Faint Object Spectrograph (FOS), a fixed format cross-dispersing spectrograph, covering the spectral range 3500–11 000 Å. Higher resolution spectra were obtained using the Intermediate Dispersion Spectrograph (IDS). Details of the observations are presented in Table 3.2.

Additional high resolution spectra were obtained in December 1991 with the Intermediate-dispersion Spectroscopic Imaging System (ISIS) on the William Herschel Telescope, and in February 1992 again with the IDS on the INT.

Date	Instrument	CCD	Slit (arcsec)	Coverage (Å)	Dispersion (Å pixel^{-1})
16.02.91	FOS-1	GEC P8603	1.1	3230–5630	5.4
				5070–11270	10.7
22.02.91	IDS	GEC P8603	1.1	6430–6710	0.5
17.12.91	ISIS	EEV P88300	0.4	4010–4950	0.7
		EEV P88200		5810–7570	1.4
27.02.92	IDS	GEC P8603	1.4	6330–6780	0.8

Table 3.2: *Observing log for RE1016−05.*

The FOS spectrum of object A(N) (Figure 3.2) shows it to be a star of late spectral type. The original dispersion is 10 Å pixel^{-1} in the first order (red) and 5 Å pixel^{-1} in the second order (blue); the merged spectra are re-binned to 10 Å.

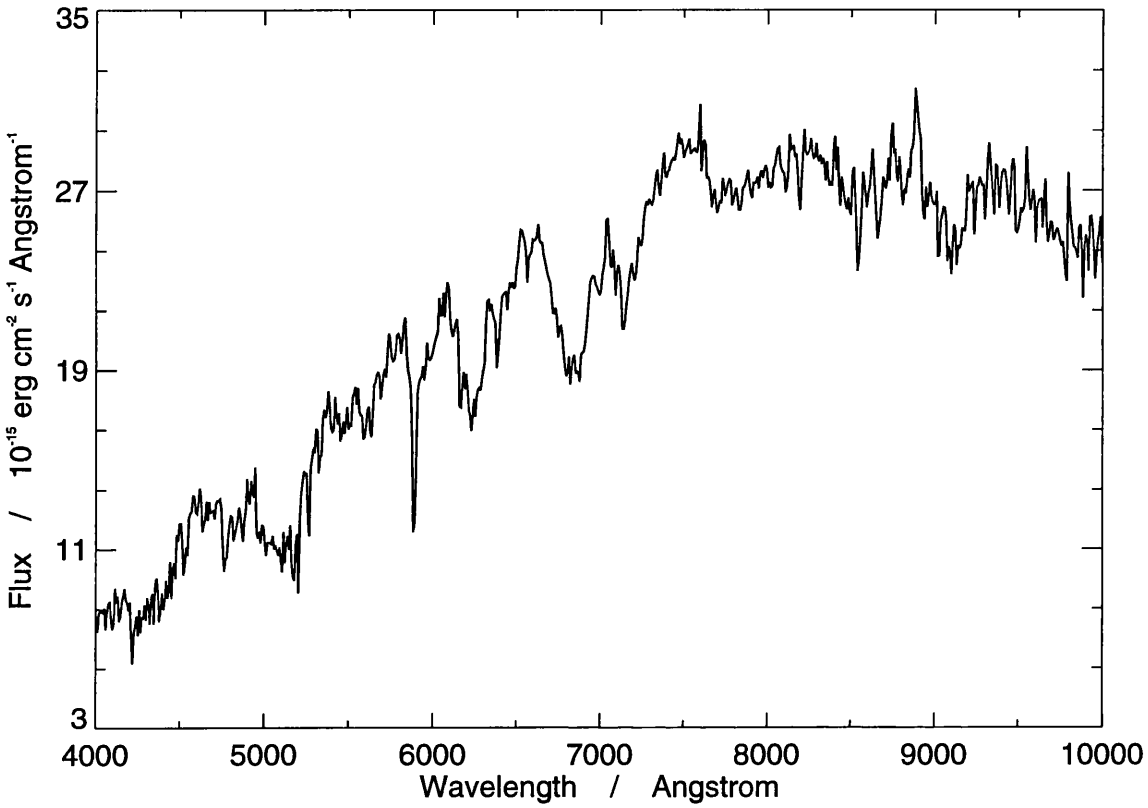

Figure 3.2: *FOS spectrum of star A(N).*

3.2.1 Classification of stellar types

After correcting the spectrum for atmospheric extinction effects (Rayleigh scattering and Telluric absorption bands) and flux calibration (see Appendix A), the *BVRI* magnitudes (Table 3.3) were obtained by convolving the calibrated FOS spectrum with the Johnson *BVRI* filter response functions. The colour indices $B-V$, $V-R$ and $V-I$ can be compared with values published for Main Sequence and giant models (Table 3.4; Zombeck 1982) to obtain a spectral type

(table 3.4). I checked this by comparing spectral features of the target star with those of standard stars, e.g., the relative strengths of 5448-5497, 5810-5862, 6158, 7054-7126 Å (TiO), 7945 Å (CN), 8320-8433 Å (TiO, CN) absorption lines and also the slope of the long wavelength spectrum (table 3.5). Standards were taken from two sources—the STARLINK DIPSO software package and the MSSL database of previous FOS observations. Finally, I used software recently written for the optical identification programme to perform a cross-correlation of star A(N) spectra with those of the standard stars. Combining all three results, for star A(N) I arrive at an overall classification of dM0 $\pm$ 1 ($V = 13.5 \pm 0.2$).

Star	V	$B-V$	$V-R$	$V-I$
A(N)	13.5 ± 0.2	1.2 ± 0.1	1.6 ± 0.1	2.3 ± 0.1
A(S) M-star	15.3 ± 0.2	1.7 ± 0.1	1.5 ± 0.1	2.3 ± 0.1
A(S) total	14.2 ± 0.2	0.1 ± 0.1	0.8 ± 0.1	1.2 ± 0.1

Table 3.3: *Johnson magnitudes and colours for stars in the field containing RE1016−05. 'A(S) total' refers to the magnitudes for the composite spectrum, 'A(S) M-star' refers to the magnitudes extracted for the M-star component alone.*

Star	$B-V$	$V-R$	$V-I$
K7 V	1.3	1.2	1.9
M0 V	1.4	1.3	2.2
M1 V	1.5	1.4	2.5
M2 V	1.5	1.5	2.7
M3 V	1.6	1.6	2.9
M4 V	1.6	1.7	3.2
M5 V	1.6	1.8	3.5
M0 III	1.6	1.2	2.2
M1 III	1.6	1.3	2.3
M2 III	1.6	1.3	2.4
M3 III	1.6	1.5	2.8
M4 III	1.6	1.7	3.4
M5 III	1.6	2.2	4.1
A(N)	1.2	1.6	2.3
A(S)	1.7	1.5	2.3

Table 3.4: *Johnson colours for standard stars similar to RE1016−05.*

Stellar type	Slope
	10^{-4} erg s^{-1} cm^{-2} Å^{-2}
M0 V	-3
M1 V	-1
M2 V	0
M3 V	1
M4 V	2
M5 V	5
A(S)	0
A(N)	-2

Table 3.5: *Comparison of the long-wavelength spectral slope of the M-star in RE1016−05 with standard M stars. The slope is that of a simple straight line fit to the continuum, measured over the wavelength region 8000–9500 Å.*

The FOS spectrum of object A(S) is shown in Figure 3.3. The dispersion is 10 Å pixel^{-1} in the first order (red) and 5 Å pixel^{-1} in the second order (blue), the merged spectra were re-binned to 10 Å.

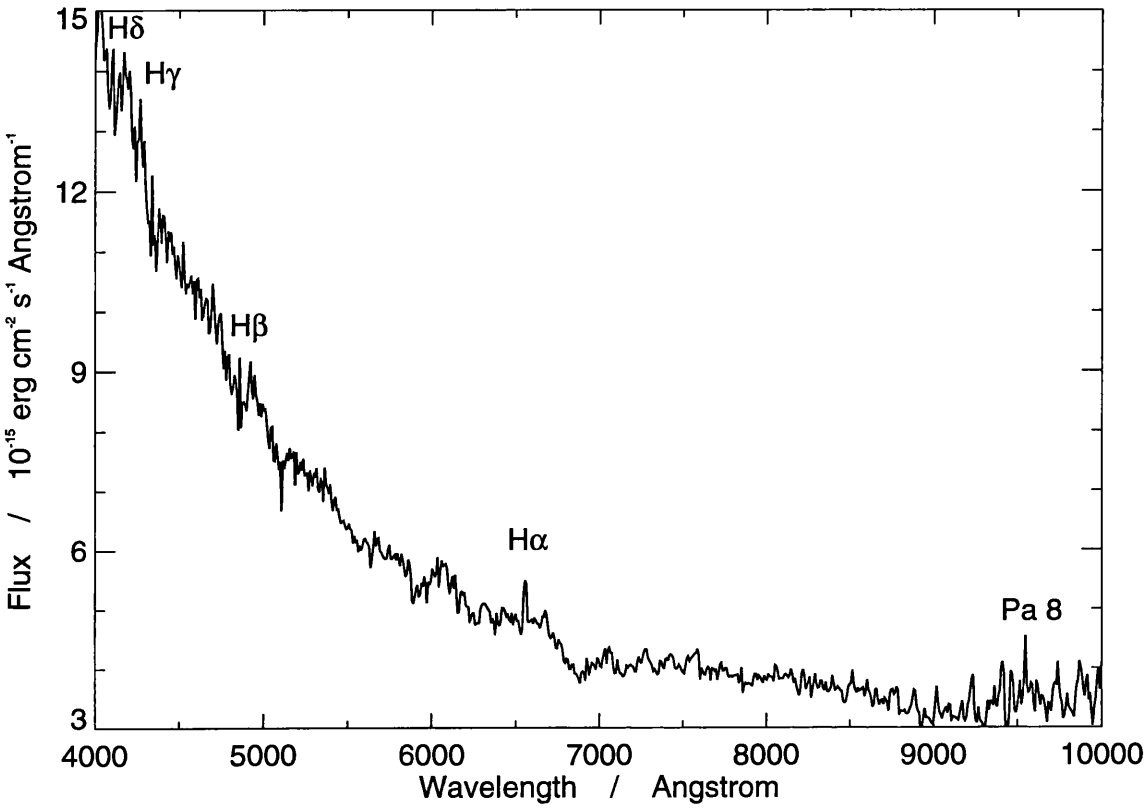

Figure 3.3: *FOS spectrum of A(S).*

Towards the blue it exhibits a steeply rising continuum with broad absorption lines—characteristic of a white dwarf. Prominent absorption bands characteristic of a late type dwarf are present in the red. In addition Hα line emission is discernable. Using the same procedure as for A(N) I obtain a V magnitude of 14.2 ± 0.2 for A(S).

Detailed inspection of the FOS spectrum of A(S) reveals hydrogen Balmer lines in absorption at Hα, Hβ, Hγ and Hδ, which are broad, but very shallow. There are no discernable helium absorption features. I infer a hot, mainly hydrogen atmosphere white dwarf component, of type DAwk (Jaschek & Jaschek 1987).

There are also detections of narrow emission lines at Hβ, Hγ, Hδ, He I 6678 Å and Paschen series lines Pa8, Pa9, Pa10.

3.2.2 Stellar parameters

The IDS spectrum (Figure 3.4) taken in February 1991 confirms the presence of narrow Hα line emission (with an upper limit to the FWHM of 1.9 Å) in the spectrum of object A(S) superposed on the broader absorption line typical of a white dwarf. However, I cannot derive an absolute flux from the IDS spectrum since conditions were not photometric. The IDS spectrum of star A(N) (also Figure 3.4) does not show any evidence of line emission.

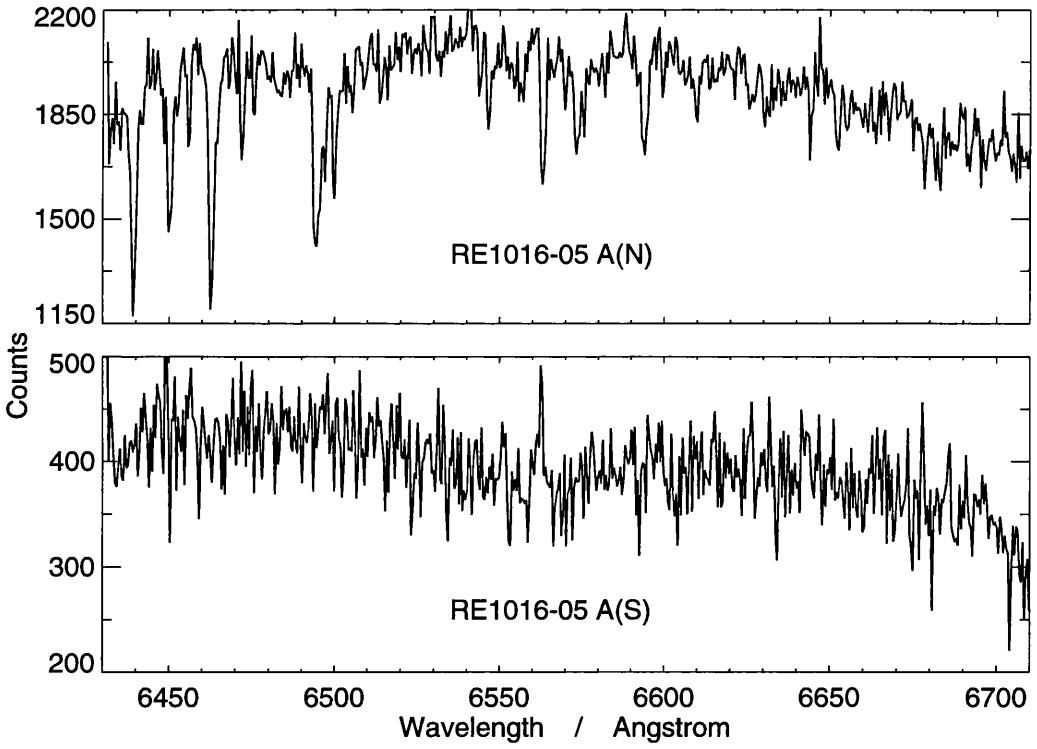

Figure 3.4: *IDS spectra of the M stars in A(S) and A(N).*

A simple preliminary modelling of the overall shape of the spectrum of object A(S) was attempted. Using a range of late type standard star templates and a set

of white dwarf model atmospheres (Jordan & Koester 1986; Koester 1991), I find that a good fit to the FOS spectrum is obtained with a M0–M5 dwarf ($M_{Vm*} \sim$ 9–12) and a $40\,000 \pm 15\,000$ K DA white dwarf ($M_{Vwd} \simeq$ 9–10). Figures 3.5 and 3.6 compare individual spectra for a M2 dwarf and a 40 000 K DA white dwarf against the observed spectrum of A(S). The relative flux contribution in the V band of the white dwarf is almost twice that of the M star. Assuming the quoted intrinsic magnitudes of the mean fitted template stars ($M_{Vm*} \sim 10$, $M_{Vwd} \sim 9.5$), I estimate a combined intrinsic magnitude of ~ 9, thus the distance modulus is $\sim$ 5.

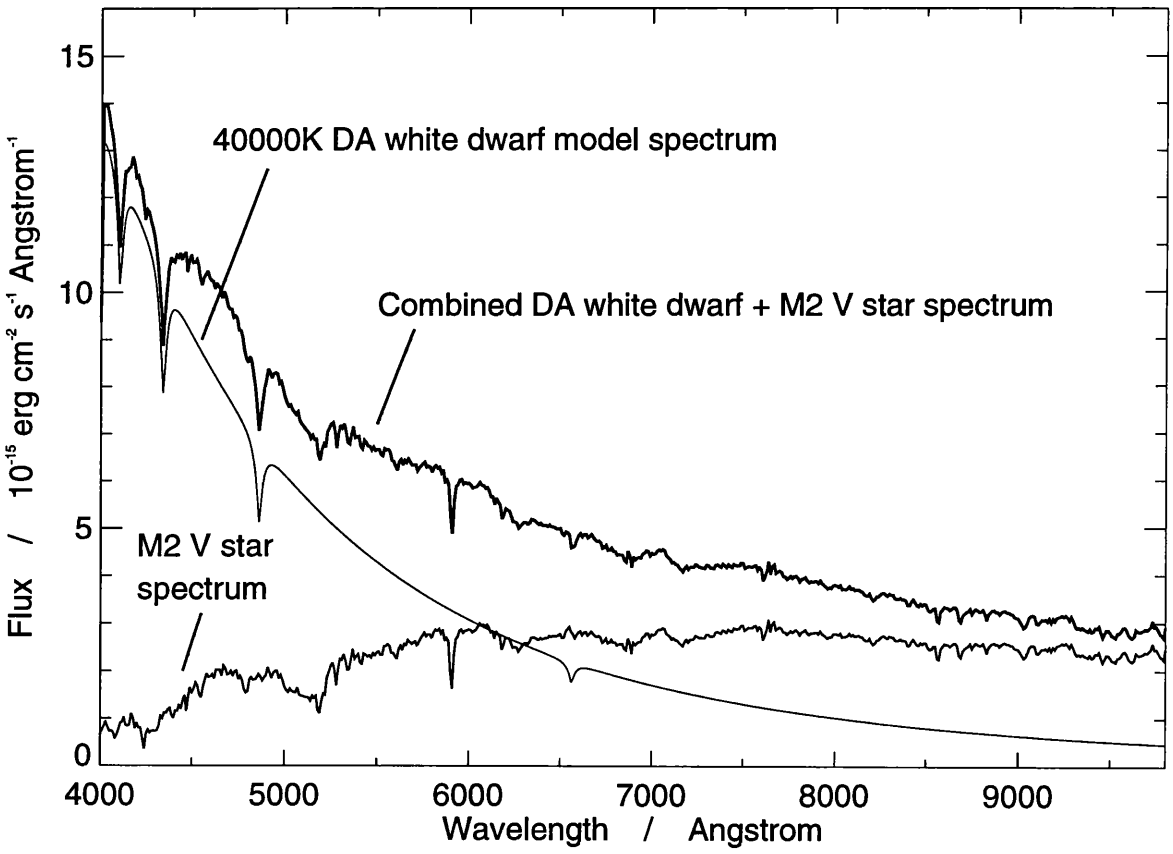

Figure 3.5: *Modelling of the white dwarf and M star components of A(S): individual spectra of a 40 000 K DA white dwarf atmosphere and an M2 dwarf star are shown alongside the combined spectrum.*

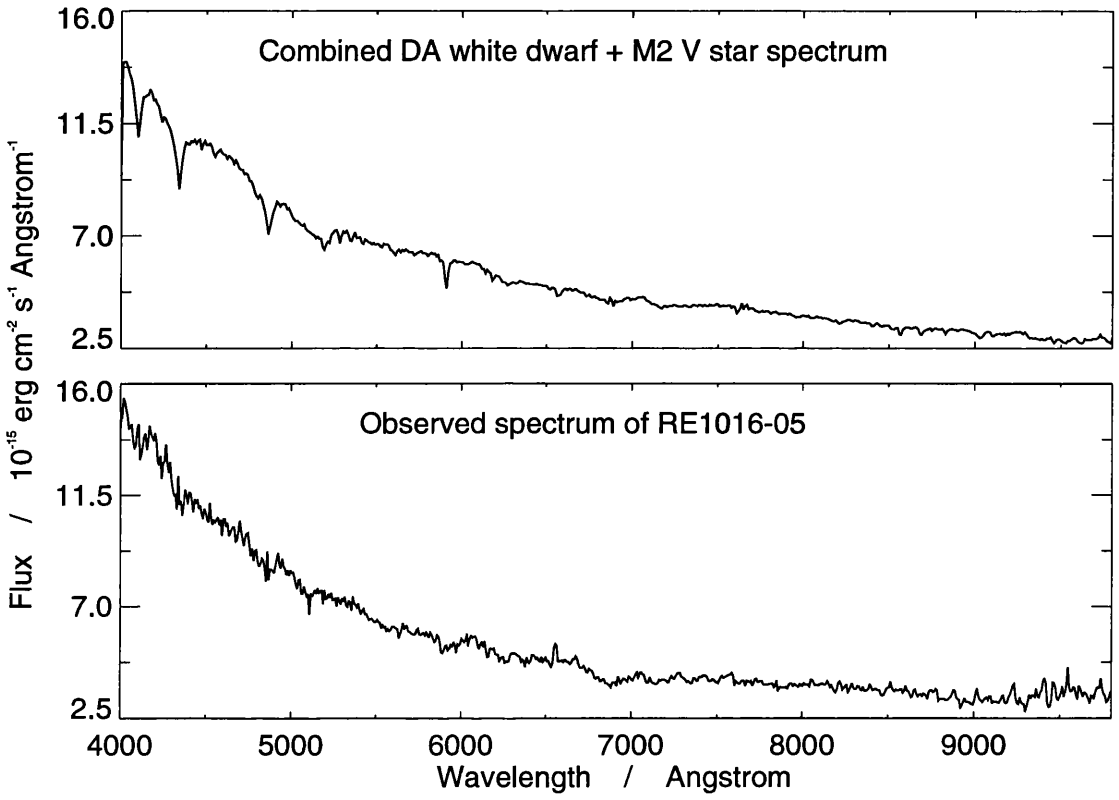

Figure 3.6: *Modelling of the white dwarf and M star components of A(S): the observed spectrum is compared to the simulated spectrum. Note that there are no Balmer emission lines included in the simulated spectrum.*

The December 1991 ISIS spectra reveal, for the first time, clear evidence of He I emission at 4471, 4921, 5874 and 7065 Å in addition to the 6678 Å line already seen, and Balmer emission down to Hδ. Figures 3.7 and 3.8 show the blue and red arm ISIS spectra respectively.

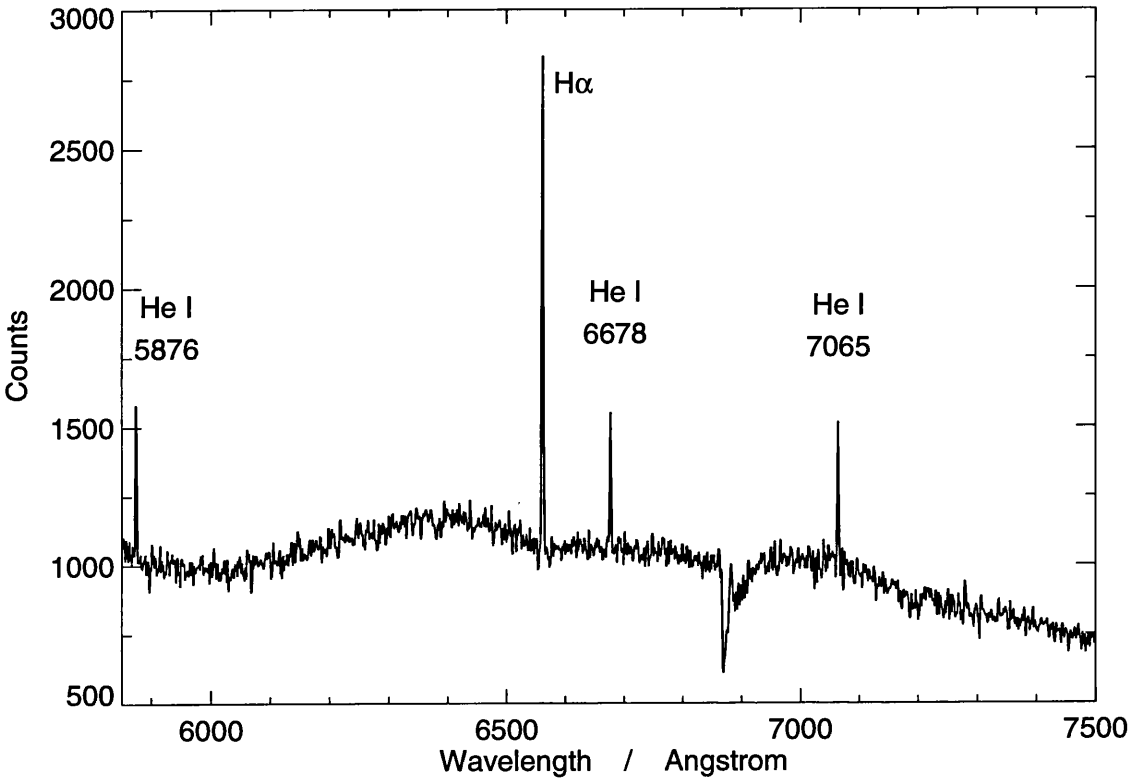

Figure 3.7: *ISIS 'red arm' spectrum of A(S). The dispersion is 1.4 Å pixel^{-1}. He I lines at 5874, 6678 and 7065 Å are seen in emission. Hα is strong in emission. Note this spectrum is not flux calibrated.*

3.2.3 Emission line variability

The IDS spectra taken in February 1992 (figures 3.9 and 3.10) show evidence for variability in the flux level of the Hα line emission over a period of a few hours. A problem with the CCD electronics on the night of observation resulted in a variable response, so these spectra cannot be used to make an absolute measurement of the

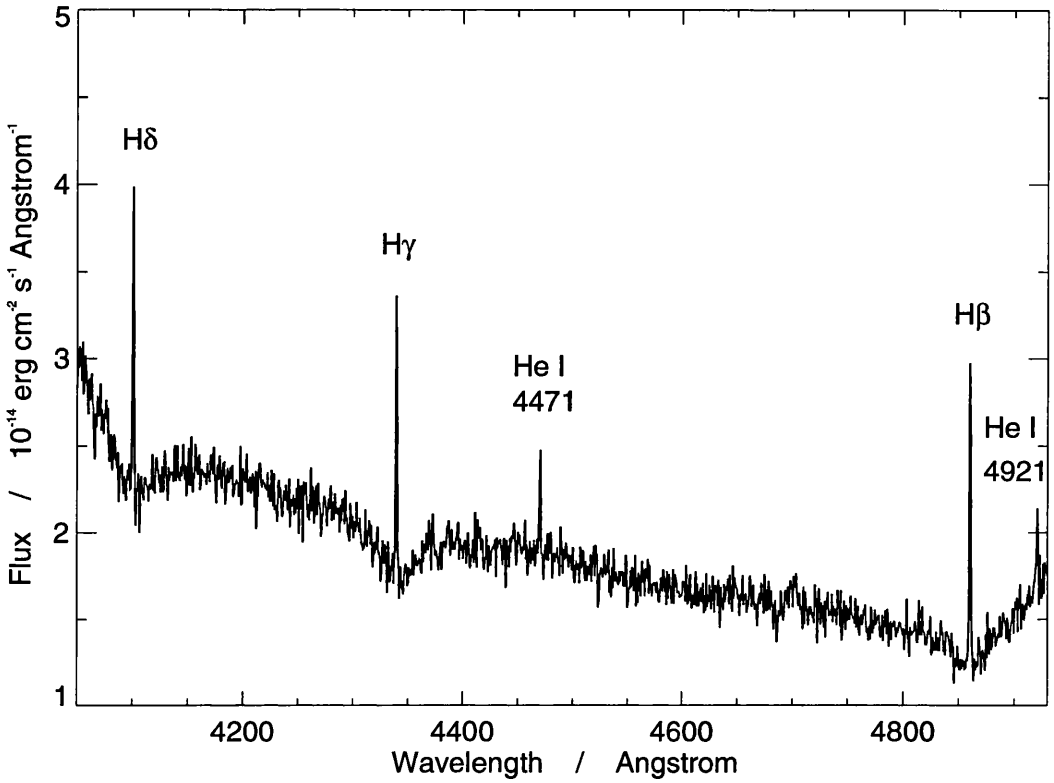

Figure 3.8: *ISIS 'blue arm' spectrum of A(S). The dispersion is 0.7Å pixel^{-1}. He I lines at 4471 and 4921 Å are seen in emission. The Hβ, Hγ and Hδ Balmer lines are seen as broad absorption lines with narrow emission cores.*

flux variation (i.e. the flux levels are consistent during the night, but varied between the nights).

However, one can estimate the changes in line flux relative to continuum by a comparison of the equivalent widths. The spectra show the equivalent width of the Hα emission line decreases by almost a factor of 3 over a period of 3.5 hours. Table 3.6 summarises the velocities, fluxes, FWHM and equivalent widths of the detected lines from those spectra (FOS, IDS and ISIS) which have reliable calibrations.

Date	Line	Velocity ($km\,s^{-1}$)	Flux ($10^{-14}\,erg\,s^{-1}\,cm^{-2}$)	FWHM ($km\,s^{-1}$)	Eq. W (Å)
	Hα	–	2 ± 2	–	4 ± 3
	Hβ	–	1 ± 2	–	1 ± 2
02.91	Hγ	–	3 ± 2	–	2 ± 2
	Hδ	–	3 ± 2	–	2 ± 2
	Hα	-55 ± 3	–	100 ± 5	5.3 ± 0.3
	Hβ	-75 ± 5	2.7 ± 0.6	55 ± 12	1.9 ± 0.4
	Hγ	-75 ± 6	2.2 ± 0.7	45 ± 14	1.1 ± 0.4
	Hδ	-68 ± 9	2.2 ± 0.6	57 ± 17	0.9 ± 0.2
12.91	HeI λ4471	-69 ± 13	0.7 ± 0.9	47 ± 13	0.4 ± 0.7
	HeI λ4921	-67 ± 12	0.6 ± 0.4	49 ± 12	0.3 ± 0.3
	HeI λ5876	-66 ± 9	–	55 ± 11	1.5 ± 0.3
	HeI λ6678	-59 ± 7	–	36 ± 9	1.2 ± 0.2
	HeI λ7065	-59 ± 7	–	42 ± 9	1.3 ± 0.2
	Hα 01:11	-90 ± 6	2.1 ± 0.3	40 ± 10	3.4 ± 0.5
02.92	Hα 03:40	-60 ± 14	0.8 ± 0.3	60 ± 30	1.6 ± 0.6
	Hα 04:31	-70 ± 19	0.5 ± 0.3	0 ± 40	1.2 ± 0.7

Table 3.6: *Optical emission line parameters for RE1016−05.*

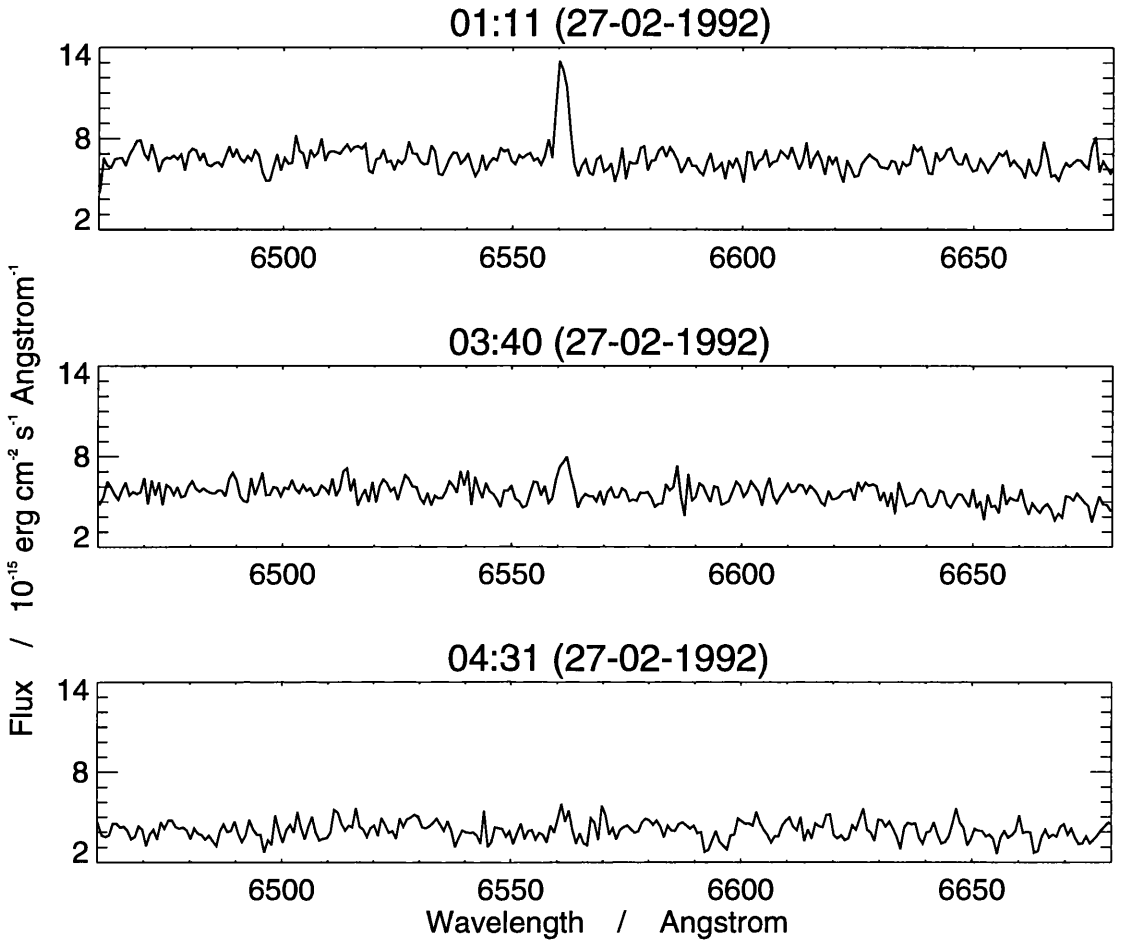

Figure 3.9: *IDS 'red' spectra*

3.2.3.1 *Continuum variability*

Closer inspection of the February 1992 IDS spectra (figures 3.9 and 3.10) seems to reveal a further change. Looking at the blue and red spectra in time sequence, we see that not only does the Hα emission vanish from the red spectra, but the Hδ absorption disappears from the blue spectra. Furthermore, there is an overall flux decrease in both the red and blue spectra. The continuum slope of the blue spectra becomes redder i.e. there is a greater loss of blue light, while the continuum slope

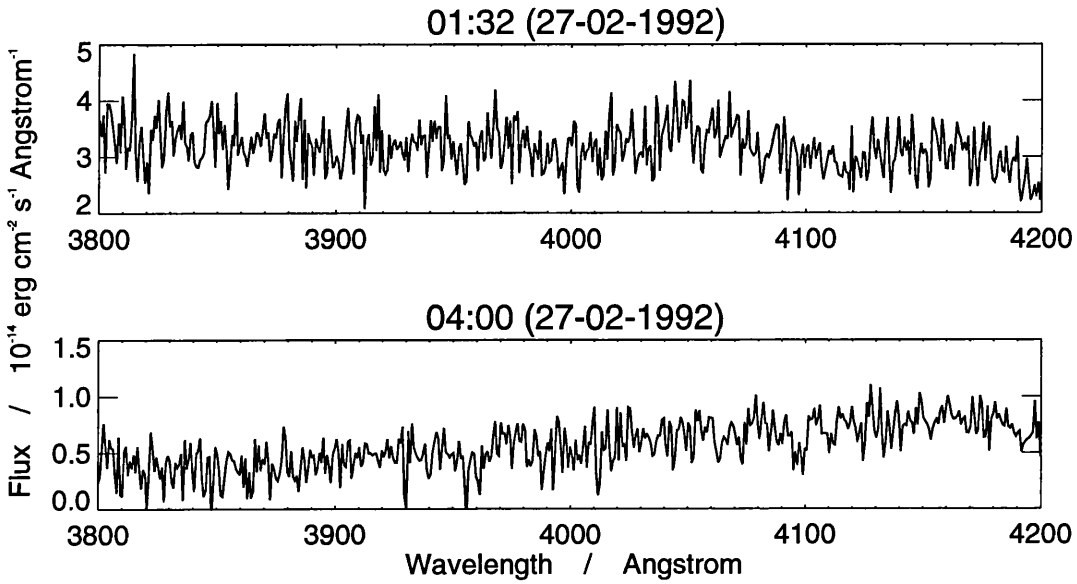

Figure 3.10: *IDS 'blue' spectra*

of the red spectra stays constant. To quantify these apparent changes I measured a crude 'V/R' ratio for each spectrum (simply breaking the spectrum into two halves and dividing the average flux level in the short wavelength half by that in the longer wavelength half). I also fitted a power law model to each spectrum to obtain a slope indicator in the form of the power law index, α. The results are tabulated in table 3.7. I have included, for comparison, values obtained for some IDS spectra taken at other dates. As can be seen, there is a definite loss of blue light in the blue spectra, while the relative slope of the red spectrum is unchanged. It is important to determine if these changes are real or not, since exactly these set of circumstances could be caused by an eclipse in a high-inclination close binary system when the white dwarf passes behind the M-star, if the Balmer lines are emitted from the irradiated face of the M-star. A simple flare, which could explain the emission line changes, could not explain the other changes.

The most common cause of blue light loss in a spectrograph is a difference between the position angle of the spectrograph slit and the parallactic angle. The

parallactic angle is that angle which, projected onto the sky, is vertical. Ideally, the slit should be rotated to the parallactic angle in order to avoid differential refraction losses, since the differential refraction occurs in the vertical direction.

The telescope logs show that all the observations on 27.2.1992 were made with a *constant* position angle. Thus during the night the difference between the position angle of the slit and the parallactic angle grew larger. The actual discrepancies are given in table 3.7. From this, we can see that by the time of the second observation in the blue, the slit has rotated to a much greater angular distance from the parallactic angle. This may be enough to account for the severe loss of blue light in these spectra. The red spectra, while undergoing a similar increase in the angular distance away from the parallactic angle, may be less affected, since the loss of red light is much less severe in the case of differential refraction (because refraction follows a wavelength dependent relationship). There should be an overall flux level reduction, as we observe in both sets of spectra. This theory can explain the apparent loss of the Hδ line, since the greatly reduced S/N may no longer be sufficient to resolve it. However, it does not explain in itself the large reduction in the Hα line equivalent width since I judge the overall loss of red light is only slight. This is more likely due to intrinsic variability in the line emission itself.

Another possibility for the loss of blue light is an incorrect extinction calculation. I note that the airmass the objects were observed through was increasing during the night, such that each exposure has a greater airmass than the previous exposure. If there is an insufficient extinction correction, this could lead to an artificially reduced flux, which becomes more severe at shorter wavelengths. To investigate this possibility, I have calculated the value of extinction used by the original reduction and compared this with the value of extinction I calculate (based on the data measured by the Carlsberg Automatic Meridian Circle [CAMC] on the night of the observations) with a more rigorous procedure. A full theoretical calculation of the extinction involves three components: Rayleigh scattering; molecular absorption; aerosol scattering (see appendix A). The correction used by the data

Spectrum (No.)	Continuum Flux 10^{-15} erg s^{-1} cm^{-2}	Power law index α	V/R	Divergence from p.a. degrees	Airmass
24-02-91					
red					
814	4.7	-6.0 ±1.0	1.2 ±0.1		
815	4.7	-6.0 ±1.0	1.2 ±0.1		
27-02-92					
red					
215	6.6	-3.5 ±0.5	1.1 ±0.1	63	1.2
225	5.5	-4.7 ±0.5	1.2 ±0.1	105	1.5
229	4.1	-5.3 ±0.5	1.2 ±0.1	112	2.0
16-02-91					
blue					
554	23.0	-1.6 ±0.4	-		
27-02-92					
blue					
217	26.0	-1.8 ±0.4	1.1 ±0.1	71	1.2
227	4.5	+11 ±0.8	0.6 ±0.1	108	1.7

Table 3.7: *Power law fits and 'V/R' for RE1016−05 spectra.*

processing software is based only on the Rayleigh scattering component. While this is sufficient in many cases, the presence of ozone and more importantly, dust, in the atmosphere can significantly alter the value of the extinction. Unfortunately, dust will in general produce a 'grey' extinction, i.e. non-wavelength dependent. This would result in an flux decrease over the whole spectrum. It is apparent from the red spectra that there is only a minimal change in the overall flux level, which (if it was due to dust) could not account for the drastic loss of blue light in the blue spectra. If I hope to explain the change in terms of extinction, I must look for an underestimation of the wavelength dependent terms. To do this, I performed a worst case analysis. On the assumption that all the extinction measured by the CAMC on the night of observation was caused by Rayleigh scattering and molecular absorption, with no aerosol contribution, I recalculated the extinction at the wavelengths and airmasses of the object spectra. The maximum extinction difference between the blue spectra in this case is 0.34 magnitudes. Even assuming no correction was made by the original processing, this change will not account for flux level change by a factor of 6. Furthermore, and this is the crucial test, there is a maximum change in extinction across the blue spectrum itself of 0.15 magnitudes between the two exposures. This is not enough to produce the required change in slope of the blue spectrum. My conclusion is that an incorrect extinction correction cannot in itself be the cause of the selective loss of blue light, although it may contribute a small part to the overall effect.

To summarise, it is most likely that the changes seen are due to a progressive wavelength dependent light loss at the spectrograph, caused by differential refraction with the slit not rotated to the parallactic angle, rather than any eclipse of the components in the binary system or an incorrect extinction correction.

3.3 Data analysis: Optical, EUV, X-ray

In this analysis I assume not only that the pair of stars in A(S) form a physical binary but that it is the white dwarf which emits practically all of the EUV emission detected by the *WFC* . Preliminary optical modelling (section 2.2.1) shows the white dwarf has a higher optical flux (figure 3.5) than the M star; the EUV/optical ratio of even very active dM stars, 10^{-2} (Jeffries *et al.* 1991), is many orders of magnitude lower than that of a typical DA white dwarf, ≥ 10, so any EUV contribution from the dM star in A(S) is likely to be negligible i.e. $\leq 0.1\%$ (in fact, the EUV/optical ratio I derive for RE1016−05 from later analysis is $\simeq 100$, close to that calculated for a pure hydrogen model atmosphere).

3.3.1 *WFC* Survey EUV data

The *WFC* EUV data on RE1016−05 were manually reduced, using the ASTERIX software system, as a check against the automated reduction of the survey processing. The relevant event data were sorted into a set of (background subtracted) images and timelines representing the three scans *ROSAT* made over the source area in each of the survey filters. The source count rates in each filter were measured and a set of fluxes derived, assuming a spectral model for the emission mechanism. Figure 3.11 displays for both survey filters the images created from the scans over RE1016−05. The corresponding timelines are shown in figure 3.12.

The PSS count rates derived in this manner are $0.53 \pm 0.02\,\mathrm{ct\,s^{-1}}$ in the S1a filter, and $0.60 \pm 0.03\,\mathrm{ct\,s^{-1}}$ in the S2a filter. These count rates are close to the values derived by the automated survey processing, thus I have confidence in using them in my calculations. The EUV timelines show no visually apparent periodic or aperiodic flux variation. The lightcurves were passed through two different period searching routines which also detected no significant periods. However, given that the timelines are of very short duration (shorter than the spin periods of many white dwarfs in binary systems) one cannot rule out the existence of a

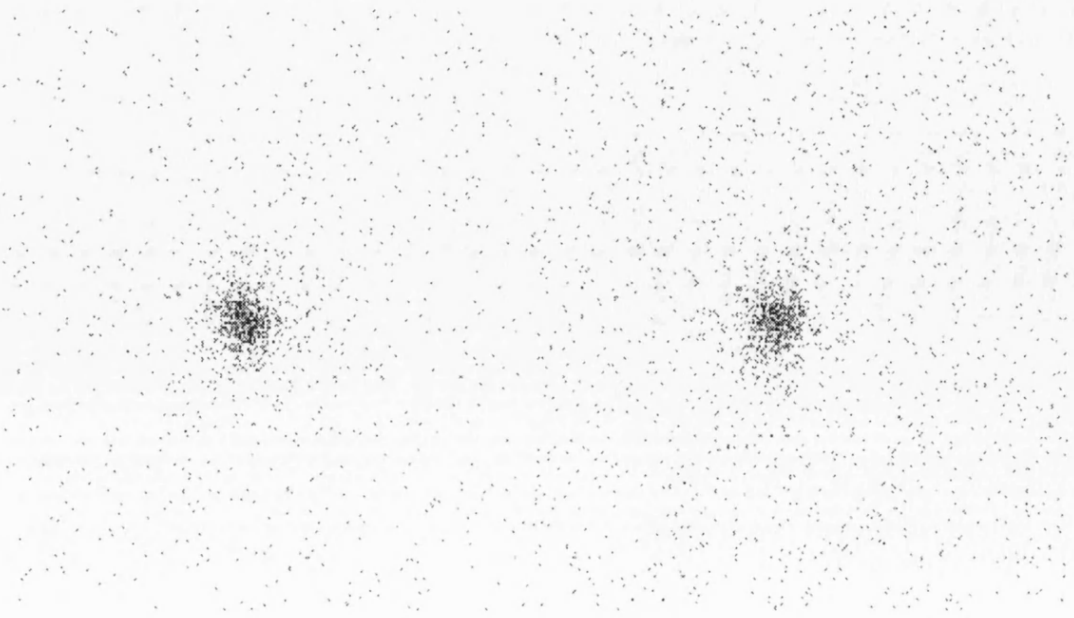

Figure 3.11: *EUV images (S1 and S2 filters) of RE1016−05 produced from the* WFC *survey scans.*

long-timescale periodic variation in the EUV emission from RE1016−05.

3.3.2 *WFC* Survey EUV data: model fitting

The use of both *WFC* filter count rates can, in principle, constrain the effective temperature of the white dwarf and the interstellar absorbing column density to the system (and with some assumptions, the elemental abundance of the white dwarf atmosphere). To achieve this, model DA white dwarf spectra are normalised to the apparent magnitude of the white dwarf component of RE1016−05 (V_{wd} = 14–15, calculated from the intrinsic magnitude and distance modulus estimated in section 2) and folded through the *WFC* S1 and S2 filter responses. Assuming the atmosphere is hydrogen with homogeneously mixed trace helium, for any particular ratio of these elements, value of surface gravity, and *WFC* filter, curves of constant count rate (mean value plus error estimates) are generated in an effective temperature versus column density plane. If the generated count rates are set equal to the observed count rates, the area between each set of curves represents

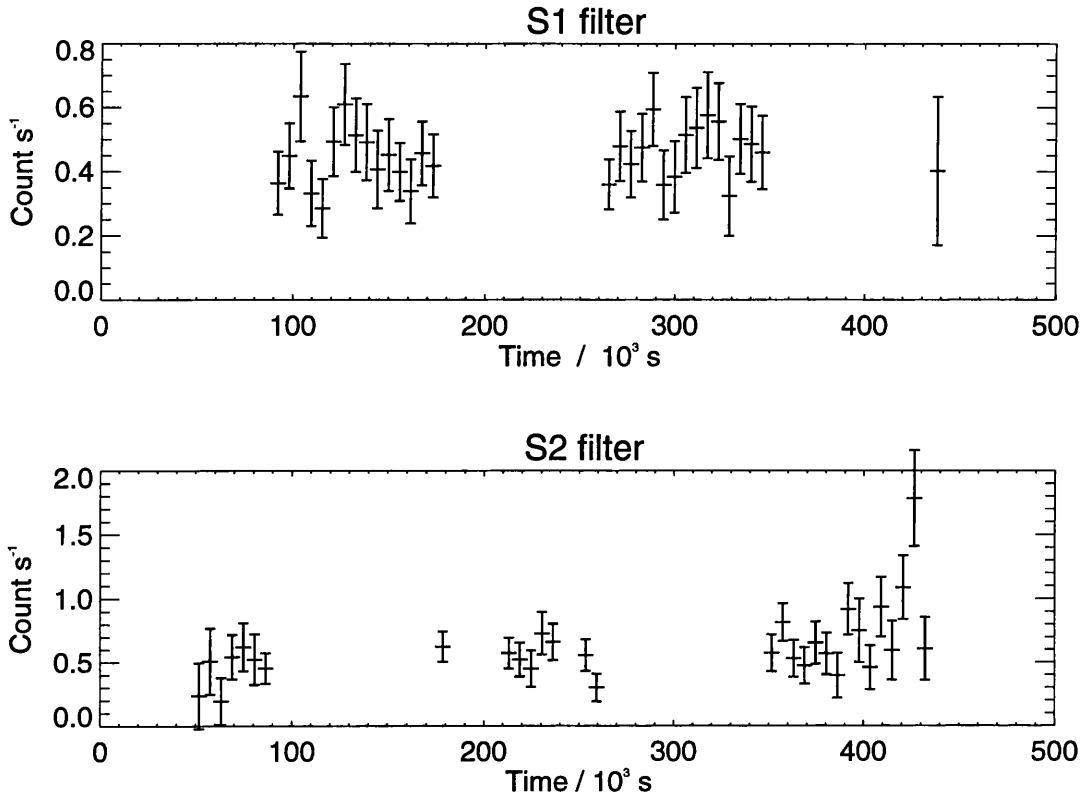

Figure 3.12: WFC *EUV timelines of RE1016−05.*

the parameter range for which the white dwarf model is consistent with the data in that filter. The area defined by the intersection of both filter curve sets is the model temperature–column density range consistent with both *WFC* filter data. Models ranging from pure hydrogen to He/H ratios of 10^{-3} (Table 3.8) were used. In practice, however, the two survey filters are insensitive to the precise helium abundances and do not alone select any particular abundance model (the pointed mode *WFC* filter P1 [56–83 eV, 150–220 Å] would be more suited for this task, lying close to the 228 Å He edge). I regard the model richest in He (He/H = 10^{-3}) as unreasonable since it requires an abnormally low column density plus a high effective temperature for the white dwarf. Considering the other models, I derive an acceptable temperature range of 37 000–49 000 K, with a column density of N_H = (1–4) $\times 10^{19}$ atm cm^{-2}.

He/H Ratio	Temperature (K)	N_H (cm^{-2})
0	37 000–47 000	(1.0–4.0) $\times 10^{19}$
10^{-5}	37 500–48 000	(0.63–3.2) $\times 10^{19}$
10^{-4}	43 000–49 000	(0.00032–1.6) $\times 10^{19}$
10^{-3}	59 000	(0.00032–3.2) $\times 10^{17}$

Table 3.8: *White dwarf atmospheric parameters from EUV fit to RE1016−05.*

Figure 3.13 shows the results for models with varying log (g) and helium abundance.

3.3.3 *WFC* Pointed mode EUV data

A 4.3 ks *ROSAT* pointed observation of RE1016−05 was obtained during December 1991. The aim of the observation was to detect the source with the *WFC* and P1 filter and with the XRT and PSPC detector. However, after the proposal had been approved and the observation scheduled, the *WFC* detector suffered a response degradation that greatly reduced the effectiveness of the observation in the EUV band. The *WFC* event data were processed to produce images of the observed area (the 4.3 ks observation consisted of three separate exposures), which were then searched for sources. No significant sources were found at or near the expected location of RE1016−05. This is probably due to the reduced efficiency of the *WFC* detector, assuming that the source had not varied since the survey detection (although I cannot rule out this possibility). Upper limits (3σ) to the count rate were derived to be 0.0018 ct s^{-1}, 0.0025 ct s^{-1} and 0.0031 ct s^{-1} for the three exposures. It was hoped that these data should feed back into the EUV modelling of the white dwarf atmospheric parameters (section 2.3.1), to refine the

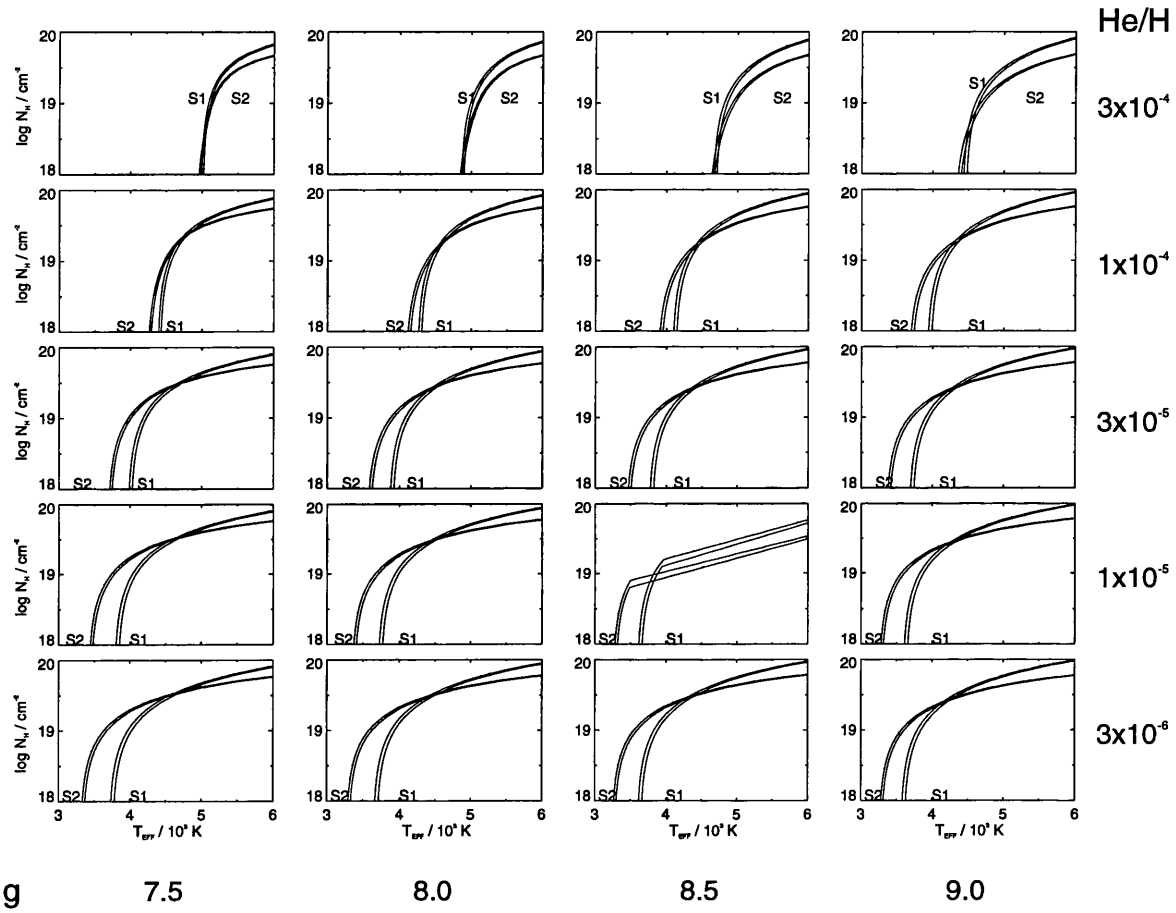

Figure 3.13: *Curves of constant* WFC *count rate plotted in the log* (N_H) *versus* T_{eff} *plane, for white dwarf model atmospheres of differing surface gravity and abundance. The region delineated by the overlap of the S1 and S2 curves gives the possible range of white dwarf effective temperatures and interstellar absorption column densities allowed by each model.*

constraints on the effective temperature, surface gravity and column density. The P1 filter is a very sensitive indicator of helium abundance, since its passband lies close to the helium edge at 228 Å. However, I find that the measured upper limits in the P1 filter cannot constrain the parameters any further, since, in all cases, the bounding curves generated in the T_{eff} versus log (g) plane encompass the area delineated by the intersection of the S1 and S2 curves.

3.3.4 *XRT* Pointed mode X-ray data

Simultaneous with the *WFC* EUV observations, the XRT also observed, and detected, RE1016−05 with a total count rate of 0.49 ± 0.01 ct s^{-1} (in the boron filter). The data were processed to produce a set of images, timelines, and X-ray spectra of the source during the three exposures. RE1016−05 can clearly be seen in the centre of the image shown in figure 3.14. The source is obviously non-pointlike, and has been drawn into a elongated shape by a small satellite wobble (see Appendix B) uncorrected for by the data processing software. This should not affect the timeline or spectral results severely, since one can specify any size region about the source image for inclusion in the subsequent processing.

3.3.4.1 Lightcurves

The timelines are shown in figure 3.15.

There are no obvious visual periods in the dataset. The Fourier transforms of the three timelines show significant power at periods of 202 s and 80 s in order of decreasing power (the power spectra are shown in figure 3.16). Each period is not necessarily significant in all three of the exposures. It can be seen that during the second observation, the 80 s period is considerably stronger than the 202 s period, the opposite of the case for the other two observations. The periods are more clearly seen when the three individual observations are combined and Fourier transformed (bottom panel).

Folding the timeline data on either of these periods produces no apparent trend

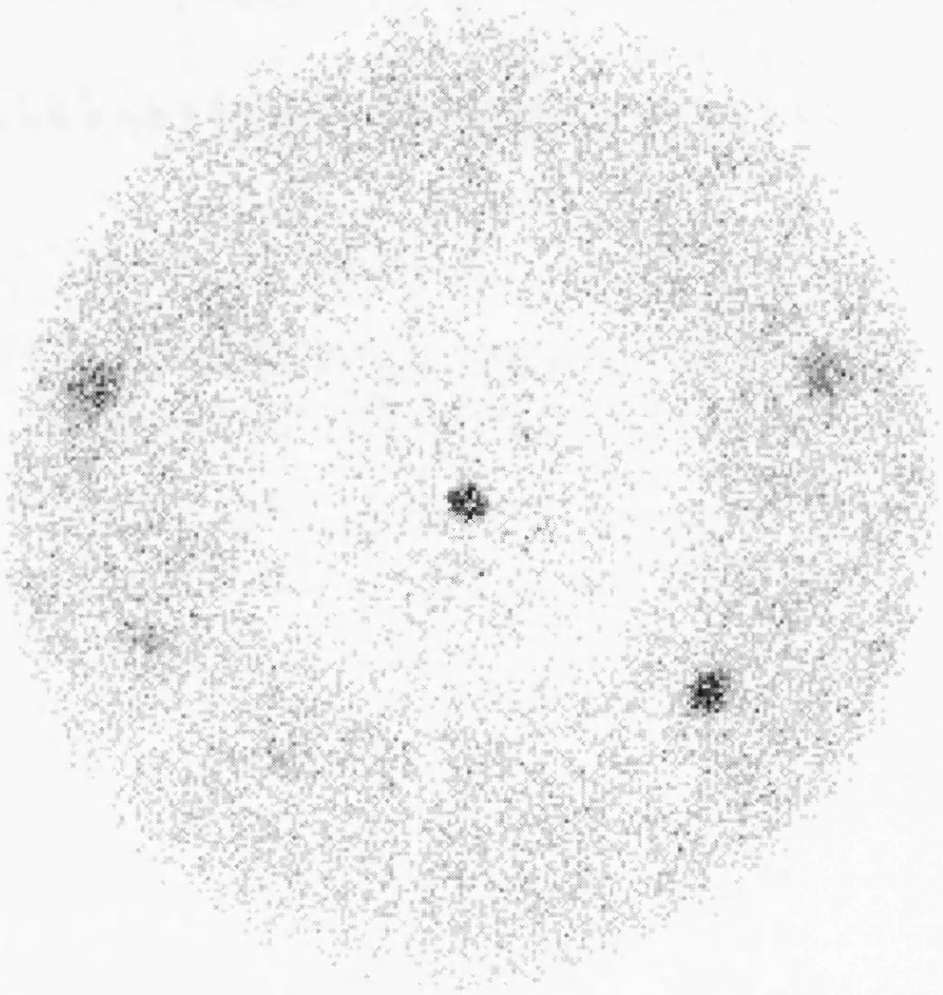

Figure 3.14: *XRT PSPC image of the field centred on RE1016−05.*

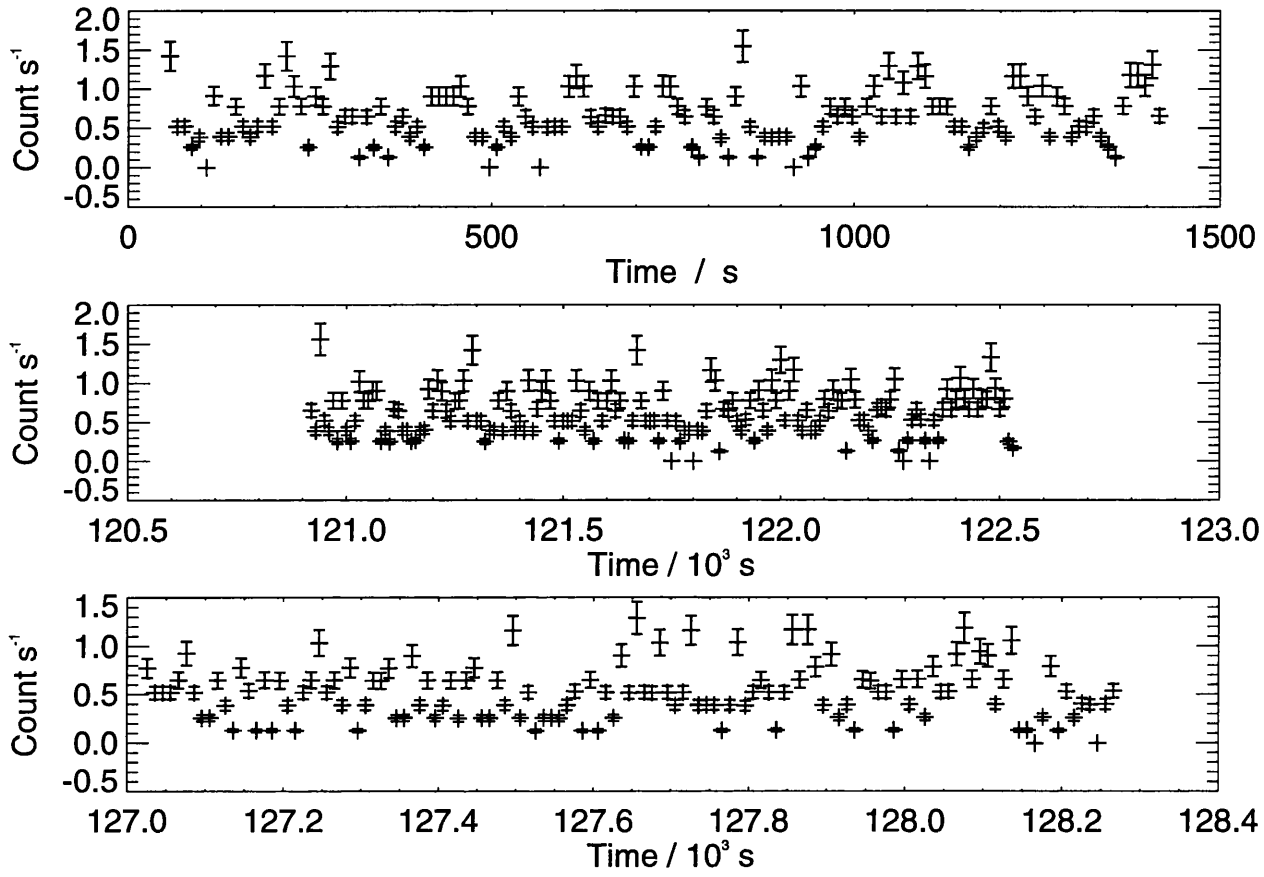

Figure 3.15: *XRT PSPC timelines of RE1016−05.*

in the data. If these periods are real, they all much shorter than one would expect to obtain from any stellar spin, orbit or pulsation modulation. They would have to originate within a small region of space or matter.

It is more likely that the periods are associated with the wobble of the *ROSAT* during XRT observations, which is induced to prevent obscuration of sources by the wire mesh. *ROSAT* is slewed in Right Ascension and Declination over a 400 second period (with a shorter period variation in roll angle). Thus any source will be occulted (in a generally uncorrectable manner, especially for an on-axis source) as it passes behind the mesh wires. Since there are three different meshes of varying size and thickness, and the whole array is effectively rotating due to the varying roll angle, with an unknown relationship between the mesh placements, it is possible to obtain an occultation of the target at any period (or several different periods) equal to or shorter than the spacecraft wobble period. To investigate the possibility of causation by the *ROSAT* wobble and mesh wires, I constructed a general model of the flux level of a pointlike source moving behind a wire mesh, at a varying speed, angle and period. The results confirm that many 'artificial periods' may be caused by this phenomenon. In general such a observation (where time-line analysis is critical) would be carried out off-axis (to prevent obscuration). However, since the main aim of this observation was to obtain a crude spectral estimate of the source flux (no variations were expected to be detectable), the best policy is an on-axis observation. As there is no method to definitively prove the cause of these periods, further speculation on their origin is deferred until observations warrant a full discussion.

After subtracting the 202 and 80 s periods there are no significant aperiodic variations remaining i.e. no flaring is observed in the lightcurve. Although this is consistent with the optical line emission being due to steady fluorescence from the irradiated atmosphere of the M-star, an intrinsically active M-star (where stochastic variability in the lightcurves is well documented) cannot be ruled out, since the flare periods are often much longer than the *ROSAT* observation duration (4 ks).

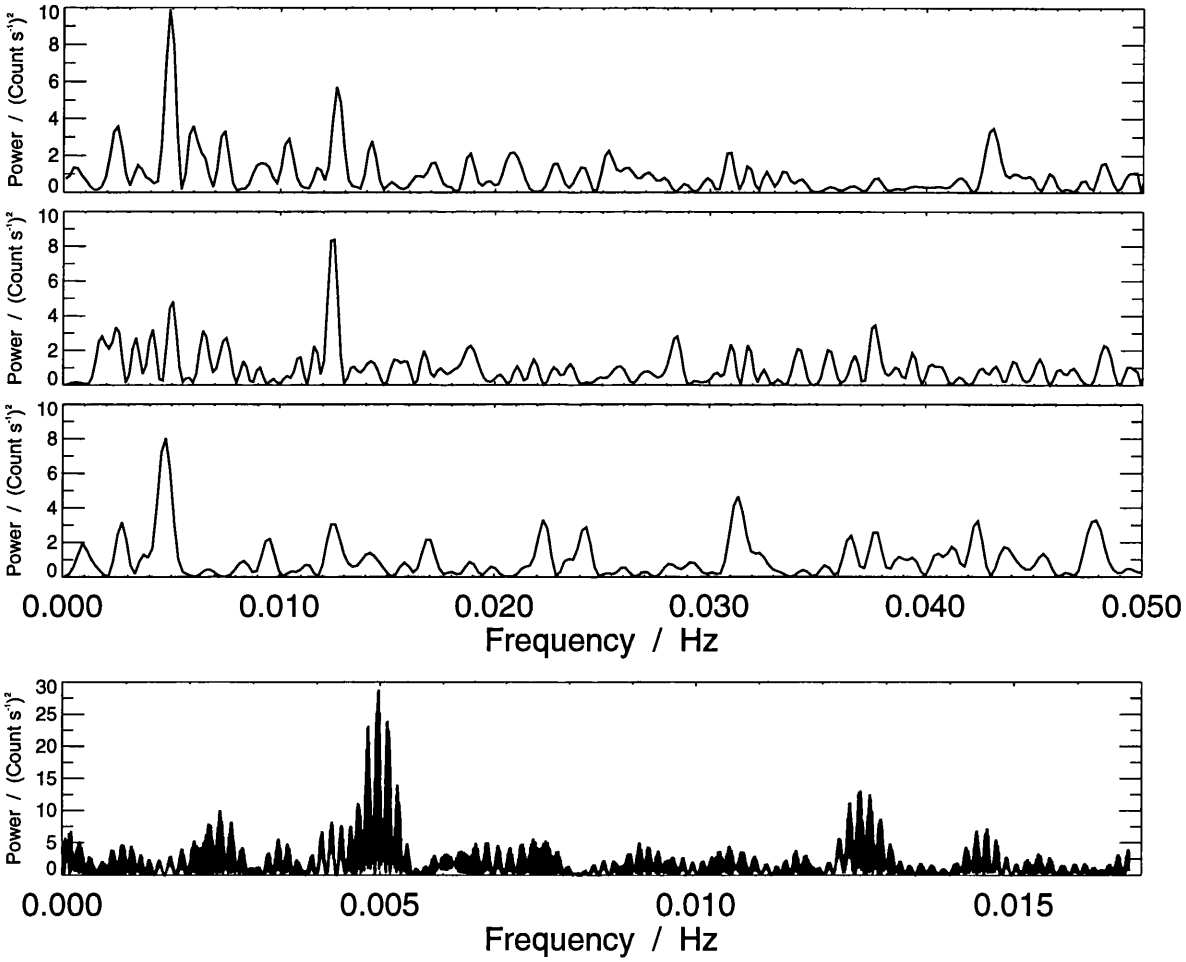

Figure 3.16: *Power spectra of the XRT PSPC timelines of RE1016−05. The top three panels show the power spectra of the three individual observations. The bottom panel shows the power spectrum of the combined exposures.*

The spectral profile of the PSPC X-ray data (Figure 3.17) shows the source to be very soft. The flux distribution peaks (with a value of 8 $\times 10^{13}\,\mathrm{erg\,s^{-1}\,cm^{-2}}$) at the lowest (reliable) energy channels observable with the PSPC ($E \sim 100\,\mathrm{eV}$) and gradually diminishes until falling below the detection threshold at $E \sim 450\,\mathrm{eV}$ (the total integrated flux is 2 $\times 10^{11}\,\mathrm{erg\,s^{-1}\,cm^{-2}}$). Since typical coronal sources, such as active M-stars, exhibit flux distributions with E >400 eV, the two close-by M-stars are unlikely to be the source of the X-rays. Even extremely soft coronal sources (such as Barnard's star) cannot account for the emission distribution, since these sources fall below the detection threshold of the *ROSAT* PSPC at only a few parsecs distance. The origin of the X-rays is more consistent with thermal emission from the white dwarf.

3.3.5 Optical data: absorption line fitting

One can independently estimate the temperature and surface gravity of the white dwarf component by modelling the Balmer absorption line profiles (cf. Bergeron *et al.* 1992). Each of the available Balmer lines (Hα, Hβ, Hγ, Hδ) is correlated against a grid of model profiles (Jordan & Koester 1986; Koester 1991), ignoring the regions affected by the narrow emission components. The models contained in the grid have pure hydrogen atmospheres, spanning the range T_{eff} = 20 000–60 000 K (in thirteen steps) and log (g) = 7.5–8.5 (three steps). For each model in the grid I calculate the correlation coefficient and χ^2 of the fit. I can then derive the 68% (1σ) and 90% (1.6σ) confidence levels in the log (g) versus T_{eff} plane. The results (Table 3.9 and Figure 3.18) show a wide spread in temperature, with the average at 44 000 K. The fits exclude (at the 90% confidence level) temperatures below 25 000 K, and the 1σ (68%) confidence levels indicate the temperature is in the range 29 000–47 000 K. The fits are not sensitive to the value of log (g).

These results have significantly larger uncertainties than those obtained by Bergeron *et al.* (1992), which were at the level of a few percent in the fitted value of T_e. Two factors may combine to explain the apparent difference. Firstly, the

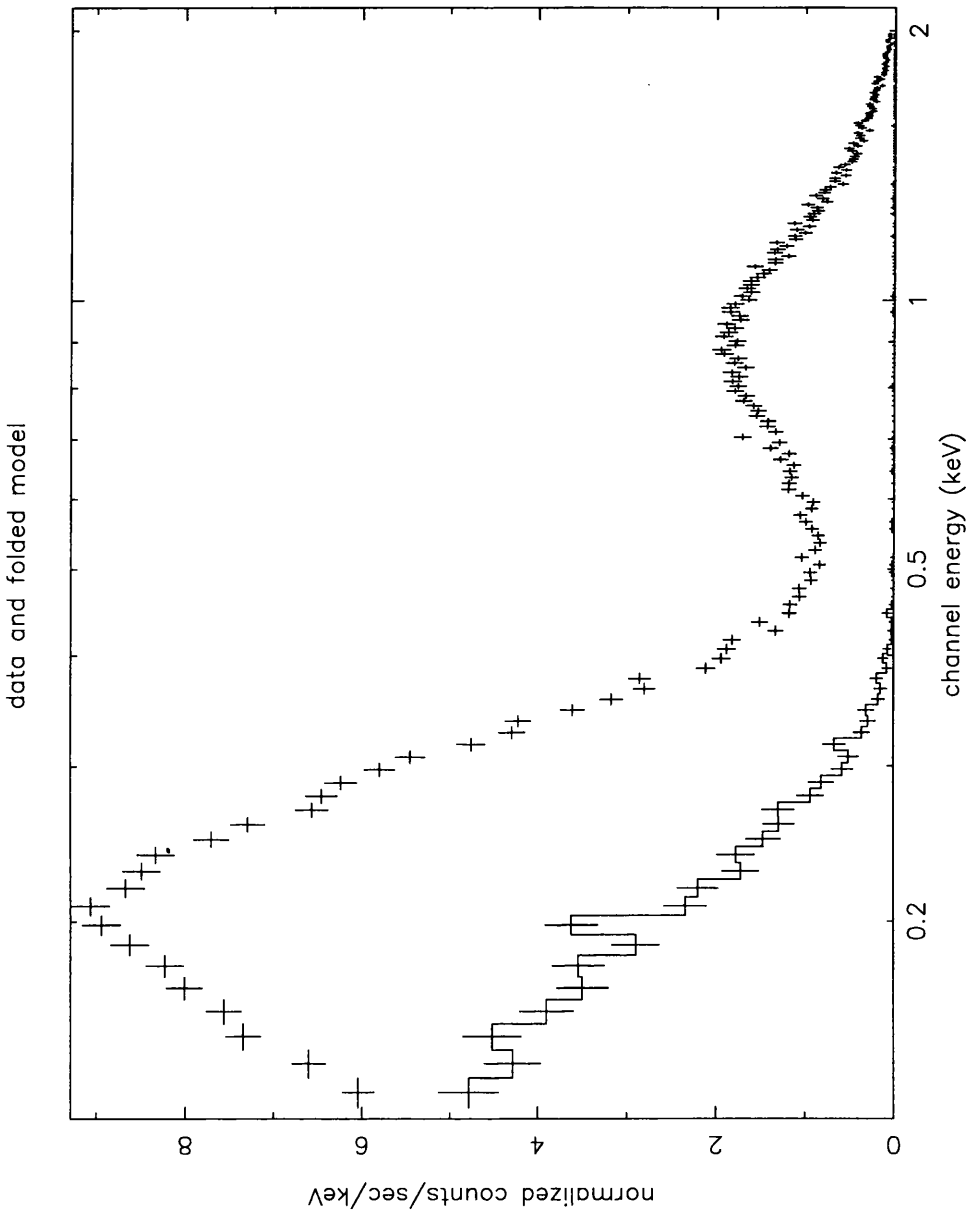

Figure 3.17: *Pulse Height Distribution of the PSPC data on RE1016−05 (lower curve). A typical coronal source (upper curve, shown offset) is given for comparison. Note the lack of hard photons (>400 eV) in the RE1016 PHD.*

partial filling of the absorption cores by the emission lines: Bergeron *et al.* exclude a similar case, HZ9, from their analysis because of this very problem. Instead, I attempt the fits after removing the emission region from our data. As there is more power in the line wings than in the core, this is not expected to affect our results significantly. The second and more likely cause of our large errors lies in the poorer signal-to-noise ratio (S/N) of our FOS spectrum. Bergeron *et al.* stress that a high S/N, preferably > 80, is necessary in order to tightly constrain the error on the resulting fits (to < 500 K), whereas our FOS spectrum has a S/N $\simeq$ 15. Moreover, our spectra have slightly poorer resolution than those of Bergeron *et al.* (8 Å as opposed to 6 Å FWHM).

Line	Best fit T_{eff} (K)	1σ constraints (K)	Best fit $\log(g)$)
Hα	60 000	no constraints within grid	7.5
Hβ	25 000	$T_{eff} \geq 24\,000$	8.5
Hγ	45 000	$28\,000 \leq T_{eff} \leq 47\,000$	8.5
Hδ	46 000	$29\,000 \leq T_{eff} \leq 48\,000$	8.5
Average	44 000	$29\,000 \leq T_{eff} \leq 47\,000$	8.5

Table 3.9: *White dwarf atmospheric parameters from RE1016−05 line profile analysis.*

In summary, my optical fits for the white dwarf component in RE1016−05 imply a temperature regime overlapping that obtained from the EUV modelling, with a common allowable range (for a pure H atmosphere) of 37 000–47 000 K.

3.3.5.1 Spectral modelling

All the available data (X-ray, EUV, optical) may be combined with the intent of using the multi-region dataset against the various models (for this I have used the

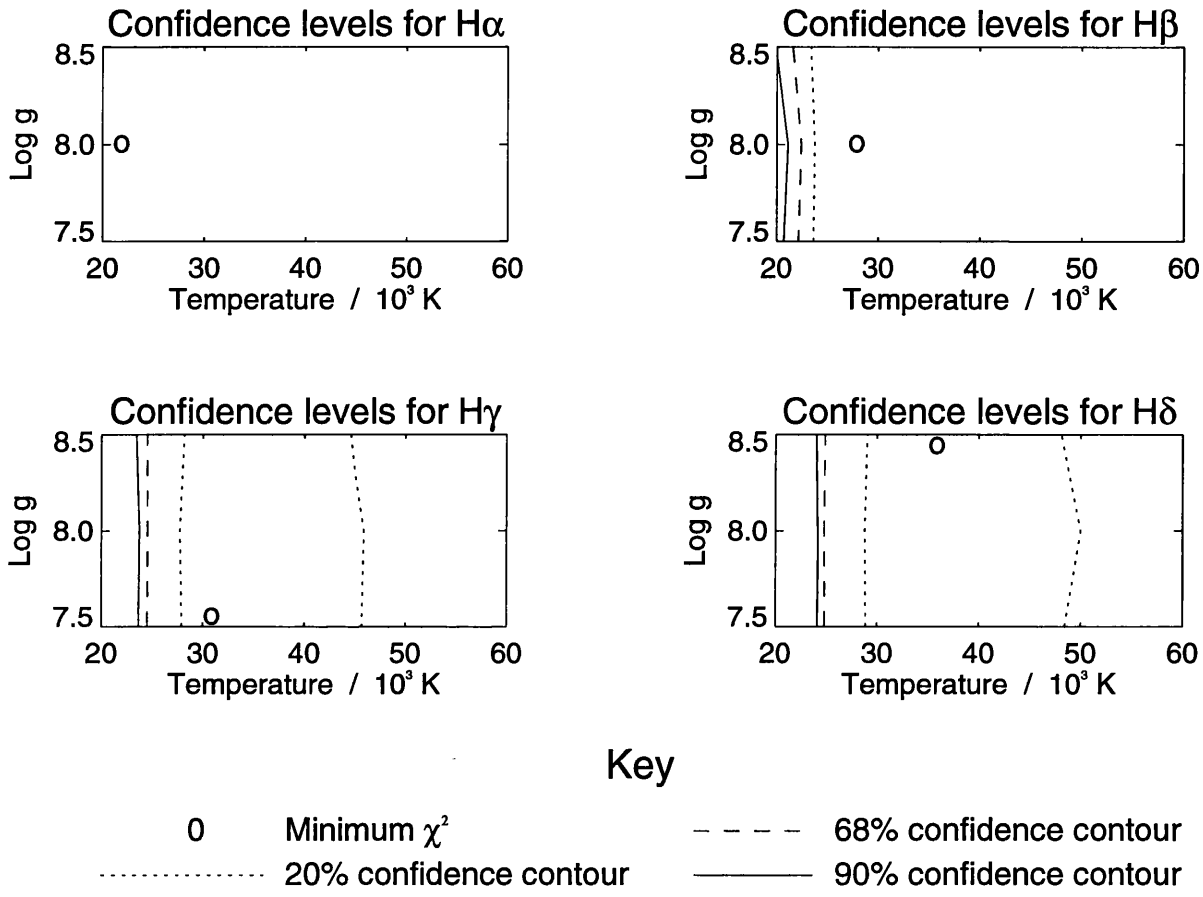

Figure 3.18: *Contour plots of temperature-gravity confidence levels derived from optical line profile fitting.*

NIPS count rates rather than PSS).

The S1 and S2 survey count rates were first corrected for the gradual degradation in efficiency during the survey period. The relation I have used is as follows:

$$Countrate = (MJD - 48103) \times \frac{Cf}{178} + 1 \tag{3.1}$$

where ($\mathrm{Cf}_{S1} = 0.3$, $\mathrm{Cf}_{S2} = 0.17$)

I have also added a 10% systematic error, in quadrature with the statistical error on the count rates, to allow for errors in the photometric calibration of the *WFC* . To obtain a count rate from the V magnitude I have used the relation

$$log(F_\lambda) = -0.4 m_\lambda + log(F_{\lambda 0}) \tag{3.2}$$

where $F_{\lambda 0} = 3.64 \times 10^{-9}$ for V. I have obtained the PSPC survey count rate (Barstow, priv. comm.) which I use unchanged from the survey-extracted values.

The four data points (S1, S2, PSPC, V) were converted into an ASTERIX-accessible format and the modelling performed with XSPEC at Leicester University. This software contains chemically stratified models for which the hydrogen layer-mass is allowed to vary as a free parameter. Thus we have four datapoints, and five parameters: T_{eff}; N_H; log (g); log (P_g), which is related to the H-layer mass by the relation $M_H = 5 \times 10^{-23}$. log (Pg) (also see § 3.6) and n, the normalisation. Fixing log (g) = 8.0, the canonical value for white dwarf atmospheres, and initialising the procedure with the best estimates of the other parameters, the best fit converges to $\mathrm{T}_{eff} = 47\,000$ K, $N_H = 4 \times 10^{19}$, log (P_g) = 9, which implies a H-layer mass of 5 $\times 10^{-14}\, M_\odot$. The fit has a reduced χ^2 which is on the verge of being discarded as unacceptable i.e. not statistically significant (e.g., see Barstow 1993c). Contrary to my expectations, this multi-wavelength fit does not improve the situation. This is almost certainly due to the presence of trace heavy metals in the white dwarf photosphere, adversely affecting the EUV portion of the fit more acutely than the optical region. The most effective remedy is to obtain an accurate optical fit to the temperature and surface gravity of the white dwarf via Balmer line fitting. These parameters may then be fixed at the optically determined values, and in

turn allow a better determination of the hydrogen layer mass and column density to the system, although any values must remain suspect until models including trace heavy metals can also be fitted against the revised data-points (see § 3.6).

3.3.6 M-star parameters

I subtract the white dwarf spectral model with parameters closest to those obtained above (T_{eff} = 45 000 K, log (g) = 8.0, $N_H = 2{\times}10^{19}$ atm cm^{-2}) from the calibrated FOS composite spectrum to obtain a spectrum of the cool secondary star (Figure 3.19).

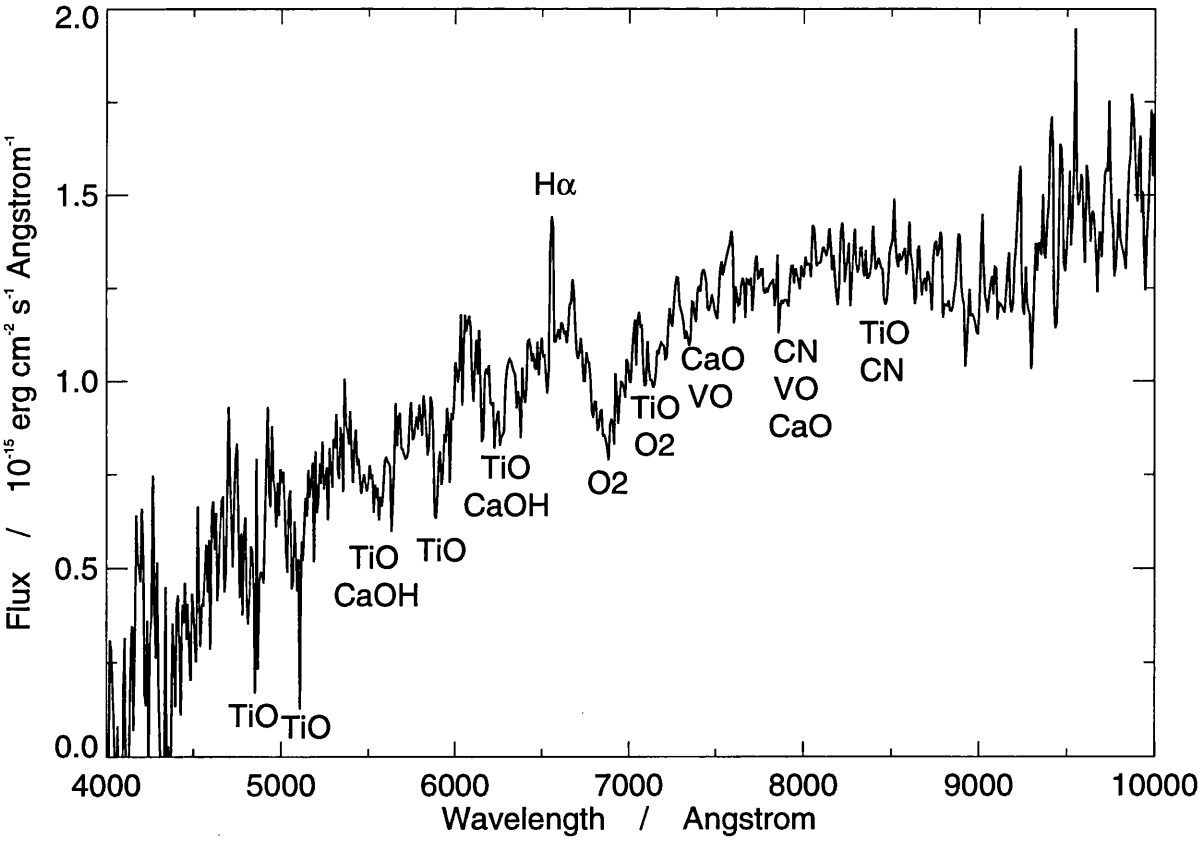

Figure 3.19: *Spectrum of M star in A(S) extracted from the composite FOS spectrum by removal of a white dwarf model atmosphere.*

As for star A(N), I obtained *BVRI* magnitudes by a convolution of this spectrum

with the Johnson filter response functions (see Table 3.3), and used the colour indices to estimate the spectral type. This was double-checked by comparing the spectral features against those found in standard stars. I classify the secondary as a M2 ± 1 dwarf. As a check, I also performed the above procedure with the next closest white dwarf model ($T_{eff} = 40\,000$ K, log $(g) = 8.0$, $N_H = 2{\times}10^{19}$ atm cm^{-2}). As before I arrive at the classification M2 ± 1 dwarf.

The total (white dwarf + M star) V magnitude of RE1016−05 (section 2) is 14.2 ± 0.2. I calculate the V magnitude of each star by using the ratio of their flux outputs in that bandpass derived from the modelling. This yields $V = 15.3 \pm 0.3$ for the red dwarf and $V = 14.7 \pm 0.3$ for the white dwarf. For the dM2 ± 1 star, I take $M_V = 10.0 \pm 0.5$ (Zombeck 1982). The relative fluxes of the modelled components then lead to $M_V = 9.4 \pm 0.7$ for the white dwarf, assuming the two stars to be physically associated. The distance modulus of the system is 5.3 ± 0.8 in the V band, leading to a systemic distance of 115^{+50}_{-35} pc. Even the largest of the intervening column densities allowed by the models in Table 3.8 ($N_H = 4{\times}10^{19}$ atm cm^{-2}) does not imply significant optical extinction—less than $0.04^{\rm m}$ in the V band (Bohlin *et al.* 1978) and the distance modulus of the system remains virtually unchanged.

3.3.7 A third component?

The dM0 star A(N) nearby must also be considered. Taking $M_V = 9.0 \pm 0.5$, the distance modulus is 4.5 ± 0.7, leading to a distance of 80^{+30}_{-20} pc, which overlaps with the error bounds on the A(S) pair. The measured separation of the two objects on the CCD (10.7 pixels) projects back to an angular separation of 3″.2, or 320 AU on the plane of the sky, if the two objects are physically associated and at a distance of 100 pc. The wavelength calibration on the high-resolution spectra of A(N) and A(S) is not secure enough for an absolute velocity measurement, but the difference in the position of the only commonly discernable line in both objects (Hα in absorption in A(N) and emission in A(S)) is 0.5 Å or 23 km s^{-1} . Thus I cannot rule out the possibility that star A(N) is a distant member of the same

system as the two components in A(S).

I can ascribe an upper limit to the separation of the two components of A(S), given that they are an unresolved pair. The FWHM of the A(S) profile projected onto the plane of the sky is 1″.5. This translates to a maximum separation (at a distance of 100 pc) of 150 AU during the observation, which allows the system components to be well separated.

A lower limit to the orbital period may be inferred, given that the system does not appear to be a CV (i.e. the secondary does not fill its Roche lobe). A theoretical Period-Mass formula for Roche-lobe filling secondary stars near the MS is given in Frank, King & Raine (1992) as

$$M_{secondary} \sim 0.11 P_{orb} \tag{3.3}$$

For our best estimate of dM2, it follows $P > 3.5\,h$. If the secondary is actually a dM3, $P > 2.5\,h$.

Perhaps a more accurate relationship is given by the empirical formula of Patterson (1984).

$$M = 0.38(P_{orb}/4)^{1.22} \tag{3.4}$$

For the above cases, this leads to $P > 4\,h$ (dM2 secondary) or $P > 2.6\,h$ (dM3 secondary).

3.4 Discussion

This system would appear to be the second EUV-bright, emission-line white dwarf/red dwarf binary discovered in the *WFC* All-Sky Survey. The first such object discovered, RE1629+781 (Cooke *et al.* 1992), has roughly double the *WFC* count rate (in the survey filters) and is three times as bright in the optical (V = 13.0). Cooke *et al.* found that RE1629+781 consisted of a 35 000–40 000 K DA white dwarf and a dM2-dM5 companion, with emission lines at Hα, Hβ and Ca K (which is often an indicator of coronal activity). Note that no Ca K emission is

seen in RE1016−05. The EUV lightcurves of both RE1629+781 and RE1016−05 are consistent with no significant variation in intensity and both have similar white dwarf effective temperatures. My data are not good enough to allow a comparison of atmospheric abundances.

3.4.1 Line emission mechanisms

The exact nature of RE1016−05 (and by association, RE1629+781) is still unclear. It is highly likely that the two components of A(S) are related, given they are visually unresolved. The observed continuum emission can be successfully modelled by a combination of the continua from a dM star and a hot DA white dwarf. However, the origin of the optical line emission is uncertain. One possibility is emission line production powered by the white dwarf. Several mechanisms are possible, such as gaseous emission from a remnant planetary nebula or local interstellar medium illuminated by the white dwarf (Durisen *et al.* 1976), or production in the white dwarf photosphere (Reid & Wegner 1988). However, the non-detection of forbidden lines, e.g., [O III] 4959, 5007 Å , the strong presence of He I lines and the small Balmer decrement argue for line emission by collisional de-excitation rather than a low density nebular recombinational region. The photospheric production theory encounters problems with the apparently strong detections of Balmer lines other than Hα, plus the helium lines—previous studies of non-magnetic DA white dwarfs show Balmer emission cores no further than Hβ (Reid & Wegner 1989). Moreover, this theory provides no explanation for the change in equivalent width of the Hα emission line—I should expect no variation if the lines are produced in the photosphere. Further tests could be performed, since the emission lines should maintain a constant position with respect to the absorption line cores as the orbit progresses. The position determination of the shallow absorption lines in our current spectra is not precise enough to constrain any relative line motion. In addition, if the lines are produced near the white dwarf, one should expect to see high excitation absorption lines such as N V, C IV and Si IV in the ultraviolet (Fontaine & Michaud

1979, Vauclair *et al.* 1979) as observed in G191-B2B (Bruhweiler & Kondo 1981).

Another possibility arises if the dM star is sufficiently close to the white dwarf: the atmosphere of the red dwarf may be heated by the white dwarf EUV flux, stimulating line emission. Six white dwarf/red dwarf binaries exhibiting this effect are known: Feige 24 (Liebert & Margon 1977; Thorstensen *et al.* 1978; Vennes *et al.* 1991); BE UMa (Ferguson *et al.* 1987); V471 Tau (Young *et al.* 1983); HZ9 (Stauffer 1987); GK Vir (Green *et al.* 1978); Case 1 (Stauffer 1987).

These systems are thought to be short period (8-100 hr) post common-envelope detached binaries, and part of the larger class of so-called pre-cataclysmic binary systems (PCBs, see de Kool & Ritter 1993 for descriptions of individual systems). The white dwarf EUV radiation is reprocessed in the photosphere and/or chromosphere of the cool companion, leading to the enhancement of its photospherically produced continuum emission and/or the production of fluorescence induced chromospheric line radiation (Ferguson *et al.* 1987; Young, Skumanich & Paylor 1988). Whether the photospheric or chromospheric processes apply, and to what extent, is determined by the temperature of the white dwarf and the separation of the two components. Only narrow optical emission lines are expected since they are produced on an illuminated region on one hemisphere of the secondary. There are none of the broad emission lines typical of interacting binaries, such as those produced by an accretion disk or infalling gas close to the white dwarf surface. If RE1016−05 is of this type, there should be significant chromospheric changes, resulting in Ca H and K emission and the 3444 Å Bowen fluorescence pumping indicator, as well as Balmer series line emission. The spectra obtained so far do not show features other than the H and He I emission lines.

I expect the emission lines in such a system will shift in the opposite direction to the absorption lines as the stars orbit, and the velocity variations will be large ($\simeq 100\,\mathrm{km\,s^{-1}}$), due to the compact orbit. The line strengths will also be modulated with the orbital phase as the emission region's visible surface area changes. If the intensity variations (~ 4 hr) seen in the February 1992 spectra are an orbital

phase effect, their timescale would suggest a short period, but within the range of the Feige 24 type systems (8–100 hr). On the other hand, if line emission is due to reprocessing of the white dwarf EUV flux, then the variations in optical line intensity could also indicate underlying variations in the white dwarf EUV output. However, I see no significant flux variations in the *WFC* time-series. Of the previously known Feige 24 type systems, BE UMa shows far-UV variability (Hutchings & Cowley 1985, where no correlation with orbital phase or any optical variations in the companion was found) and V471 Tau shows soft x-ray/EUV variability (Jensen *et al.* 1986). The nature of the rapid variations (on a timescale of hours) in BE UMa is unclear, but may be pulsational. The BE UMa white dwarf temperature is significantly higher (80 000–130 000 K) than RE1016−05, which may place the star in an instability strip (Starrfield *et al.* 1984) causing the pulsations. The other previously known Feige 24 type systems have been reported to exhibit both orbital and non-orbital X-ray and optical variability (e.g., Young *et al.* 1983; Liebert & Margon 1977).

The X-ray timelines show no flaring behaviour, although this may simply be due to the short duration of the exposures. However the shape of the detected X-ray flux distribution indicates that their source is not coronal, such as an active M-star would produce. This does not necessarily favour one scenario over the others, however, since the observations of optical line emission are not simultaneous with the *ROSAT* observations. It is possible that one of the nearby M-stars is active either below the detection threshold of the PSPC, or was quiescent during the observation, and its as yet unobserved flaring behaviour is responsible for the optical line emissions.

One significant difference between the Feige 24 type binaries and the *WFC*-selected white dwarf binaries (RE1629+781 and RE1016−05) is in their relative EUV output. RE1016−05 appears 100 times brighter than Feige 24 (which has the largest EUV flux of the previously known PCB sources) in the S1 filter but has $\simeq$ 5 times less flux in the V band (Feige 24, $V = 12.4$). Feige 24 also has

a much steeper spectral slope. Given that the two white dwarfs have overlapping temperature determinations ($\sim$ 55 000 K; see § 3.6) I conclude that the composition of RE1016−05 (and of the similar *WFC* -selected system RE1629+781) differs greatly from that of Feige 24 and the other previously known systems in having either much lower metal abundances, which would otherwise extinguish the EUV flux, or a much thicker H-layer if assuming a stratified atmosphere. If I assume RE1016−05 to have a comparable surface gravity to the white dwarfs in the Feige 24 type systems, then the lack of metals or a thicker H-layer could indicate that relatively little common envelope evolution has occurred. This would be consistent with a wide separation between the components, rather than the close Feige 24 type systems.

A third possibility for emission line production is an intrinsically active M star secondary. An example of such a white dwarf/red dwarf binary is HZ43 (Lampton *et al.* 1976; Margon *et al.* 1976). This and similar systems have separations large enough to render the white dwarf EUV flux insignificant at the surface of the secondary, line emission naturally arising in its corona. As before, the emission lines will shift in the opposite sense to the absorption lines. However, the velocity variations will be much smaller than for a close Feige 24 type binary. HZ43 itself has a nearly pure hydrogen atmosphere, resulting in a bright EUV source as for both RE1016−05 and RE1629+781. The variation I see in Hα line flux from RE1016−05 may be associated with flares on the dM star. Short timescale variability is a well known feature of the optical line emission from an active M star, and this will be unrelated to the EUV flux from the distant white dwarf. The flaring activity may produce a significant increase in the EUV output of the red dwarf, but this should still fall well below the level of the white dwarf emission.

3.5 Summary

Optical, EUV and X-ray data of the *WFC* -discovered object RE1016−05 have been presented. These show a hot DA white dwarf and dM2 star binary system, with narrow line emission in the Balmer and Paschen series hydrogen lines, and some helium line emission. I find that the system has a distance of 115^{+50}_{-35} pc, and that the white dwarf surface temperature is within the range 37 000–47 000 K. A nearby M star may be a distant third member of the system. After considering several possible scenarios for the optical line emission, it is not possible to rule out either emission from an active M-dwarf or fluorescence emission from an M-dwarf irradiated by the white dwarf. This line emission is superposed on the continuum emission from both the M-dwarf and white dwarf. However, it is the white dwarf which provides all of the *WFC*-detected EUV flux and the XRT-detected X-ray flux.

3.6 Addendum

In a recent paper, Tweedy *et al.* (1993) use improved data to re-determine the classification and temperature of the white dwarf in RE1016−05. They obtained higher S/N optical spectra, which reveal He II absorption (4686 Å ; E.W. = 250 ± 50 mÅ) indicating that the white dwarf is of type DAO (the first detected at EUV and X-ray energies) and determine $T_e = 55\,800 \pm 1000$ K, $\log(g) = 7.81 \pm 0.07$ (via Balmer line fitting). As before, their EUV fits derive a considerably lower temperature (T_e =49 000 K) suggesting significant opacity from trace heavy elements. They find no evidence for photometric variability in the B waveband, suggesting either a cool secondary, or large separation between the components. However, they maintain that the system is a PCB, due to the strong variation of narrow optical H, He and Ca emission lines, which are apparently absent at some phases (unlike most active stars which maintain emission cores even when quiescent). They derive a systemic distance of 113 ± 12 pc, and a white dwarf mass of $0.57 \pm 0.03\,M_\odot$. Tweedy *et*

al. speculate that since the majority of white dwarfs in PCB systems now appear to be DAO, that the AGB evolution of these systems may be significantly different from a typical, isolated, white dwarf star (i.e. they undergo further mass-loss).

I have recalculated my multi-wavelength fits (using chemically stratified models), fixing the temperature and surface gravity at the above optically-determined values. This produces a much improved fit, with $N_H = 5.0 \pm 0.2 \times 10^{19}$, log $(p_g) = 8.3 \pm 0.04$, with a reduced $\chi^2 = 0.66$. This implies a H-layer mass of $1.0 \pm 0.1 \times 10^{-14} M_\odot$, which is at the upper limit of H-layer mass which could be expected to allow the detection of weak He absorption lines (E.W. $\sim$ 100 mÅ) in the optical. The strength of detection Tweedy *et al.* report may thus imply a thinner H-layer, if the atmosphere is stratified, although they find a homogenous atmosphere model to be satisfactory.

Chapter 4

ROSAT DA + dM binaries

Intellectuals solve problems, geniuses prevent them.

Albert Einstein.

The largest class of object identified with the EUV emitters discovered in the *WFC* survey is that of late-type active stars (spectral types F-M) mostly belonging to the Main Sequence (Pounds *et al.* 1992), with over 180 such stars identified. The EUV emission arises from the coronal disturbance in such stars. These objects are amongst the brightest (almost all, 97%, have $m_v < 12$) of the optical counterparts to the *WFC* sources, since they must be relatively close-by in order for their low EUV output to avoid excessive attenuation by the interstellar medium. Interestingly, there is a discrepancy between the pre-survey predictions of the number of M stars expected to be discovered (Vedder *et al.* 1991; Pye & McHardy 1988) and the actual numbers detected—there is a deficiency in detections by a factor of ~ 5. However, the F, G and K type stars yielded numbers of detections comparable to the predicted numbers (Pounds *et al.* 1992). This is most likely due to our poor pre-*ROSAT* understanding of the coronal temperatures of such sources (which was overestimated) and the sparse sampling of the X-ray stellar luminosity functions obtained with Einstein (Rosner *et al.* 1985), which were used to derive the predicted number of detections.

The second largest group identified with the *WFC* EUV sources is that of hot degenerate stars i.e. white dwarfs with $T_{eff} > 20\,000$ K. There have been 120 such stars identified as the optical counterparts of all-sky-survey sources. These sources include some of the the brightest EUV emitters seen in the survey, but are conversely amongst the fainter optical sources (90% have $m_v > 12$), since they have an EUV/optical ratio much higher than any of the other stellar types identified with EUV emission sources. The interesting feature about the degenerates is that the ratio of the counts in the two survey filters (S1/S2) is just as variable within this single class of object as it can be between the different classes of objects themselves (due to the effects of atmospheric composition and structure on the spectral flux distribution of the stars). As previously mentioned, there is a deficiency in the number of stars detected (120; Pounds *et al.* 1992) when compared to the numbers predicted ($\sim$ 1000; Barstow & Pounds 1988; Finley 1988). This is due to the unforseen EUV (and X-ray) opacity blocking much of the flux, especially in the hotter stars, until they are below the all-sky-survey sensitivity threshold. The exact cause of the opacity is in contention between a stratified atmosphere with thin hydrogen layer and trace metals levitated into the photosphere by radiation pressure. However, recent evidence (e.g., Wilkinson, Green & Cash 1992; Tweedy 1993; Barstow *et al.* 1993c) is pointing to trace metals as being the more likely situation in at least some, if not most stars. In this chapter, I will attempt to shed further light on this situation, with the aid of further data.

Most of the optical counterparts of the *WFC* EUV sources are identified with a single emitting body. However, there are a number of binary or multiple systems which are identified with *WFC* EUV sources. These can again be arbitrarily broken down into two types: those which are mere 'optical' binaries in which the optical companion object plays no rôle in the *WFC* detection of the system, i.e. has no comparible intrinsic or stimulated EUV emission of its own; and those whose EUV emission is caused by the very fact that they are in a binary system. For instance, magnetic CVs are expected to have an enhanced EUV emission from polecap accre-

tion on the white dwarf (Watson 1986), and even non-magnetic CVs benefit from EUV emission in the boundary layer. These objects (most of which inhabit the fainter end of the apparent brightness distribution) are thus EUV brighter than, say, many (optically brighter) field white dwarfs, and are thus seen when they would have remained unknown if only optical detection methods were available. Such surveys as the all-sky-survey are thus extremely potent techniques for discovering such astrophysically important systems. However, it is not generally possible to discriminate which type of binary system an EUV source is (or indeed if it is part of a binary system) from the survey *WFC* count rates alone. This requires further data from other instruments/wavelength regions. Thus, it was during the optical identification programme (as was the intention) that the nature of many of these EUV sources was resolved.

This thesis is concerned with the first type of binary system described above, and in particular the class of object now commonly being called the pre-cataclysmic binary (PCB). These systems are comprised of a white dwarf plus a late-type (spectral type K–M) dwarf star, the two most common objects responsible for isolated EUV sources detected in the all-sky-survey, in a close but detached orbit. In many cases the companion late-type star is stimulated into emission by the irradiation from the white dwarf. Chapter 3 explored RE1016−05, a candidate PCB system which, as far as the *WFC*-detected EUV flux is concerned, is no different from an isolated white dwarf i.e. the M-star has no significant contribution in this region—regardless of the true nature of the M-star activity. However this does not mean that the binarity of the system must have no effect upon the nature of the emissions from it. For instance, the M star may well be stimulated into optical, EUV and X-ray emission by the EUV illumination from the degenerate companion—it is just that the level of, for example, the EUV emission from the M-star is much lower than that from the white dwarf itself, and the only way to determine the M-star parameters is from other wavelength regions.

During the optical ID programme, a number of similar systems to RE1016−05

were discovered, mainly from visual examination of the optical spectra as they were observed at the telescope. This, of course, means that only the 'obvious' candidate PCB systems would be selected at this stage i.e. only those systems with relatively comparable flux levels in each component or else large emission features or other anomalies caused by the binarity of the systems. There may be more systems 'hiding' in the residue of apparently isolated stars observed in the optical identification programme i.e. a bright white dwarf with a very faint late type companion or vice versa. For this reason, I carried out a systematic search of all the white dwarf spectra (§ 2.8) to discover if such 'hidden' systems existed.

In this chapter I will describe the DA + dM binary systems and candidate PCB systems (other than RE1016−05) detected in the *WFC* all-sky-survey (listed in table 4.1). These systems were identified as binaries on the basis of their optical spectra, during the *ROSAT* optical ID programme.

The first section in this chapter deals with RE1629+78, for which I have obtained additional *ROSAT* data. I first briefly discuss the observations obtained during the survey phase and then analyse the data I obtained during the pointed phase. The second section of this chapter deals with those sytems for which I only have the survey data itself.

Since these DA + dM systems were discovered with the same instrument as RE1016−05 (EUV-selected) I would expect them to be more similar in their behaviour and parameters to each other and RE1016−05, than with the previously known (optically-selected) systems, most of which which were not detected in the *WFC* survey.

4.1 Countrate correction and combined fits

I have obtained the survey S1 and S2 count rates for all the *WFC* sources listed in table 4.1 from the Bright Source Catalogue (Pounds *et al.* 1992). I have also obtained the XRT/PSPC survey count rates on these sources (Martin Barstow,

Source	α_{2000}	δ_{2000}	V magnitude
RE1340+60	13 40 58.6	+60 26 32	16.0
RE1426+50	14 26 41.5	+50 06 42	14.0
RE1629+78	16 29 14.5	+78 04 28	13.75
RE1711+66	17 11 26.9	+66 45 55	17.1
RE2013+40	20 13 10.2	+40 2 44	14.6
RE2024+20	20 24 15.0	+20 00 31	16.4

Table 4.1: *Optically determined Parameters for DA + dM binaries discovered with the WFC. Magnitudes are from the FOS spectra and APM except for RE1629.*

priv. comm.). These count rates are given in table 4.2. Firstly, the *WFC* count rates must be corrected for the efficiency drift that occured during the survey phase. I use the technique described in § 3.3.5.1 (using equation 3.1). The degradation-corrected count rates are listed in table 4.3. I then use these three *ROSAT* data-points, plus the V magnitude of the star (acquired from the FOS spectrum or the APM scan) plus any other data-points I have acquired in the pointed phase, such as P1 observations, in a combined fitting procedure using XSPEC, using the procedure as described for the fits to the RE1016−05 data in § 3.3.5.1. The results of the multi-region fits are given in tables 4.8 and 4.7. I also model the Balmer line profiles in the optical spectra (table 4.6).

I will give a brief synopsis of the data-analysis on each individual system, then take an overall look at the implications of the *ROSAT* data on the atmospheric debate at the end of chapter 5.

Source	Observed *ROSAT* count rates			
	PSPC (err)	S1 (err)	S2 (err)	P1 (err)
RE1340+60	0.045 (10)	0.009 (4)	0.016 (5)	-
RE1426+50	0.121 (22)	0.026 (4)	0.045 (5)	-
RE1629+78	8.629 (168)	0.908 (14)	1.406 (18)	0.03 (2)
RE1711+66	0.215 (35)	0.005 (1)	0.005 (-)	-
RE2013+40	1.413 (82)	0.055 (6)	0.031 (6)	-
RE2024+20	0.592 (42)	0.020 (5)	0.017 (-)	-

Table 4.2: ROSAT *count rates for DA + dM binaries discovered with the WFC. Numbers in parenthesis indicate the error on the count rates.*

Source	Corrected *ROSAT* count rates			
	PSPC	S1	S2	P1
RE1340+60	0.045 (10) (11)	0.013 (4) (6)	0.017 (5) (8)	-
RE1426+50	0.121 (22) (25)	0.033 (4) (5)	0.052 (5) (7)	-
RE1629+78	8.629 (168) (879)	1.180 (14) (14)	1.640 (18) (18)	0.03 (2)
RE1711+66	0.215 (35) (41)	0.006 (1) (1)	0.006 (-) (-)	-
RE2013+40	1.413 (82) (163)	0.062 (6) (9)	0.033 (6) (7)	-
RE2024+20	0.592 (42) (72)	0.022 (5) (6)	0.018 (-) (-)	-

Table 4.3: *Corrected* ROSAT *count rates for DA + dM binaries discovered with the WFC. Numbers in parenthesis indicate first the error on the count rate and then the error including systematic calibration component.*

4.1.1 RE1629+78

4.1.1.1 History

This was the first *ROSAT* discovery of a white dwarf/red dwarf system, and indeed the first discovery with the *WFC* (Cooke *et al.* 1992). RE1629+78 ($V = 13.0$) was found to be an extremely bright EUV source, with a count rate of 0.9 ± 0.1 and 1.4 ± 0.2 $ct\,s^{-1}$ in the S1 and S2 filters respectively.

Cooke's modelling of the *WFC* S1 and S2 count rates leads to the conclusion that RE1629+78 contains a 35 000–40 000 K DA white dwarf and a dM2-dM5 companion star. They found the optical spectrum exhibited emission lines of the Balmer series and Ca K, but no Ca H emission was seen. Ca H and K are, for instance, indicators of chromospheric activity.

4.1.2 Pointed mode data

I have obtained further data with the *ROSAT WFC* and XRT instruments, which allow a refinement of the previous model parameters. During December 1991 a 2802 s *WFC* exposure was taken through the pointed mode 'P1' filter (centred at 69 eV) of the field containing RE1629+78. Simultaneous data were also obtained with the XRT, using the PSPC detector and the boron filter swapped in.

Reducing the *WFC* event dataset leads to a weak detection of a source (a significance of 4.8) at the coordinates $\alpha_{2000} = 16^h\ 29^m\ 14\overset{s}{.}5$, $\delta_{2000} = +78^\circ\ 04'\ 28''$, which I identify with RE1629+78. Manually extracting the source counts, correcting for background, dead time and vignetting, I obtain a source flux of 0.005 ± 0.002 ct s^{-1}. However, in order to compare this result with the survey EUV fluxes, a correction must be made for the change in detector response which has occurred over the life of the instrument. The relative performance factor is 0.155 times that of the launch value, which leads to an efficiency-corrected flux of 0.03 ± 0.01 ct s^{-1}

The S1/S2 ratio, ~ 0.6, is typical of the average survey-detected white dwarf ratio. The S1/P1 ratio is ~ 30.

The PSPC data show that the source has an extremely soft X-ray flux (as is the case for RE1016−05). The peak flux level is at 100 eV, with a value of $\sim 6 \times 10^{13}\,\mathrm{erg\,s^{-1}\,cm^{-2}}$and gradually diminishes with increasing energy, becoming virtually extinguished by 450 eV. There is no sign of harder X-rays (> 0.5 keV) caused by coronal activity of the type seen in active late-type stars. The X-ray emission seen in my PSPC exposure is more consistent with a tail-off of the thermal emission from the hot white dwarf (however, no acceptable fits to the pulse height spectrum can be obtained with either blackbody or thin plasma models, whether including an absorbing component for the intervening column or not. The only acceptable fits are obtained with a powerlaw).

The PSPC data can be used in conjunction with the *WFC* datapoints (survey/calibration and pointed modes) and the V magnitude point (a total of five data-points) to better constrain the atmosphere fits.

Fits to the count rates including the extra *WFC* and PSPC data points, using chemically homogenous atmospheres supports a $T_{eff} = 37\,500 \pm 1\,500$ K, with an intervening column density $= 2.7 \pm 0.6 \times 10^{19}\,\mathrm{atm\,cm^{-2}}$. The H/He abundance is constrained to be $0 < H/He < 10^{-4}$, with a best fit surface gravity of 8.0 (table 4.7), an improvement over the fits of Cooke *et al.* (1992).

In a fit to the model parameters of a chemically stratified atmosphere (table 4.8), the fit converges to $T_{eff} = 49\,100$ K, which is somewhat higher than the value derived from the optical measurements, $\log g = 7.4$, lower than the optically-derived value, and $N_H = 3.2 \times 10^{19}$. Fixing the surface gravity at the optical value of $\log g = 8.2$ (Barstow, priv. comm.) does little to alter the other fit parameters. When the temperature and gravity are *both* fixed at the optical values of 42 500 K, and $\log g$ 8.2, the fit gives $N_H = 2.5 \times 10^{19}$, with a H-layer mass of $5 \times 10^{-13}\,M_\odot$.

There is no evidence for any significant periodic variation or aperiodic variation (flaring) in the X-ray or EUV (P1) timelines from my *ROSAT* pointed mode observations.

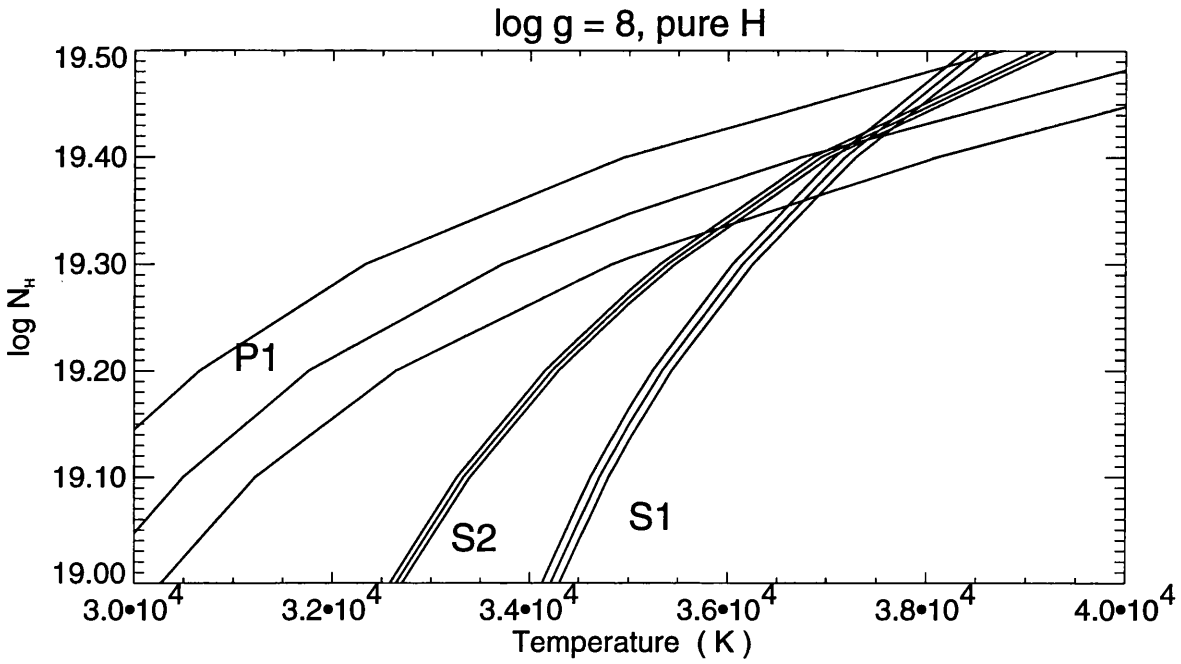

Figure 4.1: *PHOTAN fit to RE1629+78 data, plot of T_{eff} versus log N_H.*

4.1.3 RE2013+40

RE2013+40 (α_{2000} = $20^h\ 13^m\ 10\overset{s}{.}2$, δ_{2000} =40° 2′ 44″, S1 = $0.055 \pm 0.006\,\mathrm{ct\,s^{-1}}$, S2 = $0.031 \pm 0.006\,\mathrm{ct\,s^{-1}}$, PSPC = $1.413 \pm 0.082\,\mathrm{ct\,s^{-1}}$) is a DA plus late-type star binary system, first noted during the optical ID programme.

Inspection of the FOS spectrum (figure 4.2) quickly reveals activity in this source. There are emission lines present at Hα, Hβ, Hγ and Hδ. Balmer line modelling is made difficult on most of the lines due to the interference of the emission components. I therefore initially used only the line least affected by the emission, i.e. Hδ. Then I attempted to remove the emission cores from the remaining absorption lines (Hα, Hβ, Hγ) and fit these . The overall temperature I derive from these line profiles is $40\,000 \pm 4000$ K.

Interestingly, the S1/S2 ratio for RE2013+40 is one of the largest for any white dwarf at 1.8. EUV modelling with homogenous atmospheres leads to an estimated $T_{eff} = 37\,000 \pm 3000$ K, N_H = 4–7 $\times 10^{19}\,\mathrm{atm\,cm^{-2}}$.

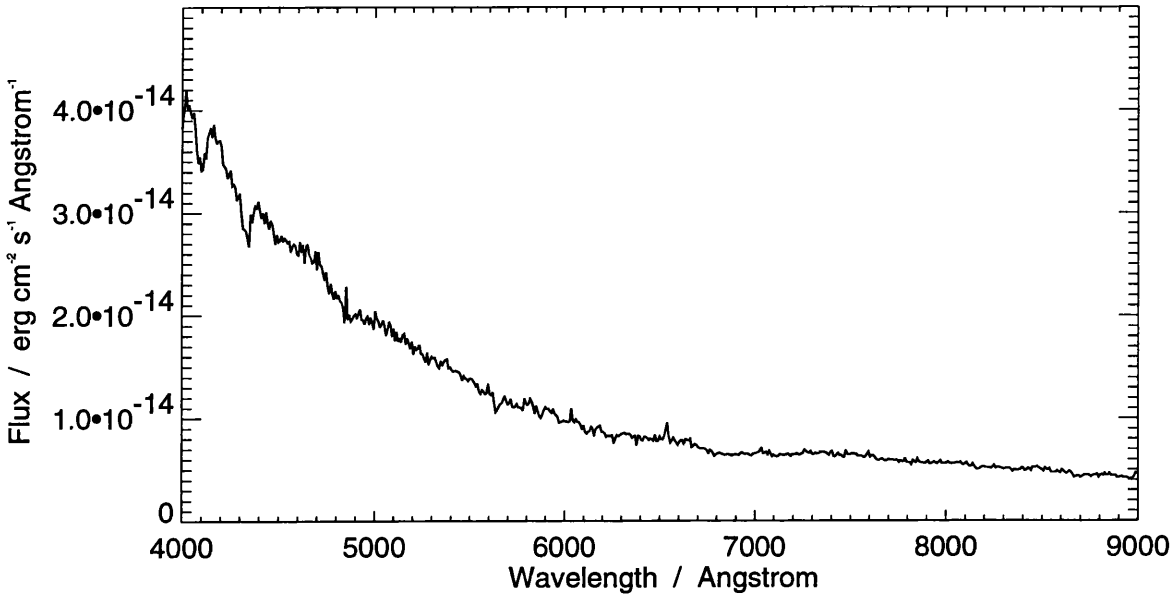

Figure 4.2: *RE2013+40 FOS spectrum*

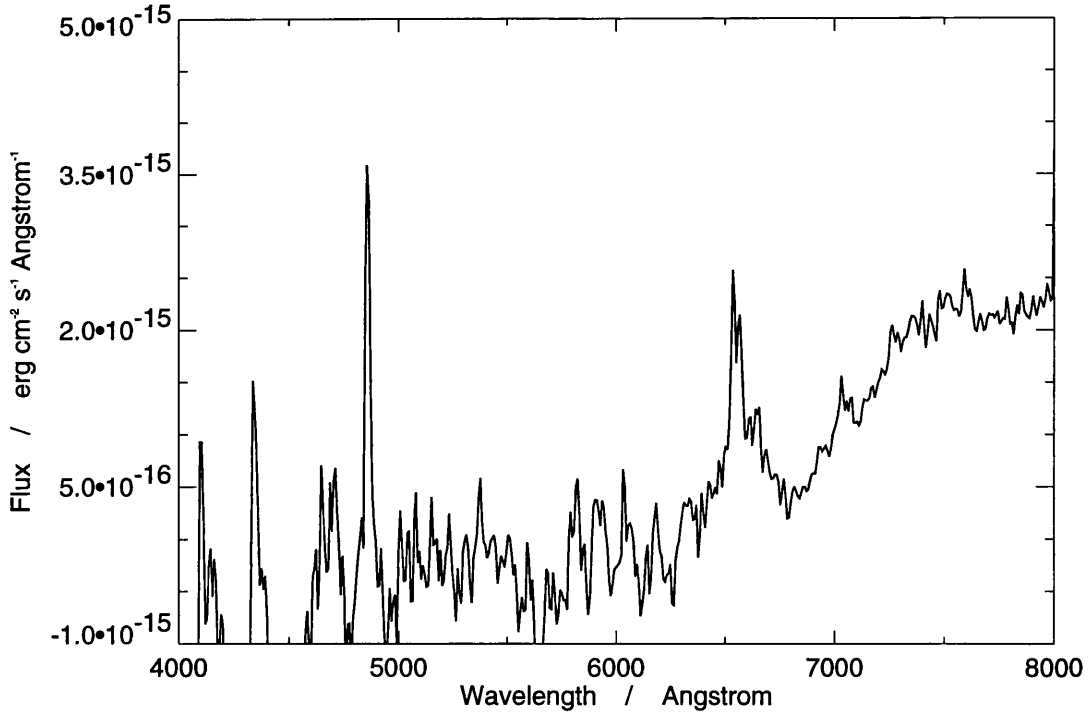

Figure 4.3: *Extracted companion spectrum in RE2013+40*

I can obtain no acceptable fits to the *WFC* and XRT data-points using stratified model atmospheres.

Subtracting the closest fit model white dwarf, I obtain an estimate of the companion type as dM2-4 (figure 4.3). The emission line fluxes and equivalent widths I measure are given in table 4.4.

Line	Flux	Eq.W.
	$10^{-15}\,\mathrm{erg\,s^{-1}\,cm^{-2}}$	Å
Hα	24.0 ± 0.7	3.1 ± 1.0
Hβ	6.3 ± 0.9	0.5 ± 1.4
Hγ	5.3 ± 1.3	0.5 ± 1.5
Hδ	2.9 ± 2.0	0.3 ± 2

Table 4.4: *Line fluxes for RE2013+40.*

There have since been follow-up investigations on RE2013+40 by others (see Barstow *et al.* 1993a). RE2013+40 exhibits radial velocity variations of $300\,\mathrm{km\,s^{-1}}$ in the emission lines and is required to have a short period ($P < 8.7 M sin^3 i\,\mathrm{hr}$, where i is the system inclination and M is the system mass). He II is seen in absorption at 4686 Å, making the white dwarf of type DAO. Since this system appears to be such a close WD + dM binary (thus post-CE), exhibiting orbitally-variable emission-line features, yet has no apparent mass-transfer it is classed as a PCB. Again, this confirms the trend for the degenerate stars in these systems to be of type DAO. However, the failure of stratified atmosphere fits indicates there may be some heavy element opacity in the photosphere.

4.1.4 RE2024+20

RE2024+20 (α_{2000} = $20^h\ 24^m\ 15\overset{s}{.}0$, δ_{2000} =20° 0′ 31″, S1 = $0.020 \pm 0.005\,\mathrm{ct\,s^{-1}}$, PSPC = $0.592 \pm 0.042\,\mathrm{ct\,s^{-1}}$, S2 upper limit = $0.017\,\mathrm{ct\,s^{-1}}$) is noted as being a possible DA plus late-type star binary system from the optical ID FOS spectrum.

The optical spectrum (figure 4.4) is too noisy in the Balmer line region to obtain an acceptable fit with Balmer line modelling techniques. Even a fit to the continuum slope does not constrain the effective temperature within the model limits. It can be seen that the dominant component in the spectrum is the late-type companion star, its features being visible as early as 5700 Å.

Since the *WFC* S2 count rate is only an upper limit, I can only constrain the white dwarf to have $28\,000\,\mathrm{K} < T_{eff} < 40\,000\,\mathrm{K}$ and $N_H < 5 \times 10^{19}\,\mathrm{atm\,cm^{-2}}$ with a homogenous DA model atmosphere fit.

There are no acceptable fits to the *ROSAT* data with stratified atmosphere models.

Subtracting a nominal 35 000 K DA atmosphere reveals an M-type companion, which I classify as M3-M5 (figure 4.5). There is no evidence of significant Hα (or any other) line emission; I determine an upper limit of $7 \times 10^{-16}\,\mathrm{erg\,s^{-1}\,cm^{-2}}$to any H$\alpha$ emission, based on the continuum level.

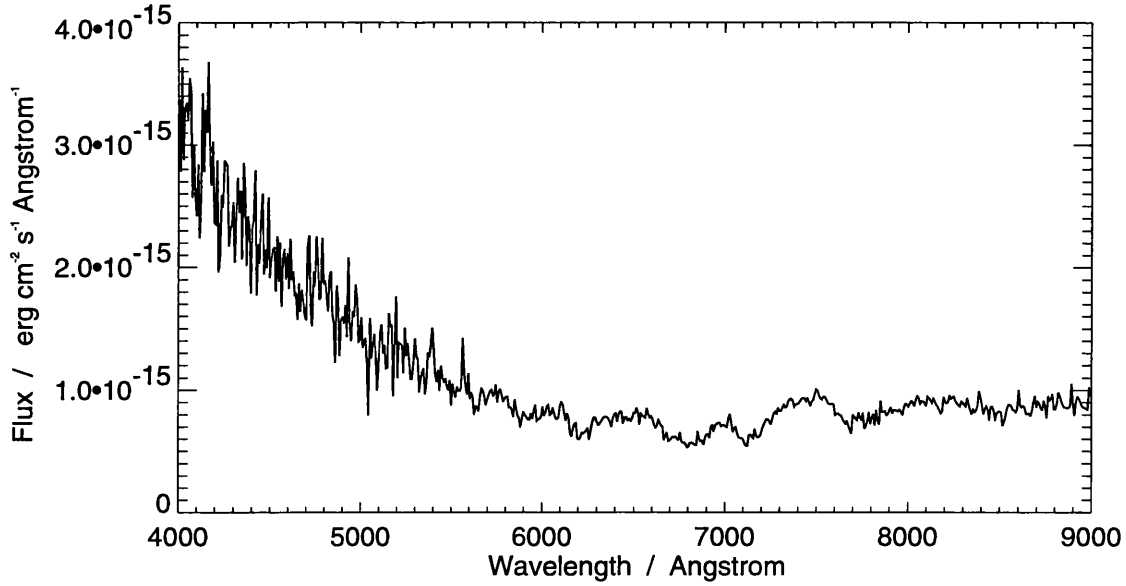

Figure 4.4: *FOS spectrum of RE2024+20.*

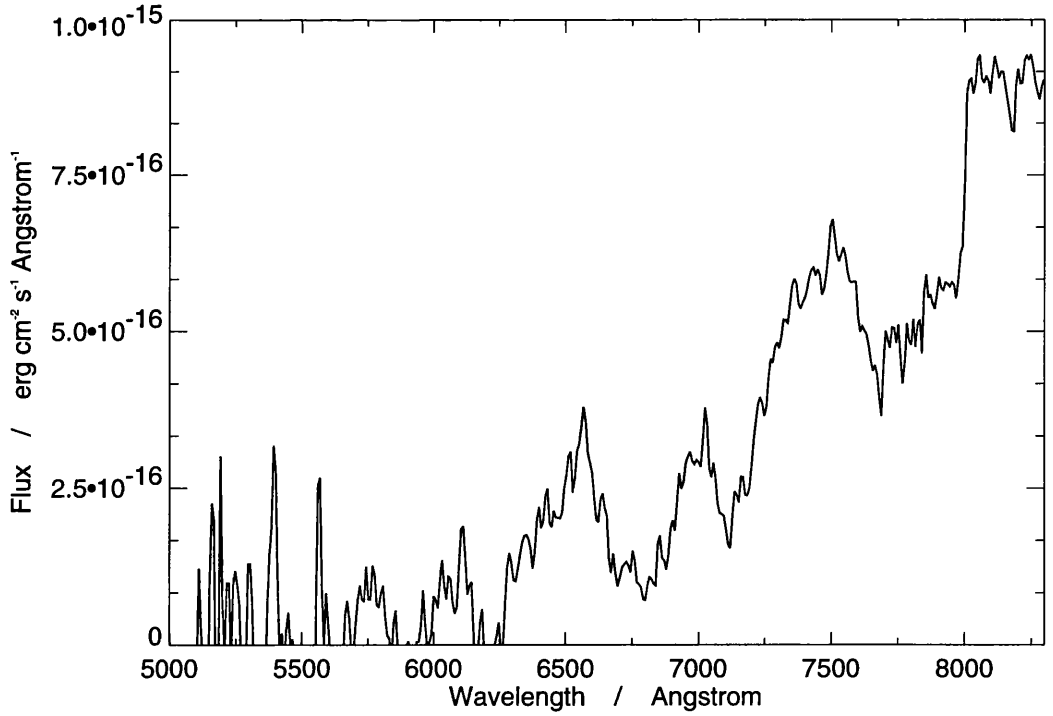

Figure 4.5: *Extracted companion spectrum in RE2024*

4.1.5 RE1711+66

RE1711 ($\alpha_{2000} = 17^h\,11^m\,26\overset{s}{.}9$, δ_{2000} =66° 45′ 55″, S1 = $0.005 \pm 0.001\,\mathrm{ct\,s^{-1}}$, PSPC = $0.215 \pm 0.035\,\mathrm{ct\,s^{-1}}$, S2 upper limit = $0.005\,\mathrm{ct\,s^{-1}}$) is noted as being a DA plus late-type star binary system from the optical ID spectrum.

Balmer line modelling using my DWARF software is complicated by the noisiness of the individual absorption lines in the FOS spectrum (figure 4.6). There are no acceptable fits to any of the visible Balmer lines. A fit to the short wavelength continuum shape (such that any late type companion flux is negligible) leads to a temperature estimate of $40\,000 \pm 5000$ K.

EUV modelling with homogenous DA atmospheres reveals a temperature range of 30 000–37 000 K, and a column density of 1–5 $\times 10^{19}\,\mathrm{atm\,cm^{-2}}$.

Fits with stratified models are unacceptable unless fixing both the temperature (I used values around the nominal Balmer modelling value of 40 000 K) *and* the surface gravity (I chose values around the canonical value of $\log g = 8.0$). In these cases the fits derive a column of $5.5 \pm 0.6 \times 10^{19}\,\mathrm{atm\,cm^{-2}}$ and a H-layer mass of $2\text{–}60 \times 10^{-14}\,M_\odot$.

Subtracting a scaled DA model atmosphere at 35 000–40 000 K reveals an M-star secondary (figure 4.7) which I classify as type M3–M4. There is no apparent Hα emission, and I place an upper limit on any of $5 \times 10^{-16}\,\mathrm{erg\,s^{-1}\,cm^{-2}}$, based on the continuum level.

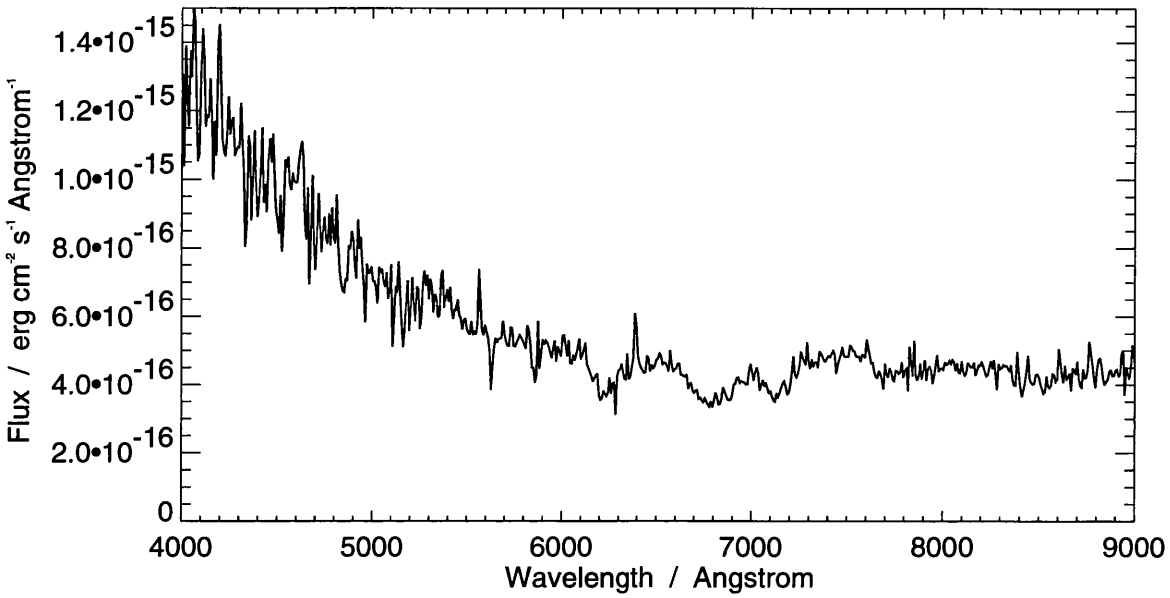

Figure 4.6: *RE1711+66 FOS spectrum*

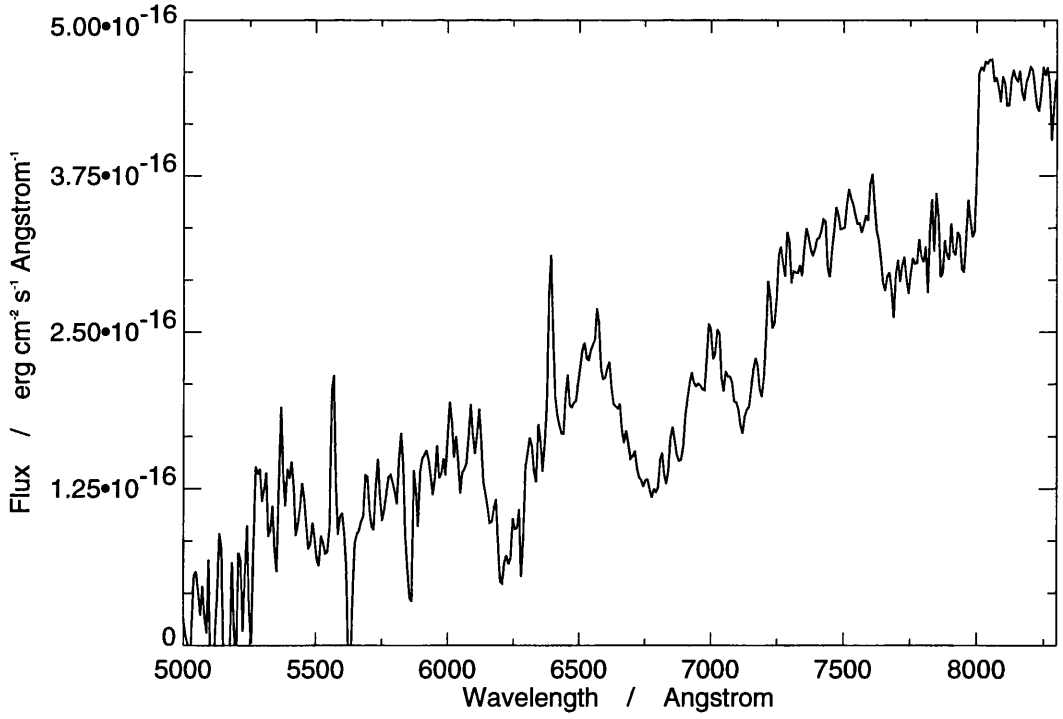

Figure 4.7: *Extracted companion spectrum in RE1711*

4.1.6 RE1340+60

RE1340+60 ($\alpha_{2000} = 13^h\ 40^m\ 58\overset{s}{.}6$, $\delta_{2000} = 60°\ 26'\ 32''$, S1 $= 0.009 \pm 0.004\,\mathrm{ct\,s^{-1}}$, S2 $= 0.016 \pm 0.005\,\mathrm{ct\,s^{-1}}$, PSPC $= 0.045 \pm 0.010\,\mathrm{ct\,s^{-1}}$) is noted as being a possible DA plus late-type star binary system from the optical ID spectrum.

Balmer line modelling on individual lines does not give any acceptable fits due to the noisiness of the spectrum (figure 4.8). A fit to the short-wavelength continuum shape leads to a temperature estimate of $45\,000 \pm 5000$ K.

EUV modelling with homogenous atmospheres leads to an allowed range of $30\,000\,\mathrm{K} < T_{eff} < 50\,000\,\mathrm{K}$, $N_H < 7 \times 10^{19}\,\mathrm{atm\,cm^{-2}}$.

Stratified atmosphere fits do not lead to viable results even when constraining the temperature to be at or about the Balmer-line derived value and the surface gravity near the canonical value.

Subtracting the best fit white dwarf model leads to the companion's spectrum (figure 4.9) which I can only tentatively type as K5–M5, due to the noisiness of the spectrum. There is a feature at 6550 Å, which may be low-level Hα emission, but it is not significant (above the continuum level). I place an upper limit on the line of $8 \times 10^{-16}\,\mathrm{erg\,s^{-1}\,cm^{-2}}$, based on the continuum level.

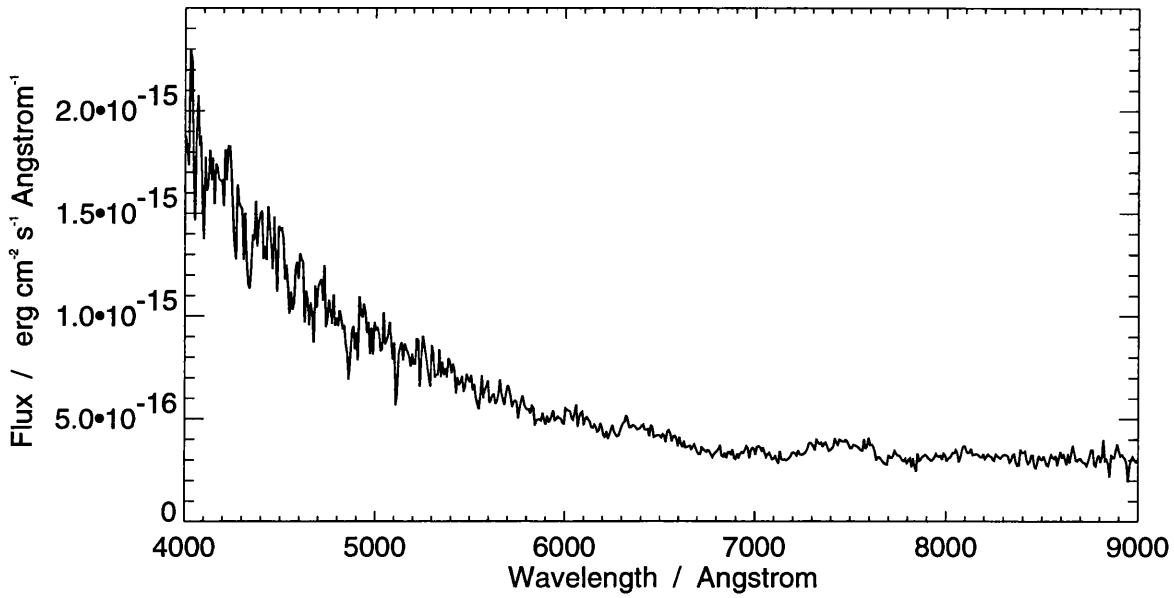

Figure 4.8: *FOS spectrum of RE1340+60.*

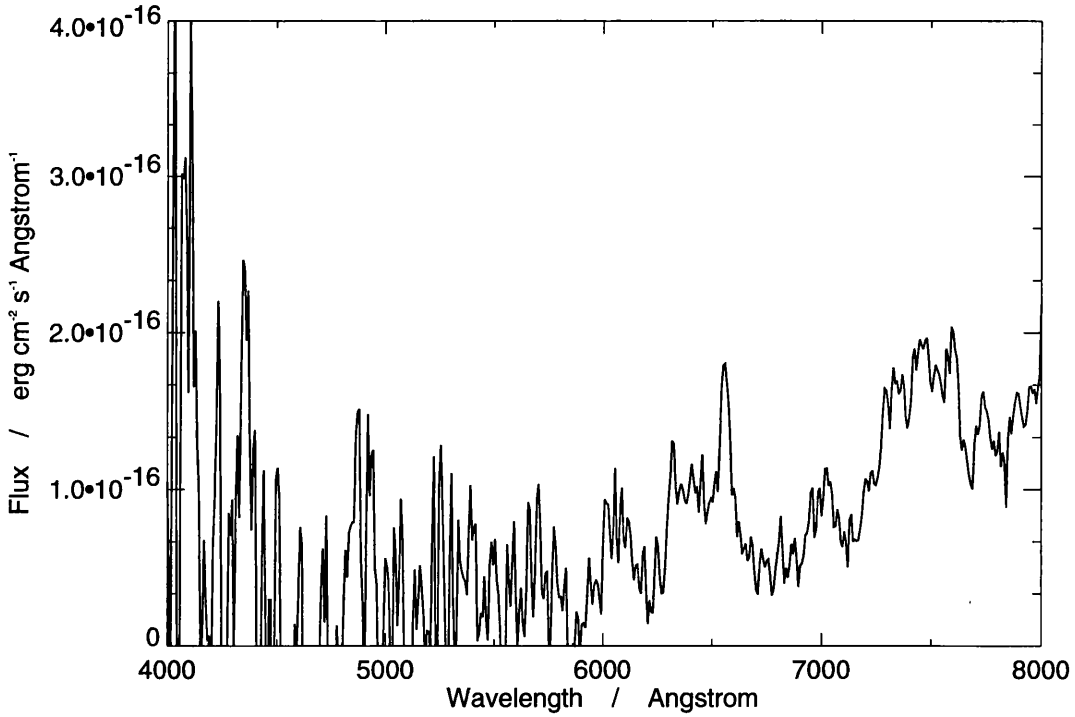

Figure 4.9: *Extracted spectrum of companion in RE1340*

4.1.7 RE1426+50

RE1426+50 ($\alpha_{2000} = 14^h\ 26^m\ 41\overset{s}{.}5$, δ_{2000} =50° 6′ 42″, S1 = $0.026 \pm 0.004\,\mathrm{ct\,s^{-1}}$, S2 = $0.045 \pm 0.005\,\mathrm{ct\,s^{-1}}$ PSPC = $0.121 \pm 0.022\,\mathrm{ct\,s^{-1}}$) is noted as being a possible DA plus late-type binary system from the optical spectrum taken during the optical ID programme.

This target is a much more suitable candidate for Balmer line modelling than many of the other stars, since it is one of the cooler DAs and thus the lines are much more pronounced. Balmer absorption lines are easily visible in the FOS spectrum from Hα to Hϵ (figure 4.10). At this low temperature the line changes are also much more pronounced as the temperature is altered up or down slightly, making it easier to discriminate accurately between the models. There also is a prominent narrow absorption line at 5110 Å seen in the FOS spectrum. Closer inspection also reveals possible evidence for low-level emission components in each of the Balmer absorption lines Hα to Hϵ. An emission spike of similar shape appears offset into the red wing of each of these absorption lines. However, the wavelength shift from the absorption line centre is 15-20 Å, implying a velocity shift of $1000\,\mathrm{km\,s^{-1}}$. This is obviously too large to be a shift due to orbital motion, throwing doubt on the validity of the lines as emission features. Furthermore, an IDS spectrum taken of the Hα region a few hours later shows no sign of narrow Hα line emission (although the broad absorption line from the white dwarf may be partially filled in).

I have fitted the profiles of the Hβ, Hγ and Hδ lines individually (attempting to exclude the emission features), as well as fitting the short wavelength continuum including the Balmer lines. The best fits I obtain for the lines are shown in table 4.5.

The fits are not sensitive to the value of log g within the model limits.

A fit to the *WFC* EUV count rates with a homogenous DA atmosphere constrains $T_{eff} = 28\,000 \pm 1500\,\mathrm{K}$ and $N_H = 0.6\text{–}3.0 \times 10^{19}\,\mathrm{atm\,cm^{-2}}$.

Fits with stratified atmospheres are very poor. Fixing either the effective temperature at the value I derive from the Balmer line modelling, or the surface gravity at the canonical value, results in no real constraints within the model limits upon

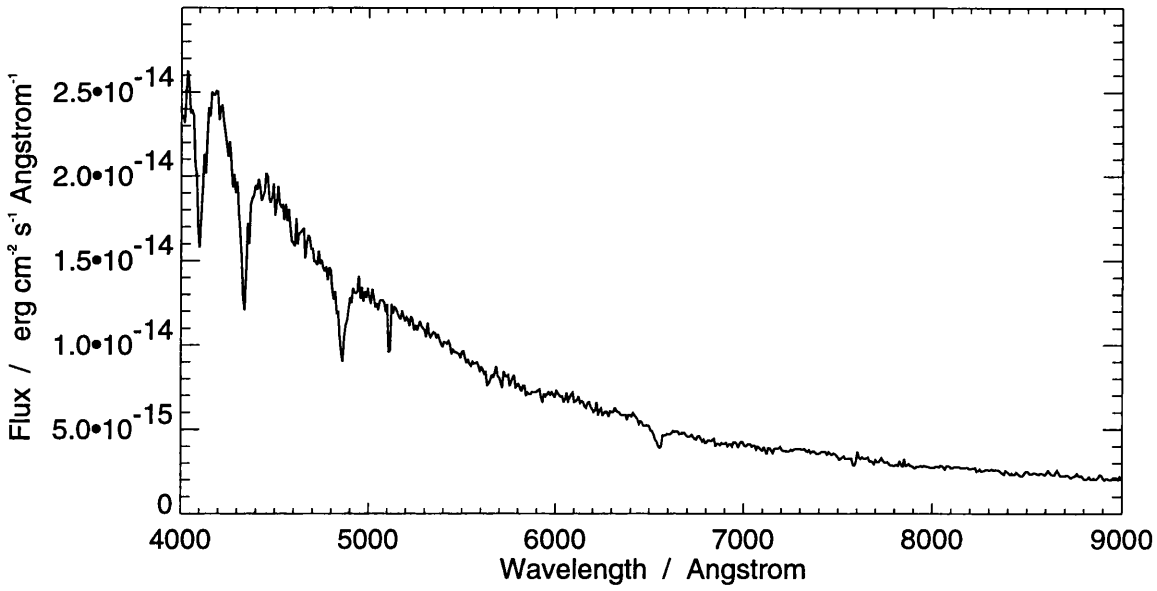

Figure 4.10: *FOS spectrum of RE1426+50.*

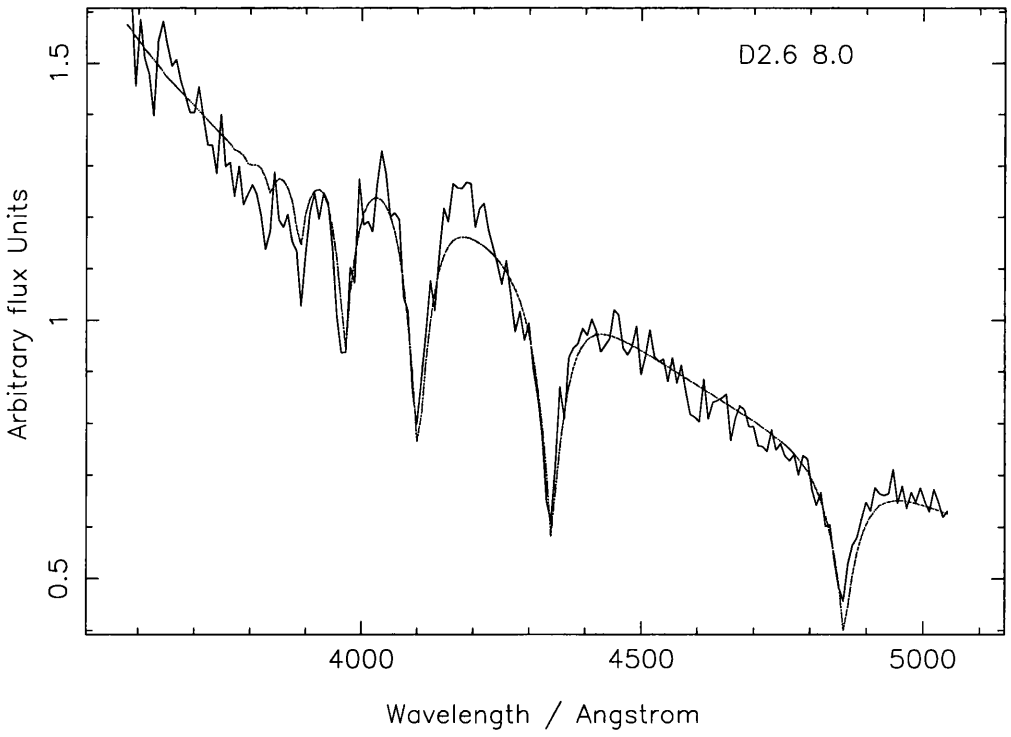

Figure 4.11: *Balmer line profile fit to FOS spectrum of RE1426.*

Line	Best fit T_{eff} K	1σ constraints K	Best fit $\log(g)$
Hβ	24 000	$20\,000 \leq T_{eff} \geq 24\,000$	7.5
Hγ	28 000	$26\,000 \leq T_{eff} \leq 31\,000$	8.5
Hδ	24 000	$22\,000 \leq T_{eff} \leq 27\,000$	8.0
Continuum	26 000	$23\,000 \leq T_{eff} \leq 28\,000$	7.5
Average	26 000		

Table 4.5: *Atmospheric parameters from RE1426+50 Balmer line profile fits.*

the H-layer mass or column density. Fixing both of these parameters (temperature and gravity) simultaneously constrains the column to $< 3 \times 10^{19}$ atm cm^{-2} but does not restrict the H-layer mass. As the χ^2 on the fits is large (7) given the number of degrees of freedom (1), the probability of a good fit is very low, thus I determine that no fit is acceptable (e.g., see B93).

Scaling and subtracting the best fit model atmosphere (26 000 K) from the FOS spectrum of RE1426+50, I extract the spectrum of the optical companion (figure 4.12) for which I derive a spectral type of K5-M0 (using the same methods as in § 3.2.1).

I have made a further examination of the emission features. Since an incorrect subtraction of the Balmer absorption lines in the white dwarf model can lead to apparent emission features in the extracted spectrum, I have concentrated on the IDS and uncorrected FOS spectra. The most prominent feature in the FOS spectrum is near the Hα position, but offset by a unaccountably large velocity. It is only 1σ above the continuum. No emission lines are visible in the IDS spectrum. I have also examined the profile of this and the other possible emission features. I conclude that at this time there is no justification for claiming the lines are genuine Balmer emission.

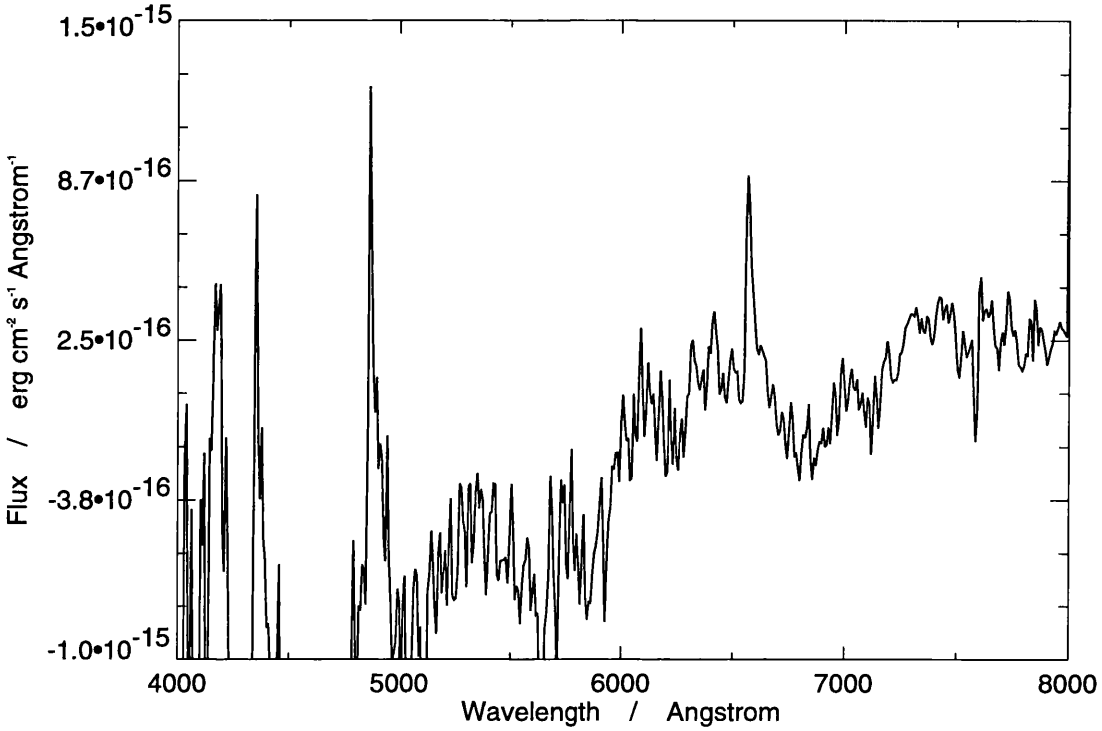

Figure 4.12: *Extracted companion spectrum in RE1426+50.*

4.2 Summary

The nature of most of these systems is still unclear.

Two of them (RE1629+78 and RE2013+40) exhibit Balmer emission lines. It is clear from further investigations that RE2013+40 is a close binary system, probably a PCB, whereas the situation for RE1629+78 is less certain. Follow-up investigations (e.g., see Tweedy 1993a) show it is likely to be a well separated system with line emission from a coronally active M-star, rather than under any influence from the white dwarf, since it has exhibited quiescent emission line cores and emission line outbursts.

The other systems studied in this chapter appear to have, on average, very late companion stars. This is probably due to the selection effect of two stars with different flux output regions being easier to see in a composite spectrum, since all of these sytems were identified visually at the telescope. None of them

Source	$T_{eff}(err)$ K	Log (g) (err)
RE1340+60	45000 (5000)	8.0 (-)
RE1426+50	26000 (3000)	8.0 (-)
RE1629+78	37500 (1500)	8.0 (-)
RE1711+66	40000 (5000)	8.0 (-)
RE2013+40	40000 (4000)	8.0 (-)
RE2024+20	no fit	

Table 4.6: *Balmer profile fits to DA + dM binaries discovered with the WFC.*

Source	$T_{eff}(err)$ K	$N_H(err)$ 10^{19} atm cm^{-2}	Log (g) (err)
RE1340+60	40000 (10000)	<7	8.0 (-)
RE1426+50	28000 (1500)	1.8 (1.2)	8.0 (-)
RE1629+78	37500 (1500)	2.7 (0.6)	8.0 (-)
RE1711+66	33500 (3500)	3.0 (2.0)	8.0 (-)
RE2013−70	37300 (3000)	5(2)	8.0 (-)
RE2024+20	34000 (6000)	<5	8.0 (-)

Table 4.7: *PHOTAN Homogenous atmosphere fits to DA + dM binaries discovered with the WFC.*

Source	T_{eff} (err) K	N_H (err) 10^{19} atm cm^{-2}	M_H (range) $10^{-13}\,M_\odot$	log (g) (err)	χ^2
RE1340+60	no fit				
RE1426+50	no fit				
RE1629+78	49100 (7100)	3.2 (0.5)	-	7.4 (1.3)	4.6
RE1629+78	49300 (9900)	3.3 (0.6)	0.39 (0.03–5.5)	8.2 (-)	0.96
RE1629+78	42500 (-)	2.5 (0.1)	5.0 (0.5–50)	8.2 (-)	1.80
RE1711+66	40000 (-)	5.5 (0.6)	0.32 (0.2–6)	8.0 (-)	1.8
RE2013+40	no fit				
RE2024+20	no fit				

Table 4.8: *XSPEC stratified atmosphere fits to DA + dM binaries discovered with the WFC. A dash in the error column indicates that the parameter has been fixed at that value. A dash in the parameter column indicates no constraints within model limits.*

show convincing evidence of line emission, indicating they are all well-separated or have cool white dwarf components. A look at the derived temperatures shows they are all in the range 26 000–50 000 K. Since there are many reflection-effect binaries with white dwarf temperatures in this range, I assume these systems must be well-separated.

Fits with homogenous atmospheres can be made to all of the systems (if constraining the surface gravity of the white dwarf at the canonical value). However, they do little to significantly constrain the column density in most cases, except for RE1629+78. I can obtain no acceptable fits with stratified atmosphere models for four of the six stars in this sample (RE1340, RE1426, RE2013, RE2024).

A full discussion of these systems will take place in chapter 5, after I have analysed the data from the known DA + dK–M binary systems detected with *ROSAT* .

Chapter 5

Known DA + dK–M systems

Once the validity of this mode of thought has been recognized, the final results appear almost simple; any intelligent undergraduate can understand them without much trouble. But the years of searching in the dark for a truth that one feels, but cannot express; the intense desire and the alternations of confidence and misgiving, until one breaks through to clarity and understanding, are only known to him who has himself experienced them.

Albert Einstein

5.1 Introduction

This chapter deals with three post-CE binaries known to exist before the *ROSAT* survey. The systems studied are GD123, Feige 24 and V471 Tau. I use the optically-determined temperatures and gravities of Kidder (1991; table 5.1). I have obtained the *WFC* survey count rates from the Bright Source Catalogue (Pounds *et al.* 1992) and the PSPC survey count rates (Barstow priv. comm.), which are shown in table 5.2. I have then corrected the *WFC* survey count rates for the degradation in instrument response during the survey in accordance with the method used in

§ 3.3.5.1, the revised rates being shown in table 5.3. I fit homogenous and stratified model atmospheres (e.g., Koester 1991) to the data, the results of which are listed in tables 5.4 and 5.5.

5.2 RE1036+46: GD123

RE1036+46 was detected in the *WFC* survey S1 and S2 bands with counts of 0.051 ± 0.006 and $0.199 \pm 0.012\,\mathrm{ct\,s^{-1}}$ respectively. Its position was cross-correlated with the known DA+K binary system GD123 (also WD1033+464; Green, Schmidt & Liebert 1986) during the initial processing stages and was thus it was not a target for the optical ID programme. Some parameters of the system are already known from optical work. For instance Finley *et al.* (1990) find a surface effective temperature of $T_{eff} = 31\,050^{+4500}_{-2900}\,\mathrm{K}$ (they classify the degenerate as DA1), and Kidder (1991) derived $T_{eff} = 30\,200 \pm 300$ (both $1\,\sigma$ bounds).

During November 1991 I obtained further *WFC* and PSPC observations of this source. Four observing slots were allocated, which consisted of 1401, 2031 144 and 1248 s observations through the S2B, P2, P2 and P1 filters respectively. Again, PSPC data (with boron filter) were collected during these exposures.

The *WFC* data show a weak source detected at:

$$\alpha_{2000} = 10^h\,36^m\,23\overset{s}{.}7\ ,\ \delta_{2000} = 46^\circ\,8'\,8''$$

I obtain count rates for the source in two of the filters: $0.08 \pm 0.02\,\mathrm{ct\,s^{-1}}$ in S2B; $0.03 \pm 0.02\,\mathrm{ct\,s^{-1}}$ in P1 (1σ errors). For the third filter, P2, I estimate un upper limit of $0.02\,\mathrm{ct\,s^{-1}}$ (3σ above the local background).

The X-ray detection for GD123 is very weak, with a count rate of only 0.018 ± 0.002 ct s^1. The integrated flux is $10^{-12}\,\mathrm{erg\,s^{-1}\,cm^{-2}}$(0.1–2.5 keV). The pulse height spectrum resembles those of RE1016 and RE1629, except that the GD123 is much brighter in the *WFC* relative to the PSPC than the two other sources. The peak of the PSPC data is at 100 eV ($2 \times 10^{-14}\,\mathrm{erg\,s^{-1}\,cm^{-2}}$) and diminishes towards higher energies. The survey X-ray detection of GD123 was at a

Source	V magnitude	T_{eff} (error) K	Log (g) (error)
GD123	14.34	30200 (300)	7.95 (0.06)
Feige 24	12.56	59800 (3400)	7.45 (0.51)
V471 Tau	13.65	34200 (600)	8.8 (0.28)

Table 5.1: *Optically determined parameters for WD + dK-M binaries. Taken from Kidder (1991).*

Source	Observed *ROSAT* count rates			
	PSPC (err)	S1 (err)	S2 (err)	P1 (err)
GD123	0.294 (26)	0.051 (6)	0.199 (12)	0.03 (1)
Feige 24	0.014 (-)	0.0049 (23)	0.704 (28)	-
V471 Tau	1.11 (25)	0.340 (20)	1.040 (29)	-

Table 5.2: ROSAT *count rates for WD + dK–M binaries. Numbers in parenthesis indicate the error on the count rates.*

Source	Corrected *ROSAT* count rates			
	PSPC (err)	S1 (err)	S2 (err)	P1 (err)
GD123	0.294 (26) (39)	0.057 (6) (9)	0.213 (12) (24)	0.03 (1)
Feige 24	0.014 (-) (-)	0.039 (-) (-)	0.823 (28) (87)	-
V471 Tau	1.11 (25) (27)	0.342 (20) (39)	1.056 (29) (110)	-

Table 5.3: *Corrected* ROSAT *count rates for WD + dK–M binaries. Numbers in parenthesis indicate first the error on the count rate and then the error including systematic calibration component.*

count rate of 0.294 ± 0.026 ct s^1 (without the boron filter). A good fit to the pulse height spectrum cannot be obtained with any models other than a powerlaw (i.e. plasma or blackbody).

There is no evidence for significant periodic variations or aperiodic variations (flaring) activity in any of the EUV or X-ray timelines.

Atmospheric (PHOTAN) fits to the count rates encounter severe difficulties (table 5.4 and figure 5.1). From the survey S1/S2 ratio alone one would assume the white dwarf to either have a large metal content levitated into the atmosphere or a relatively thin hydrogen layer if a stratified atmosphere (which would lead to the required loss of harder EUV flux). However, while the pointed-mode P1 and survey-mode S2A filter constant-count rate curves may be made to agree at a temperature consistent with that derived by Finley *et al.* (1990), and indeed even the survey S1A curve intersects with the P1 curve near the lower limit of the Finley estimate, the survey S1A curve does not intersect with the survey S2A curve.

Another point of note is the discrepancy between the pointed-mode S2B count rate I derive and the survey value for the S2A filter. Manually re-extracting the survey data (to obtain a consistent analysis between the two data sets) and analysing them produces results in agreement with the pipeline analysis. The discrepancy is probably best explained in that the 'correction' for the efficiency degradation calculation is uncertain and it is perhaps not surprising that the survey and pointed count rates do not match. It is not sufficient evidence that the source has varied its output level (and spectral quality) of EUV emission, given that the intrinsic EUV emission from the white dwarf is expected to be stable.

As an experiment, substituting the value of the pointed mode S2B count in the analysis for the survey S2A count rate does alleviate the problem somewhat. The S2 curve is made 'cooler' until it intersects with the S1 curve and the P1 curve simultaneously (the curves overlap for a large portion of the temperature-column plane, assuming 3σ error limits). The common range is now $T_{eff} = 27\,000$–$29\,000$ K, $N_H = 0.5$–2×10^{19} atm cm^{-2}. However, there is no justification for placing

any weight in this argument. If the discrepancy occurs anywhwere, it is in the conversion from pointed mode to survey countrates, and the survey and pointed mode count rates should not be used in the same analysis.

Using the XRT PSPC data points in the homogenous atmosphere (PHOTAN) analysis is of no benefit, the extra curves do not serve to constrain the analysis any further, given that no fit is acceptable with even the three *WFC* data-points.

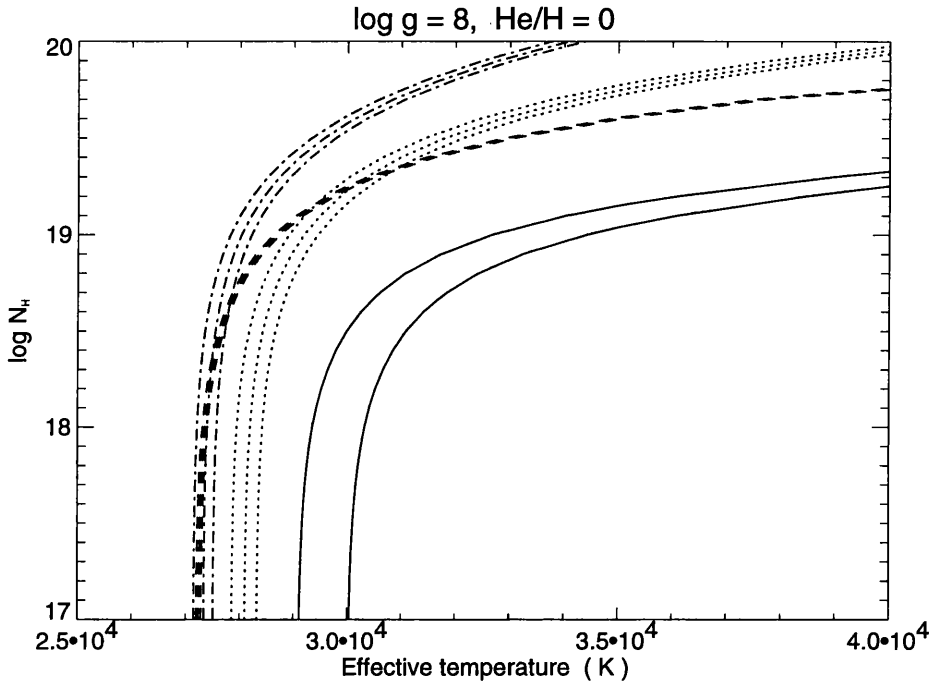

Figure 5.1: *PHOTAN fit to GD123 data, plot of T_{eff} versus log N_H. S1 = dot-dash line, S2 = dotted line, P1 = dashed line PSPC = solid line.*

I have also performed fits to the data including the pointed-mode P1 filter count rate, and the PSPC countrate, using the XSPEC code and chemically stratified models (see table 5.5). Using the S1, S2, P1, PSPC and V magnitude data-points, and a free fit with all parameters allowed to float, the parameters are not constrained well. The 1σ error limits encompass the range T_{eff} = 30 500–60 000 K, N_H = 0–5×10^{19} atm cm^{-2}, M_H is unconstrained within model limits. Fixing the temperature at the optically-determined value improves the fit greatly, deriving

best fit parameters of $N_H = 5.1{\times}10^{18}\,\mathrm{atm\,cm^{-2}}$, $M_H = 6.3 \times 10^{-14}\,M_\odot$. Fixing the surface gravity at the optically determined value leads to best fit parameters of $T_{eff} = 31\,440\,\mathrm{K}$ $N_H = 1.2{\times}10^{19}\,\mathrm{atm\,cm^{-2}}$, $M_H = 1.99 \times 10^{-14}\,M_\odot$.

5.3 Feige 24

Feige 24 was the second extra-solar source detected in the EUV band (Margon *et al.* 1976). It was determined from optical spectra to be a binary system comprised of one of the hottest known (60 000 K) DA degenerate stars and a M1–M2 dwarf star (Holm 1976; Liebert & Margon 1977). The optical spectrum was found to exhibit sharp Hα and He I emission lines, which varied in strength smoothly with the orbital phase, reaching maximum at superior conjunction, and the velocity of which varied in accordance with that of the absorption lines from the M dwarf. The orbital period, at 4.2 d (Thorstensen *et al.* 1978), ruled out significant mass transfer, thus the majority of the emission was determined to arise from reprocessing of the white dwarf's EUV radiation in the M dwarf's facing hemisphere. The system was also found to show ultraviolet resonance lines of Si IV, N V and C IV (Dupree & Raymond 1982), interpreted as originating in both the photosphere and a Strömgren sphere ionized by the white dwarf. The *EXOSAT* EUV spectrum (Paerels *et al.* 1986) could only be matched by assuming radiatively levitated traces of heavy elements (Vennes *et al.* 1989) and not H + He stratified atmospheres. Feige 24 is the prototype post-CE, interacting, non-cataclysmic WD + MS binary. Its orbit is too wide for it to be considered a bona-fide PCB and the companion is too late to have evolved off the MS within the current lifetime of the galaxy.

Feige 24 was detected in the WFC S2a filter band with a count rate of $0.704 \pm 0.028\,\mathrm{ct\,s^{-1}}$. An upper limit for the S1a filter is calculated of $0.030\,\mathrm{ct\,s^{-1}}$. An upper limit of $0.014\,\mathrm{ct\,s^{-1}}$ (maximum likelyhood 2 σ upper limit) can also be obtained from the XRT PSPC survey data. Since we already have several accurate temperature determinations (e.g., $T_{eff} = 59\,800 \pm 3400\,\mathrm{K}$; Kidder 1991) this pa-

rameter can effectively be fixed in any analysis to attempt and constrain the other parameters. However, I find no acceptable fits are obtained to the combined *WFC* and PSPC data-points, either using homogenous H + He models or stratified H + He models. While this may be partially due to having only an upper limit in the S1 filter and PSPC, I expect the actual cause to be not having model atmospheres with a realistic mixture of selected trace heavy elements: for Feige 24 it has been shown that trace abundances of heavy elements can successfully fit the previous *EXOSAT* EUV spectra (Vennes *et al.* 1989) where stratified models cannot, and this situation has not changed with this new data from the *ROSAT WFC* and XRT.

5.4 V471 Tau

V471 Tau is a $P = 0.52\,\mathrm{d}$ binary system containing a hot DA (35 000 K; Jensen, Petrie, Sion & Shipman 1986) and a detached K2V companion. The system displays 9.25 min X-ray and optical oscillations, photometric wave variability, orbital X-ray dips, narrow ultraviolet absorption lines, optical emission lines and flare events (Jensen *et al.* 1986). The system is conjectured to have a stellar wind from the K star (Mullen *et al.* 1989) with a mass loss rate lower limit of $2 \times 10^{-11}\,M_{\odot}\ \mathrm{yr}^{-1}$. Sion *et al.* (1989; 1990) find a circumbinary shell and argue that mass-transfer from the cool star onto the degenerate is negligible due to its rotating magnetosphere.

V471 Tau was detected in the *WFC* EUV survey filters with count rates of $0.256 \pm 0.015\,\mathrm{ct\,s^{-1}}$ in S1a; $1.048 \pm 0.031\,\mathrm{ct\,s^{-1}}$ in S2a, and in the XRT survey with $1.11 \pm 0.25\,\mathrm{ct\,s^{-1}}$.

I can find no acceptable fits given by any of the homogenous atmosphere models, whether attempting to constrain the temperature and surface gravity to be near the optically-derived values or not.

I have also performed fits to the data using the XSPEC code and chemically stratified models: using the S1, S2, PSPC and V data-points, and fixing $\log g$

at 8.0, the best fit parameters are T_{eff} = 32 740 K, N_H = 4.6×10^{18} atm cm^{-2}, M_H unconstrained within model limits. However the 1σ error limits are so large on M_H and N_H as to render the fit unacceptable. Fixing the surface gravity at the optically-determined value leads to best fit parameters of T_{eff} = 33 880 K N_H = 7×10^{18} atm cm^{-2}, M_H = 1.1 × 10^{-13} $M_\odot$. However, the errors are still large. Fixing the temperature at the optically-determined value and keeping log g also fixed improves the fit further, deriving N_H = 7.2×10^{18} atm cm^{-2}, M_H = 1.1×10^{-13} $M_\odot$ with an acceptable χ^2 (table 5.5).

Source	T_{eff}	N_H
	K	10^{19} cm^{-2}
GD123	no fit	
Feige 24	no fit	
V471 Tau	no fit	

Table 5.4: *PHOTAN homogenous atmosphere fits to WD + dK–M binaries.*

5.5 Additional studies

Recently, B93 also report an analysis of these stars using the new modelling code (XSPEC), and determines for GD123 a hydrogen mass layer of 3 × 10^{-13} $M_\odot$ and a column of 5×10^{18} atm cm^{-2}, when fixing the temperature at the optically determined value. The fit obtained by B93 for V471 Tau gives 29 000 < T_{Eff} < 33 000 K, 0 < N_H < 3 × 19 atm cm^{-2} , 0.2 ×10^{-13} < M / $M_\odot$ < 0.7 × 10^{-13}, if the temperature is *not* fixed within the optical limits. There are no acceptable fits obtained for the Feige 24 data.

Source	T_{eff} (err) K	N_H (err) $10^{18}\,\mathrm{cm}^{-2}$	M_H (err) $10^{-14}\,M_\odot$	log (g) (err)	χ^2_r
GD123	30 500 (28 760–60 000)	10 (0–60)	no constraint	9 (7-9)	5
GD123	31 440 (4320)	12 (5)	2.0 (0.3–12.6)	7.84 (-)	1.1
GD123	30 000 (-)	5.2 (2.1)	6.3 (1.6–25)	7.84 (-)	1.7
Feige 24	no fit				
V471 Tau	32 740 (6150)	4 (0–21)	no constraint	8 (-)	8
V471 Tau	33 880 (28 420–55 000)	7 (0–32)	11 (0.001–1000)	8.8 (-)	6.6
V471 Tau	34 200 (-)	7.2 (2.5)	11 (6–19)	8.8 (-)	2.8

Table 5.5: *XSPEC stratified atmosphere fits to WD + dK–M binaries. A dash in the error column indicates that the parameter has been fixed at that value.*

5.6 Discussion

None of the systems dealt with in this chapter can be fitted with any homogenous atmosphere models. This firstly adds yet more weight to the already overwhelming evidence that there is a wavelength-dependent flux discrepancy between the observations of degenerate stars and the predictions of the chemically homogenous models (e.g., Paerels *et al.* 1986; Barstow 1992, 1993c).

In the optical region, all these stars fit the predicted flux distribution very closely, it is the data-points in the EUV and X-ray regions that cannot be made to converge with the model predictions; they are lower than calculated. I have tried to fit these stars' data with chemically stratified atmospheric models, in order to see if this phenomenon could be responsible for the short-wavelength opacities. For two of the stars, GD123 and V471 Tau, it is indeed possible to fit the data. In the case of GD123 and V471 Tau, it is possible to obtain a fit to the data with most of the parameters allowed to float. However, the quality of the fit is poor, and the error limits encompass virtually the entire range of the models available. Fortunately, there have been high S/N optical spectra taken of both these stars, and thus reliable determinations for the surface gravity and effective temperature. By fixing these two parameters at the values derived from the optical spectra, the fits are improved and I can constrain the remaining parameters to a narrower region. In the case of GD123 and V471 Tau this leads to sufficiently good fits that I find a chemically stratified atmosphere consisting only of H + He to be an acceptable solution to the atmospheric structure. It is interesting to note that B93 find that acceptable fits to the V471 Tau data may be obtained only when not fixing the temperature to be at the optically-derived values. However, the temperature the fits converge at when it is allowed to float *are* close to the optically-derived values. In my analysis, when constraining the temperature to the optical values a better fit was obtained.

Feige 24, on the other hand, cannot be fitted by any stratified model. Assuming that the problem lies with the theory (not the implementation of the model) this

indicates that the EUV and X-ray opacity is not formed by a stratified atmosphere but is almost certainly due to the heavy element flux-blocking. This is further evidence that radiative acceleration of metals plays a significant part in the spectral output of degenerate stars, confirming the work of e.g., Vennes *et al.* (1989), who showed that the *EXOSAT* spectrum of Feige 24 could only be fitted by the inclusion of trace heavy elements (C, N, O Ne, Na, Si, S, Ar and Ca) into the atmospheric models.

If a self-consistent set of model atmospheres including the effects of heavy-elements was available for all stars, we may find that it will successfully fit the stars I was unable to fit with homogenous atmospheres (GD123 and V471 Tau), and that a stratified atmosphere model is no better at fitting the data. However, the test of which is the better theory must await the formulation of a suitable model atmosphere for these cases.

In chapter 4, poor fits to the data on four out of six DA + dM binaries were obtained with stratified-atmosphere models. Homogenous atmospheres proved better at fitting the data, but provided little constraint to the range of the intervening column.

Note that in the population of white dwarfs as a whole (chapter 2), the fraction of the population that cannot be fitted by, say, a homogenous atmosphere, or whose EUV-derived effective temperature deviates from the Balmer profile derived effective temperature, is much lower than the fraction of the binary systems (studied at the end of chapter 2, and in chapters 4 and 5) which exhibit a deviation or inability to fit.

To quantify the flux obscuration, I calculate the normalised fluxes of the sources (as in chapter 2). I can also calculate the *WFC* to PSPC flux ratios, as I have the PSPC data-points. The results are shown in table 5.6. I also include the systems studied in chapter 4.

These results are plotted in figures 5.2 and 5.3.

Interstellar absorption will act to preferentially absorb the lower energies, i.e.

Source	Normalised fluxes			Flux ratios	
	PSPC	S1	S2	S1/PSPC	S2/PSPC
RE1340+60	0.119	1.17	2.87	9.8	24.1
RE1426+50	0.051	0.47	1.39	9.2	27.3
RE1629+78	2.87	13.33	34.86	4.6	12.1
RE1711+66	1.57	1.48	<2.79	0.94	>1.7
RE2013+40	1.03	1.53	1.53	1.49	1.49
RE2024+20	2.27	2.85	4.39	1.26	1.93
GD123	0.169	1.108	7.797	6.56	46.14
Feige 24	<0.002	<0.147	5.847	-	>2924
V471 Tau	0.337	3.523	20.474	10.45	60.75

Table 5.6: *Normalised fluxes and flux ratios for DA + dM binaries discovered with the WFC.*

S2, S1 and PSPC in decreasing order. In the plot of normalised flux, this will shift all of the filter points downwards, with the lower energy filters suffering the most shift. Any intrinsic opacity sources that preferentially extinguish the higher energies will move the points with the higer energy filters suffering the most shift.

In the plot of flux ratio, if higher energies are preferentially extinguished then the ratio will increase and the points shift upwards. The S2/PSPC point should undergo less shift than the S1/PSPC point. If lower energies are preferentially extinguished, then both points will shift downwards, with the S2/PSPC undergoing more shift.

From the plots I deduce the following: for the sources RE1340, RE1426 and RE1629 the S1 and PSPC points are consistent with the sources having an $N_H > 3 \times 10^{18}\,\mathrm{atm\,cm^{-2}}$, and an opacity consistent with interstellar absorption, although the S2 flux is somewhat more strongly absorbed than predicted for a pure H atmosphere. Neither RE1340 nor RE1426 could be fitted by a stratified atmosphere, but homogenous fits were acceptable. In the case of RE1629, homogenous and stratified models can be fit, but the error limits on the H-layer mass of the stratified model span layers massive enough ($10^{-11}\,M_\odot$) to give the appearance of a pure H atmosphere. Thus there would appear to be no photospheric opacity source preferentially obscuring the harder EUV flux in these stars. If anything, the lower energy bands are over-absorbed. From the analysis in chapter 4, it appears that all three of these sytems have well-separated components.

For GD123 and V471 Tau, their flux output is consistent with equivalent absorption between all of the passbands. Since interstellar column has an increasing cross-section at lower energies, this implies there may be some high-energy absorption in the star itself. In the atmospheric model fitting procedure, I found that no homogenous atmosphere fits were acceptable, both stars requiring a stratified atmosphere (with temperatures and gravities constrained to be at the optical values) to fit the data. In both cases the H-layer derived is allowed to be thin enough that the underlying He-layer will significantly absorb in the EUV and possibly show He

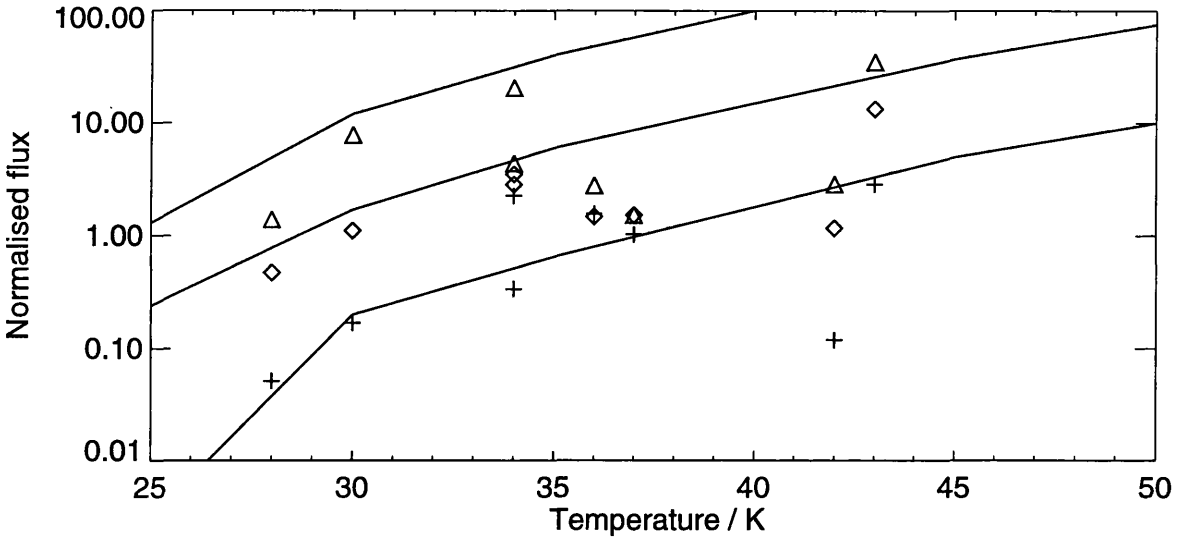

Figure 5.2: *Normalised fluxes versus effective temperature for EUV-selected sample of white dwarf binary systems. Crosses, diamonds and triangles indicate the PSPC, S1 and S2 fluxes respectively. The top, middle and bottom curves represent the S2 and S1 and PSPC fluxes for a pure H atmosphere, with* $N_H = 3 \times 10^{18}\, atm\, cm^{-2}$.

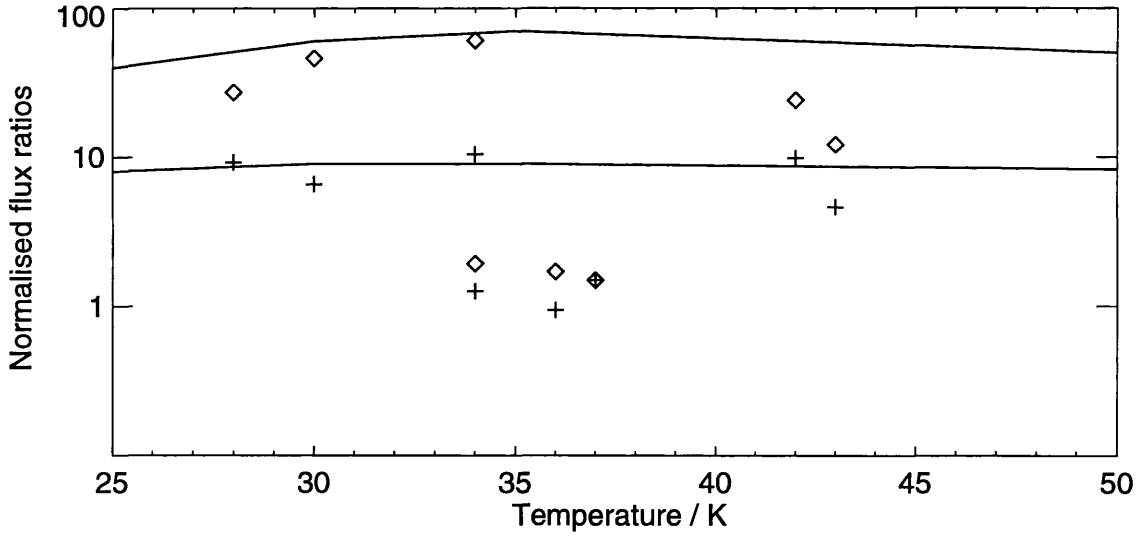

Figure 5.3: *Normalised flux ratios versus effective temperature for EUV-selected sample of white dwarf binary systems. Crosses and diamonds indicate the S1/PSPC and S2/PSPC ratios respectively. The top and bottom curves represent the S2/PSPC and S1/PSPC ratios for a pure H atmosphere, with* $N_H = 3 \times 10^{18}\, atm\, cm^{-2}$.

features in the optical. Note that V471 Tau is a close binary with many observed continuum and emission line phenomena, conjectured circumbinary material and wind-loss from the late-type companion.

For Feige 24 the data strongly indicate a source of high-energy obscuration. The PSPC and S1 fluxes are extremely absorbed compared to the S2 point. The ratio of S2/PSPC is a factor of 50 above any of the other stars' points on this plot. From the model fitting we see that no homogenous or stratified atmosphere model will fit the data. Thus this is the strongest case for a star with metal opacities in the photosphere, as shown by Vennes *et al.* (1989). It is notable that the WD in Feige 24 is indeed a DAZ (in the optical), and it has been postulated to accrete metals via a wind from the M-star (Sion & Starrfield 1984).

The remaining sources, RE2013, RE2024 and RE1711 all appear to have extreme absorption in both the S1 and S2 bands as compared to the PSPC. This may be interpreted to mean that there is a large intervening column. In fact the model fitting indicates these three have the largest columns of the sample. Stratified atmosphere models cannot fit the data for either the RE2013 or RE2024, whilst homogenous models can. For RE1711, both models can be fitted to the data, with an overlapping range of column density. However, the derived H-layer of the stratified model spans two orders of magnitude. RE2013 is known to be a close binary system with a short orbital period. The other two systems are assumed to have well-separated components from the analysis in chapter 4.

Except for RE2013, the WD in close-binary systems with late-type companions thus seem to have extra opacity sources in their photospheres, and these data indicate that the opacity source is at least in some cases due to heavy elements rather than a stratified atmosphere.

Most of the systems analysed in chapter 4 appear well separated and some will not have undergone CE phases. If there is a correlation between a close binary and photospheric opacities, we should expect most of these systems to fit the homogenous models, as is the case.

Note also that most of the degenerates in this subsample have low effective temperatures. If metal levitation is the cause of much EUV opacity, it would not be expected to operate in these systems, except for Feige 24 (which is what I find).

The question is now raised, what causes the distinction between the three stars analysed in this chapter (and the others which cannot be fitted with homogenous atmospheres) and those which I can fit with homogenous models. They are not simply all hotter, as can be seen from their derived effective temperatures. For Feige 24, we can be certain the opacity is caused by metals levitated in the photosphere (due to a high temperature and low gravity), but the other systems are too cool (GD123 and V471 Tau are comparible in temperature to the stars which do fit with homogenous atmospheres), nor do they all have significantly lower surface gravities, the two parameters thought to be responsible for the effective levitation of heavy elements. Thus the differences we see at present may result from either differing initial composition or differing ongoing evolutionary process (see chapter 1) not necessarily temperature dependant. The former can be ruled out, since these stars are cool enough (i.e. old enough) to have their original heavy-elements sink into the core under the action of diffusion. Any heavy elements present now must be due to either accretion or levitation, as convection cannot bring them back up from the core (even if it was active in these stars).

Of the currently known PCB, virtually none are strong EUV emitters. I have checked through the survey data, and found that the only PCB detected in either band are in fact V471 Tau and the new discoveries RE2013+40 and possibly RE1016−05.

Of the known WD + dK–M close-binaries (post-CE, but not necessarily PCB) these three (GD123, V471 Tau, Feige 24) were the only ones detected in the WFC EUV survey.

The close WD + dK–M systems not detected in the *WFC* survey include: NN Ser (WD = DAO, $T_{eff} = 55\,000$ K), GK Vir (DA, 50 000 K), HZ 9 (DA, 22 000 K), PG0308+096 (DA, 15 000 K), Case 1 (DA, 13 000 K), PG1026−002 (DA), RR Cae

(DA), and BE UMa (DO, 80 000 K). Excluding Case 1, PG0308 and BE UMa as being too cool DAs and too hot a DO to be detetcted by the *WFC* , respectively, this indicates that the rest of these systems may have large photospheric opacities.

These systems are conventionally non-interacting, that is there is no mass-transfer between the stars. However, it is feasible that tidal stresses are affecting the compositional structure of the degenerate star by causing, for example, rotational currents in the degenerate star's photosphere (Nather, Robinson & Stover 1981). The white dwarf evolution may also be affected by the CE phase, resulting in an increased loss of hydrogen. Depending upon the time since the CE phase, when heavy elements may be stirred up, and the diffusion timescale, all heavy elements should have sunk into the core within 10^4 yr, unless maintained by radiative levitation or other mechanisms.

The degenerate star in these binary systems may be accreting matter from the M-companion, via a stellar wind, as is proposed in the case of V471 Tau (Sion, Dermott, Mullan & Shipman 1990; Mullen *et al.* 1989). No winds have been detected in any of the other systems, although one has been postulated for Feige 24 (Sion & Starrfield 1984) in order to explain the observed metal abundances in the optical spectra. It is not yet known how such a late-type (M) star would support such an outflow. Alternatively, perhaps the M-star is not yet fully detached from its Roche lobe or, more likely, there is circumbinary material left over from the Roche-lobe overflow event (as in V471 Tau). Thus matter may be gradually accreted onto the degenerate star, from this pool of material, rather than a conventional wind.

If this scenario is correct, it is likely that the heavy-element (and He) opacity is the result of a subtle balance between the evolutionary history, accretion rate, radiation pressure, tidal influences and gravitation (Chayer *et al.* 1987; Chayer, Fontaine & Wesemael 1988). Thus the difference between which systems exhibit the opacities and to what extent may not be easily predictable.

The paucity of EUV output from close WD + dM binaries may turn out to be a very significant finding. Most of the degenerates in PCB systems now seem

to be of type DAO (Tweedy *et al.* 1993), inferring that there is a difference in the evolution between the WD in close and well separated binaries, at least on the AGB and probably thereafter. This implication is that either the He is not allowed to settle below a thick H-layer or that there is a deficiency of total H compared to an isolated degenerate star, leading to a stratified configuration with a thin H layer.

Thus there would seem to be two different mechanisms for obtaining photospheric opacity in close binary systems: accretion from the cool companion and an evolutionary divergence from isolated stars, leading to an over-abundance of He.

The search for late-type companions to degenerates that I conducted in § 2.8 revealed candidates which on the whole had photospheric opacity towards the upper limits of that seen amongst the entire sample of stars I was studying. At the time I was unable to provide an acceptable explanation. However, if there is a correlation between the prescence of a companion star and the prescence of extra photospheric opacity in the degenerate star, via one of the mechanisms as proposed above, this would explain the finding.

Supporting this view, the average H-layer mass of the three stars analysed in this chapter seems to be slightly lower than the mean of the B93 sample. This correlates with the fact most degenerates in PCB and similar close binary systems are type DAO, since the layer-masses in some of these stars are tending towards the mass required to show faint He traces in the optical spectra. If these stars are at the upper ranges for the H-layer mass in these systems, then it would explain why the other sytems are not detected, effectively having a larger He opacity. It should be instructive to check if the undetected PCB and related systems have relatively more prominent He features in the optical, as this could help determine if stratified atmospheres are the cause of EUV opacity.

If the opacity is due to metals, then the models I have been using may not strictly be applicable, but the low H-layer mass is indicating that there are heavy elements in the photosphere. These stars would thus represent the cases with the

smallest abundances of the class. I thus propose that looking at IUE spectra of the stars *not* seen in the EUV, to determine metal abundances in relation to the detected stars, should indicate whether heavy elenents are a source of EUV opacity in these systems. Unfortunately, not all of the elements visible in the EUV show strong line transitions in the UV.

However, if these two observations could be made for many stars it would help constrain the source of the EUV opacity, and hence the mechanism by which it is produced, and the evolutionary history of these binary sytems.

5.6.1 H-layers

The thin H-layer masses derived in the previous chapters of this thesis are in conflict with evolutionary calculations (Iben & Tutakov 1984; Koester & Schönberner 1986), which require much thicker atmospheres.

These evolutionary calculations predict that stars with thin H-layers evolve similarly to He stars, but those with thick H-layers evolve differently from He/thin H-layer stars. Since there is a class of very hot, high-gravity He stars (PG1159 stars) Wesemael, Green & Liebert (1985) and Fleming, Liebert & Green (1986) argue that if DA stars have thin H-layers, an analagous class of hot DA stars should be seen; yet no DA stars as hot as 70 000 K, have yet been observed.

However, several current lines of investigation are providing evidence that the evolutionary models are in error.

Models of ZZ Ceti stars require H-layers of mass $<10^{-8}\,M_{\odot}$ if their atmospheres are to become unstable.

The distortions of the high-order Balmer line profiles of most cool DA stars found by Bergeron *et al.* (1990, 1991) are due to the presence of He (Liebert & Wehrse 1983) and imply that most DA stars below 11 500 K have significant amounts of He in their atmospheres, due to the onset of convective remixing at this temperature. In order to produce the He/H ratios observed for most DA stars, these data imply a mass for the H-layer of 10^{-14}–$10^{-11}\,M_{\odot}$.

The DO–DB gap may be explained as the result of the cooling sequence on a white dwarf with an initially predominantly helium atmosphere with trace hydrogen. Initially, due to the short diffusion time-scale, the hydrogen is hidden and the star appears as type DO (Nather, Robinson & Stover 1981). Hydrogen will float to the surface as the star cools, to give the star the characteristics of a DAO (Vennes *et al.* 1988). Eventually, a thin surface H-layer builds up, reaching $10^{-11}\,M_{\odot}$ by the time the star has cooled to 45 000 K. The star is classified as a DA. With further cooling, convection will mix in He from the transition zone, turning the star into a DAB/DBA (Shipman *et al.* 1986). When T_{eff} is down to 30 000 K enough He has been mixed in to convert the star into a DB. This theory sets an upper limit to the allowed H abundance, and thus the implied H-layer masses, of $\sim 10^{-11}\,M_{\odot}$.

Although Nather, Robinson & Stover (1981) found no viable mechanism to allow such a small H-layer to remain on the degenerate star after the PN stage, wind loss and diffusion-induced nuclear burning have been advanced as two possible solutions (Michaud, Fontaine & Charland 1984)

5.6.2 Levitation or stratification?

G191-B2B, one of the hottest DA degenerate stars known (and inferred to have formed relatively recently from a hot PNN subdwarf star), shows the presence of weak, narrow absorption lines due to NV, CIV and SIV (Bruhweiler & Kondo 1981). Similar high-excitation lines have been found in Feige 24 (Dupree & Raymond 1982). However, the lines in G191-B2B show none of the Zeeman splitting nor circular polarisation found in magnetic stars (Angel, Borra & Landstreet 1981). Bruhweiler & Kondo (1981, 1982, 1983) have proposed that these lines in G191-B2B are due to metals which have been radiatively levitated to the surface of the star and then expelled in a low-velocity stellar wind, the lines originating in an expanding shell about the degenerate star. Calculations by Fontaine & Michaud (1979) and Vauclair, Vauclair & Greenstein (1979) show that levitation could produce sufficient quantities of carbon, nitrogen and oxygen. Expelling these metals in a wind is a

more difficult problem. Dupree & Raymond (1983) propose that they are instead formed by the hot star ionising the local interstellar continuum. Reid & Wegner (1988), show, with remeasured radial velocities for the lines, that they *are* formed in the WD photosphere, as is the Hα emission line observed in the core of the absorption line. In the case of Feige 24, it has been argued (Dupree & Raymond 1983) that the metals are accreted from a stellar wind originating on the M-dwarf companion, or that the lines originate in the stellar wind itself (Sion & Starrfield 1984).

Vennes *et al.* (1988) showed that radiation pressure is far too low to account for much He to be levitated into the upper atmosphere, and thus expect G191-B2B to have a strongly stratified atmosphere, with a H-layer mass $< 10^{-14}\,M_{\odot}$. This is thin enough to allow domination of the EUV flux by the underlying helium. Indeed the H-layer mass derived by Koester (1989) is $5{\times}10^{-16}\,M_{\odot}$. However, B93 show that neither homogenous nor stratified H + He models can account for the EUV and X-ray opacity observed in recent *ROSAT* data; the photosphere must contain other metal species. Furthermore, Wilkinson, Green & Cash (1993) have recently obtained the first EUV spectrum of G191−B2B, which demonstrates Fe VI and O III ions in the stellar photosphere, yet a lack of He features, conclusive evidence that it is heavy elements and not a stratified atmosphere that is providing the EUV opacity in this star, similar to the case for Feige 24.

The EUV, optical and X-ray data analysis of the *ROSAT* identified white dwarfs contained within this thesis, and the analysis of B93 finds that isolated DA stars below 40 000 K can be fitted by either homogenous atmospheres of nearly pure H or stratified atmospheres with H-layers on the order of $10^{-13}\,M_{\odot}$. Opacity due to He is almost negligible in either case. For many stars above 40 000 K, there is an obscuration of the EUV flux, and the data cannot be fitted by homogenous or stratified models containing H and He only. This implies that the obscuration is due to metals, maintained by radiative levitation, a conclusion supported by Tweedy (1993b). No DA stars are seen above 60 000 K, which implies that enough

metals (e.g., Fe, at this high temperature) are levitated to block the EUV flux almost completely.

In order to determine the true nature of the opacities in the white dwarf photospheres, it will be necessary to develop self-consistent models of the spectral distribution of a degenerate star with many heavy elements present in trace abundances, and compare this to the predictions of the stratified model atmospheres. At the current time, modelling of stars with trace metals has only been conducted by constructing models of each individual star's spectrum. However, progress is being made towards the goal of a obtaining a realistic theoretical model of the flux distribution.

Figure 5.4 illustrates the relative flux output of model atmospheres with varying metal abundances. The solid curve is the flux from a comparison model of pure hydrogen. The dashed curves represent successively increasing metal abundances (as they depart further from the pure H curve). Note the backwarming excess at the FUV end. This may be searched for in UV spectra or photometry to determine in which stars heavy element opacity is an importnt contributor.

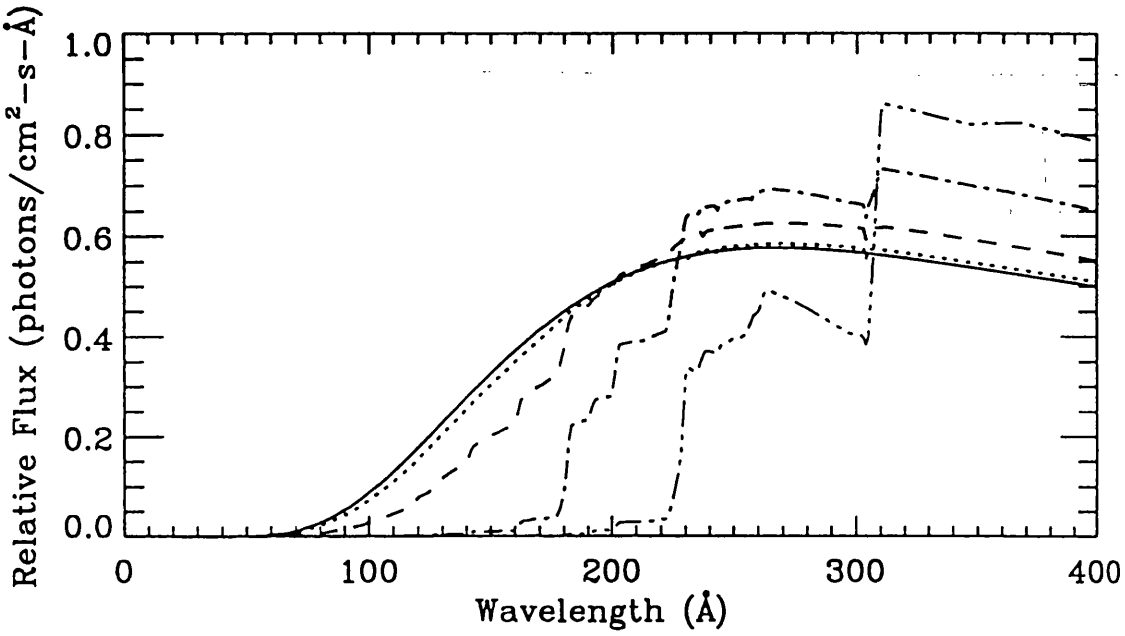

Figure 5.4: *Relative flux ouput of model atmospheres with differing metal abundances. The solid line is that for a pure H atmosphere at 54 000 K, log (g) = 7.5; the dotted, dashed, dot-dash and dot-dot-dot-dash lines indicate atmospheres of successively increasing metal abundances, at the same effective temperature and surface gravity. As can be seen, flux is increasingly blocked from the shorter wavelengths (<200 Å), and re-radiated at longer wavelengths. Taken from Finley, Dupuis, Paerels & Koester (1993).*

Chapter 6

Conclusions

The great tragedy of Science—the slaying of a beautiful hypothesis by an ugly fact.

T. H. Huxley

6.1 Summary

I shall give a brief overview of the work completed in this thesis, and the deductions that are made possible by the analysis in each chapter.

The data used in this thesis are from the *ROSAT WFC* EUV and XRT X-ray all-sky-survey and pointed mode phases, and from the optical follow-up identification programme.

After an introductory chapter on the state of white dwarf astronomy, in binary and isolated systems, a study of newly-discovered apparently isolated white dwarfs (Chapter 2) shows that there is a marked discrepancy between the effective temperatures assigned to some of them via fits to the optical Balmer absorption lines and fits to the EUV data. This discrepancy is worst for the hottest stars. Fits to the EUV data underestimate the temperatures in comparison to the optical fits. This indicates there is an unaccounted opacity source in the hot stars which affects

the EUV flux output much more severely than the optical flux output. It is shown that this is not an interstellar column effect, but the opacity source must reside in the photosphere of the white dwarf. This opacity is generally assumed to be due to either helium (homogenously mixed in with the hydrogen or in a stratified configuration) or to heavy elements levitated into the atmosphere by the radiation pressure. The data are not sufficient to discriminate between these options.

The EUV-selected white dwarf distribution function is comparible to that of optically-selected white dwarfs.

A detailed search through all the white dwarf optical spectra reveals several peculiar examples, which may be binary systems with low-lumonosity late-type dwarf companions. A proportion of these stars also exhibit apparent Balmer line emission cores. This may be due to one or a combination of several reasons, such as line reversal near the top of NLTE atmospheres, active companion stars or nebula emission. These stars exhibit a more marked discrepancy between their EUV-derived and optically-derived effective temperatures than the general population.

In chapter 3 I make a detailed study of the EUV, X-ray and optical data on RE1016−05, a DA + dM binary system. This leads to estimates of the white dwarf temperature (47 000 K), systemic distance (115 pc), line parameters and secondary spectral type (dM2). I show that the observed EUV and X-ray emission originate from the white dwarf rather than the M-star. There is no definite flaring activity or any significant periods seen in the EUV, X-rays or optical data. A discussion of the possible configurations and evolutionary history of the system is considered. With my data it is not possible to conclusively determine if the system is a PCB. Later data obtained by Tweedy *et al.* strongly indicate this to be the case.

A study of the white dwarf binary systems discovered with the *ROSAT WFC* (chapter 4) and of previously known binary systems detected with *ROSAT* (chapter 5) shows that in some of the systems where the EUV data are impossible to fit with a homogenous atmosphere model, they may be modelled by a stratified H + He atmosphere with a thin topmost H-layer. However, a significant proportion of the

white dwarf atmospheres still cannot be fitted by a simple H + He model, whether homogenous or stratified. This is conclusive evidence that, at least in some hot stars, there must be significant opacity caused by heavier elements, presumably levitated by radiative acceleration.

There appears to be a correlation between close binary systems and extra opacities in the white dwarf photospheres. This may be related to the finding that most of the degenerate stars in PCB systems now appear to be of type DAO.

In conclusion, the following are the main results of this thesis:

- Hot white dwarfs often exhibit an enhanced photospheric EUV opacity source, which is not seen in the cooler stars. Helium is not the sole cause of this extra EUV opacity. In some stars it must be due to heavier elements, levitated by radiative acceleration. Helium may still be responsible for the EUV opacity in some cases, however, when a stratified atmosphere is invoked.

- In a stratified atmosphere, thin H layers ($\sim 10^{-13}\,M_{\odot}$) seem to be prevalent, rather than the thicker layers ($\sim 10^{-4}\,M_{\odot}$) derived via evolutionary calculations, suggesting they are inadequate.

- RE1016−05 is most likely a PCB, though this is only confirmed with the latest evidence.

- The evolution of the atmospheres of white dwarfs in binary systems is significantly different from that for single star evolution, leading to a preponderance of stars with photospheric opacities.

6.2 In the future...

With the guest observer program for *EUVE* well underway, it is now possible to spectrally resolve metal lines in the EUV (with a dedicated observatory, as opposed to the occasional sounding rocket experiment). Thus direct observational evidence

should be forthcoming to show if metals or helium provide the opacity in many peculiar stars, both as individuals and as a class.

There is also work being done on the inclusion of heavy elements into the white dwarf model atmospheres, which should lead to a much better test of the theories competing to explain the atmospheric composition, structure and evolution in white dwarf stars.

With additional observations the *ROSAT* data may be used to calculate formal luminosity functions and mass-distributions of the white dwarf population. Since the volume of known white dwarfs is being increased by the *ROSAT* observations, this should lead to improved data about the scaleheight, distribution, formation rates and evolution of these objects, and ultimately the MS stars from which they evolve.

Appendix A

Data Reduction

The only uniform CCD is a dead CCD

Craig Mackay

A.1 Introduction

This chapter deals with the reduction procedures used both in the automated reduction software I wrote for the *ROSAT* Optical Identification Programme and in the analysis of the other observations described in this thesis. It is essentially intended to provide a background explanation of the basic reduction techniques used and then describe those novel procedures which I have used or 'new' software I have written to overcome particular problems.

A.2 Software written for Optical ID Programme

I developed an automated reduction procedure for use with the data obtained by the *ROSAT* Optical Identification Programme. The concept was to be able to sufficiently reduce the large volume of spectra being acquired at the telescopes each night, before the next night's observing began. This would provide the observing

team with the ability to make decisions about the best observing policy for each night. I attended two of the Optical Identification observing runs; January 1991 and December 1991, during which I set up and modified the processing software and was part of the observing team.

A.2.1 The Faint Object Spectrograph

The Faint Object Spectrograph (FOS) is a fixed format low-resolution cross-dispersing spectrograph with CCD detector. FOS-1 (the original instrument) is in operation on the INT, while FOS-2 (an improved version) is in operation on the WHT. The *ROSAT* Optical Identification Programme made use of the INT so we were concerned mainly with FOS-1, but the software could easily be used for the FOS-2 with little alteration.

The FOS-1 is mounted below the Intermediate Dispersion Spectrograph (with which it shares the A & G unit) at the Cassegrain focus of the Isaac Newton Telescope (INT). The optical layout is based on a Schmidt camera (without collimator) in the diverging beam from the Cassegrain focus. Spectral coverage is from 3500–11 000 Å in two dispersion orders. Dispersion is provided by a transmission grating followed by a cross-dispersing grism (150 lines mm^{-1} transmission grating blazed at 7300Å cemented to cross-dispersing prisms). The camera consists of an aspheric corrector plate, a silver-coated spherical mirror and a field flattening lens. The aspheric corrector plate is cemented to the underside of the grating/grism combination. The detector is a coated GEC P8603 CCD mounted inside the camera body, cooled by copper conductors leading to the cryostat.

The FOS-1 parameters are shown in table A.1. A diagram of the instrument and a plot of its throughput are shown in figures A.1 and A.2.

In what follows I will describe the various steps used in the reduction procedure. These are: debiasing; flatfielding; spectral extraction; wavelength calibration; fluxing; extinction corrections. Then I will summarise the automated software system, method/techniques of implementation, and quality of the results.

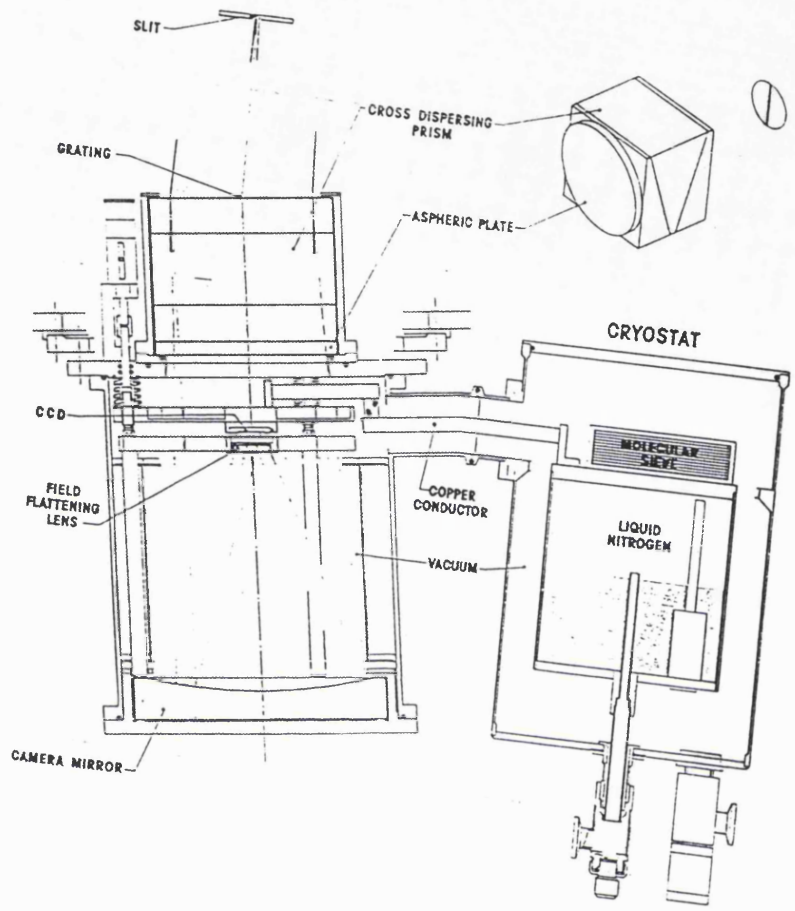

Figure A.1: *FOS instrument*

Instrument	FOS-1
Telescope	INT
Focal ratio	f/15 (from Cassegrain focus)
Image scale (slit)	5.41 arcsec mm^{-1}
Image scale (detector)	58 arcsec mm^{-1}
Detector	Coated GEC P8603 CCD, 578x385 pixels
Pixel size	22μ square, or $1''.24$
Camera focal ratio	f/1.4
Grism grating	150 lines mm^{-1}, 7300Å blaze
Spectral orders	Two : 5070–11 270Å & 3230–5630Å
Reciprocal dispersion	486 & 245Å mm^{-1}
at detector	10.7 & 5.4 (Å $pixel^{-1}$)
Optical system resolution	33μ (Zero Slit Width)
	$1''9$ spatial
Wavelength resolution	16 & 8Å(1st & 2nd orders)
Pixel resolution	1.5

Table A.1: *FOS parameters.*

A.2.1.1 Debiasing

All pixels in CCD images are given a zero-offset value, so as to avoid obtaining any negative values in the dataset. This is called the *bias value* of the CCD image. This bias value must be subtracted from the whole image area before the data can be usefully processed. Since the exact value of the offset is subject to some random variation, the same correction cannot be applied to all the frames; rather it must be individually measured for each frame. The bias value of each CCD frame can be measured from the underscan region, which is the unexposed portion of the chip

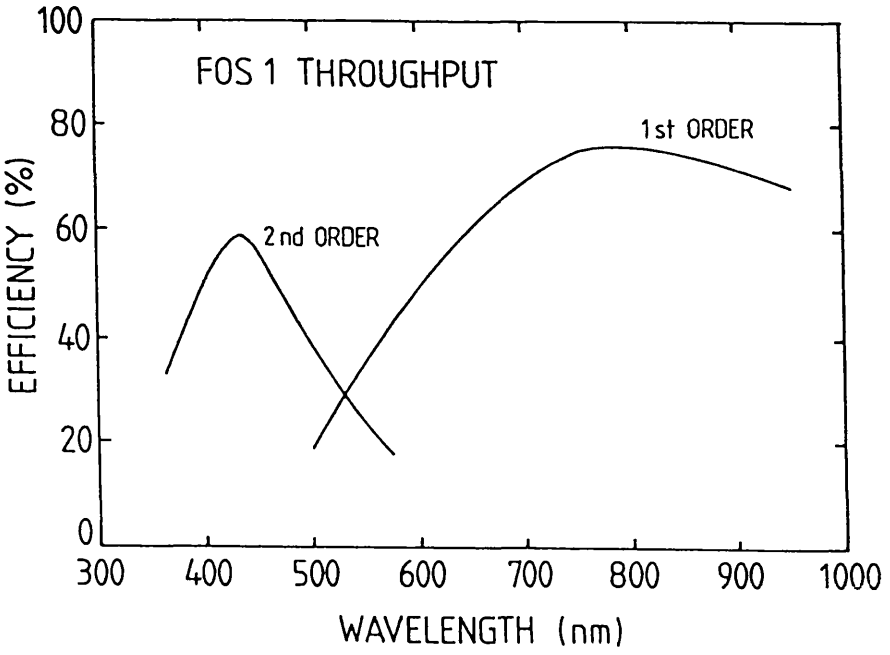

Figure A.2: *FOS throughput*

at the top and left hand edges, when seen from above. There is also an overscan region, occupying the right hand and bottom edges of the chip. These two regions are subject to all the conditions and instrumental effects that the rest of the chip experiences, save the exposure to starlight. Thus correction is a simple matter of subtracting from all pixels that value of the bias determined by averaging the count per pixel in the underscan region.

Bias must not be confused with pre-flash. Pre-flashing is a short pre-exposure illumination of the chip. This is done to ensure correct charge transfer on certain (mainly older) CCDs where only charges over a certain threshold value are transferred properly. Bias is an electronic offset applied to the data to avoid negative values. The CCDs we used in the FOS and IDS do not need to be pre-flashed, since their charge transfer characteristics are very good.

At this stage there are two other effects to consider: dark currents and readout noise. The dark current is simply the charge accrued via thermal generation of electrons during the exposure. To alleviate this problem the CCDs are cryogenically cooled to $< 180\,\mathrm{K}$. At this temperature, the quantity of electrons released due to

thermal effects is negligible (e.g., for the GEC CCD, $< 1\,\mathrm{ADU\,pix^{-1}\,hr^{-1}}$, or, for our average exposure, $<0.1\,\mathrm{ADU\,pix^{-1}}$).

The readout noise is the noise generated when measuring the charge quantity in each pixel. This is typically ~ 8 electrons per pixel. As long as this is a known quantity we can take it into account during the data reduction.

A.2.1.2 Flatfielding

The sensitivity of any CCD will naturally vary across its surface in two different ways. Firstly, there will be large scale variations across the whole chip (as a function of, for example, substrate thickness) and secondly much smaller scale sensitivity variation from pixel to pixel, called 'granularity'. Both effects must be removed before the reduction of the data can be considered complete.

The response variation across the chip is generally smooth and can be satisfactorily modelled with a low order polynomial. In practice, the gross variation of *count rate* over the area of the CCD will also be dependant on other factors such as the instrumental setup and illumination, not just the intrinsic variation. Thus this effect is best studied by exposing an image of the twilight sky, so that the detector is illuminated in the same manner as for the object exposures. We can then model the gross variations (in turn sum up the data along each axis of the CCD and fit polynomials to the result) and remove them from the other CCD frames (simply by dividing these by our fitted polynomials). This technique is most useful for long-slit exposures, to measure the illumination variation along the slit due to vignetting.

The pixel-to-pixel variation or granularity, however, is in practice random (i.e. not smoothly varying), but is fixed for that device (i.e. constant for all exposures). Thus one can make a measurement of the variation and correct *all* frames for this effect. To do this an exposure is made of the twilight sky, a tungsten lamp, or the inside of the telescope dome (under good lighting), the task being to obtain an even illumination of as much of the CCD as possible. It is important to have

no sharp variations in the illumination (such as stars) which might be confused with the granularity. The bias value and gross variation are removed, as explained previously, to leave just the pixel to pixel variation. Divide any de-biased CCD frame by this pixel variation file, and the pixel to pixel variation is removed. As this granularity is actually very small (usually at the level of a few percent in the average pixel count) the counts per pixel needed for this type of flat-field are fairly high ($\sim$ 5000 per pixel) otherwise the noise level of the exposure itself will be comparable to the granularity.

A.2.1.3 Extraction

The next step in the data reduction is to transform the two-dimensional raw FITS data files into a one-dimensional 'spectrum' of counts versus channel number. There are several competing methods of achieving this, as described below.

A.2.1.4 Optimal versus Standard

In a standard extraction, the columns on the CCD containing significant starlight are summed, then a scaled amount of the sum of those columns containing sky is subtracted from this value. The spectrophotometric accuracy of the observation is increased when all the star columns are summed; however, this may actually decrease the S/N, since some of the outer star columns contain very little signal. Excluding these columns compromises the spectrophotometric accuracy of the spectrum. The optimal extraction technique was developed (Robertson 1986; Horne 1986) to overcome this quandry of maintaining spectrophotometric accuracy whilst obtaining a high S/N in the reduced spectrum. The method is based upon assigning a weighting to each pixel when performing the summation, based upon the signal strength of that particular pixel. The weighting may take the form of a fixed value for each column (i.e. simply proportional to the summed signal of all the pixels in that column) or it may be allowed to vary smoothly down the column i.e. as a function of wavelength. The variation is constrained to be smooth to avoid

statistical noise on individual pixel strengths. Optimal extraction programmes are often used in the reduction of straight spectra, with orders parallel to the edges of the CCD chip.

A.2.1.5 Curved and straight spectra

Most spectrographs (for example the IDS on the INT or ISIS on the WHT) produce straight dispersion orders. These are generally arranged to be parallel to one of the CCD axes, for ease of data reduction, although there are some spectrographs where the dispersion orders fall at a diagonal to the axes. Cross-dispersing spectrographs such as the Faint Object Spectrograph (FOS) use a second grating or grism to obtain more than one spectral order on the same CCD chip. This leads to curved spectral orders. These present a more difficult problem at the extraction stage than do the straight order spectra, since the spectra produced by cross-dispersing instruments do not have smooth variations in signal from pixel to pixel along one column.

My initial approach was to straighten the curved spectrum by 'resampling' the raw CCD data, then use a linear extraction algorithm. However, this can lead to a number of problems. The spatial profile of the resampled light source is slightly altered from the true shape, and the alteration is wavelength-dependent. The resampled profile will coincide with and deviate from the true profile at the integer and half-integer values of where the resampled 'pixel' edges cross the detector pixel edges respectively. Given that the optimal extraction procedure makes an estimate of the spatial profile of the source, this introduces spurious humps into the reduced spectrum since the profile is either held constant or allowed to vary smoothly, which is usually not enough to account for the rapid variations in the stellar profile caused by the resampling. The problem becomes severe in the case of a spatial profile which is of comparable size to the pixel size—which is indeed the case with the FOS and the good seeing conditions at La Palma. Most other spectrographs would exhibit less of a problem since the spatial profile is covered

by many more pixels. Bright stars are most afflicted by this phenomenon, and as predicted, the humps show up at the brightest part of the spectral order i.e. where the instrumental response is greatest.

One solution to the curvature problem is to perform a 'virtual' resampling, as described by Mukai (1989). In this procedure the data are resampled onto a much finer grid than the detector pixels themselves, but solely to determine the weighting values. The spatial profile fit in this new grid is allowed to vary not only as a smooth function of wavelength but also as a function of the resampling noise, as described above. For each column in this new grid, only those virtual pixels close to the nearest detector pixel centre are picked, and a low-order polynomial fitted. To calculate the weighting factor for any pixel in the real spectrum, a value is interpolated between the fitted polynomials to the two nearest virtually resampled columns. With these new weightings, the spectral orders need never actually be 'straightened'. In fact, this approach is the one I eventually adopted, after comparisons of the efficiency and overall quality of reduced spectra I tested with both methods showed that it was superior.

A.2.1.6 Wavelength calibration

To calibrate the IDS and FOS spectra, exposures were made of CuAr and CuNe arc lamps. The spectral lines were identified, and low-order polynomials fitted to their wavelengths (orders higher than 5 can introduce spurious features into the calibration). The polynomial coefficients were then used to provide the wavelength scales for the other exposures. To check stability (since it is not unlikely that telescope flexure or other problem can cause a shift in the wavelength scale), several arc exposures were made throughout the night, and compared against each other. Where a difference was noted, an the polynomial coefficients were interpolated given the time separation between the arcs and the object spectrum.

A.2.1.7 Flux calibration

In order to measure the true flux output of the object stars, we need some way of calibrating for the instrument response. This is achieved by observing (with an identical setup to that of the target stars) several photometric 'standard' stars for which very precise absolute flux measurements have been made (usually in 40 or 80 Å bins over a wide wavelength region). We can in theory divide the absolute flux in each bin of the absolute spectrum by the observed count rate in this bin range, to obtain our Instrument Response Function (IRF), which we then fit with some function. Thus is should be possible to correct for the response at all points in our observed spectrum.

In practice it is not this simple, since there is no guarantee that the IRF can be fitted by a simple function. What we can do is fit the difference between this IRF and an IRF created at a previous observation.

A.2.1.8 Correcting for atmospheric absorption lines

A number of telluric absorption features (the A band, B band etc) usually appear in spectroscopic observations at these wavelengths (6000–10000Å). However, the extent of these features is highly variable, depending upon the precise atmospheric conditions at the time of observation (i.e. airmass, humidity, atmospheric particulates), which makes them difficult to remove from an object spectrum, especially in an automated reduction procedure. The best way to eliminate these features in general is by eye, but for the automated procedure some other way had to be found.

To obtain a measure of the parameters of the telluric absorption lines an observation of a nearby F8 star was made for every field observed at the telescope. F8 stars were chosen because they have no intrinsic absorption features apart from Hα in the region occupied by the telluric absorption. As long as the F8 star was observed close in time and sky coordinates to the field stars, then its light should have encountered the same atmospheric conditions, so that the absorption features

should follow the same pattern as those in the field stars. The task was to fit the absorption features in this F star spectrum, and deduce a correction spectrum to be applied to all the other field star spectra.

Initially, the method chosen was to fit the extracted but pre-fluxed F8 spectrum with multiple cubic splines *outside* the wavelength region of the absorption features (to follow as closely as possible the real shape of the continuum), but to ignore the features themselves, and interpolate a smooth fit to represent the intrinsic stellar continuum. The real spectrum is then divided by this fit, to produce an inverse map of the absorption features. The continuum level outside the lines should now be set to unity (being divided by itself) whereas the absorption features should appear as emission 'spikes'. This correction spectrum was multiplied with all the extracted object spectra to correct for their absorption features. In general a visual check of the reduced spectra will reveal if the process has been a success; since the majority of object spectra (which are obviously not the identification for the EUV source) will be normal midrange dwarfs, they should show no excessive emission or absorption in these regions. Any resultant wide absorption features from an under-correction or even an emission feature from an over-correction can be readily spotted.

As the software evolved, it was switched to using the post-fluxing F8 star spectrum, which resulted in better telluric line removal.

A.2.1.9 Correcting for atmospheric extinction

Atmospheric extinction can be broadly divided in three main components: Rayleigh scattering; molecular absorption; aerosol scattering. The first two contributors have a wavelength dependency in their effect, the third is usually 'grey' i.e. it affects all wavelengths equally.

All the spectra processed by my software received a standard treatment based on the extinction of Hayes & Latham (1975). This treatment, however, only extends as far as the Rayleigh scattering component. This formula used is given in the

equation

$$A_{Rayleigh}(\lambda, h) = 9.4977 \times 10^{-3} \left(\frac{1}{\lambda}\right)^4 \left[\frac{(n-1)_\lambda}{(n-1)_{\lambda=1}}\right]^2 exp\left(\frac{-h}{7.996}\right), \quad (A.1)$$

where the index of refraction term is given by

$$\frac{(n-1)_\lambda}{(n-1)_{\lambda=1}} = 0.23465 + \frac{1.076 \times 10^{-2}}{146 - (1/\lambda^2)} + \frac{0.93161}{41 - (1/\lambda^2)}. \quad (A.2)$$

The molecular absorption contribution can be separated into two sources; ozone absorption and telluric absorption. The former contributor resides in a fixed height range above ground level, and once measured for any particular site will remain fairly consistent over a long timespan. Hayes & Latham provide a means for calculating the ozone absorption thus

$$A_{ozone} = 1.11\ T_{ozone}\ k_{ozone}(\lambda), \quad (A.3)$$

where $k_{ozone}(\lambda)$ is the absorption coefficient in cm^{-1}, from Gast (1960), and T_{ozone} is the total ozone above the observatory in atm-cm, from Allen (1963).

The telluric component is much more variable, since at any given time the amount of water vapour in the atmosphere above any site will depend on many prevailing conditions such as ambient temperature, humidity, cloud cover. The absorption is thus extremely difficult to calculate theoretically and no attempt is usually made in spectral reductions to account for this effect. I have followed this convention, so users of the data should be aware that telluric absorption may account for an extinction of up to 0.01 magnitudes per airmass in severe conditions.

Hayes & Latham deduce that the aerosol scattering may also be approximated thus

$$A_{aerosol}(\lambda, h) = A_0 \lambda^{-\alpha} exp\left(\frac{-h}{H}\right). \quad (A.4)$$

However α, H and A_0 are not easy to determine. This is why it is more conventional and more accurate to measure the total extinction while observing and

thus deduce the contribution from aerosols from the data rather than attempt a tricky calculation. This is the convention I have used in performing my checks on the 'colour' change in the IDS spectra observed in February 1992 (see § 3.2.3.1). Otherwise, no routine correction is made by the processing software.

A.2.1.10 Spectral results

Once all the spectra have been fully calibrated, they are passed through a set of routines which extracts the Johnson magnitudes and colours of each object.

A.2.2 The Intermediate Dispersion Spectrograph

The Intermediate Dispersion Spectrograph (IDS) is a variable format medium dispersion spectrograph with a choice of two different detector types. Either a CCD or the Image Photon Counting System (IPCS) may be used as the detector, depending on the type of work being done. The IPCS has a much lower detector noise but is also less efficient than the various CCDs available (GEC P8603 RCA SID501, and more recently an EEV chip). For the optical ID programme the IDS was always used with the CCD as detector because of the greater efficiency and the greater ease with which the data may be reduced.

A.2.3 IDS automatic reduction software

This procedure is potentially more complicated than the FOS spectral reduction, because of the variable wavelength range and dispersion available, unlike those of a fixed format device.

The adjustments that need to be made for this imply that a method be found for automatically measuring and applying wavelength scale calibrations.

Movements of the telescope while re-orienting, or general flexure of the structures due to thermal changes or movement may cause a shift in the wavelength offsets of the spectrograph. Thus spectra taken over any period may have a grad-

ual zero point offset which varies with time. Experience from previous spectra suggests that this offset may reach a value of up to 1 Åin particular severe cases. Fortunately the dispersion of the IDS (using the same grating!) over a particular observing session is very stable, which reduces the problem to that of finding the value of the offset. The general method used is simply to take many arc spectra, one for every object that is observed (or every exposure taken in cases where wavelength is critical). Then the arc spectra are calibrated from wavelength tables by eye and the object spectra calibrated by the relevant arc spectrum or an interpolated value between the two arc spectra nearest to it. As the range of dispersions and wavelength centres is multitudinous, it would be almost impossible for any software to determine which grating/dispersion/wavelength centre was used for any particular arc spectrum. However, since the same grating is kept for may exposures, it is reasonable to assume that the only change between most arc spectra is a linear shift.

The method chosen for the automated reduction was for the software to perform a cross-correlation between the various arc spectra to determine what the relative change in the wavelength axis is. The observer is required to manually calibrate the *first* arc spectrum taken for each different arc lamp/grating/grating angle configuration. The software is then able to determine from the grating/grating angle stored in the FITS header which wavelength range the spectrum should occupy, and deduces the linear offset value, which it then applies to the relevant spectra. When it encounters a new grating/grating angle configuration it looks for the appropriate calibrated arc spectrum.

No correction is attempted for the telluric absorption bands in the IDS spectra. This is due to the vast variability of the wavelength coverage possible with the device. The majority of the spectra would fall outside the ranges where any significant telluric bands occur, thus any correction is superfluous, and any attempted could only degrade the spectra. Even in the spectra where a telluric absorption band may be present, it may fall anywhere within the spectra, even halfway off the

end of the spectra, which would cause major problems for any software reduction. Since this problem occurs much less frequently than in the FOS spectra, and may be a more difficult problem, it is probably still a job for a manual analysis, at least at this stage of the software package.

The other IDS spectra reduction stages, apart from those described above, follow the same pattern as for the FOS spectra, and can be reduced in the same manner.

Although I embarked upon the coding of this part of the software, I was not able to complete it due to time constraints. The development was taken over by Jon Mittaz.

A.2.4 FOS automatic reduction software

Several methods of achieving a satisfactory automatic reduction procedure were tested. The main decision was whether to write the reduction procedure based around the STARLINK FIGARO spectral reduction packages (which are a 'standard' set of programs, but which do not have a full implementation at MSSL) or instead to use the ARK software packages (developed at Oxford, Cambridge and MSSL) which in many cases are superior to the FIGARO equivalents in terms of quality of results (although originally they did not have a full implementation at La Palma, where the reduction software would mainly be of benefit, and at some other sites).

The 'handling' software which has the job of controlling and passing the data to the various reduction procedures in turn was written in VMS DCL. The extra utility programs necessary were written in FORTRAN. A log file of the entire processing run is kept for fault tracing.

I wrote a preliminary automatic reduction procedure based around each of the two possible software suites, and tested the competing packages on a large volume of spectra previously acquired at La Palma. I then compared the resultant reductions for the stability against spectral defects (such as cosmic rays or bad chip pixels)

and the quality of the spectrum (i.e. signal-to-noise ratio, S/N). In general, the algorithms written for the ARK software were marginally superior, as in many cases they were written specifically to either overcome the problems associated with the curved FOS spectra (see previous explanation) for which the FIGARO procedures were no more than adequate, or compensate for unsuitable or even non-existent reduction procedures. The results produced with the ARK software had greater S/N and often showed features difficult to see in the FIGARO reduced spectra, although the difference was in most cases small, being mainly noticeable in those exposures with an inherently low S/N or count rate.

I also tested the packages against each other in terms of robustness. An automatic reduction procedure is fraught with dangers, and an ability to run flawlessly, even when operated by a novice, is of great benefit. The software must produce reliable results, or give some indication if things are going wrong, rather than simply crash with no helpful error messages. In this respect each of the systems have similar strengths and weaknesses. Simple problems with the processing pipeline such as incorrect filenames being passed to programs are well catered for, with specific error messages from the software package. The processing will in general exit cleanly (but in bad cases may crash out) from the current reduction but will carry on with the next one in line. Thus not much data may be lost, and the user can go back later on and manually reduce the offenders or else resubmit the processing having made the requisite changes. However it should be noted that if the incorrect name has been arrived at for one dataset, it is highly likely this is due to some basic underlying cause, and will re-occur for other, if not all, files. Also if the one file that is misread and skipped is an important file e.g., a photometric standard, then it may have ramifications later on when the other processing requires the missing file. This will usually cause the later processes to exit (or crash) without reducing the data any further, although the pipeline is designed to try and run to completion, in case the error is trivial or so the user can trace the cause of the problems.

Problems with the reduction processing itself (i.e. a star too faint for the automated procedure to extract) are in general also handled well, producing a clean exit rather than a crash. Enough information is produced by the reduction packages to allow the user to work out why the problem has occurred. The reduction will then be able to run on to completion without affecting the other datafiles being reduced, unless it is a critical file such as standard star or arc lamp, which again may be the cause of later crashes, or worse, if the output from one package is erroneous but completed, may subtly alter the subsequent processing. As before the user can rectify the situation easily given the level of information output, and this course is recommended in all cases, to ensure the integrity of the resultant data. I found the ARK packages to be slightly better in this respect, and this is undoubtedly due at least in part because one of the many reasons this software was written was to provide a more stable environment and user-friendly interface. Most problems such as these would not cause a crash in the ARK packages, and a string of error messages is output when succeeding operations are tried without the necessary files. The FIGARO environment was slightly worse at handling these problems, being less informative and/or more likely to crash rather than exit.

In fact, some of the problems with the reduction processing itself stem from the first problem discussed; misdirected files. For example, attempting to 'extract' an arc lamp exposure as if it were an object spectra will create a 'No stars found' type error since the illumination will not have the gaussian spatial profile the software expects. This type of problem generally does not crash the package (and, indeed, in some cases is allowed to happen because it is known not to) but may cause errors later in the processing if the reduction is needed (not one of the intentional misdirections). This type of problem can be the most serious of all, since the user may not realise it has happened if no crashes or obvious error messages are produced, yet the data may be corrupted by processing with the incorrect files. Thus it is recommended that the log file is checked for every reduction run performed regardless of whether it crashes or not, and the user should always be

on the lookout for 'strange' spectral effects. A good test of the integrity of the data is to calibrate the photometric 'flux' standard stars with each other, and check the output spectra against the published spectra for any deviations.

Other errors can occur when the software conflicts in some way with the operating system directives e.g., overrunning file-space or writing to protected directories. This usually causes a fatal crash from the application running and thus will terminate some or all the rest of the processing (all in the case of the two examples cited, since it will re-occur for every file). The cause may be clear if the system error message is lucid, but this is not always the case. The simplest cure is to re-run the processing after clearing the system problem. I regard these type of problems as trivial since they have no effect on the scientific quality of the data reduction, merely whether it can actually take place or not. Re-running at an appropriate time will produce correct results without alteration of the software or processing methods. These problems will affect both reduction systems equally.

To summarise, in most cases where an error is found and its ramifications are uncertain, it is advisable to re-run the whole pipeline. In any case, one must be aware that subtle problems may occur and should carefully check the spectra for unexpected effects. Given the above scenarios, it was decided that the ARK reduction software was a better choice for the automated reduction system than the FIGARO software.

A.2.5 Software performance

After a short period of testing and improvement the reduction procedure was found to be very stable, running through to completion most of the time. If a problem was encountered, it was normally very easy to spot the reason and re-run the software, (since the log is made of all the various reduction attempts). The main problem area is the accuracy of the flux calibration, which is a very difficult correction to automate. After many revisions the software is now much improved and used at many other sites than La Palma. It has been used to perform a complete and

consistent re-analysis of all the data taken at La Palma for the *ROSAT* optical ID programme, which are now collated in the *ROSAT* Optical ID Database.

A.2.6 Spectral problem: ripple effects

During the first *ROSAT* optical ID observing run (January 1991) it was noticed that some of the spectra exhibited a curious 'rippling' effect. This seemed to occur mainly with short exposure bright objects (usually standard stars or F8 stars) and was most severe at the point in the spectra with the greatest count rate and curvature (i.e. the short wavelength portion of the first order, 6000Å). An example spectrum is shown in figure A.3.

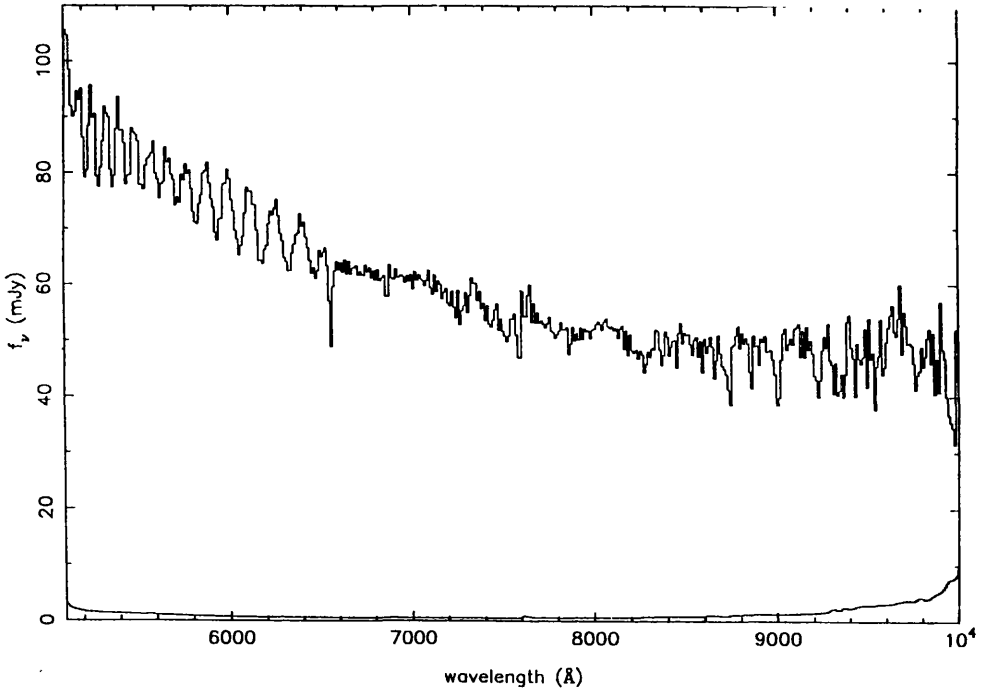

Figure A.3: *Undersampling ripple in the FOS spectra*

This effect is caused by undersampling. As the curved spectral order passes over the pixel boundaries on the CCD the spectral light falls onto a varying number of rows of pixels and inter-pixel gaps. Normally the profile is large enough compared to the pixel gap size that negligible amounts of light are lost between the pixels. However, in the case of good seeing conditions, such as we has for this observing

run, the spatial profile can become narrow enough compared to the pixel size (1.2 arcsec) that significant light *is* lost in the inter-pixel gaps. The period of the ripple will depend upon the rate at which the spectrum crosses the pixel boundaries, which is dependant upon the curvature and inclination of the spectral order. Thus the ripple is much 'faster' and thus appears more pronounced at the bluer wavelengths, occurring over a scale of $\sim$ 10Å, whereas it may occur over a scale of up to 500Å at the far-red end of a spectrum where the spectral curvature on the CCD is slight. Looking at the variation in the amplitude of the ripples, I calculate that it peaks at a semi-amplitude on the order of 10% (in the blue), which I consider very severe. The effect drops off significantly to the red of the first order, and is not apparent in the second order. However this may be because the much lower count rate and greater curvature is hiding the ripples amongst the noise.

There appears to be no easy way to theoretically solve this dilemma, since it would depend on many temporally variable parameters. After a short investigation, I concluded that a treatment of the problem would require a modelling of the ripple in each spectrum. Even then, it may not be possible to recover the full data. Due time constraints, the affected spectra had been noted, but no corrective action had been taken.

Since that time, the problem has been reported by other observers. Rutten *et al.* (1992) present a means for correcting the ripples, based upon an empirical modelling of the spectra. This involves modelling the shape and amplitude of the ripple on an isolated part of the spectrum with no intrinsic features. Firstly, they fit a smooth curve to the spectrum, then divide the spectrum by the fit to obtain a normalised spectrum. Next they trace the spectrum across the CCD to determine the wavelength to pixel boundary relationship, convert this to a CCD spatial position to pixel boundary relationship and fold it to reveal an expected flux versus pixel boundary position. This curve is then applied to the data, factoring in the amplitude of the ripples, which must be measured for each spectrum (and may vary along the wavelength of the spectrum).

It is my opinion that this technique could be instigated for the afflicted spectra taken during the *ROSAT* optical ID runs, with the possibility of obtaining much cleaner spectra than those currently reduced.

A.2.7 Standard star selection software

During the survey runs it is necessary to have standard stars ready to observe for each field of target stars. Both a photometric standard star for flux calibration and an F8 star for calibration of atmospheric telluric absorption bands are needed. As the order in which targets were observed and even which targets were actually observed was constantly changing during the run, it was necessary to have some means of quickly identifying the relevant standard stars for each field. Thus I wrote a software package to calculate the nearest bright F8 star and photometric standard star to the field stars for any position on the sky and time of day. The F8 stars I obtained from the SAAO catalogue on magnetic tape. The photometric standards I obtained from the ARK database at MSSL (which is based upon the list of photometric standards at the La Palma observatory).

Initially the concept behind this program was to allow a schedule for a night's observing to be drawn up in advance by the computer. However, after the observing runs started, and it became clear how variable and flexible the actual target list might become, it was realised this was not really feasible and the program evolved into the simpler form of a standard star allocation utility as described above.

A.3 Other reduction techniques used

A.3.1 White dwarf line profile fitting

A particular task required in the analysis of *ROSAT* Optical ID Programme data was that of fitting the Balmer absorption lines present in white dwarf spectra. To this end I obtained some white dwarf model atmospheres from D. Koester, which

are based upon pure hydrogen atmospheres (DA stars) at various temperature (T_{eff} = 20 000–60 000 K) and surface gravity levels (log (g) = 7.5–8.5).

My procedure, called DWARF, allows the cross-correlation and χ^2 test of the similarity between a particular stellar atmosphere model and the object spectrum. Any portion of the spectra (whole continua or individual Balmer line profiles) can be compared against each other. I then use the method of χ^2 minimisation to obtain error estimates on the best fit model.

Models are available with temperatures and surface gravities as follows:

T_{eff} = 20 000, 24 000, 25 000, 26 000, 26 000, 28 000, 30 000, 35 000, 40 000, 45 000, 50 000, 55 000, 60 000 K.

Log (g) = 7.5, 8.0, 8.5.

A.4 ROSAT data reduction

Here I give a brief description of the reduction of the *ROSAT* data. In general the same techniques used for the survey data applies to the pointed phase data also, although in a few cases there is a different implementation of the software to perform it.

A.4.1 X-ray data

This data was reduced using the ADAM and ICL environments and the ASTERIX software processing system.

The dataset is received on a magnetic tape, in the form of FITS type files. It is then converted to STARLINK SDF format. An image of the source field is created from the event data, which is then used as the basis for future reduction decisions; when an area of interest in the image is decided, the image plot is used to delineate the portions of the dataset used for the subsequent processing. A source and background region are defined, and the data within these area is processed for either spectral, temporal or image use. The background data is subtracted from

the source data, the resulting file is exposure corrected for dead-time losses and then corrected for the detector response. The output file is then suitable for use by the observer, and may be fitted within the ASTERIX system or exported for use in other software packages, for example XSPEC.

A.4.2 EUV data

The survey data was reduced using the ADAM environment and extraction and detection software developed by the consortium institutes—the Point Source Searching algorithm—PSS.

The process is similar to that for the X-ray data. The EUV data is received on magnetic tape and downloaded to disk. One particular filter type is selected and a source and background dataset created. The background is removed from the source data, and the result output for analysis.

A.4.2.1 Temperature vs. Column density modelling with WFC points

Given that our EUV counts are produced almost exclusively by the white dwarf components in our systems, it is possible to perform a modelling of the atmospheric parameters of the white dwarf and the distance to the system.

The software package PHOTAN at Leicester contains a selection of various white dwarf model atmospheres. These are normalised to the magnitude of the white dwarf in the target system and folded through the filter responses to produce an expected count rate assuming no interstellar absorption. However, there is significant absorption present and at any particular wavelength the same count rate may be produced by many different combinations of white dwarf flux (thus surface temperature) and absorption column to the system (i.e. an increase in temperature and thus flux can be counterbalanced by an increased absorption). The software calculates the differing parameter range of absorption and temperature for which the observed count rate can be achieved in that filter and outputs the result as a curve of constant count rate in surface temperature versus column density space.

With more than one set of filter count rates, it is theoretically possible to determine the exact temperature and column density, since the curves must agree at one point only. However, there is obviously some error range and in general the more data points available the better the constraints possible.

The standalone PHOTAN software was eventually outdated, with the inclusion of this aspect of the modelling into the standard XSPEC software package. This allowed a more formalised fitting procedure, including the calculation of a χ^2 statistic on the derived parameters.

A.5 White dwarf photometric regressions

Taken from Fleming, Liebert & Green (1986).

From Greenstein (1984), an empirical relationship between M_v and multichannel colours is found:

$$M_v = 11.857 + 2.882(U-V) - 0.519(U-V)^2 \tag{A.5}$$

and

$$M_v = 13.033 + 3.114(G-R) - 0.799(G-R)^2 \tag{A.6}$$

for which the zero-point is corrected to AB79.

In Strömgren colours, Green (1980) finds

$$M_v = 11.50 + 7.56(b-y) \tag{A.7}$$

In Johnson colours Greenstein (1988) derives

$$M_v = 11.61 + 5.11(B-V) - 1.11(B-V)^2 \tag{A.8}$$

and Sion & Liebert (1977) deduce

$$M_v = 11.246(B-V+1)^{0.60} - 0.045 \tag{A.9}$$

Fleming, Liebert & Green also derive an empirical relation between Hβ equivalent width and absolute magnitude:

$$H\beta_{ew} = -13.13 + 71.32(M_v - 10) - 20.22(M_v - 10)^2 \qquad \text{(A.10)}$$

for stars with $M_v > 10.5$

Appendix B

The ROSAT mission and follow-up

It is alledged that when Einstein and his wife visited the Mount Wilson Observatory in California, Mrs. Einstein pointed to a particularly complex piece of equipment and asked its purpose. Their guide said that it was used to determine the shape of the universe. "Oh," she said, not at all impressed, "my husband uses the back of an old envelope to work that out."

B.1 Instrumentation

ROSAT carries two main instruments. The X-ray Telescope (XRT) which operates in the band 0.1–2.4 keV, and the Wide Field Camera (*WFC*) operating in the band 17–210 eV. The XRT may be used either with the position sensitive proportional counter (PSPC) or the High Resolution Imager (HRI) as the detector, receiving the photons from the X-ray Mirror Assembly (XMA). The Wide Field Camera project is supported by the UK Science and Engineering Research Council. The *WFC* was developed by a consortium of five UK institutes: the Universities of Birmingham and Leicester, the Mullard Space Science Laboratory of University College London,

SERC's Rutherford Appleton Laboratory and the Imperial College of Science and Technology, London (Wells *et al.* 1991).

B.1.1 The *WFC*

The optics consist of three gold-coated aluminium Wolter-Scwarzschild type I mirrors in a nested configuration (for a fuller description see the *ROSAT* Technical Description manual). The detector has two curved Microchannel Plates (MCPs) and a resistive anode readout system (the curvature is to match the optimum focal surface). The front end MCP has a CsI photocathode on the front face to enhance XUV efficiency. There are eight filters contained in a filter wheel. Six of these are science filters, which are comprised of two pointed phase filters, P1 (56–83 eV) and P2 (17–24 eV) , plus two of each of the survey filters, S1a (90–185 eV) and S1b (90–210 eV), S2a and S2b (62–111 eV). The remaining two are an opaque filter and a UV interference filter. The pointed phase and survey phase filters have different diameters. Although all cover the full field-of-view of the *WFC* , the pointed filters will be vignetted if observing towards the edges.

B.1.2 The XRT

The XMA consists of four nested gold-coated Zerodur grazing incidence Wolter type I mirrors.

The PSPCs are multiwire proportional counters with a cathode strip readout configuration to allow position determination. The are positioned behind carbon and lexan coated polypropylene entrance windows.

The window supports consist of several mesh structures and a rib. Owing to the sharp focus of the optics, there is the possibility of an object being obscured behind one of the thick mesh wires; thus whenever the XRT is observing, *ROSAT* is set on a slow 'wobble' diagonal to the mesh wire direction.

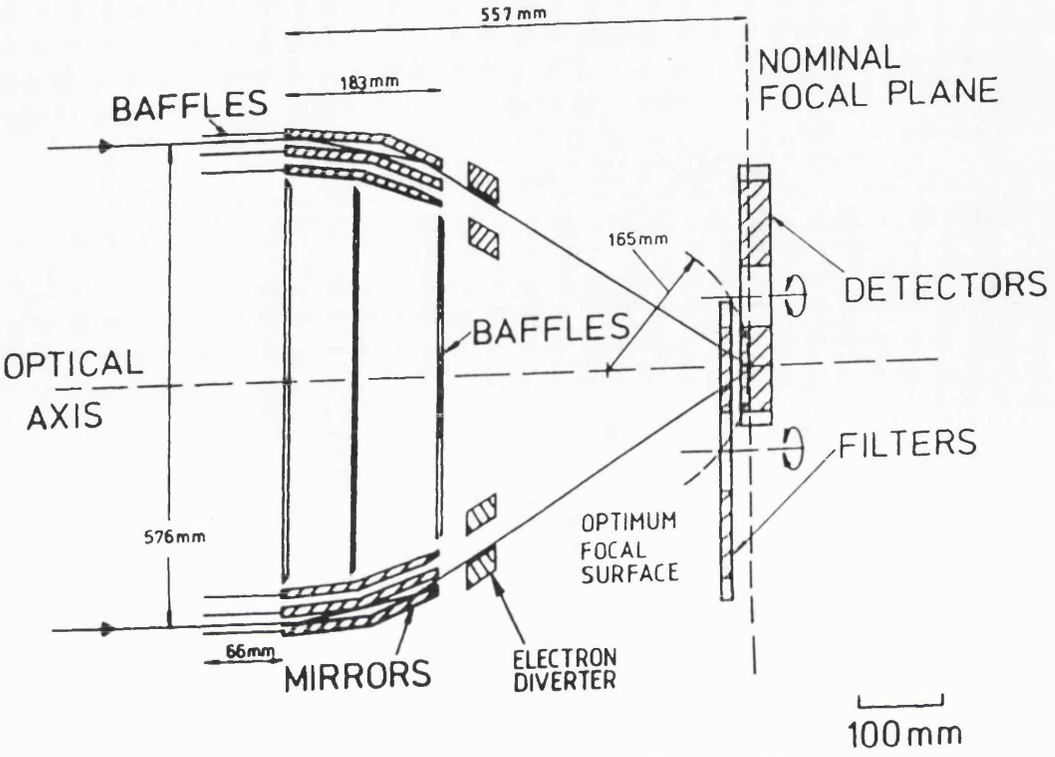

Figure B.1: *A schematic of the WFC assembly*

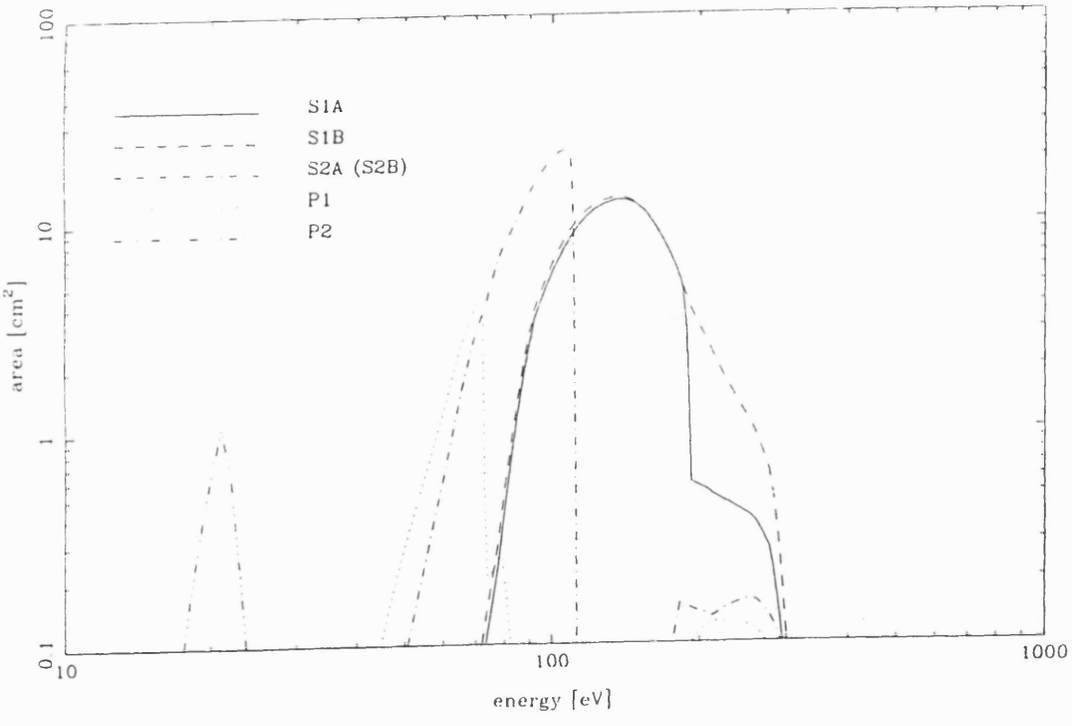

Figure B.2: *Effective areas of the WFC filters, at the beginning of the survey phase.*

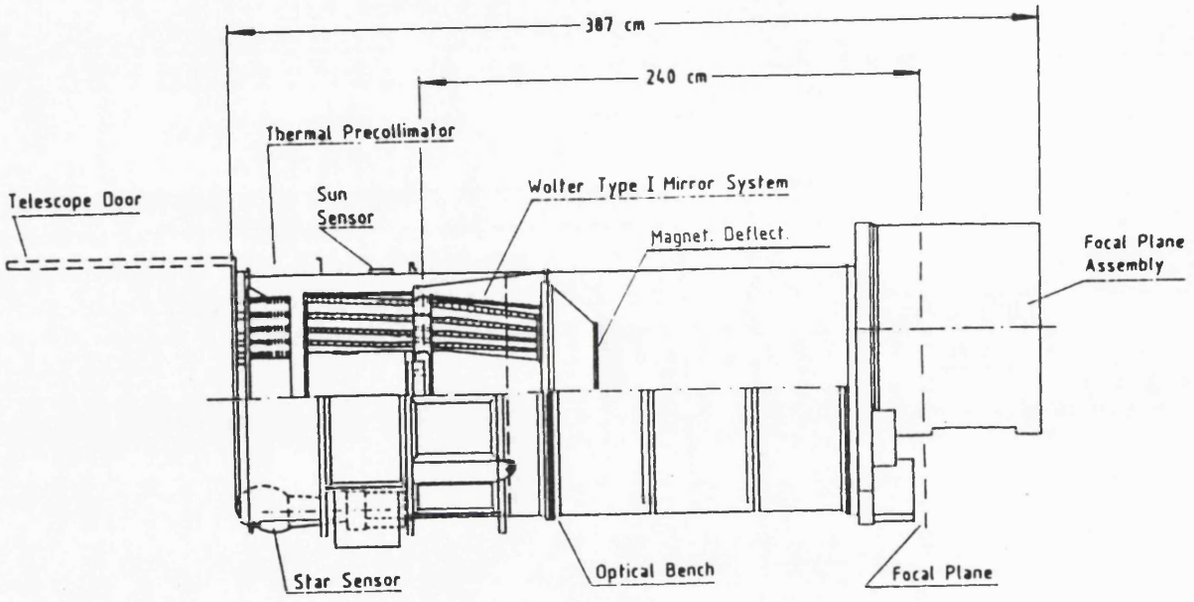

Figure B.3: *A schematic of the XRT assembly*

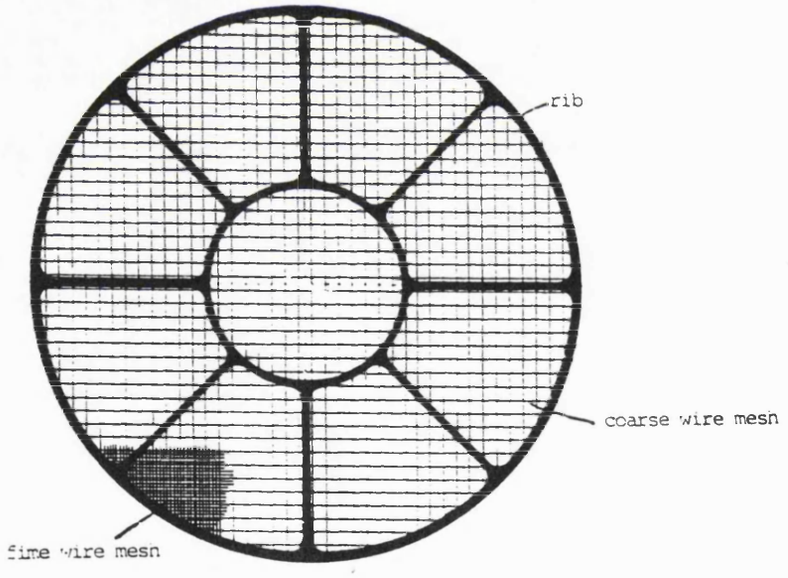

Figure B.4: *The PSPC window support structure*

B.2 *WFC* survey Data processing

Each of the participating consortium institutes was allocated a specific area of sky for which they were responsible for the data reduction and source analysis. The *WFC* data for each time slot and region of sky was received at the relevant institute on magnetic tape after initial pre-processing at the UK Data Centre (UKDC) at Rutherford Appleton Laboratory. The data was down-loaded to disk and sent through the automated pipeline-processing software. This processing broke down the raw event dataset into a series of images along the *ROSAT* scan path. The software attempted to identify and remove all potential sources from each image, to leave the background noise. A series of splines was fitted to this to produce a model for the background level in each image. The newly calculated background level was subtracted from each of the raw images to obtain a properly background-subtracted image data-set. Each of these was re-searched by the relevant source searching package in use by that institute (PSS or NIPS) to detect any significant point sources. Those sources were passed through a set of routines to obtain information such as source count rate, filter ratio, position. The positions were cross-correlated against a set of existing X-ray, EUV and optical source catalogues to determine if any sources could be identified with known objects. The results were output to log files for verification.

After each day's processing was completed, one of the workers (of which I was one) manually checked through all of the images to determine if the software had performed the extractions correctly or not. Each of the background spline fits was plotted and examined. A series of statistical results output from the processing software was checked. If the spline fits were generally smooth, as the background should be, with a low χ^2 to the fits, and the resultant background subtracted image looked reasonable, then that image was passed. If the spline fit had singularities or sharp deviations or the χ^2 to the fit was very high then it was likely that an initial source had not been properly subtracted. That particular image was then re-submitted by the checker, manually adjusting the reduction parameters, until a

resonable background fit was achieved, and the images checked again.

Each of the sources flagged by the software and any detected in the re-submitted images were individually extracted. The first job was to flag the validity of the source. The count rates were re-calculated manually and checked against the pipeline values. Many sources detected by the pipeline were obviously spurious, many were dubious but some were quite obviously real. The user prioritised those found by the pipeline with a simple scale designed to assign a confidence to the source validity. Those found to be good identifications had further analysis performed upon them, such as creation of the timeline.

The final source list from each institute was passed on to be merged together in a complete source listing. This was then updated after every dataset was received and processed. This source listing was used as the input to the Optical Identification Programme.

B.3 Optical ID programme

The task of the optical ID programme was to identify as many as possible of the optical counterparts to the *WFC* EUV sources discovered during the sky survey.

The initial effort of the optical identification process was to scan existing optical sky survey plates to produce finding charts for the *WFC* sources. The northern sky scans were mainly produced by the APM from the Palomar Optical Sky Survey plates, the southern scans by the COSMOS machine (MacGillivray & Stobie 1984) from the SERC UK Schmidt Plates. These plate scans produced a database of stellar positions and magnitudes much deeper than any other large coverage database.

The next task was to prioritise the potential counterparts for the optical identification effort.

B.3.1 Strategy & scheduling

The priority of each source depended on several factors, such as if there was a corresponding XRT detection and the source significance above the background level. Sources were assigned a priority from 1 (high) to 5 (low) to determine which should be observed first. Several separate blocks of observing time were obtained on the INT, such that the sources also had to be arranged in celestial position order to ensure that there would be sufficient targets to observe at all times during the year (i.e. all observing sessions). When the set of observations for each observing session was known, a set of finding charts was generated, with corresponding lists of all the potential optical counterparts in the field and information on each, such as magnitude and colour. This information was also represented graphically (in colour-magnitude diagrams), since the likelyhood is that an EUV source is also very blue optically (although not necessarily so).

B.3.2 Observations

At the telescope, before each night's observing, the list of objects to observe was sorted through and reprioritised to account for information that became available after the initial decisions had been made. Each field was turned to and we began observing each candidate star in that field in order of (usually) magnitude and proximity to the EUV, and if possible any XRT detections. This continued until we had reasonably determined the probable optical counterpart to the *WFC* /XRT source or else had decided there was little chance of observing the actual counterpart, due to faintness or large number of remaining candidates with equal likelyhood of being the counterpart.

As we were pressed for time, we did not complete (observe all the stars) in each field after we had determined that we had found the probable counterpart. There is the likelihood that some of the resulting identifications were not the true counterpart (merely a coincidental superposition of sources) and that there was another fainter or more distant star which was the real counterpart. However, it was

decided that this would be uncommon enough (e.g., Pounds *et al.* 1992) that the time spent completing the field to obtain more statistically valid results would result in many less real identifications. Later on, some of these fields (and those with no detected counterpart after an intial scan though the most obvious candidates) could be searched systematically down to the magnitude limit to perform a few complete fields which would give us data on how complete the rest of the identifications were.

B.3.3 Software

After each night's observing, the data was run through my automated reduction software (see appendix A), and (hopefully) by next morning, this had reduced the spectra of all the observed sources (and extracted magnitudes and colour indices) for more detailed analysis by the team members. Thus we could check that we had indeed a suitable candidate for the optical counterpart and could measure some of its parameters such as continuum and line fluxes (absorption and emission).

B.3.4 End products–database

After each run, the data was brought back to the UK and collated into a database of all the observations and identifications. This was linked with the *ROSAT* data so that a user could access the EUV and X-ray count rates, timelines, and optical spectra and parameters all in the same place. This has now been completely re-processed to give a consistent analysis of all the spectra in the database and is online to the astronomical community.

Acknowledgements

Rest is not idleness, and to lie sometimes on the grass on a summer day listening to the murmur of water, or watching the clouds float across the sky, is hardly a waste of time.

Sir J. Lubbock

...and now the difficult bit. The production of this thesis would not have possible without a great many people, who I will now, in true Oscar winning fashion, attempt to thank.

My supervisor, Graziella Branduardi-Raymont, has been invaluable throughout the long haul of this thesis; guiding me, correcting my (many) mistakes and prodding me into activity whenever I lapsed into depression. She, more than anyone else, is responsible for my completion before the heat death of the Universe. Well done! I thank Keith Mason, the head of the group for convincing me to attempt the daunting task of a Ph.D. thesis in the first place, and giving me the opportunity to participate in such a ground-breaking project as the *ROSAT* all-sky-survey, and optical follow-up. I have received much help in my work on white dwarfs from Martin Barstow, and given my initial state of knowledge about these objects, this was gratefully received indeed!

I would like to thank all my fellow workers, students and Cyberdyne systems T69 androids (hi, Phil) both in the X-ray group and the student flats at MSSL, for putting up with me for so long without braining me with a very large crowbar. In particular Lee 'E-lio-sent-ric jool-e-an dee-ytt, ammuh!' Sproats, whose ample belly, acting as the butt for all of my jokes, has allowed me to release my tensions in

a non-violent manner. I thank Mick Edgar and Sri Moorthy, first amongst my fellow non-people, who for so long gave me someone to look at and say "Yes, someone *is* worse off than me." I must thank Jon Mittaz for always being there... to assure me it could only get *worse!* His software was also always there, for better *or* worse. I congratulate the Director of MSSL, Len Culhane, for running such a wonderful establishment as MSSL.

There are still more people to thank, so here I go: Koji Mukai, Alan Smale, Robin Corbett and Tim Naylor, for writing the ARK software which I used for much of the data reduction for this thesis. Phil Smith, for showing that mono-elemental diets are possible. Mark Garlick, for being a complete home entertainment centre with a fleshy covering. Roger Woodliffe, for making me ponder many things I had not previously thought to question. Ian Davenport, for providing a science fiction video library in those rare cases when Mark can't quote the entire film script. Andy Phillips, for introducing me to 'Conquer'. Simon Phillips, for his stories of bravado in Israel. Carolin Crawford, Malcom Bremer and Bob Abrahams, for showing me how to feed cats and drive safely at La Palma. Dave Pike, for beating me at pool at extreme altitude. Ata Etermadi, for immortalising myself and others in GIF form. Caroline '7 out of 10' Allen. Charles Wiles, for the 'ejector' bed, being further behind in his PhD than I am in mine, inviting me out on blind dates (well, ok, one blind date), and still visiting us poor 'Sloiders' occasionally. Julie Cave, for allowing me to earn some badly needed cash. Sarah Szita, Gavin 'absolutely barking' Ramsey, Andy Harris, Ady 'that's rude' James, Nick 'Hussar!' Flowers, Tom and Sheila Foster, Simon 'expletive deleted' Rosen, Liz Puchnarewicz, Barbara Hassall, Ken Elliot, Alisdair 'nine Pliedes' Davey, Dolores 'the Fixer' Rawlings, Matthew 'guest author' Kenworthy, Eva 'ten things you didn't know about...' Alam (for not losing *my* Star Trek videotape!), 'Don' Vito Graffagnino, Jacqui 'honeydew' Russell, Dave 'Wonky' Wonnacott, Francisco Carrera, Mathew Page, Encarni 'Tell/bell' Romero-Colmenero and, finally, Don Knuth, for writing TEX.

I commend you all for bearing with me. Have fun and stay loose.

Ain't got no time for no jibber-jabber, fool!

Mr T. in 'The A-Team'

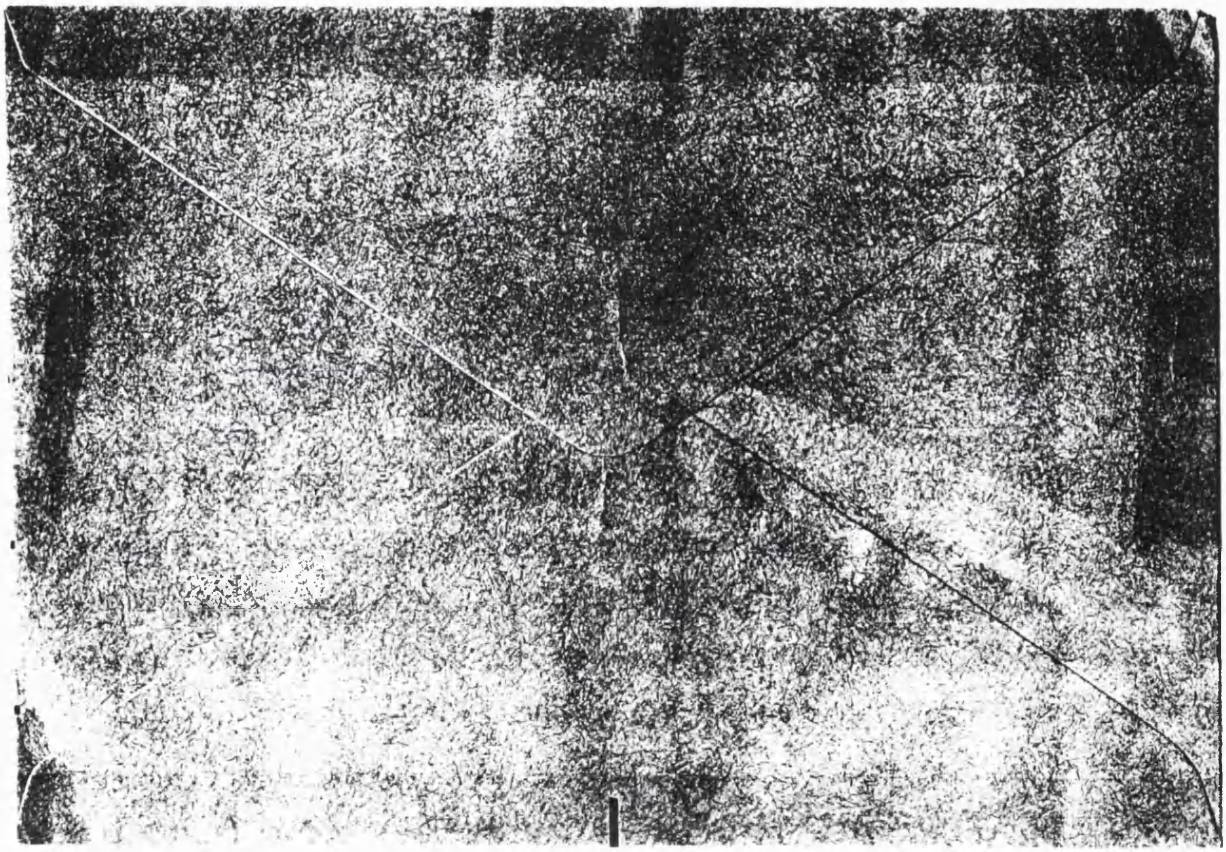

A picture of the back of an envelope. To work out the meaning of the Universe is left an an exercise for the reader...

Bibliography

My brain hurt like a warehouse it had no room to spare, I had to cram so many things to store everything in there.

David Bowie, "Five Years"

Adams W. S. 1914, PASP, 26, 198

Alcock C. & Illarionov A. 1980, ApJ, 235, 534

Allen C.W. 1973, in Astrophysical Quantities, (London: Athlone Press)

Angel J. R. P, Carswell R.F., Strittmatter P. A., Beavér E. A. & Harms R. 1974, ApJL, 194, L48

Angel J. R. P., Borra E. F. & Landstreet J. D. 1981, ApJS, 45, 474

Auer L. H. & Shipman H. L. 1977, ApJL, 211, L103

Barstow M. A. & Pounds K. A. 1988, in Proc. NATO ASI: Hot Thin Plasmas in Astrophysics, 359

Barstow M. A. 1989, in White Dwarfs, ed. Wegner G., (Berlin: Springer-Verlag), 156

Barstow M. A., Schmitt J. H. M. M., Clemens J. C., Pye J. P., Denby M., Harris A. W. & Pankiewicz, G. S. 1992, MNRAS, 255, 369

Barstow M. A., Hodgkin S. T., Pye J. P., King A. R., Fleming T. A., Holberg J. B. & Tweedy R. W. 1993a, in White Dwarfs: Advances in Observation and Theory, ed. Barstow M. A. (Dordrecht: Kluwer), 433

Barstow M. A., Fleming T. A., Finley D. S., Koester D. & Diamond C. J., 1993b, MNRAS, 260, 631

Barstow M. A., Fleming T. A., Diamond C. J., Finley D. S., Sansom A. E., Rosen S. R., Koester D., Marsh M. C., Holberg J. B. & Kidder K. 1993c, MNRAS, 264, 16

Berg C., Wegner G., Foltz C. B., Chaffee F. H. & Hewett P. C. 1992, ApJS, 78, 409

Bergeron P., Wesemael F., Fontaine G. & Liebert J. 1990, ApJL, 351, L21

Bergeron P., Wesemael F. & Fontaine G. 1991, ApJ, 367, 253

Bergeron P., Saffer R. A. & Liebert J. 1992, ApJ, 224, 132

Bergeron P., Saffer R. A. & Liebert J. 1992b, ApJ, 394, 228

Bohlin R. C., Savage B. D., & Drake J. F. 1978, ApJ, 224, 132

Böhm K. H. 1979, in IAU Colloq. 53: White Dwarfs and Variable Degenerate Stars, ed. van Horn H. & Weidemann V., (Rochester: Univ. Rochester press), 223

Böhm K. H. & Kapranidis S. 1980, A&A, 87, 307

Bohm-Vitense E., Dettman T. & Kapranidis S. 1979, ApJL, 232, L189

Bond H. E. 1976, PASP, 88, 192

Bond H. E. 1985, in Cataclysmic Variables and Low-Mass X-Ray Binaries, ed. Lamb D. Q. & Patterson J. (Dordrecht: Reidel), 15

Bond H. E. 1993, in White Dwarfs: Advances in Observation and Theory, ed. Barstow M. A. (Dordrecht: Kluwer), 85

Bowers R. & Deeming T. 1984, in Astrophysics I: Stars, ed. Kelly A., (Boston: Bartlett), 183

Boyle B. J. 1989, MNRAS, 240, 533

Braggaglia A., Greggio L., Renzini A. & D'Odorico S. 1990, ApJL, 365, L13

Bruhweiler F.C. & Kondo Y. 1981, ApJL, 248, L123

Bruhweiler F.C. & Kondo Y. 1982, ApJ, 259, 232

Bruhweiler F.C. & Kondo Y. 1983, ApJ, 269, 657

Caloi V. 1989, A&A, 221, 27

Cannizzo J. K., Wheeler J. C. & Ghosh P. 1982, ApJL, 260, L83

Chayer P., Fontaine G. & Wesemael F. 1988, in IAU Colloq. 114: White Dwarfs, ed. Wegner G., (New York: Springer-Verlag)

Chayer P., Fontaine G., Wesemael F. & Michaud G. 1987, in IAU Colloq. 95: The Second Conference on Faint Blue Stars, ed. Phillip A. G. D., Hayes D. & Liebert J. (Schenectady: Davis), 653

Cooke B. A., Barstow M. A., Breeveld E. R., Charles P. A., Goodall C. V., Gourlay J. A., Hassall B. J. M., Huckle H. E., Kent B. J., Pye J. P., Richards A. G., Sims M. R., Sumner T. J., Watson M. G., Wells A., Willingale R. & Wright J. S. 1992, Nature, 355, 61

Córdova F. & Mason K. 1981, in Accretion Driven Stellar X-ray Sources, (Cambridge: Cambridge Univ. Press)

Cottrell P. L., Bessel M. S. & Wickramasinghe D. T. 1977, ApJL, 218, L133

Cowie L. L., Taylor W. & York D. G. 1981, ApJ, 248, 528

Crampton D., Cowley A. P., & Fisher W. A. 1986, ApJ, 300, 788

Cropper M. S. 1990, Spa. Sci. Rev., 54, 195

de Kool M. & Ritter H. 1993, A&A, 267, 397

Dorren J. D., Guinan E. F. & Sion E. M. 1982, in Advances in Ultraviolet Astronomy: Four Years of IUE Research, NASA Conference Publication 2238 , 517

Dupree A. K. & Raymond J. C. 1982, ApJL, 263, L63

Dupuis J., Fontaine G. & Wesemael F. 1993, ApJS, 87, 345

Durisen R. H., Savedoff, M. P. & van Horn H. M. 1976, ApJL, 206, L149

Eggleton P. P. 1976, in IAU Symp. 73, 209

Faulkner J. & Lin D. 1983, AAS meeting, Boston

Ferguson D. H., Liebert J., Cutri R., Green R. F., Willner S. P., Steiner J. E., & Tokarz, S. 1987, ApJ, 316, 399

Finley D. S. 1988, PhD thesis, Univ. California, Berkeley

Finley D. S., Basri G., & Bowyer S. 1990, ApJ, 359, 483

Finley D. S., Koester D. & Basri G. 1993a, in preparation

Finley D. S., Dupuis J., Paerels F. & Koester D. 1993b, in White Dwarfs: Advances in Observation and Theory, ed. Barstow M. A. (Dordrecht: Kluwer), 191

Fleming T. A., Liebert J. & Green R. F. 1986, ApJ, 308, 176

Fontaine G., McGraw J. T., Dearborn D. S. P., Gustafson J. & Lacombe P., 1982, ApJ, 258, 651

Fontaine G. & van Horne H. M. 1976, ApJS, 31, 467

Fontaine G. & Michaud G. 1979, ApJ, 231, 826

Fontaine G. & Wesemael F. 1987, in IAU Colloq. 95: The Second Conference on Faint Blue Stars, ed. Phillip A. G. D., Hayes D. & Liebert J. (Schenectady: Davis), 319

Frank J., King A. R. & Raine D. J. 1992, in Accretion Power in Astrophysics, ed. Carswell R. F., Lin D. N. C. & Pringle J. E., (Cambridge: Cambridge Univ. Press), 51

Fulbright M. S., Liebert J. W., Bergeron P. & Green R. F., ApJ, 1993, in press

Fujimoto M. Y. 1982a, ApJ, 257, 752

Fujimoto M. Y. 1982b, ApJ, 257, 767

Fusi-Pecci F. & Renzini A. 1976, A&A, 46, 447

Gast P. R. 1960, in Handbook of Geophysics, U. S. Air Force Cambridge Research Center Geophysics Research Directorate (Rev. ed.; New York: Macmillan), 16

Grauer A. D. & Bond H. E. 1981, PASP, 93, 388

Grauer A. D. & Bond H. E. 1983, ApJ, 271, 259

Green R. F. 1980, ApJ, 238, 685

Green R. F., Richstone D. O. & Schmidt M. 1978, ApJ, 224, 892

Green R. F., Schmidt M. & Liebert J. 1986, ApJS, 61, 305

Greenstein J. L. 1958, in Handbuch der Physik, (Berlin: Springer-Verlag), 50, 161,

Greenstein J. L. 1979, ApJ, 233, 239

Greenstein J. L. 1984, ApJ, 276, 602

Greenstein J. L. 1986, ApJ, 304, 334

Greenstein J. L. 1988, PASP, 100, 82

Greenstein J. L. & Sargent A. I. 1974, ApJS, 28, 157

Greenstein J. L., Boksenberg A., Carswell R. & Shortridge K. 1977, ApJ, 212, 186

Greenstein J. L. & Oke J. B. 1979, ApJL, 229, L141

Greenstein J. L. & McCarthy J. K. 1985, ApJ, 289, 732

Greenstein J. L., Henry R. J. W. & O'Connell R. F. 1985, ApJL, 289, L25

Greggio L. & Renzini A. 1983, A&A, 118, 217

Hamada T. & Salpeter E. E. 1961, ApJ, 134, 683

Hayakawa S., Murakami T., Nagase F., Tanaka Y. & Yamashita K. 1975a, IAU/COSPAR Symp.: Fast Transients in X- and γ-rays, Varna, Bulgaria

Hayakawa S., Tanaka Y., Yamashita K., Bleeker J. A. M., Deerenberg A. J. M. & de Korte P. A. J. 1975b, PASJ, 27, 615

Hayes D. S. & Latham D. W. 1975, ApJ, 197, 593

Heise J. 1986, in Invited Review Talk: 167 Meeting of the American Astronomical Society, Houston, Texas, USA

Heise J. & Huizenga H. 1980, A&A, 84, 280

Henry P., Cruddace R., Paresce F., Bowyer S. & Lampton M. 1975, ApJ, 195, 107

Henry P., Bowyer S., Lampton M., Paresce F. & Cruddace R. 1976, ApJ, 205, 426

Hills J. G. 1972, A&A, 17, 155

Hoshi R. 1979, Prog. Theor. Phys., 61, 1307

Hoshi R. 1981, Prog. Theor. Phys. Suppl., 70, 181

Hoshi R. 1982, Prog. Theor. Phys., 67, 179

Humason M. L. & Zwicky F. 1947, ApJ, 105, 85

Hutchings J. B. & Cowley A. P. 1985, PASP, 97, 328

Iben I. Jr. 1984, ApJ, 277, 333

Iben I. 1985, QJRAS., 26, 1

Iben I. 1991, ApJS, 76, 55

Iben I. Jr.& Tutakov A, V. 1984, ApJ, 282, 615

Iben I. & Tutukov A. V. 1986, ApJ, 311, 742

Illarionov A. F. & Sunyaev R. A. 1975, A&A, 39, 185

Jaschek C. & Jaschek M. 1987, in The Classification of Stars, (Cambridge: Cambridge Univ. Press), (377)

Jeffries R. D., Jewell S. J., Barstow M. A., Bromage G. E., Hodgkin S. T., Mason K. O., Matthews L., Mittaz, J. P. D., Pye J. P., Quenby J. J., Rosen S. R. & Sidher S. D. 1991, Vistas in Astronomy, 34, 267

Jenkins E. B. 1978, ApJ, 220, 107

Jensen K., Swank J., Petrie R., Guinan E., Sion E. & Shipman H. 1986, ApJL, 309, L27

Jomaron C. M., Branduardi-Raymont G., Bromage G. E., Hassall B. J. M., Hodgkin S. T., Mason K. O., Naylor T. & Watson M. G. 1993 MNRAS, 264, 219

Jones D. H. P. 1984, RGO/La Palma Technical Note 10

Jordan S. & Koester D. 1986, A&AS, 65, 367

Jordan S. & Heber U. 1993, in White Dwarfs: Advances in Observation and Theory, ed. Barstow M. A. (Dordrecht: Kluwer), 47

Kahn S. M., Wesemael F., Liebert J., Raymond J. C., Steiner J. E. & Shipman H. L. 1984, ApJ, 278, 255

Kidder K. M. 1991, PhD. thesis, University of Arizona

Kilkenny D., Hilditch R. W. & Penfold J. E. 1978, MNRAS, 183, 523

King D. L. 1985, RGO/La Palma Technical Note 31

Kippenhahn R. & Weigert A. 1967, ZAp, 65, 251

Koester D. 1976, A&A, 52, 415

Koester D. 1978, A&A, 65, 449

Koester D. 1987, in IAU Colloq. 95: The Second Conference on Faint Blue Stars, ed. Phillip A. G. D., Hayes D. & Liebert J. (Schenectady: Davis), 329

Koester D. 1989, ApJ, 342, 999

Koester D. 1991, in IAU Symposium 145: Evolution of Stars: the Photospheric Abundance Connection, ed. Michaud G. & Tutukov A. (Dordrecht: Kluwer), 435

Koester D. & Schönberner D. 1986, A&A, 154, 125

Koester D., Weidemann V. & Zeidler-K. T. E. M. 1982, A&A, 116, 147

Kohoutek L. 1964, Bull. Astr. Inst. Czech, 15, 161

Kopal Z. 1978, in Dynamics of Close Binary Systems, (Dordrecht: Reidel)

Kraft R. P. 1967, PASP, 79, 395

Kraft R. P., Mathews J. & Greenstein J. L. 1962, ApJ, 136, 312

Kudritzki R. P. & Simon K. P. 1978, A&A, 70, 653

Kuiper G. P. 1940, PASP, 53, 248

Kuzma T. J. 1979, ApJ, 227, 548

Labay J., Canal R. & Isern J. 1983, A&A, 117, L1

Lampton M., Margon B., Paresce F., Stern R. & Bowyer S. 1976, ApJL, 203, L71

Lanning H. H. 1982, ApJ, 253, 752

Lanning H. & Pesch P. 1981, ApJ, 244, 280

Law W-Y. & Ritter H. 1983, A&A, 123, 33

Liebert J. W. 1980, ARA&A, 18, 363

Liebert J. 1986, in IAU Colloq. 87: Hydrogen Deficient Stars and Related Objects, (Dordrecht: Reidel)

Liebert J. & Margon B. 1977, ApJ, 216, 18

Liebert J. & Wehrse R. 1983, A&A, 122, 297

Liebert J., Wehrse R. & Green R. F. 1987, A&A, 175, 173

Liebert J., Fontaine G. & Wesemael F. 1987, Mem. Soc. Astr. Italiana, 58, 17

Liebert J., Dahn C. C. & Monet D. G. 1988, ApJ, 332, 891

Liebert J., Green R., Bond H. E., Holberg J., Wesemael F., Fleming T. A. & Kidder K. 1989, ApJ, 346, 251

Lightman A. P. & Grindlay J. E. 1982, ApJ, 262, 145

Livio M. 1982, A&A, 105, 37

Lucy L. B. & Ricco F. 1979, AJ, 84, 401

Luyten W. J. 1952, ApJ, 116, 283

Luyten W. J. 1969, Proper motion survey with the 48-inch Schmidt telescope, No. XVIII

Luyten W. J. 1971, in IAU Symp., 42, 1

Luyten W. J. 1979, University Minnesota L. II

MacGillivray H. T. & Stobie R. S. 1984, Vistas in Astronomy, 27,433

Malina R. F., Bowyer S. & Basri G. 1982, ApJ, 262, 717

Margon B. & Bowyer S. 1975, Sky and Telescope, 50, 4

Margon B., Liebert J., Gatewood G., Lampton M., Spinrad H. & Bowyer S., 1976, ApJ, 209, 525

Mason K. O., Branduardi-Raymont G., Bromage G. E., Buckley D., Charles P. A., Hassall B. J. M., Hawkins M. R. S., Hodgkin S. T., Pike C. D., Jomaron C. M., Jones D. H. P., McHardy I., Naylor T., Ponman T. J. & Watson M. G. 1991, Vistas in Astronomy, 34, 343

Mazurek T. J. 1973, Ap&SS, 23, 365

Mazzitelli I. 1989, in IAU Colloq. 114: White Dwarfs, ed. Wegner G. (Berlin: Springer-Verlag), 29

McCook G. P. & Sion E. M. 1987, ApJS, 65, 603

McGraw J. T. 1979, ApJ, 229, 203

McMahan R. K. 1989, ApJ, 336, 409

Mendez R. H. & Niemela V. S. 1977, MNRAS, 178, 409

Mendez R. H. & Niemela V. S. 1981, ApJ, 250, 240

Michaud G. & Fontaine G. 1982 ApJL, 253, L29

Michaud G., Fontaine G. & Charland Y. 1984, ApJ, 280, 247

Muchmore D. 1984, ApJ, 278, 769

Mullen D. J., Sion E. M., Carpenter K. G. & Bruhweiler F. C. 1989, ApJL, 339, L33

Nather R. E. 1978, PASP, 90, 477

Nather R. E., Robinson E. L. & Stover R. J. 1981, ApJ, 244, 269

Nelson B. & Young A. 1970, PASP, 82, 699

Oswalt T. D., Hintzen P. M., Liebert J. & Sion E. M. 1988, ApJL, 333, L87

Paerels F. B. S., Bleeker J. A. M., Brinkman A. C. & Heise J. 1986, ApJL, 309, L33

Paerels F. B. S. & Heise J. 1989, ApJ, 339, 1000

Paczyński B. 1976, in IAU Symp. 73: Structure and Evolution of Close Binary Systems, ed. Eggleton P. P., Mitton S. & Whelan J. (Dordrecht: Reidel), 75

Paczyński B. 1985, in Cataclysmic Variables and Low-Mass X-Ray Binaries, ed. Lamb D. Q. & Patterson J. (Dordrecht: Reidel)

Paczyński B. & Rudak B. 1980, A&A, 82, 349

Paczyński B. & Trimble V. 1973, A&A, 22, 9

Patterson J. 1979, AJ, 84, 804

Patterson J. 1984, ApJS, 54, 443

Pelletier C., Fontaine G., Wesemael F., Michaud G. & Wegner G. 1986, ApJ, 307, 242

Pilachowski C. A. & Milkey R. W. 1984, PASP, 96, 821

Pounds K. A., Allan D. J., Barber C., Barstow M. A., Bertram D., Branduardi-Raymont G., Brebner G. E. C., Buckley D., Bromage G. E., Cole R. E., Courtier M., Cruise A. M., Culhane J. L., Denby M., Donoghue D. O., Dunford E., Georgantopoulos I., Goodall C. V., Gondhalekar P. M., Gourlay J. A., Harris A. W., Hassall B. J. M., Hellier C., Hodgkin S., Jeffries R. D., Kellet B. J., Kent B. J., Lieu R., Lloyd C., McGale P., Mason K. O., Matthews L., Mittaz J. P. D., Page C. G., Pankiewicz G. S., Pike C. D., Ponman T. J., Puchnarewicz E. M., Pye J. P., Quenby J. J., Ricketts M. J., Rosen S. R., Sansom A. E., Sembay S., Sidher S., Sims M. R., Stewart B. C., Sumner T. J., Vallance R. J., Watson M. G., Warwick R. S., Wells A. A., Willingale R., Willmore A. P., Willoughby G. A. & Wonnacott D. 1992, MNRAS, 260, 77

Probst R. G. 1983, ApJS, 53, 335

Pye J. P. & McHardy I. M. 1988, Ap&SSL, 143, 241

Rappaport S., Joss P. C. & Webbink R. F. 1982, ApJ, 254, 616

Reid N. & Wegner G. 1988, ApJ, 335, 953

Reid N. & Wegner G. 1989, in IAU Colloq. 114: White Dwarfs, ed. Wegner G. (Berlin: Springer-Verlag), 396

Reid N., Saffer R. A. & Liebert J. 1993, in White Dwarfs: Advances in Observation and Theory, ed. Barstow M. A. (Dordrecht: Kluwer), 441

Reynolds R. J. 1977, ApJ, 216, 433

Reynolds R. J. 1980, ApJ, 236, 153

Reynolds R. J. 1987, ApJ, 315, 234

Riegler G. R. & Garmire C. P. 1974, J. Geophys. Res., 79, 226

Ritter H. 1976, MNRAS, 175, 279

Ritter H. & Burkert A. 1986, A&A, 158, 161

Robinson E. L. 1976, ARA&A, 14, 119

Roche E. A., 1849a, Mem. Acad. Sci. Montpellier, 1, 243

Roche E. A., 1849b, Mem. Acad. Sci. Montpellier, 1, 383

Roche E. A., 1851, Mem. Acad. Sci. Montpellier, 2, 21

Roche E. A., 1873, Ann. de l'Acad. Sci. Montpellier, 8, 235

Rosner R., Golub L. & Vaiana G. S. 1985, ARA&A, 23, 413

Rutten R., Dhillon V. & Horne K. 1992, Gemini: Newsletter of the Royal Greenwich Observatory, 22, 38

Saffer R. A., Liebert J. & Olszewski E. W. 1988, ApJ, 334, 947

Sandage A. 1973, ApJ, 183, 711

Schönberner D. 1983, ApJ, 272, 708

Shipman H. L. 1979, ApJ, 228, 240

Shipman H. L. & Greenstein J. L. 1983, ApJ, 266, 761

Shipman H. L., Liebert J. & Green R. F. 1987, ApJ, 315, 239

Shipman H. L., Liebert J. & Green R. F. 1987, ApJ, 315, 239

Simon T., Fekel F. & Gibson D. M. 1983, BAAS, 14, 982

Sion E. M. 1984, ApJ, 282, 612

Sion E. M. 1986, PASP, 98, 821

Sion E. M. & Liebert J. 1977, ApJ, 213, 468

Sion E. M. & Starrfield S. G. 1984, ApJ, 286, 760

Sion E. M., Greenstein J. L., Landstreet J. D., Liebert J., Shipman H. L. & Wegner G. A. 1983, ApJ, 269, 253

Sion E. M., Shipman H. L., Wagner R. M., Liebert J. & Starrfield S. G., 1986, ApJL, 308, L67

Sion E. M. & Guinan E. F. 1983, ApJL, 265, L87

Sion E. M., Dermott J., Mullan D. J. & Shipman H. L. 1990

Sion E. M., Bruhweiler F. C., Mullan D. J. & Carpenter K. 1989, ApJL, 341, L17

Sion E. M., Hammond G. L., Wagner R. M., Starrfield S. G. & Liebert J., 1990, ApJ, 362, 691

Sion E. M. 1993, in White Dwarfs: Advances in Observation and Theory, ed. Barstow M. A. (Dordrecht: Kluwer), 311

Smak J. 1971, Acta Astron., 21, 15

Smith E. P. & Jacobs K. C. 1973, in Introductory Astronomy and Astrophysics, (Philadelphia: Saunders)

Spruit H. C. & Ritter H. 1983 A&A, 124, 267

Starrfield S., Cox A. N., Kidman R. B. & Pesnell W. D. 1984, ApJ, 281, 800

Stauffer J. R. 1987, AJ, 94, 996

Stephenson C. B. 1971, in IAU Symp. 42: White Dwarfs, ed. Luyten W. L. (Dordrecht: Reidel), 61

Strittmatter P. A. & Wickramasinghe D. T. 1971, MNRAS, 152, 47

Tassoul M. & Tassoul J.-L. 1983, ApJ, 267, 334

Taylor J. H. & Weisberg J. M. 1982, ApJ, 253, 908

Thorstensen J. R., Charles P. A., Margon B. & Bowyer S. 1978, ApJ, 223, 260

Trimble V. 1982a, The Observatory, 102, 133

Trimble V. L. 1982b, Rev. Mod. Phys., 54, 1183

Trimble V. & Greenstein J. L. 1972, ApJ, 177, 441

Tweedy R. W., Holberg J. B., Barstow M. A., Bergeron P., Grauer A. D., Liebert J. & Fleming T. A. 1993a, AJ, 105, 1938

Tweedy R. W. 1993b, in White Dwarfs: Advances in Observation and Theory, ed. Barstow M. A. (Dordrecht: Kluwer), 317

van Buren D., Charles P. A. & Mason K. O. 1980, ApJL, 242, L105

Vassiliadis E. & Wood P R. 1993, ApJ, 413, 641

Vauclair G. 1989, in White Dwarfs, ed. Wegner G., (Berlin: Springer-Verlag), 176

Vauclair G., Vauclair S. & Greenstein J.L. 1979, A&A, 80, 79

Vaz L. P. R. 1985, Ap&SS, 113, 349

Vedder P. W., Vallerga J. V., Jelinsky P., Marshall H. L. & Bowyer S. 1991, in Extreme Ultraviolet Astronomy, ed. Malina & Bowyer, (Pergamon press), 120

Vennes S., Chayer P., Fontaine G. & Wesemael F. 1989, ApJL, 336, L25

Vennes S., Pelletier C., Fontaine G. & Wesemael F. 1988, ApJ, 331, 876

Vennes S., Thorstensen J. R., Thejll P. & Shipman H. L. 1991, ApJL, 372, L37

Vennes S. & Thorstensen J. R., 1994, in press.

Verbunt F. & Zwaan C. 1981, A&A, 100, L7

Watson M. G. 1986, in Physics of Accretion onto Compact Objects, ed. Mason K. O., watson M. G. & White N. E., (Berlin:Springer-Verlag), 97

Webbink R. F. 1976, ApJ, 209, 829

Webbink R. F. 1979, in IAU Colloq. 53: White Dwarfs and Variable Degenerate Stars, ed. van Horn H. & Weidemann V., (Rochester: Univ. Rochester press), 426

Webbink R. F., Livio M., Truran J. W., Orio M. 1987, ApJ, 314, 653

Wegner G. & Nelan E. P. 1987, ApJ, 319, 916

Wegner G. & Yackovich F. H. 1983, ApJ, 275, 240

Wegner G. & Yackovich F. H. 1984, ApJ, 284, 257

Wehrse R. 1977, MSAI, 48, 13

Weidemann V. 1977, A&A, 59, 411

Weidemann V. 1977, A&A, 61, L27

Weideman V. & Koester D. 1983, A&A, 121, 77

Weideman V. & Koester D. 1984, A&A, 132, 195

Weigert A. 1966, Z. Astrophys, 64, 395

Wells A. A., Abbey A. F., Barstow M. A., Cole R. E., Pye J. P., Sims M. R., Spragg J. E., Watson D. J., Willingale R., Courtier G. M., Gourlay J. A., Kent B. J., Richards A. G., Wright A. S., Goodall C. V., Breeveld E. R., Huckle H. E., McCalden A. J., & Sumner T. J., 1990, Presented at the SPIE Conference on EUV, X-ray and Gamma-ray instrumentation for Astronomy and Atomic Physics, San Diego, California, in Proc. SPIE, 1344, 230

Wesemael F 1979, A&A, 72, 104

Wesemael F., Auer L. H., van Horn H. M. & Savedoff M. P. 1980, ApJS, 43, 159

Wesemael F, Green R. F.& Liebert J. 1985, ApJS, 58, 379

Wesemael F. & Truran J. W. 1982, ApJ, 260, 807

Wesselius P. R. & Koester D. 1978, A&A, 70, 745

Wilson J. 1980, Proc. N.Y. Acad. Sci., 336, 358

Wilson J. 1983, in Numerical Astrophysics, ed. Centrella J., Bowers R., LeBlanc J. & LeBlanc M., (Boston: Jones & Bartlett), 422

Wilson R. E. 1990, ApJ, 356, 613

Winget D. E. & Fontaine G. 1982, Pulsations in classical and cataclysmic variables ed. J. P. Cox & C. J. Hansen (Boulder: JILA), 46

Winget D. E., Robinson E. L., Nather R. E. & Fontaine G. 1982, ApJL, 262, L11

Winget D. E., van Horn H. M., Tassoul M., Hansen C. J. & Fontaine G., 1983, ApJL, 268, L33

Wood M. A. 1990, Ph.D. thesis, University of Texas

Wood J. H., Zhang E-H. & Robinson E. L. 1993, MNRAS, 261, 103

Wood P. R. & Cahn J. H. 1977, ApJ, 211, 499

Woosley S. E. & Weaver T. A. 1986, ARA&A, 24, 205

Young A., Klimke A., Africano J. L., Quigley R., Radick R. R. & Van Buren D. 1983, ApJ, 267, 655

Young A., Nelson B. & Mielbrecht R. M. 1972, ApJ, 174, 27

Young A., Skumanich A., & Paylor V. 1988, ApJ, 334, 397

Zeidler-K. T. E. M. , Weidemann V. & Koester D. 1986, A&A, 155, 356

Zombeck M. V. 1982, in Handbook of Space Astronomy and Astrophysics, (Cambridge: Cambridge Univ. Press), 68

Zuckerman B. & Becklin E. E. 1992, ApJ, 386, 260